The Asymptotic Structure Of Excitable Systems Of Equations

Thesis submitted in accordance with the requirements of the University of Liverpool for the degree of Doctor in Philosophy

by

Rebecca Suckley

July 2004

Declaration

No part of the work referred to in this thesis has been submitted in support of an application for another degree or qualification of this or any other institution of learning. However some parts of the material contained herein has been previously published.

Acknowledgements

I would like to thank my supervisor Dr V.N. Biktashev for giving me the opportunity to do my PhD and for all the time, help and understanding he has shown to me during my research.

Also I acknowledge the University and the Department of Mathematics for allowing me to study for my PhD and for the use of their facilities for my research.

I thank the governing body EPSRC for the financial support I have received for my project.

I thank Marc Courtemanche for giving me the program file to draw the graphs from the 1998 paper he wrote with Ramirez and Nattel. I also thank Alan Vinet for sending me a copy of the master thesis and the paper written by Friedman.

Also, an acknowledgement goes to all my friends in the department, especially Martyn Hughes and Alana Selsil, for all the support and friendship that they have given me since I started.

I thank my family and friends for giving me the support to achieve my goal.

For the most important person in my life, my fiancé Carl, there are not enough words or gestures in this world to show how much I appreciate all the support, love and guidance he has given me during my research. I would never have achieved so much without his understanding of all the time I've put into my research, and the little time I've spent with him.

Also I thank him for the many hours of proof reading he has done for me.

Abstract

This thesis is concerned with using asymptotic methods to study high-order, non-linear systems of differential equations for nerve fibres and cardiac muscles.

We use these methods because these systems cannot be solved analytically, and numerical study is complicated due to the stiffness of the equations, i.e. the presence of small parameters.

We use well-known asymptotical methods, which describe the fast and slow processes that occur at different moments in time, so that we can gain a better understanding of the ways the biological systems work. To achieve this we obtain simplified models, from our methods, which exhibit the same qualitative features as the detailed model. From this we can study the simplified models numerically and analytically.

New asymptotic methods are also derived to obtain simplified models, because the standard asymptotic methods did not describe some qualitative features of the solutions. Our new methods also help to solve the systems analytically.

The following properties of the systems of equations are taken into account to derive the new asymptotic methods:

1. the fact that some small parameters appear in a non-standard way,

2. identifying the most important parameter as being the ionic conductance g_{Na} characterising the sodium current, this is because g_{Na} is large and its inverse is small, and

3. the almost perfect closure of the gating variables for the sodium current in certain ranges of voltage.

The thesis begins with the study of simple classical biological excitable models, and then moves to studying a more accurate and complicated model.

Publications And Presentations

The following papers have appeared and are going to appear in the following journals:

1. Suckley R and Biktashev V.N, "Comparison of asymptotics of heart and nerve excitability", Phys. Rev. E, 68, 011902, 2003,

2. Suckley R and Biktashev V.N, "The asymptotic structure of the Hodgkin-Huxley equations", Int. J. Bifurcation and Chaos, 13 (12), 3805-3826, 2003,

3. Biktashev V.N and Suckley R, "Non-Tikhonov asymptotic structure of cardiac excitation equations", submitted to Phys. Rev. Lett.

4. Biktashev V.N, Suckley R and Elkin Y.E, "Asymptotic structure and analytical solutions for a model of cardiac excitation", to be submitted to Physica D.

The following presentations have been given and are going to be given at conferences:

1. "The asymptotical structure of the Hodgkin-Huxley equations", Departmental Seminar, May, 2002,

2. "The asymptotic structure of the Hodgkin-Huxley equations", Poster for the EPSRC workshop in Leeds, "Virtual Tissues and Organs", June 2002,

3. "The asymptotic structure of the Hodgkin-Huxley equations", Poster for the IUTAM Symposium in Liverpool, July 2002,

4. "A comparison of asymptotics of heart and nerve excitability", Poster for the University Poster Day, 1st, April 2003,

5. "A comparison of asymptotics of heart and nerve excitability", BAMC in Southampton, 8th, April 2003,

6. "A comparison of asymptotics of heart and nerve excitability", Departmental Seminar, 16th, April 2003,

7. "A comparison of asymptotics of heart and nerve excitability", International Conference Of Mathematical Biology (SMB03) in Dundee, 7th, August 2003,

8. "Non-Tikhonov asymptotic structure of cardiac excitation equations", BAMC in Norwich, 19th, April 2004,

9. "Non-Tikhonov asymptotic structure of cardiac excitation equations", Departmental Seminar, 30th, April 2004.

List of Tables

2.1 Terms and definitions for Courtemanche et al's model 27
2.2 Gating variables and their values for α and β for Courtemanche et al's model 36
2.3 The other gating variables and their τ's and quasi-stationary values $\overline{y}$ for Courtemanche et al's model. 36
2.4 The initial values for all the dynamic variables for Courtemanche et al's model. 37

6.1 Defining the different time stages and corresponding variables for Courtemanche et al's model. 147
6.2 Time steps, in ms, admissible for different versions of Courtemanche et al's model. 234
6.3 Description of the ϵ's and where they are used in Courtemanche et al's model. 239

List of Figures

1.1 A diagram representing the processes in the cell membrane. 2

2.1 The action potential for the Hodgkin-Huxley system. 13
2.2 Solutions of the Hodgkin-Huxley system for V, m, n and h. 13
2.3 Graph of $\overline{m}$ for Hodgkin-Huxley and Noble's system. 18
2.4 Graph of α_m's and β_m's for Hodgkin-Huxley and Noble's system. . 19
2.5 Action potential for Noble's system. 21
2.6 Action potential for Courtemanche et al's system 39
2.7 Graphs of the currents and F_n, Cai, $Caup$, and $Carel$ variables for Courtemanche et al's system. 40
2.8 (a,c) Phase portrait of the FitzHugh system. (b,d) The action potential. 42
2.9 (a,c) Projection of the Hodgkin-Huxley system to a two-dimensional subspace. (b,d) The action potential. 44
2.10 (a) Phase portrait of Zeeman's "heart" model. (b) The "heart" action potential. 57
2.11 (a,b) Phase portrait of Zeeman's "nerve" model. (c) The "nerve" action potential. 63
2.12 Projection of the slow manifold of Zeeman's "nerve" model. . . . 65
2.13 Phase portrait of the new FitzHugh system. 66
2.14 (a) Graph of the τ's. (b) Graph of $\overline{n}$, $\overline{m}$ and $\overline{h}$ for the Hodgkin-Huxley system. 68
2.15 Graph of $G{=}\overline{n} + \overline{h}$ for the Hodgkin-Huxley system. 69
2.16 Graph of $\ln(\tau)$'s for the Hodgkin-Huxley system. 71
2.17 Graph of $\frac{\tau_m}{\tau_n}$ for the Hodgkin-Huxley system. 73
2.18 Phase portrait of the second order and the original Hodgkin-Huxley system. 76

3.1 Graph of the τ's for the Hodgkin-Huxley system, including τ_V. . . 82
3.2 Graphs of m, $\overline{m}$ and $-V * 0.01$ for the Hodgkin-Huxley system. . 82
3.3 Graphs of $-V$ for the reduced and original Hodgkin-Huxley system. 84
3.4 Graphs of $-V$ for the reduced and original Hodgkin-Huxley system for ϵ=0.1. 85
3.5 Graph of the τ's for the Hodgkin-Huxley system. 86
3.6 Graph of r in Hodgkin-Huxley's system. 87
3.7 Graph of $-V$ for the new reduced and original Hodgkin-Huxley system. 90
3.8 (a) The graph of n^4. (b) The projection of the fold curve in the (n, h) plane for E_l=10.613 for the Hodgkin-Huxley system. 95
3.9 Graph of F'' for the Hodgkin-Huxley system. 96
3.10 (a,b) The phase portrait of the reduced Hodgkin-Huxley system for E_l=10.613. (c) The action potential. 97
3.11 Graph of $q_1(E)$, $q_2(E)$ and $\mu(E)$ for (a) E_l=10.613 and (b) E_l=25 for the Hodgkin-Huxley system. 98
3.12 (a) The graph of n^4. (b) The projection of the fold curve in the (n, h) plane for E_l=25 for the Hodgkin-Huxley system. 99
3.13 (a,b)The phase portrait of the reduced Hodgkin-Huxley system for E_l=25. (c) The action potential. 100

4.1 Graph of the τ's for Noble's system. 105
4.2 Graph of the original and the reduced Noble system. 106
4.3 Pacemaker potential for the reduced Noble system. 108
4.4 The graph of $\overline{h}$ for Noble's system. 109
4.5 Graph of $\mathrm{Tr}(J_{Eh})$ and $10 * \det(J_{Eh})$ for Noble's system. 112
4.6 Phase portraits of the fast leaves for Noble's system. 114
4.7 (a,b) The projection of the phase portrait of Noble's system onto the (n, E) plane. (c) The pacemaker potentials of the original and embedded systems. 114
4.8 (a) Same as Fig. 4.3(a). (b) The fast time scale T for (a). (c) Same as Fig. 4.5. With E_K=−110. 116
4.9 Same as Fig. 4.6 with E_K=−110. 117
4.10 Same as Fig. 4.7 with E_K=−110. 118

5.1 Action potential for Noble's excitable system with h and n. 122

5.2 (a) Graph of $\overline{m}^3$, $\overline{h}$, $100\overline{m}^3\overline{h}$ and $1000\overline{m}^3\overline{h}'$. (b) Action potential for Noble's excitable system with approximations and h and n. . . 122
5.3 (a,b) Graphs of the currents and the action potential for the reduced system with and without the approximations for Noble's excitable system, and (c) for Courtemanche et al's system. 124
5.4 Action potential of the modified and the original system with h and n for Noble's excitable system. 128
5.5 Action potential for Noble's excitable system with n and h. 130
5.6 Graph of $\mathrm{Tr}(J_{En}) * 0.01$ and $\det(J_{En})$ for Noble's excitable system. 132
5.7 (a,b)Phase portrait for the slow system for Noble's excitable system. 133
5.8 Action potential for Noble's excitable system with h and n. 133
5.9 Phase portrait for the fast system for Noble's excitable system. . . 135

6.1 Action potential for Courtemanche et al's system. 138
6.2 Graph of $\ln(\tau)$'s for Courtemanche et al's system. 140
6.3 Graphs of CRN-21 with the super-slow variables frozen. 142
6.4 Graphs of the super-fast variables and their quasi-stationary values for CRN-17. 144
6.5 Action potential of CRN-17 and CRN-14. 145
6.6 (a) Action potential for CRN-17 with m, u_a and w adiabatically eliminated separately. 146
6.7 Graph of the τ's for CRN-14. 149
6.8 (a,b,c) Graphs of the fast variables and their quasi-stationary values and (d) graph of the currents for CRN-14. 150
6.9 (a,c) Graphs of the slow system and (b,d) graphs of the fast system for E and h in CRN-14. 151
6.10 (a,c) Graphs of the slow system and (b,d) graphs of the fast system for o_a and d in CRN-14. 152
6.11 Graphs of CRN-14 with the slow variables frozen. 153
6.12 Graphs of CRN-14 and CRN-4. 155
6.13 Phase portrait for the sodium embedding for τ_h=constant. 159
6.14 Graphs of $\ln(\mu)$ and μ and their approximations. 160
6.15 Phase portrait for the sodium embedding for μ=Ke^{mE}. 161
6.16 Graph of μ and μ=$(a+bE)e^{-cE}$. 162
6.17 Phase portrait for the sodium embedding for $\mu(E)$=$(a+bE)e^{-cE}$. 162
6.18 Graph of $E(T)$ for the sodium embedding. 164

6.19 Graph of E_∞ for τ_h=const. 164
6.20 Graph of the τ's for CRN-11. 168
6.21 Graphs of y_1 and y_2 for CRN-11. 171
6.22 Graph of y_1 and y_2 for CRN-11 for t=29.05132. 173
6.23 (a,b) The action potentials for CRN-11 and (c,d) graphs of u, $\overline{u}$, $\overline{u}_2$, $\overline{u}_3$ and $\overline{u}_1$. 174
6.24 Action potential for CRN-11 and CRN-10. 176
6.25 Graph of u and its quasi-stationary value for CRN-11. 176
6.26 (a) Graph of y. (b) Graph of $\overline{d}$ and (c) graph of $\overline{d}(E_{Ca,L} - E)$ for the lower equilibrium. 179
6.27 Graph of y for CRN-11 for the upper equilibrium. 182
6.28 Graph of $\overline{w}$ and $\overline{d}$ for CRN-11. 183
6.29 (a) Graph of $I_{Ca,L}$ against K with a trajectory. (b,c,d) Phase portrait of the calcium subsystem for different z axes. 188
6.30 Phase portrait of the calcium subsystem for two viewpoints. . . . 189
6.31 Action potential for CRN-11 for the slow variables. 190
6.32 Action potential for CRN-11 and CRN-8. 191
6.33 Graph of $Cai * 1000$ and $Carel$ for CRN-8. 192
6.34 Graphs of CRN-8 with $(Carel - Cai) \approx Carel$ in I_{rel}. 193
6.35 Graphs of CRN-8 and CRN-6. 195
6.36 Graphs of CRN-8 and CRN-6 with minor currents neglected. . . . 196
6.37 Graphs of CRN-6 and CRN-5. 198
6.38 Action potential for CRN-6 (E) and CRN-6 (E_1) for E_0=$-$10.8425.199
6.39 Graphs of CRN-6. 200
6.40 Graphs of CRN-6 (E)and CRN-6 (E_1) for E_0=21.7785. 201
6.41 Graphs of CRN-6 for E_0=21.7785 for Cai_1. 203
6.42 Graph of iterations for $Carel$ for the initial point $Carel_0$=1.488. . 205
6.43 Graphs of (a) G and (b) $Carel$. 206
6.44 Graph of $Carel$ with different approximations for $Carel$. 207
6.45 Graph of the τ's for CRN-11. 209
6.46 Action potential of CRN-11 with $(Carel - Cai) \approx Carel$ in I_{rel}. . 210
6.47 Graphs of the fast variables and their quasi-stationary values for CRN-11 for the slow scale. 211
6.48 Graphs of the fast variables and their quasi-stationary values for CRN-11 for the fast scale. 211

6.49 Graphs of CRN-11 for the slow time scale. 212
6.50 Action potential of CRN-11 for the slow scale. 213
6.51 Graphs of CRN-11 for the fast scale. 214
6.52 Graphs of CRN-11 for the fast scale. 215
6.53 Graphs of u and the original and Heaviside $\overline{u}$ for CRN-11 and the action potential with original and Heaviside $\overline{u}$. 216
6.54 Action potential of CRN-11 and CRN-7. 217
6.55 Graphs of currents in CRN-11 and CRN-7. 218
6.56 Graph of $Carel$ and the approximation $(Caup - Carel) \approx Caup$. . 221
6.57 Graph of $Carel$ and the approximation for $Carel(G)$. 221
6.58 Graphs CRN-7 and CRN-5a. 224
6.59 Graphs of CRN-5a for the gating variables and their quasi-stationary values. 225
6.60 Graph of the τ's for CRN-5a. 225
6.61 Graphs of currents for CRN-5a. 226
6.62 Graphs of $\frac{\mathrm{d}E}{\mathrm{d}t}$ for CRN-5a. 227
6.63 Graphs of CRN-5a for the gating variables with their approximations. 228
6.64 Graphs of CRN-5a and CRN-3. 229
6.65 Graphs of I_{kr} and I_{ks} for CRN-5a and CRN-3. 230
6.66 Graph of the τ's for CRN-5. 230
6.67 Graphs of (a) original and Heaviside $\overline{f}$, (b) original and Heaviside τ_f, and (c,d,e) CRN-3 with original and Heaviside τ_f and $\overline{f}$. . . . 232

Contents

List of Tables **v**

List of Figures **vi**

Contents **xi**

1 Introduction **1**

2 Literature Review **7**

2.1 Cardiac Excitation Models: from Hodgkin-Huxley to Modern Systems 7

2.1.1 The Hodgkin-Huxley 1952 system of equations 7

2.1.2 Noble's 1962 system of equations 14

2.1.3 Development of cardiac excitation models after 1962 . . . 22

2.1.4 Courtemanche et al's 1998 system of equations 26

2.1.5 Summary 38

2.2 The FitzHugh System 39

2.2.1 Summary 43

2.3 The Classical Perturbation Theory 45

2.3.1 Tikhonov's theorem 45

2.3.2 Pontryagin's theorem 50

2.3.3 Geometry of the slow manifold 52

2.3.4 Parametric embedding 52

2.3.5 Summary 53

2.4 Two Excitable Systems by Zeeman 53

2.4.1 The "heart" by Zeeman 54

2.4.2 The "nerve" by Zeeman 57

2.4.3 Applying Zeeman's method to the FitzHugh system 65

2.4.4 Summary 65

2.5 Reduction of the Classical Models to a Second Order System by Krinsky and Kokoz 66
2.5.1 Reduction of the Hodgkin-Huxley system to a third order system 68
2.5.2 Reduction of the third order system to a second order system 71
2.5.3 Phase portrait of the second order system 74
2.5.4 Reduction of Noble's 1962 model by Krinsky and Kokoz . 75
2.5.5 Further models using Krinsky and Kokoz's methods 77
2.5.6 Summary 79

3 Hodgkin-Huxley Model: Tikhonov's Approach 80
3.1 Looking For Small Parameters In The Hodgkin-Huxley Model . . 80
3.1.1 The V, n, h reduced system 83
3.1.2 Introducing a small parameter ϵ 83
3.1.3 If the voltage was the fastest variable 89
3.1.4 Summary 91
3.2 Properties of the Third Order Reduced Hodgkin-Huxley System . 91
3.2.1 Hodgkin-Huxley's third order system 91
3.2.2 Slow manifold and fast foliation 92
3.2.3 Fold curve 93
3.2.4 Finding the cusp point 94
3.2.5 The phase portrait 96
3.2.6 Finding where n^4 is positive 97
3.2.7 Changing the value of E_l 97
3.2.8 The phase portrait for E_l=25 98
3.2.9 Reducing the system by using the $\dot{E}$ and $\dot{m}$ equations . . . 100
3.2.10 Summary 103

4 Noble's 1962 Model Of The Purkinje Fibres: Tikhonov's Approach 104
4.1 Reduction of Noble's Heart Equations 104
4.2 Finding which Variable is the Fastest 105
4.3 Eliminating the m Variable 105
4.4 The Slow Manifold and Fast Foliation 107
4.5 Phase Portraits 109

4.6 Using Tikhonov's Approach for an Excitable Version of Noble's Model . . . 115
4.7 Summary . . . 116

5 Noble's 1962 Model: Non-Tikhonov Approach 120
5.1 Non-Tikhonov Embedding of Noble's Model . . . 120
5.2 Replacing $\overline{m}^3$ and $\overline{h}$ with Heaviside Functions . . . 121
5.3 Axiomatic Approach . . . 123
5.4 Modifying System (5.1) . . . 127
5.5 Slow System . . . 130
5.6 Fast System . . . 132
5.6.1 If we consider τ_h as a constant . . . 134
5.7 Summary . . . 136

6 The Human Atrial Cell Action Potential-Courtemanche et al Model 137
6.1 Time Scales and Time Stages . . . 137
6.1.1 The action potential solution . . . 137
6.1.2 Speed analysis . . . 140
6.1.3 Elimination of the super-slow variables . . . 141
6.1.4 Adiabatical elimination of the super-fast variables . . . 143
6.1.5 Definition of the fast, intermediate and slow time stages . 146
6.1.6 Summary . . . 147
6.2 The Fast Stage $[t_0, t_1]$ . . . 148
6.2.1 Phase portrait for sodium embedding . . . 156
6.2.2 Replacing τ_h with a constant or a function of E . . . 157
6.2.3 Representing μ as an exponential function . . . 159
6.2.4 Approximating μ by a quasi-polynomial using the Marquardt-Levenberg procedure (best fit) . . . 160
6.2.5 Obtaining $E(T)$ using the solution from τ_h=constant . . . 163
6.2.6 Summary . . . 165
6.3 Calcium Subsystem in the Intermediate Stage . . . 166
6.3.1 Considering u as a fast variable . . . 167
6.3.2 Comparing u and $\overline{u}$ . . . 175
6.3.3 Finding the threshold for E where the intersections change from three to one in Fig. 6.21, lower equilibrium disappears 177

6.3.4 Finding the threshold for E where the intersections change from three to one in Fig. 6.21, upper equilibrium disappears 180
6.3.5 Summary . . . 184
6.4 Other Variables in the Intermediate Stage $[t_1, t_2]$ . . . 189
6.4.1 Neglecting dependence of I_{rel} on Cai . . . 191
6.4.2 Explicit solution for u and v in the intermediate stage . . . 192
6.4.3 Neglecting the minor currents . . . 194
6.4.4 Iterations for constant E=E_0 . . . 196
6.4.5 Dynamics of $Carel$ . . . 203
6.4.6 Finding a simpler approximation for $Carel$ . . . 204
6.4.7 Summary . . . 206
6.5 The Slow Stage $[t_2, \infty]$ . . . 208
6.5.1 Analysis of u and $\overline{u}$ . . . 214
6.5.2 Eliminating minor currents . . . 218
6.5.3 Iterations for $\frac{\mathrm{d}Carel}{\mathrm{d}t}$ . . . 219
6.5.4 Finding a good reduction for CRN-7 . . . 222
6.5.5 Empirical elimination of x_r and x_s from CRN-5a . . . 226
6.5.6 Replacing $\overline{f}$ and τ_f with a Heaviside function in CRN-3 (system (6.37)) . . . 231
6.5.7 Summary . . . 232
6.6 Properties of Various Reduced Models with Respect to Numerical Simulations . . . 233
6.7 Main Results . . . 234
6.7.1 Hierarchy of small parameters for Courtemanche et al's model . . . 238

7 Conclusion **241**

Bibliography **246**

Chapter 1

Introduction

This thesis describes a study of systems of first order ordinary differential equations that describe the electrical behaviour of nerve and cardiac cells. We analyse the asymptotic structure of those systems by identifying the classes of processes of different speeds and the speed of the corresponding variables.

The nerve and cardiac cells that we study are called excitable cells by physiologists. The cells have membrane currents flowing through their membranes, which maintain the polarization of the cells at their resting state. The cell membrane is modelled as a capacitor connected in parallel with variable resistances and batteries representing the ionic channels and external currents.

If small external currents are applied to the resting state, then these currents cause small perturbations, which are below the critical level (threshold) of that system, and they decay straight away back to the resting state. If a perturbation exceeds the critical level of that system, due to large external currents entering the cells, then this causes excitation to happen. The cells are then depolarized, which means that the transmembrane voltage is moved away from its resting state. This happens for a considerable length of time. This corresponds to the action potential, as the action potential shows the cell moving away from the resting state, and then returning to the resting state, which can be either monotonically or after a plateau stage that exhibits a dome shape.

Excitable cells do not just contain transmembrane processes, processes that happen in the membrane of the cell, which separates the cell interior from the outside, but also contains intracellular processes, e.g. the calcium dynamics. Intracellular processes happen in the interior of the cell and the calcium dynamics flow between the compartments inside the cell. These compartments are called the sarcoplasmic reticulum and are surrounded by myoplasm. Sarcoplasmic retic-

ulum is an arrangement of membranous vesicles and tubules found in the muscle fibres of the heart. The sarcoplasmic reticulum plays an important role in the transmission of nervous excitation to the contractile parts of the fibres. The sarcoplasmic reticulum acts as an excitable system within the cell. It contains two more intercellular compartments called the network sarcoplasmic reticulum and the junctional sarcoplasmic reticulum. Calcium ions flow into the network sarcoplasmic reticulum from the myoplasm as the calcium uptake current. Once inside the sarcoplasmic reticulum, calcium is transferred from the network sarcoplasmic reticulum into the junctional sarcoplasmic reticulum, as the calcium transient current. Not all of the calcium is transferred, as some is leaked back into the myoplasm as the calcium leakage current. This process where the calcium is transferred from the network sarcoplasmic reticulum into the junctional sarcoplasmic reticulum is called calcium transient. The calcium is then released from the junctional sarcoplasmic reticulum back into the myoplasm if the cell is depolarized to a critical level by a stimulus of sufficient magnitude to initiate a travelling pulse, which propagates through the cell. This process is called calcium induced calcium release. Figure 1.1 shows these processes.

Calmodulin, troponin and calsequestrin are the Ca^{2+} buffers within different sections of the cell. Troponin and calmodulin are in the cytoplasm and calsequestrin is in the release compartment.

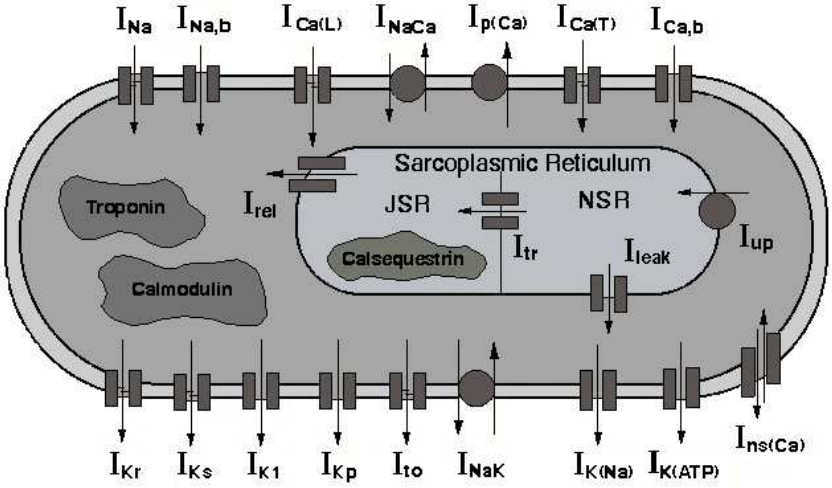

Figure 1.1: A diagram representing the processes in the cell membrane. From http://www.cwru.edu/med/CBRTC/ and similar to the cell diagram in Courtemanche et al's paper[1].

So far the models have been described in a physiological context. In a mathematical context the models can be called fast-slow systems of equations, because the equations describe the fast and slow processes in the models; e.g. the fast processes correspond to the upstroke of the action potential, this happens for a short time at the beginning of the action potential, and the slow processes correspond to the plateau stage and the return of the action potential. We are interested in the fast and slow processes because we want to use an asymptotic theory to study the models, and this asymptotic theory is for fast-slow systems of equations.

Some of the models that we study are relatively simple models, which only contain four equations, e.g. Hodgkin-Huxley's 1952 model[2] for a giant squid axon, and Noble's 1962 model[3] for mammalian Purkinje fibres. Still, they are generally considered too complicated to be solved analytically and can only be solved numerically. We modify these systems to make them even simpler while preserving their behaviour qualitatively, and we do this by reducing them to fewer equations, as we want to try and solve the equations analytically rather than just numerically.

We also consider a more complicated model, e.g. Courtemanche, Ramirez and Nattel's 1998 model[1] on the human atrial cell action potential. This is a modern and very detailed model of cardiac cells compared to the simple models. We apply the methods that we developed on the simple models, to reduce the complicated model to a simpler version, which still preserves the behaviour qualitatively. We do this so we can solve the original model analytically rather than numerically, and if we can't solve the model analytically then we want to cut down the number of time steps the computer takes to calculate the solution. This will help to consider models that have large numbers of equations to solve, e.g. if the complicated model described a piece of heart tissue containing millions of cells, instead of a single cell, and there were 21 equations in each cell in the tissue, then if the 21 equations contained fast equations, smaller time steps are needed to solve the model; and the reduced models, after the fast equations have been eliminated, can tolerate much larger time steps. Therefore a smaller number of time steps are needed to cover the required time interval.

Chapter 2 is our literature review and we talk about analysis that has been used on systems of equations that are used to describe excitable properties in mammalian heart fibres.

In Section 2.1 we give a brief description for each model before we look at other models, and more detailed analysis are in separate chapters later on.

We describe FitzHugh's 1961 system of equations[4] in Section 2.2, which is a modified version of the van der Pol system. FitzHugh takes the van der Pol system, which consists of two variables, to represent the Hodgkin-Huxley model, which has four variables and suggests that if you project the Hodgkin-Huxley phase space onto a plane it produces a similar phase portrait as the van der Pol phase portrait.

We have the definitions that are used throughout our work and a 1952 theorem by Tikhonov[5] for fast-slow systems in Section 2.3. We use this theorem to establish new methods for analysing the asymptotic structure of the Hodgkin-Huxley model, Noble's model and Courtemanche et al's model.

We also describe Zeeman's two "toy" models for "heart" and "nerve" in Section 2.4, which are described in his 1972 paper[6] and his 1977 book[7]. They are called toy models because he used simple systems of equations to demonstrate two different types of asymptotic behaviour of the shape of the action potential, which he believed resembled the shapes of the action potentials in nerve and cardiac tissue. In his paper Zeeman suggested using the concepts of a slow manifold and fast foliation for the formal analysis of the properties of the "heart" and "nerve" models. The slow manifold and fast foliation are defined in Tikhonov's section of Chapter 2.

This observation leads to his hypothesis of there being a cusp catastrophe in the "nerve" membrane model. We test this hypothesis and draw the resulting phase portrait to see if we can find a cusp and verify his hypothesis. The action potentials for both the "heart" and "nerve" models are also drawn for comparison.

We use Zeeman's analysis on the FitzHugh system to see what happens to the phase portrait and we want to know if the system has a slow manifold and a fast foliation. To do this we transform the FitzHugh system to look similar to Zeeman's "heart" model.

In Section 2.5 we describe the methods that Krinsky and Kokoz used in their 1972 papers[8] to reduce the Hodgkin-Huxley model to a second order system of equations. They used two factors to be able to do this:

1. the elimination of the fastest variable and,

2. the approximation of two other variables.

We also briefly describe how Krinsky and Kokoz[9] reduced Noble's model to a second order system of equations.

In Chapter 3 we study the first of the two classical models which is Hodgkin-Huxley's 1952 model[2]. We use Krinsky and Kokoz's analysis to reduce the Hodgkin-Huxley system to a third order system of equations and what the resulting action potential will look like compared to the original systems action potential. The question is "Can we successfully reduce the Hodgkin-Huxley system to a third order system of equations without causing too much change to the behaviour of the action potential?" as we want to keep the qualitative properties of the system.

After looking at Zeeman's "nerve" model in Section 2.4.2, we decided to test Zeeman's hypothesis on the Hodgkin-Huxley equations. This is that for a third order system of equations there exists a cusp catastrophe and we ask the question "What is the geometrical representation of the fold curve and does it form a cusp?"

We change one parameter in the Hodgkin-Huxley model to see if the geometry of the slow manifold will change, and the two branches of the fold curve will join together to produce a cusp.

In Chapter 4 we study the second classical model, which is Noble's 1962 model[3] on the Purkinje fibres of the heart.

In his 1962 paper[3], Noble observed that if he modified the Hodgkin-Huxley equations, then the properties of excitable membranes may also be used to describe the long-lasting action and pace-maker potentials of the Purkinje fibres of the heart. The Hodgkin-Huxley equations were used for nerve fibres; and the Purkinje fibres are muscle fibres in the heart, through which the atrio-ventricular node passes signals to the ventricles. The Purkinje fibres are different from the nerve membrane, because the action potential for the Purkinje fibres exhibits a much sharper onset compared to the onset of the action potential for nerve fibres.

In Chapter 5 we want to further develop the results from Chapter 4, by using a non-Tikhonov embedding method on Noble's model. The reason we do this is because by using Tikhonov's method, the reduced system has a fast onset and sharp (jump) return. So we do not retain the qualitative properties of the system by using Tikhonov's method.

So by using a non-Tikhonov embedding we can retain the slow (smooth)

return of the original system. We do this by modifying the model to obtain an excitable system instead of an oscillatory system. Then we study the reduced model using a non-Tikhonov method and compare our results with the results from Chapter 4.

In Chapter 6 we study the model by Courtemanche et al in their 1998 paper[1] on the human atrial cell action potential. We considered a more complicated system than we have already been studying and to analyse its asymptotic structure compared to our two previous models. The reason for this is that Courtemanche et al's model is an example of a modern model than Hodgkin-Huxley and Noble's models. We also wanted to see if Tikhonov's method for fast-slow systems will work on a more complicated model or if we will need to use a non-Tikhonov embedding method to obtain solutions that we can study.

The results of our study are summarized in Chapter 7.

Chapter 2

Literature Review

We first consider a literature review where we study systems of equations, the methods used to analyse their asymptotic structure and the behaviour of their solutions. The systems that we look at are Hodgkin-Huxley's 1952 model, Noble's 1962 model, Courtemanche et al's 1998 model, FitzHugh's 1961 model and Zeeman's 1972 models for "heart" and "nerve". We also describe the classic perturbation theory for fast-slow systems[10] including Tikhonov's Theorem.

2.1 Cardiac Excitation Models: from Hodgkin-Huxley to Modern Systems

We first introduce the classical model by Hodgkin and Huxley[2] for nerve membranes. The system of equations was documented in 1952 and we describe the model and the resulting action potential for different initial values of voltage.

We then introduce the second classical model which is Noble's 1962 model[3] for Purkinje fibres in the heart.

Before we describe the human atrial cell model by Courtemanche et al from their 1998 paper[1], we briefly describe some of the models that were developed after 1962.

2.1.1 The Hodgkin-Huxley 1952 system of equations

The Hodgkin-Huxley system of equations is:

$$\frac{\mathrm{d}V}{\mathrm{d}t} = \frac{I - \overline{g}_K n^4 (V - V_K) - \overline{g}_{Na} m^3 h (V - V_{Na}) - \overline{g}_l (V - V_l)}{C_M}, \quad (2.1)$$

where,

$$\begin{aligned}
\frac{\mathrm{d}n}{\mathrm{d}t} &= \alpha_n(1-n) - \beta_n n = \frac{(\overline{n}-n)}{\tau_n}, \\
\frac{\mathrm{d}m}{\mathrm{d}t} &= \alpha_m(1-m) - \beta_m m = \frac{(\overline{m}-m)}{\tau_m}, \\
\frac{\mathrm{d}h}{\mathrm{d}t} &= \alpha_h(1-h) - \beta_h h = \frac{(\overline{h}-h)}{\tau_h},
\end{aligned}$$

and

$$\begin{aligned}
\alpha_n = \frac{0.01(V+10)}{e^{\frac{V+10}{10}}-1}, \qquad & \beta_n = 0.125e^{\frac{V}{80}}, \\
\alpha_m = \frac{0.1(V+25)}{e^{\frac{V+25}{10}}-1}, \qquad & \beta_m = 4e^{\frac{V}{18}}, \\
\alpha_h = 0.07e^{\frac{V}{20}}, \qquad & \beta_h = \frac{1}{e^{\frac{V+30}{10}}+1}, \\
\overline{g}_{Na} = 120, \qquad & V_{Na} = -115, \\
\overline{g}_K = 36, \qquad & V_K = 12, \\
\overline{g}_l = 0.3, \qquad & V_l = -10.613, \\
C_M = 1.0. & \qquad
\end{aligned}$$

Variable V is the displacement of the membrane potential from its resting value in mV, and n, m and h are dimensionless gating variables which can vary between $[0, 1]$.

The α's and β's are the results of experiments and they are the gates' opening and closing rates that are functions of voltage, not time, and are in ms^{-1}. Parameters $\overline{g}_{Na}$, $\overline{g}_K$ and $\overline{g}_l$ are all constants in $\mathrm{mmho/cm}^2$. Parameters V_{Na}, V_K and V_l are the reversal potentials in mV, and they can be measured directly as displacements from the resting potential. Functions $\overline{m}$, $\overline{n}$ and $\overline{h}$ are the gates' instant equilibrium values, i.e. quasi-stationary values, which are dimensionless, and the τ's are the gates' dynamics time scales in ms.

In equation (2.1) $C_M \frac{\mathrm{d}V}{\mathrm{d}t}$ gives the capacity current, $\overline{g}_K n^4(V - V_K)$ gives the current carried by K ions, $\overline{g}_{Na} m^3 h(V - V_{Na})$ gives the current carried by Na ions and $\overline{g}_l(V - V_l)$ gives the 'leakage current'. The currents are for $1\mathrm{cm}^2$ of membrane.

Membrane current

The current carried by any ion depends on the magnitude of its electrochemical potential gradient, the work done in bringing one mole of an ion from a standard state (infinitely separated) to a specified concentration and electrical potential, and on how easy it is for the ions to cross the cell membrane, i.e. membrane conductivity for that ion.

The total membrane current is divided into a capacity current, $C_M \frac{\mathrm{d}V}{\mathrm{d}t}$, and an ionic current, I_i. This leads to equation:

$$\frac{\mathrm{d}V}{\mathrm{d}t} = \frac{(I - I_i)}{C_M},$$

where I is the total membrane current density, inward current positive, in $\mu\mathrm{A/cm}^2$, I_i is the ionic current density, inward current positive, in $\mu\mathrm{A/cm}^2$, V is the displacement of the membrane potential from the resting value, depolarization negative, C_M is the membrane capacity per unit area which is assumed constant in $\mu\mathrm{F/cm}^2$ and t is time in ms.

I is the current we measure at the end after we've put the ion currents into the membrane. We can split the ionic current I_i into components carried by sodium ions I_{Na}, potassium ions I_K, and other ions I_l which are mainly made up of chloride. So we have:

$$I_i = I_{Na} + I_K + I_l.$$

The independent ionic currents are:

$$\begin{aligned} I_{Na} &= g_{Na}(E - E_{Na}), \\ I_K &= g_K(E - E_K), \\ I_l &= \overline{g}_l(E - E_l), \end{aligned}$$

where g_{Na}, g_K and $\overline{g}_l$ are ionic conductance's and g_{Na} and g_K are functions of time and membrane potential and $\overline{g}_l$ may be taken as a constant. Parameters E_{Na} and E_K are the equilibrium potentials for the sodium and potassium ions and may be taken as a constant, E_l is the potential at which the 'leakage current' due to chloride and other ions are zero, and may be taken as a constant and E is the membrane potential.

There are two reasons why we say the ionic currents are independent. These are because:

1. the currents are carried by different ions, in our case sodium, potassium, and a 'leakage current', and

2. the current is carried through different channels in the membrane. What we mean by channels is that a protein molecule sits on the membrane and makes a hole that is of a particular shape, so only a certain ion can get through. So no other ions can get through this hole and they have to find another hole that they can fit through. Therefore the three types of ions enter the membrane through different types of channels.

Functions g_{Na}, g_K and $\overline{g}_l$ represents the sum of the overall conductance of the channels for the sodium ion, potassium ion, and other ions respectively.

Therefore from the relation $V{=}E - E_r$, the ionic current equations become:

$$\begin{aligned} I_{Na} &= g_{Na}(V - V_{Na}), \\ I_K &= g_K(V - V_K), \\ I_l &= \overline{g}_l(V - V_l). \end{aligned}$$

The relation $V{=}E - E_r$, where E_r is the resting potential, relates to Chapters 3, 4 and 5 and Section 2.5 later on.

The potassium conductance

We assume that:

$$g_K = \overline{g}_K n^4, \tag{2.2}$$

$$\frac{\mathrm{d}n}{\mathrm{d}t} = \alpha_n(1-n) - \beta_n n = \frac{(\overline{n} - n)}{\tau_n}, \tag{2.3}$$

are used to describe the potassium conductance.

We say that we have four subunits n in the membrane and these constitute the channels. To open a channel through the membrane to let the ions in we must have all four subunits open, otherwise we say that the channel is closed. If we do not have all the subunits open then the ions cannot flow through the membrane. Variable n is the probability that a subunit is open. Assuming that

these events are independent, then the probability for all subunits to be open is n^4. Functions α and β depend on V. The "Voltage-clamp" is the experimental technique used by Hodgkin and Huxley to keep V constant. The channels can either be open or closed depending on the voltage and rate of transfer of α's and β's. In equation (2.3) n represents the proportion of open subunits and $(1-n)$ represents the proportion of closed subunits. Also α_n determines the rate of transfer from the closed subunits to the open subunits and vice versa for β_n.

Functions τ_n and $\overline{n}$ are described by the following equations:

$$\tau_n = \frac{1}{\alpha_n + \beta_n}, \qquad \overline{n} = \frac{\alpha_n}{\alpha_n + \beta_n}.$$

The sodium conductance

Equations,

$$g_{Na} = m^3 h \overline{g}_{Na}, \tag{2.4}$$

$$\frac{\mathrm{d}m}{\mathrm{d}t} = \alpha_m(1-m) - \beta_m m = \frac{(\overline{m} - m)}{\tau_m}, \tag{2.5}$$

$$\frac{\mathrm{d}h}{\mathrm{d}t} = \alpha_h(1-h) - \beta_h h = \frac{(\overline{h} - h)}{\tau_h}, \tag{2.6}$$

are used to describe the sodium conductance.

Here the channel consists of four subunits, where three are of one kind of subunit m and one is of another kind of subunit h. Variables m and h represents the proportion of open subunits and $(1-m)$ and $(1-h)$ represents the proportion of closed subunits. Therefore m^3h is the probability for all subunits to be open. Functions α_m or β_h and β_m or α_h represent the transfer rate constants in the two directions.

Functions $\tau_m, \overline{m}, \tau_h$ and $\overline{h}$ are described by the following equations:

$$\overline{m} = \frac{\alpha_m}{\alpha_m + \beta_m}, \qquad \overline{h} = \frac{\alpha_h}{\alpha_h + \beta_h},$$
$$\tau_m = \frac{1}{\alpha_m + \beta_m}, \qquad \tau_h = \frac{1}{\alpha_h + \beta_h}.$$

Action potential solutions

The expressions for the α's and β's are appropriate to a temperature of 6.3°c, for other temperatures they must be scaled with a Q_{10} of 3.

If I=0:

$$\begin{aligned}
\frac{\mathrm{d}V}{\mathrm{d}t} &= -\frac{1}{C_M}(\overline{g}_K n^4(V-V_K)+\overline{g}_{Na}m^3h(V-V_{Na})+\overline{g}_l(V-V_l)), \qquad (2.7)\\
\frac{\mathrm{d}n}{\mathrm{d}t} &= \alpha_n(1-n)-\beta_n n=\frac{(\overline{n}-n)}{\tau_n},\\
\frac{\mathrm{d}m}{\mathrm{d}t} &= \alpha_m(1-m)-\beta_m m=\frac{(\overline{m}-m)}{\tau_m},\\
\frac{\mathrm{d}h}{\mathrm{d}t} &= \alpha_h(1-h)-\beta_h h=\frac{(\overline{h}-h)}{\tau_h}.
\end{aligned}$$

These four equations are used to draw the graphs in Figs. 2.1 and 2.2. Parameter V_l is the exact value chosen to make the total ionic current zero at the resting potential, $V=0$.

The equilibrium values are for $\frac{\mathrm{d}n}{\mathrm{d}t}$=$\frac{\mathrm{d}m}{\mathrm{d}t}$=$\frac{\mathrm{d}h}{\mathrm{d}t}$=0. So the values are:

$$n_0=0.3177, \qquad m_0=0.0530, \qquad h_0=0.5961,$$

to four decimal places.

The α's and β's were calculated for a temperature of 6.3°C. In our diagrams the temperatures are different so we use the equation:

$$\phi=3^{(T^o-6.3)/10}.$$

We can either multiply the α's and β's by ϕ or multiply C_m by ϕ to correct the temperature difference.

We consider the temperature T^o in this system, because in Chapter 3 we study the properties of T^o and the effect it has on the τ's.

In Figs. 2.2 we see that if the initial voltage V_0 is decreased, then the action potentials for V, m, n and h move along the time axis. This means that the latency for the rapid depolarisation of the action potentials decreases as the initial V_0 increases.

Hodgkin and Huxley used the equations to predict the qualitative behaviour of a model nerve under a variety of conditions.

The theory used by Hodgkin and Huxley also predicts that a direct current will not excite if it rises sufficiently slowly.

All that we have illustrated shows excitability especially around the threshold and the equilibrium values.

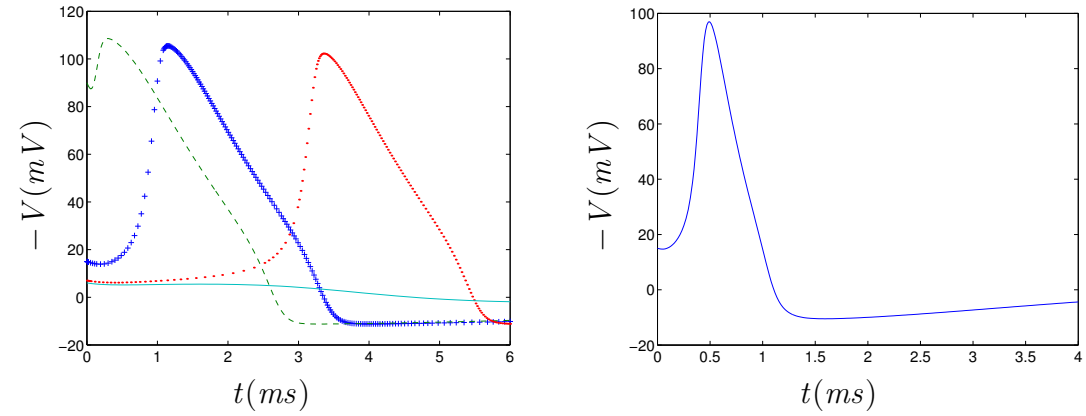

Figure 2.1: Solution of system (2.7) for (a) T^o=6°C and V_0 are 90mV (- -), 15mV (+), 7mV (.) and 6mV (-) and (b) T^o=18.5°C and V_0=15mV.

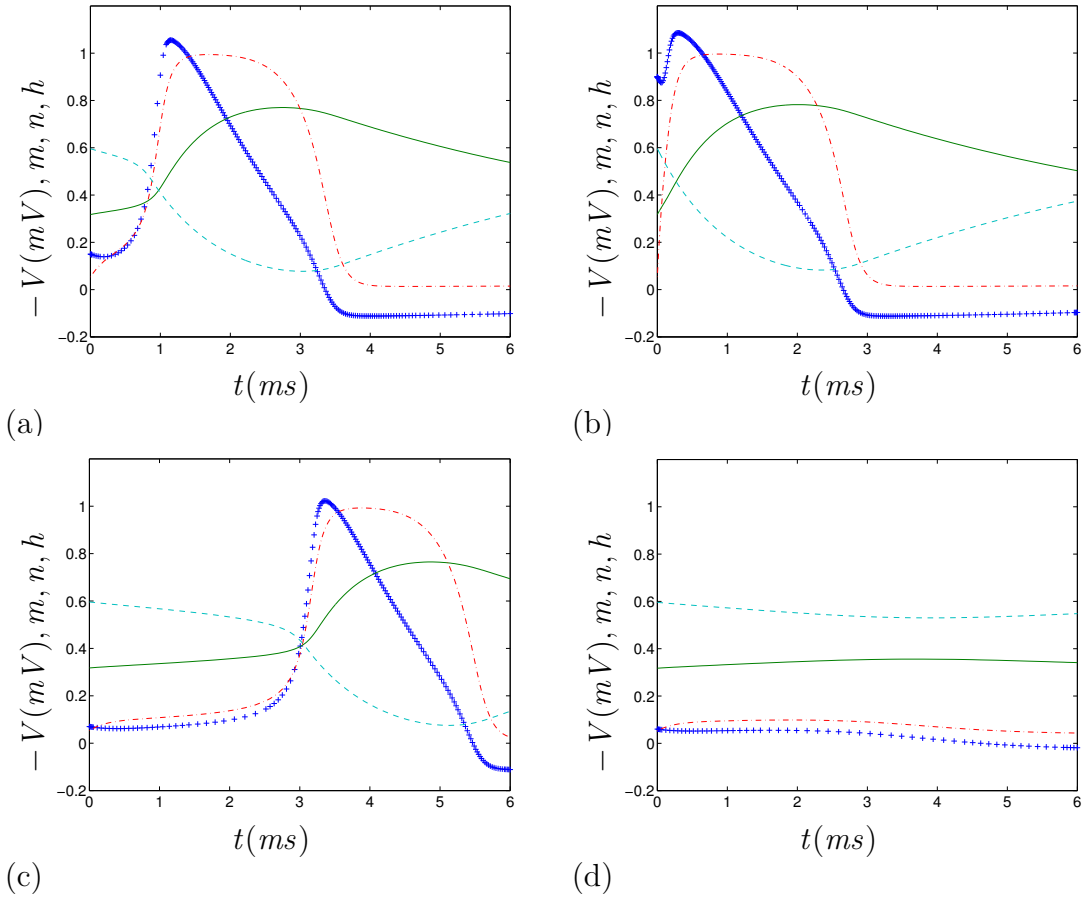

Figure 2.2: Solution of system (2.7) for V (+), m (-.), n (-) and h (- -) for T^o=6°C and (a) V_0=90mV, (b) V_0=15mV, (c) V_0=7mV and (d) V_0=6mV.

We use the computer package Matlab to compute the solutions of the models we study in this thesis. To find the numerical solutions, e.g. action potentials, we use two ODE solvers, ODE45 and ODE15s. For the simple systems we use ODE45 and for the complicated systems we use ODE15s. ODE45 is a non-stiff solver with medium order of accuracy and is most commonly used. ODE15s is a stiff solver with low to medium order of accuracy and is used only if ODE45 is slow. For the solvers, we use all default values of the parameters, which can be found in any Matlab manual[11].

2.1.2 Noble's 1962 system of equations

We now review Noble's 1962 model[3] for Purkinje fibres in the heart as it is a modified version of the Hodgkin-Huxley model. We will describe how Noble obtained his model and what the action potential looks like for different values of g_l.

Membrane current

The total membrane current (2.8) is divided into ionic currents and a capacity current, current flowing into the membrane capacity.

$$\frac{\mathrm{d}E}{\mathrm{d}t} = \frac{I - I_{Na} - I_K - I_l}{C_M}, \tag{2.8}$$

where I is the total membrane current density, I_{Na} and I_K are the ionic currents and I_l is the anion current in $\mu\mathrm{A/cm}^2$, E is the membrane potential in mV, C_M is the membrane capacity in $\mu\mathrm{F/cm}^2$, t is time in ms and $C_M\frac{\mathrm{d}E}{\mathrm{d}t}$ gives the capacity current. The resting potential is a negative quantity.

Here positive currents are taken as outward currents, where Hodgkin and Huxley took them as inward currents. Also, if we compare the equations in Noble's paper[3] to the Hodgkin-Huxley equations in their 1952 paper[2], we need the substitution:

$$E = E_r - V,$$

where E_r is the resting potential for the nerve, which is zero.

The value for C_M is 12, which is twelve times larger than it is for the nerve.

If we have an action potential that is initiated at all points along a fibre simultaneously, then the membrane potential at each instant will be uniform.

The axial current will therefore be zero and in absence of applied currents the total membrane current will also be zero. Hodgkin and Huxley called this type of response a 'membrane' action potential and is given by I=0 in equation (2.8).

As we do not consider the axial current, then we neglect it for the action potentials and so I is taken to be zero. Therefore we have the equation:

$$\frac{\mathrm{d}E}{\mathrm{d}t} = -\frac{(I_{Na} + I_K + I_l)}{C_M}.$$

The individual ionic currents are:

$$I_{Na} = g_{Na}(E - E_{Na}), \tag{2.9}$$

$$I_K = g_K(E - E_K), \tag{2.10}$$

$$I_l = g_l(E - E_l), \tag{2.11}$$

where g_{Na} is the sodium conductance, g_K is the potassium conductance, and g_l is the anion conductance and all are in mmho/cm^2, E_{Na}, E_K and E_l are the equilibrium potentials in mV.

The potassium current

Modifications are made to the potassium equations; these describe the dependence of the potassium current on potential and time, to take into account the behaviour during depolarization.

It was found that depolarization decreased the membrane conductance, which is different to what happened to the nerve. In the nerve the depolarization causes a rapid increase in sodium conductance and a slower, but maintained increase in potassium conductance.

It can be assumed that all the current measured in sodium-deficient solutions is carried by potassium ions and also that the potassium ions may move through two types of channels in the membrane. In the Hodgkin-Huxley system the potassium ions could only move through one channel of the membrane. In one channel the potassium conductance g_{K_1} is assumed to be an instantaneous function of the membrane potential and decreases if the membrane is depolarized. In the other channel the conductance g_{K_2} slowly rises if the membrane is depolarized.

The following equation is used to describe g_{K_1}:

$$g_{K_1} = 1.2e^{\frac{(-E-90)}{50}} + 0.015e^{\frac{(E+90)}{60}}.$$

For g_{K_2} we use the Hodgkin-Huxley potassium current equations:

$$\begin{aligned} g_{K_2} &= \overline{g}_{K_2} n^4, \\ \frac{\mathrm{d}n}{\mathrm{d}t} &= \alpha_n(1-n) - \beta_n n. \end{aligned}$$

Two modifications are made to these equations. The first modification is to make $\overline{g}_{K_2}$ smaller than in the nerve, so that the increase in g_{K_2} produced by depolarization should not affect the decrease in g_{K_1}. The second modification is to divide α_n and β_n by 100 in order to take account of the much slower onset of this effect in Purkinje fibres.

So the potassium equations become:

$$\begin{aligned} g_{K_2} &= 1.2n^4, \\ \frac{\mathrm{d}n}{\mathrm{d}t} &= \alpha_n(1-n) - \beta_n n, \\ \alpha_n &= \frac{0.0001(-E-50)}{e^{\frac{(-E-50)}{10}} - 1}, \\ \beta_n &= 0.002e^{\frac{(-E-90)}{80}}. \end{aligned} \tag{2.12}$$

Parameter $\overline{g}_{K_2}$=1.2 is a constant in mmho/cm^2, α_n and β_n are the gates opening and closing rates that are functions of voltage, not time, in ms^{-1} and n is a dimensionless gating variable between $[0, 1]$.

The absolute values of the conductance's have been adjusted to give a resting conductance of about 1mmho/cm^2. For E_K=−100mV the total potassium current is:

$$I_K = (g_{K_1} + g_{K_2})(E + 100).$$

Function $\overline{n}$ is described by the following equation:

$$\overline{n} = \frac{\alpha_n}{\alpha_n + \beta_n}.$$

The sodium current

The sodium equations are kept similar to the Hodgkin-Huxley ones. The solution to these equations closely resembles the Purkinje fibre action and pacemaker potentials.

The sodium equations are:

$$\begin{aligned} g_{Na} &= m^3 h \overline{g}_{Na} + 0.14, \\ \frac{\mathrm{d}m}{\mathrm{d}t} &= \alpha_m(1-m) - \beta_m m, \\ \frac{\mathrm{d}h}{\mathrm{d}t} &= \alpha_h(1-h) - \beta_h h, \end{aligned} \tag{2.13}$$

where $\overline{g}_{Na}$ is a constant in mmho/cm^2, α_m, α_h, β_m and β_h are functions of E in ms^{-1}, and m and h are dimensionless gating variables between $[0, 1]$.

The only modification made here was that the functions α_h and β_h should be shifted along the voltage axis. Therefore the equations for α_h and β_h were obtained by adjusting the constants determining the position of the curve until the potential at which $\overline{h}$=0.5 became about -7.1mV.

$$\overline{h} = \frac{\alpha_h}{\alpha_h + \beta_h}.$$

Therefore the equations for α_h and β_h are:

$$\begin{aligned} \alpha_h &= 0.17 e^{\frac{(-E-90)}{20}}, \\ \beta_h &= (e^{\frac{(-E-42)}{10}} + 1)^{-1}. \end{aligned}$$

To obtain the equations for the m variable it was observed that there is a close similarity between the processes determining h in the Purkinje fibre and the nerve fibre. Therefore it was assumed that the processes determining m are also similar. The following method was used to find suitable values for the constants in the m equations.

The action potential was used to help find the m equations. Different equations of α_m and β_m are used to see if it is possible to obtain the action potential similar to that of the Hodgkin-Huxley action potential for these equations. It was found that this worked well and a solution was obtained that resembled the Purkinje fibre action potential, but the equations for m which would also allow pacemaker activity to occur are still needed to be found.

The equations obtained are:

$$\alpha_m = \frac{0.1(-E-48)}{e^{\frac{(-E-48)}{15}}-1}, \tag{2.14}$$

$$\beta_m = \frac{0.12(E+8)}{e^{\frac{(E+8)}{5}}-1}. \tag{2.15}$$

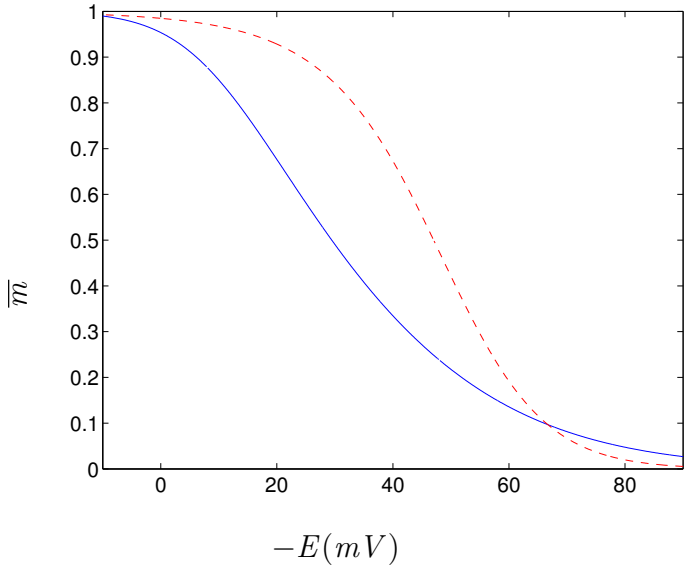

Figure 2.3: Graph of $\overline{m}$ for the Hodgkin-Huxley system (- -) and Noble's system (-).

Figure 2.3 illustrates how equations (2.14) and (2.15) are obtained. In this figure m is plotted against E. It was assumed that 0.14mmho/cm^2 is independent of E and t. Assuming this makes it easier to obtain the functions for α_m and β_m, which allow pacemaker activity to occur. This does not mean that in some channels g_{Na} is independent of E and t in cardiac muscle.

The curve $\overline{m}$ (-) in Fig. 2.3 is given by equations (2.14), (2.15) and (2.16).

$$\overline{m} = \frac{\alpha_m}{\alpha_m + \beta_m}. \tag{2.16}$$

The curve (- -) is for the Hodgkin-Huxley equations, but α_m and β_m have been shifted along the voltage axis by the same amount that the h equations were shifted by. So $\overline{m}$ is drawn using equation (2.16) and the following two equations:

$$\alpha_m = \frac{0.1(-E-47)}{e^{\frac{(-E-47)}{10}}-1},$$

$$\beta_m = 4e^{\frac{(-E-72)}{18}}.$$

In Fig. 2.3, the main difference between Noble's $\overline{m}$ and Hodgkin-Huxley's $\overline{m}$ is that $\overline{m}$ and β_m vary less steeply with E. Therefore the values $\overline{m}$=0.5 and $\overline{m}$=0.1 are separated by about 35mV in Noble's equations and by about 20mV in Hodgkin-Huxley's equations.

Therefore we obtain the equation:

$$I_{Na} = (400m^3h + 0.14)(E - 40),$$

by using the values $\overline{g}_{Na}$=400mmho/cm^2 and E_{Na}=40mV and putting them in equations (2.9) and (2.13). Here the value 0.14 is a small component of g_{Na} which is independent of voltage and time.

Following the large transient increase on g_{Na}, E is suddenly changed from -90 to -20mV and there appears a small maintained increase which persists throughout the period of the depolarization. Therefore the steady state Na current increases, even though there is a decrease in the Na electrochemical potential gradient. Because of this property the equations can be extended to describe long-lasting action potentials without any serious modification to the sodium current equations.

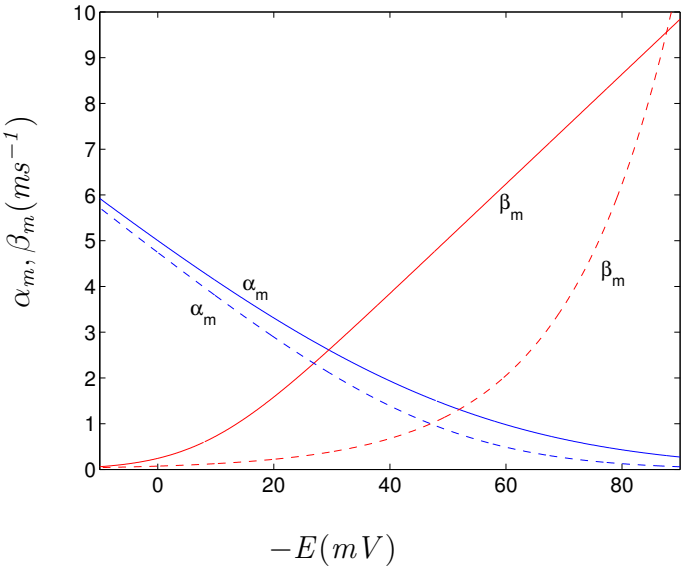

Figure 2.4: Graph of α_m's and β_m's for the Hodgkin-Huxley system (- -) and Noble's system (-).

In Fig. 2.4 we have the α_m's and β_m's for both Noble's system and Hodgkin-Huxley's system. We compare the two systems and see that α_m for Noble's system has the same shape as α_m for the Hodgkin-Huxley system, for the values

of E, but they are separated by a small distance on the E axis. For the β_m's, we see that β_m for Noble's system changes less rapidly with E than β_m for Hodgkin-Huxley's system.

Action potential solutions

If I=0, we have the following system of equations:

$$\begin{aligned}
\frac{\mathrm{d}E}{\mathrm{d}t} &= -\frac{1}{C_M}((m^3 h\overline{g}_{Na} + 0.14)(E - E_{Na}) + g_l(E - E_l) \\
&\quad +(g_{K_1} + g_{K_2})(E - E_K)), \\
\frac{\mathrm{d}m}{\mathrm{d}t} &= \alpha_m(1-m) - \beta_m m = \frac{(\overline{m} - m)}{\tau_m}, \\
\frac{\mathrm{d}h}{\mathrm{d}t} &= \alpha_h(1-h) - \beta_h h = \frac{(\overline{h} - h)}{\tau_h}, \\
\frac{\mathrm{d}n}{\mathrm{d}t} &= \alpha_n(1-n) - \beta_n n = \frac{(\overline{n} - n)}{\tau_n},
\end{aligned} \tag{2.17}$$

where,

$$\begin{aligned}
\alpha_m &= \frac{0.1(-E-48)}{e^{\frac{(-E-48)}{15}} - 1}, & \beta_m &= \frac{0.12(E+8)}{e^{\frac{(E+8)}{5}} - 1}, \\
\alpha_h &= 0.17e^{\frac{(-E-90)}{20}}, & \beta_h &= (e^{\frac{(-E-42)}{10}} + 1)^{-1}, \\
\alpha_n &= \frac{0.0001(-E-50)}{e^{\frac{(-E-50)}{10}} - 1}, & \beta_n &= 0.002e^{\frac{(-E-90)}{80}}, \\
\overline{g}_{Na} &= 400, & E_{Na} &= 40, \\
g_{K_1} &= 1.2e^{\frac{(-E-90)}{50}} + 0.015e^{\frac{(E+90)}{60}}, & g_{K_2} &= 1.2n^4, \\
E_K &= -100, & C_M &= 12, \\
g_l &= 0, & E_l &= -60.
\end{aligned}$$

In this system we have an unstable equilibrium point, as the system is an oscillatory system. The solutions of the pacemaker potentials for this system closely resemble the potential changes in Purkinje fibres.

Figure 2.5 are the pacemaker potentials for the above system (2.17) for different values of g_l. It is drawn for the initial point, (E_0, m_0, n_0, h_0)=$(-90, 0.9537, 0.8858, 0.0019)$. The solution of this system is computed for two cycles. The pacemaker potential shows the characteristic spike, which is about 600ms and 1400ms in Fig. 2.5(a). This is followed by a plateau lasting about 400ms which is terminated by a faster phase of

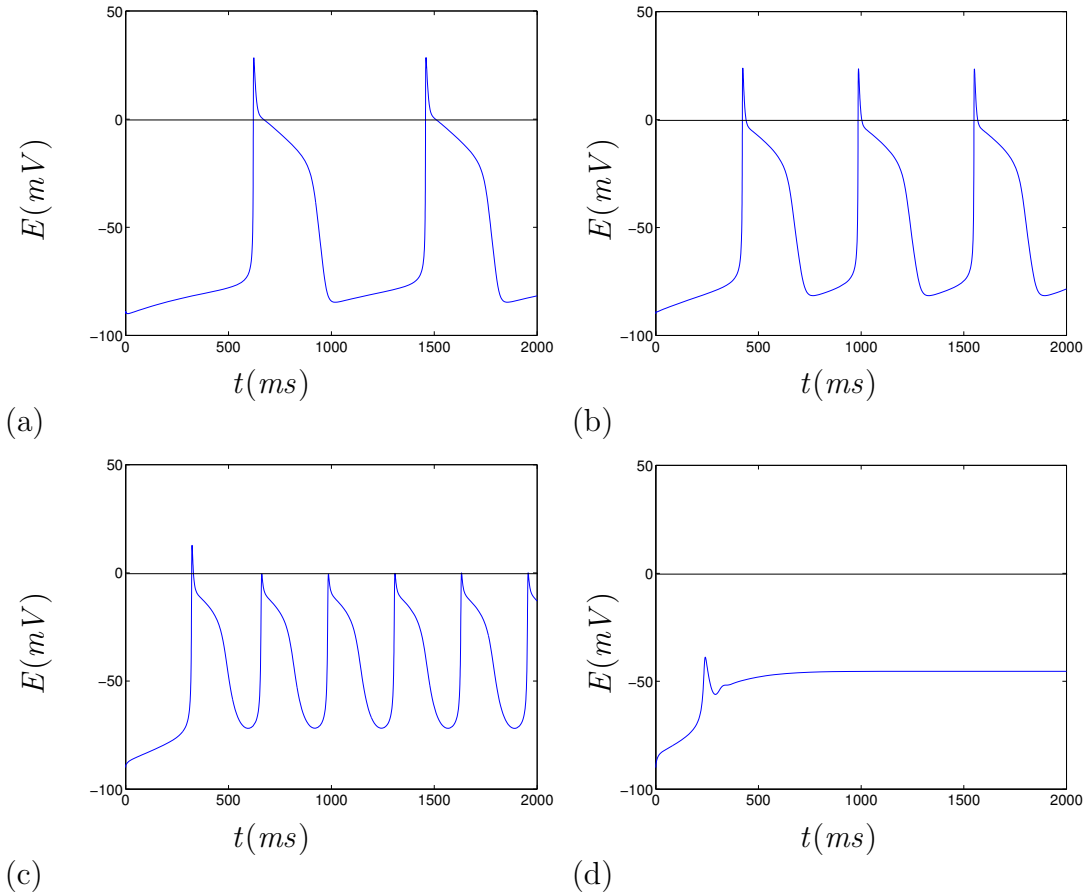

Figure 2.5: Solution of system (2.17) for the initial point (E_0, m_0, n_0, h_0)=$(-90, 0.9537, 0.8858, 0.0019)$ and (a) g_l=0, (b) g_l=0.075, (c) g_l=0.18, and (d) g_l=0.4.

repolarization. The membrane then slowly depolarizes again, which is the pacemaker potential, until the threshold is reached and another potential is initiated.

At the beginning of each pacemaker potential we have a spike which gets smaller in height as g_l increases and this transient means that the programme used to draw this reproduces the heart model. Figure 2.5(b) resembles the effect of chloride ions on the Purkinje fibres. Figure 2.5(c) resembles the effect of prolonged exposure to Nitrate ions on the Purkinje fibres and Fig. 2.5(d) resembles the effect if chloride ions are replaced by Iodine ions in the Purkinje fibres.

If we compare Fig. 2.5 to the Hodgkin-Huxley action potentials of the nerve, we see that where the Hodgkin-Huxley action potentials are more triangular in shape, the pacemaker potentials for Noble's heart is rectangular in shape, except for the spike at the top.

2.1.3 Development of cardiac excitation models after 1962

Noble wrote a paper in 2002[12] outlining the defects in the Hodgkin-Huxley model, which could only be seen years after Hodgkin and Huxley introduced their 1952 model. This was because research by other authors[13, 14, 15], found that calcium currents existed in the membrane.

Therefore it was found that the main defect in Hodgkin-Huxley's model was that it only included one voltage-gated inward current, I_{Na}, because calcium currents were not discovered.

So the sodium current acted as both sodium and calcium channels in the plateau region of the action potential, but to make the model work in this way, Hodgkin-Huxley had to extend the voltage range of the sodium "window" current. To do this they had to reduce the voltage dependence of the sodium activation processes m.

Noble says that from this, two predictions were found:

1. either sodium channels in the heart are quantitatively different from those in the nerve, or

2. other inward current-carrying channels must exist.

As we know both predictions are correct. The first prediction is confirmed by Noble's 1962 model and the second has been confirmed by numerous authors over the world.

The cardiac calcium current was discovered by Reuter[15] in 1967. Then by the 70's Noble's 1962 model was replaced by more complicated models containing calcium currents. These models are briefly described in this section with other models that concern heart and nerve analysis.

In 1975 McAllister, Noble and Tsien[14] modified Noble's 1962 Purkinje fibre model by including calcium currents. They found that there were two separate voltage ranges in which very slow conductance changes could be observed, and this introduced multiple potassium currents. Their model reconstructed a much wider range of experimental results and it did so with good accuracy in some cases.

In 1980 Ebihara and Johnson wrote a paper[16] on the fast sodium current in cardiac muscle. They had obtained new experimental kinetic data and wanted to incorporate this into the Hodgkin-Huxley model. To do this Ebihara and Johnson had to modify the α and β parameters by using curve fitting, so that the parameter's described their new kinetic data. They then substituted the new sodium current into the Hodgkin-Huxley model, and so they could compare their kinetics with other studies.

DiFrancesco and Noble wrote a paper in 1985[17] about extensive developments since McAllister et al's paper. DiFrancesco and Noble replaced the pacemaker potassium current I_{K2} in McAllister et al's model with a new hyperpolarizing-activated sodium-potassium current I_f, which was the nearest equivalent to I_{K2} in McAllister et al's model. DiFrancesco and Noble obtained an accurate mapping between the I_{K2} model and the new I_f model that could be constructed demonstrating how both models related to the same experimental results and to each other.

Hilgemann and Noble produced a paper in 1987[18] on the rabbit atrium and they studied the interactions of electrogenic sodium-calcium exchange, calcium channel and sarcoplasmic reticulum in the mammalian heart by studying simulations of extracellular calcium transients measured with a drug in rabbit atrium. They do this so that they can reconstruct the action potentials, intercellular calcium transients and extracellular calcium transients. This also provided the basis for modelling the ventricular cells in various species with short ventricular action potentials, e.g. rat and mouse. This model also addressed a number of important questions concerning calcium balance.

Drouhard and Roberge produced a paper in 1987[19] revising the sodium

current activation and inactivation gates in Beeler-Reuter's 1977 model[20] for ventricular myocardial cells. They revised this current because recent technical advances have made it possible to achieve more accurate measurements of the sodium current compared to earlier models. They used curve fitting to determine the α and β parameters and compared the steady-state gating variables with selected experimental points from the new data. They fine-tuned the steady state gating variables and its associated time constant by trial and error to allow satisfactory simultaneous fit. They then substituted the new sodium current into the original Beeler-Reuter model, and drew the action potential upstroke, as this is where I_{Na} is active, which they found is comparable to the experimental observations, but the upstroke is much faster than in the original Beeler-Reuter model. The peak depolarization is close to the sodium equilibrium potential, due to large changes in the sodium conductance.

Earm and Noble hypothesised in 1990[21] a non-linear relation between calcium current and calcium release and they investigated this using a single-cell version of the rabbit atrium model that was developed by Hilgemann and Noble. Hilgemann and Noble were more concerned with calcium release on the action potential. To measure the calcium ions in the tissue, they illuminated them using a laser light that was sensitive to calcium ions, and the signal measures how the calcium ions changed. They used this on a tissue and assumed that the amount the calcium changed in one cell happens in all the cells. So the model they created is a single cell model, based on multiple cells by assuming that all the cells behave in the same way. From Hilgemann and Noble, Earm and Noble just rescaled the qualities from multiple cells to a single cell and changed the unit of measurement.

Between the years of 1991 and 1994 Luo and Rudy[22, 23, 24] developed a model to study mammalian ventricular cells in several different species. They wanted to produce a system of equations that would successfully describe the electrophysiological responses in ventricular cells. They started in 1991 with a simple system of four currents, I_{Na}, I_K, I_{K1} and I_{Kp}, which they used to study single cell responses. Their studies for this system were based on reproducing the interaction between depolarization and repolarization processes for I_{Na}, I_K and I_{K1}.

In 1994 they took their 1991 model and introduced more sodium, potassium and calcium currents to it. Therefore the new model was able to correctly repro-

duce the action potential for the ventricular cell and the qualitative properties of the cell. A working model was then found that could be used to study the ventricular cell, and this has been the basis for many other modern day models.

In 1995 Zeng et al[25] reformulated the I_{Kr} and I_{Ks} currents, so that they could update Luo-Rudy's 1994 models. Since then Luo-Rudy's 1994 models have been developed by Rudy and various other authors[26, 27], so that it can still be used to describe ventricular cells using modern day results.

Nygren et al in 1998[28] constructed a model of the human atrial cell and we looked at this to compare the methods and results with Courtemanche et al's model[1], which we describe briefly in Section 2.1.4 and study in detail in Chapter 6. Nygren also wrote a paper in 2001[29] comparing both models and found that even though both models ([28] and [1]) are based on very similar data, they can result in contradictory results where some are of fundamental importance to human atrial cell electrophysiology and pharmacology. They analysed the reasons for these discrepancies. One difference in the two models is the action potential shape due to the sizes of the underlying ionic currents, but the main difference was regarding the role of the rapidly activating, sustained outward K^+ current, I_{Kur}. Also the currents in both models were written differently.

In 1998 Noble et al[30] constructed the guinea-pig ventricular cell model and how it has been extended to include accumulation and depletion of calcium in a diadic space between the sarcolemma and the sarcoplasmic reticulum, where, according to contemporary understanding the majority of calcium-induced calcium release is triggered. Also the delayed potassium current equations have been developed to include rapid I_{Kr} and slow I_{Ks} components of the delayed rectifier current. Their new model was tested against experimental data on action potential clamp and was found to reliably reproduce experimental observations.

Nerve excitation models have also been developed over the years, e.g. in 1998 Clay[31] re-examined the electrical properties of the Hodgkin-Huxley model. Clay said that the Hodgkin-Huxley model did not provide a good description of many electrophysiological properties of the axon. Clay modified the Hodgkin-Huxley model so that it did give a good description of many electrophysiological properties, and display modern findings.

In 2001 Noble and Rudy[32] reviewed the main models of cardiac ventricular action potentials and they focused on the interaction between simulation and experimental work. Their aim was to demonstrate that as much was learnt from

the way in which models failed as from their successes.

From all these papers we can summarise that the main mathematical features are similar and that Courtemanche et al's model[1] is a typical representative from this family; this is described in the next section.

In Noble's books and reviews[33], Noble considers in detail the underlying physiology of the biological systems of equations, but in our research we only concentrate on the mathematical properties of the systems.

2.1.4 Courtemanche et al's 1998 system of equations

Courtemanche et al developed a more accurate action potential model that models the human atrium based on ionic current data obtained directly in human atrial cells. They built their model mostly on the work of Luo-Rudy[23].

We reproduce the action potential of this model using the computer program Matlab and also in reproducing the other graphs that are in Courtemanche et al's paper[1].

For our study we choose Courtemanche et al's model because it is a system of ordinary differential equations only, unlike some other models, e.g. the Rudy et al family, and also because the original error free code of the model was available thanks to M. Courtemanche.

The action potential is going to have a definite spike and dome shape instead of a triangular shape like the Hodgkin-Huxley action potential and a rectangular shape like Noble's action potential.

We make a note here that the current equations I involved in the equation for voltage $\frac{\mathrm{d}E}{\mathrm{d}t}$ in this section are the true currents which are measured in pA. The calcium storage and release currents are the same equations that are in their paper[1], and are measured in pA/pF. The currents in Courtemanche et al's 1998 paper[1] are the normalised currents, measured in pA/pF. The true currents and the normalised currents differ by a factor of C_M.

Therefore this makes the currents and the voltage equation the same dimensions as the Hodgkin-Huxley and Noble equations, but we cannot compare the absolute values between Courtemanche et al's system and Hodgkin-Huxley's system as Hodgkin-Huxley uses per unit squared dimensions and Courtemanche et al uses the total dimensions.

Glossary of terms

Table 2.1 contains descriptions of all the terms that are used in this system and if they are constants then their values as well.

Table 2.1: Terms and definitions for Courtemanche et al's model

Variable	Definition	Value/Units
E	Transmembrane Potential	mV
Nai	Intracellular Concentration Of Ion Na^+	mmol
Ki	Intracellular Concentration Of Ion K^+	mmol
Cai	Intracellular Concentration Of Ion Ca^{2+}	mmol
$Carel$	Ca^{2+} Concentration In The Release Compartment	mmol
$Caup$	Ca^{2+} Concentration In The Uptake Compartment	mmol
m	Activation Gating Variable For I_{Na^+}	dimensionless
h	Fast Inactivation Gating Variable For I_{Na^+}	dimensionless
j	Slow Inactivation Gating Variable For I_{Na^+}	dimensionless
o_a	Activation Gating Variable For I_{to}	dimensionless
o_i	Inactivation Gating Variable For I_{to}	dimensionless
u_a	Activation Gating Variable For I_{Kur}	dimensionless
u_i	Inactivation Gating Variable For I_{Kur}	dimensionless
x_r	Activation Gating Variable For I_{Kr}	dimensionless
x_s	Activation Gating Variable For I_{Ks}	dimensionless
d	Activation Gating Variable For $I_{Ca,L}$	dimensionless
f	Voltage-Dependent Inactivation Gating Variable For $I_{Ca,L}$	dimensionless
f_{Ca}	Ca^{2+}-Dependent Inactivation Gating Variable For $I_{Ca,L}$	dimensionless
u	Activation Gating Variable For I_{rel}	dimensionless
v	Ca^{2+} Flux-Dependent Inactivation Gating Variable For I_{rel}	dimensionless
w	Voltage-Dependent Inactivation Gating Variable For I_{rel}	dimensionless

continued on next page

continued from previous page

Variable	Definition	Value/Units
t	Time	ms
E_{Na}	Equilibrium Potential For Ion Na^+	mV
E_K	Equilibrium Potential For Ion K^+	mV
E_{Ca}	Equilibrium Potential For Ion Ca^{2+}	mV
I_{ion}	Total Ionic Current	pA
I_{Na}	Fast Inward Na^+ current	pA
α_m	Forward Rate Constant For Gating Variable m	ms^{-1}
β_m	Backward Rate Constant For Gating Variable m	ms^{-1}
τ_m	Time Constant For Gating Variable m	ms
$\overline{m}$	Steady-State Relation For Gating Variable m	dimensionless
α_h	Forward Rate Constant For Gating Variable h	ms^{-1}
β_h	Backward Rate Constant For Gating Variable h	ms^{-1}
τ_h	Time Constant For Gating Variable h	ms
$\overline{h}$	Steady-State Relation For Gating Variable h	dimensionless
α_j	Forward Rate Constant For Gating Variable j	ms^{-1}
β_j	Backward Rate Constant For Gating Variable j	ms^{-1}
τ_j	Time Constant For Gating Variable j	ms
$\overline{j}$	Steady-State Relation For Gating Variable j	dimensionless
I_{K1}	Inward Rectifier K^+ Current	pA
I_{to}	Transient Outward K^+ Current	pA
α_{o_a}	Forward Rate Constant For Gating Variable o_a	ms^{-1}
β_{o_a}	Backward Rate Constant For Gating Variable o_a	ms^{-1}

continued on next page

continued from previous page

Variable	Definition	Value/Units
τ_{o_a}	Time Constant For Gating Variable o_a	ms
$\overline{o_a}$	Steady-State Relation For Gating Variable o_a	dimensionless
α_{o_i}	Forward Rate Constant For Gating Variable o_i	ms^{-1}
β_{o_i}	Backward Rate Constant For Gating Variable o_i	ms^{-1}
τ_{o_i}	Time Constant For Gating Variable o_i	ms
$\overline{o_i}$	Steady-State Relation For Gating Variable o_i	dimensionless
I_{Kur}	Ultrarapid Delayed Rectifier For K^+ Current	pA
g_{Kur}	Maximal I_{Kur} Conductance	nS/pF
α_{u_a}	Forward Rate Constant For Gating Variable u_a	ms^{-1}
β_{u_a}	Backward Rate Constant For Gating Variable u_a	ms^{-1}
τ_{u_a}	Time Constant For Gating Variable u_a	ms
$\overline{u_a}$	Steady-State Relation For Gating Variable u_a	dimensionless
α_{u_i}	Forward Rate Constant For Gating Variable u_i	ms^{-1}
β_{u_i}	Backward Rate Constant For Gating Variable u_i	ms^{-1}
τ_{u_i}	Time Constant For Gating Variable u_i	ms
$\overline{u_i}$	Steady-State Relation For Gating Variable u_i	dimensionless
I_{Kr}	Rapid Delayed Rectifier For K^+ Current	pA
α_{x_r}	Forward Rate Constant For Gating Variable x_r	ms^{-1}
β_{x_r}	Backward Rate Constant For Gating Variable x_r	ms^{-1}

continued on next page

continued from previous page

Variable	Definition	Value/Units
τ_{x_r}	Time Constant For Gating Variable x_r	ms
$\overline{x_r}$	Steady-State Relation For Gating Variable x_r	dimensionless
I_{Ks}	Slow Delayed Rectifier For K^+ Current	pA
α_{x_s}	Forward Rate Constant For Gating Variable x_s	ms^{-1}
β_{x_s}	Backward Rate Constant For Gating Variable x_s	ms^{-1}
τ_{x_s}	Time Constant For Gating Variable x_s	ms
$\overline{x_s}$	Steady-State Relation For Gating Variable x_s	dimensionless
$I_{Ca,L}$	L-Type Inward Ca^{2+}	pA
τ_d	Time Constant For Gating Variable d	ms
$\overline{d}$	Steady-State Relation For Gating Variable d	dimensionless
τ_f	Time Constant For Gating Variable f	ms
$\overline{f}$	Steady-State Relation For Gating Variable f	dimensionless
$\overline{f_{Ca}}$	Steady-State Relation For Gating Variable f_{Ca}	dimensionless
$I_{p,Ca}$	Sarcoplasmic Ca^{2+} Pump Current	pA
I_{NaK}	Na^+-K^+ Pump Current	pA
f_{NaK}	Voltage-Dependence Parameter For I_{NaK}	mV
σ	$[Na^+]_o$-Dependence Parameter For I_{NaK}	mV
I_{NaCa}	Na^+/Ca^{2+} Exchanger Current	pA
$I_{b,Na}$	Background Na^+ Current	pA
$I_{b,Ca}$	Background Ca^{2+} Current	pA
$I_{b,K}$	Background K^+ Current	pA
I_{rel}	Ca^{2+} Release Current From The Junctional Sarcoplasmic Reticulum	pA/pF
$\overline{u}$	Steady-State Relation For Gating Variable u	dimensionless

continued on next page

continued from previous page

Variable	Definition	Value/Units
τ_v	Time Constant For Gating Variable v	ms
$\overline{v}$	Steady-State Relation For Gating Variable v	dimensionless
τ_w	Time Constant For Gating Variable w	ms
$\overline{w}$	Steady-State Relation For Gating Variable w	mV
F_n	Saroplasmic Ca^{2+} Flux Signal For I_{rel}	dimensionless
I_{up}	Ca^{2+} Uptake Current Into The Network Saroplasmic Reticulum	pA/pF
I_{tr}	Ca^{2+} Transfer Current From The Network Saroplasmic Reticulum To The Junctional Saroplasmic Reticulum	pA/pF
$I_{up,leak}$	Ca^{2+} Leak Current From The Network Saroplasmic Reticulum	pA/pF
z	Corresponds To The Charge Of The Ions	dimensionless
Q_{10}	Temperature Adjustment Factor, $k(T^o)$=$k(T_0^o)Q_{10}^{(T^o-T_0^o)/10}$	dimensionless
$CaCmdn$	Ca^{2+}-Bound Calmodulin Concentration	mmol
$CaTrpn$	Ca^{2+}-Bound Troponin Concentration	mmol
$CaCsqn$	Ca^{2+}-Bound Calsequestrin Concentration	mmol
R	Gas Constant	8.3143JK^{-1}mol^{-1}
T^o	Temperature	310K
F	Faraday Constant	96.4867C/mmol
C_M	Membrane Capacitance	100pF
V_{cell}	Cell Volume	20100μm^3
V_i	Intracellular volume	13668μm^3
V_{up}	Saroplasmic Reticulum Uptake Compartment Volume	1109.52μm^3
V_{rel}	Saroplasmic Reticulum Release Compartment Volume	96.48μm^3
I_{st}	Stimulus Current	0 or -2000 pA
Nao	Extracellular Concentration Of Ion Na^+	140mmol

continued on next page

continued from previous page

Variable	Definition	Value/Units
Ko	Extracellular Concentration Of Ion K^+	5.4mmol
Cao	Extracellular Concentration Of Ion Ca^{2+}	1.8mmol
g_{Na}	Maximal I_{Na^+} Conductance	7.8nS/pF
g_{K1}	Maximal I_{K1} Conductance	0.09nS/pF
g_{to}	Maximal I_{to} Conductance	0.1652nS/pF
$K_{Q_{10}}$	Q_{10}-Based Temperature Adjustment Factor For I_{Kur} And I_{to} Kinetics	3
g_{Kr}	Maximal I_{Kr} Conductance	0.0294nS/pF
g_{Ks}	Maximal I_{Ks} Conductance	0.129nS/pF
$g_{Ca,L}$	Maximal $I_{Ca,L}$ Conductance	0.1238nS/pF
$\tau_{f_{Ca}}$	Time Constant For Gating Variable f_{Ca}	2ms
$I_{p,Ca}(max)$	Maximal $I_{p,Ca}$	0.275pA/pF
$I_{NaK}(max)$	Maximal I_{NaK}	0.60pA/pF
$K_{m,Na(i)}$	$[Na^+]_i$ Half-Saturation Constant For I_{NaK}	10mmol
$K_{m,K(o)}$	$[K^+]_o$ Half-Saturation Constant For I_{NaK}	1.5mmol
$I_{NaCa}(max)$	I_{NaCa} Scaling Factor (Maximal I_{NaCa})	1600pA/pF
$K_{m,Na}$	$[Na^+]_o$ Saturation Constant For I_{NaCa}	87.5mmol
$K_{m,Ca}$	$[Ca^{2+}]_o$ Saturation Constant For I_{NaCa}	1.38mmol
K_{sat}	Saturation Factor For I_{NaCa}	0.1mmol
γ	Voltage-Dependence Parameter For I_{NaCa}	0.35mV
$g_{b,Na}$	Maximal $I_{b,Na}$ Conductance	0.000674nS/pF
$g_{b,Ca}$	Maximal $I_{b,Ca}$ Conductance	0.00113nS/pF
$g_{b,K}$	Maximal $I_{b,K}$ Conductance	0nS/pF
K_{rel}	Maximal Ca^{2+} Release Rate For I_{rel}	$30ms^{-1}$
τ_u	Time Constant For Gating Variable u	8ms
K_{up}	$[Ca^{2+}]_i$ Half-Saturation Constant For I_{up}	0.00092mmol
$I_{up(max)}$	Maximal Ca^{2+} Uptake Rate For I_{up}	0.005mmol/ms
$Caup(max)$	Maximal Ca^{2+} Concentration In The Uptake Compartment	$15ms^{-1}$
τ_{tr}	Ca^{2+} Transfer Time Constant	180ms
$[Cmdn]_{max}$	Total Calmodulin Concentration In Myoplasm	0.05mmol

continued on next page

continued from previous page		
Variable	Definition	Value/Units
$[Trpn]_{max}$	Total Troponin Concentration In Myoplasm	0.07mmol
$[Csqn]_{max}$	Total Calsequestrin Concentration In The Junctional Saroplasmic Reticulum	10mmol
$K_{m,Cmdn}$	Ca^{2+} Half-Saturation Constant For Calmodulim	0.00238mmol
$K_{m,Trpn}$	Ca^{2+} Half-Saturation Constant For Troponin	0.0005mmol
$K_{m,Csqn}$	Ca^{2+} Half-Saturation Constant For Calsequestrin	0.8mmol

The mathematical model

The time derivative of the membrane potential E, with the assumption of an equipotential cell, is given by:

$$\frac{\mathrm{d}E}{\mathrm{d}t} = -\frac{(I_{ion} + I_{st})}{C_M}.$$

The total ionic current is given by:

$$\begin{aligned} I_{ion} &= I_{Na} + I_{K1} + I_{to} + I_{Kur} + I_{Kr} + I_{Ks} + I_{Ca,L} + I_{p,Ca} + I_{Na,K} + I_{NaCa} \\ &\quad + I_{b,Na} + I_{b,Ca} + I_{b,K}, \end{aligned}$$

and I_{st} is the stimulus current, which is a function that depends on time. The I_{st} current takes two values depending on time, as for 2ms of time a large I_{st} current enters the cell. So I_{st} can be written as follows:

$$I_{st}(t) = I_{st(max)}\theta(t - 100)\theta(102 - t),$$

where $I_{st(max)}$=−2000pA, and t is measured in ms.

The membrane currents

Here we state the equations for the membrane currents in this system and then we will list the α's, β's, τ's and quasi-stationary values in Tables 2.2 and 2.3.

The fast sodium current is:

$$I_{Na} = C_M g_{Na} m^3 hj(E - E_{Na}),$$

where,

$$E_{Na} = \frac{RT^o}{zF} \log \frac{Nao}{Nai}, \qquad z = 1,$$
$$\overline{y} = \alpha_y \tau_y, \qquad \tau_y = (\alpha_y + \beta_y)^{-1},$$

where y=m, h and n.

The inward rectifier potassium current is:

$$I_{K1} = C_M \frac{g_{K1}(E - E_K)}{1 + e^{0.07(E+80)}},$$

where,

$$E_K = \frac{RT^o}{zF} \log \frac{Ko}{Ki}.$$

The transient outward and ultrarapid rectifier potassium currents are:

$$\begin{aligned} I_{to} &= C_M g_{to} o_a^3 o_i (E - E_K), \\ I_{Kur} &= C_M g_{Kur} u_a^3 u_i (E - E_K), \end{aligned}$$

respectively, where,

$$g_{Kur} = 0.005 + \frac{0.05}{1 + e^{-\frac{(E-15)}{13}}}.$$

We see that both currents share the same structure of gating variables where the activation gating variables are to the power three and the inactivation gating variables are to the power one. I_{to} has fairly rapid inactivation kinetics; I_{Kur} displays only partial slow inactivation.

The delayed rectifier equations are:

$$\begin{aligned} I_{Kr} &= C_M \frac{g_{Kr} x_r (E - E_K)}{1 + e^{\frac{(E+15)}{22.4}}}, \\ I_{Ks} &= C_M g_{Ks} x_s^2 (E - E_K). \end{aligned}$$

We see that both currents have only a single activation gate, although I_{Ks} activation uses a squared activation gate, x_s^2.

The slow inward Ca^{2+} current is:

$$I_{Ca,L} = C_M g_{Ca,L}\, d\, f\, f_{Ca} (E - 65).$$

This includes voltage-dependent activation gate d and inactivation gate f, as well as a Ca^{2+}-dependent inactivation gate f_{Ca}. A fixed intrinsic time dependence, $\tau_{f_{Ca}}$=2ms, is incorporated into the f_{Ca} gate to better reproduce the time course of Ca^{2+}-dependent inactivation of $I_{Ca,L}$.

The sodium-potassium pump equation is:

$$I_{NaK} = C_M I_{NaK(max)} f_{NaK} \left(\frac{1}{1 + (K_{m,Na(i)}/Nai)^{1.5}} \right) \left(\frac{Ko}{Ko + K_{m,K(o)}} \right),$$

where,

$$\begin{aligned} f_{NaK} &= (1 + 0.1245 e^{-0.1(\frac{FE}{RT})} + 0.0365 \sigma e^{-\frac{FE}{RT}})^{-1}, \\ \sigma &= \frac{e^{\frac{Nao}{67.3}} - 1}{7}. \end{aligned}$$

The sodium/calcium exchanger equation is:

$$I_{NaCa} = C_M \frac{I_{NaCa(max)} (e^{\gamma(\frac{EF}{RT^o})} Nai^3 Cao - e^{(\gamma-1)(\frac{EF}{RT^o})} Nao^3 Cai)}{(K^3_{m,Na} + Nao^3)(K_{m,Ca} + Cao)(1 + K_{sat} e^{(\gamma-1)\frac{EF}{RT^o}})}.$$

The background calcium, sodium and potassium currents are:

$$\begin{aligned} I_{b,Ca} &= C_M g_{b,Ca} (E - E_{Ca}), \\ I_{b,Na} &= C_M g_{b,Na} (E - E_{Na}), \\ I_{b,K} &= C_M g_{b,K} (E - E_K), \end{aligned}$$

respectively, where,

$$E_{Ca} = \frac{RT^o}{zF} \log \frac{Cao}{Cai}, \qquad z = 2.$$

Also included in the model is a sarcolemmal Ca^{2+} pump to maintain Cai at physiological levels.

$$I_{p,Ca} = C_M I_{p,Ca(max)} \left(\frac{Cai}{0.0005 + Cai} \right).$$

The saroplasmic reticulum calcium storage and release currents are:

$$\begin{aligned} I_{rel} &= K_{rel} u^2 vw (Carel - Cai), \\ I_{tr} &= \frac{Caup - Carel}{\tau_{tr}}, \\ I_{up} &= \frac{I_{up(max)}}{1 + (K_{up}/Cai)}, \\ I_{up,leak} &= \frac{Caup}{Caup(max)} I_{up(max)}. \end{aligned}$$

Courtemanche et al claims that the voltage-dependent inactivation gate w contributes to the decrease in saroplasmic reticulum release current amplitude at positive potentials, if membrane voltage approaches the $I_{Ca,L}$ reversal potential. The activation gates u and v control the release of Ca^{2+} from the junctional sarcoplasmic reticulum compartment in the cell membrane.

The calcium flux signal for I_{rel} is:

$$F_n = 10^{-12} V_{rel} I_{rel} - \frac{5 * 10^{-13}}{F} \left(\frac{1}{2} I_{Ca,L} - \frac{1}{5} I_{Na,Ca} \right).$$

The formulae for the α's, β's, τ's and quasi-stationary values are in Table's 2.2 and 2.3 below and where the formulae produce a zero denominator then apply continuity. Also θ is the Heaviside function here.

Table 2.2: Gating variables and their values for α and β for Courtemanche et al's model, where A=$-1.2714 * 10^5$, B=V, C=$3.474 * 10^{-5}$ and D=0.04391.

Gate	α	β
m	$\frac{0.32(E+47.13)}{1-e^{-0.1(E+47.13)}}$	$0.08e^{-\frac{E}{11}}$
h	$0.135e^{-\frac{(E+80)}{6.8}}\theta(-E-40)$	$(0.13(1+e^{-\frac{(E+10.66)}{11.1}}))^{-1}\theta(E+40) + (3.56e^{0.079E} + 3.1 * 10^5 e^{0.35E})\theta(-E-40)$
j	$(Ae^{BE} - Ce^{-DE}) * \left(\frac{E+37.78}{1+e^{0.311(E+79.23)}}\right)\theta(-E-40)$	$0.3\left(\frac{e^{-2.535*10^{-7}E}}{1+e^{-0.1(E+32)}}\right)\theta(E+40) + 0.1212\left(\frac{e^{-0.01052E}}{1+e^{-0.1378(E+40.14)}}\right)\theta(-E-40)$

Table 2.3: The other gating variables and their τ's and quasi-stationary values $\overline{y}$ for Courtemanche et al's model.

Gate (y)	τ_y	$\overline{y}$
o_a	$\frac{1}{K_{Q_{10}}}(0.65(e^{-\frac{(E+10)}{8.5}} + e^{-\frac{(E-30)}{59}})^{-1} + 0.65(2.5+e^{\frac{(E+82)}{17}})^{-1})^{-1}$	$(1+e^{-\frac{(E+20.47)}{17.54}})^{-1}$
o_i	$\frac{1}{K_{Q_{10}}}((18.53 + e^{\frac{(E+113.7)}{10.95}})^{-1} + (35.56 + e^{-\frac{(E+1.26)}{7.44}})^{-1})^{-1}$	$(1+e^{\frac{(E+43.1)}{5.3}})^{-1}$
u_a	$\frac{1}{K_{Q_{10}}}(0.65(e^{-\frac{(E+10)}{8.5}} + e^{-\frac{(E-30)}{59}})^{-1} + 0.65(2.5+e^{\frac{(E+82)}{17}})^{-1})^{-1}$	$(1+e^{-\frac{(E+30.3)}{9.6}})^{-1}$
u_i	$\frac{1}{K_{Q_{10}}}(21+e^{-\frac{(E-185)}{28}})^{-1} + e^{\frac{(E-158)}{16}})^{-1}$	$(1+e^{\frac{(E-99.45)}{27.48}})^{-1}$
x_r	$(0.0003\left(\frac{E+14.1}{1-e^{-\frac{(E+14.1)}{5}}}\right) + 7.3898 * 10^{-5}\left(\frac{E-3.3328}{e^{\frac{(E-3.3328)}{5.1237}}-1}\right))^{-1}$	$(1+e^{-\frac{(E+14.1)}{6.5}})^{-1}$

continued on next page

continued from previous page		
Gate (y)	τ_y	$\overline{y}$
x_s	$\frac{1}{2}(4 * 10^{-5}\left(\frac{E-19.9}{1-e^{-\frac{(E-19.9)}{17}}}\right) 3.5 * 10^{-5}\left(\frac{E-19.9}{e^{\frac{(E-19.9)}{9}}-1}\right))^{-1}$	$(1+e^{-\frac{(E-19.9)}{12.7}})^{-1/2}$
d	$\frac{1-e^{-\frac{(E+10)}{6.24}}}{0.035(E+10)(1+e^{-\frac{(E+10)}{6.24}})}$	$(1+e^{-\frac{(E+10)}{8}})^{-1}$
f	$9(0.0197e^{-0.0337^2(E+10)^2}+0.02)^{-1}$	$(1+e^{\frac{(E+28)}{6.9}})^{-1}$
f_{Ca}	2	$\left(1+\frac{Cai}{0.00035}\right)^{-1}$
u	8	$\left(1+e^{-\frac{(F_n-3.4175*10^{-13})}{13.67*10^{-16}}}\right)^{-1}$
v	$1.91+2.09\left(1+e^{-\frac{(F_n-3.4175*10^{-13})}{13.67*10^{-16}}}\right)^{-1}$	$1-\left(1+e^{-\frac{(F_n-6.835*10^{-14})}{13.67*10^{-16}}}\right)^{-1}$
w	$6\left(\frac{1-e^{-\frac{(E-7.9)}{5}}}{(1+0.3e^{-\frac{(E-7.9)}{5}})(E-7.9)}\right)$	$1-\left(1+e^{-\frac{(E-40)}{17}}\right)^{-1}$

The system of equations

The system of 21 equations is:

$$
\begin{aligned}
\frac{\mathrm{d}E}{\mathrm{d}t} &= -\frac{(I_{ion}+I_{st})}{C_M}, \qquad (2.18)\\
I_{ion} &= I_{Na}+I_{K1}+I_{to}+I_{Kur}+I_{Kr}+I_{Ks}+I_{Ca,L}+I_{p,Ca}+I_{Na,K}\\
&\quad +I_{NaCa}+I_{b,Na}+I_{b,Ca},\\
\frac{\mathrm{d}Nai}{\mathrm{d}t} &= -\frac{3I_{NaK}+3I_{NaCa}+I_{b,Na}+I_{Na}}{FV_i},\\
\frac{\mathrm{d}Ki}{\mathrm{d}t} &= \frac{2I_{NaK}-I_{K1}-I_{to}-I_{Kur}-I_{Kr}-I_{Ks}-I_{b,K}}{FV_i},\\
\frac{\mathrm{d}Cai}{\mathrm{d}t} &= \frac{B1}{B2},\\
B1 &= \frac{2I_{NaCa}-I_{p,Ca}-I_{Ca,L}-I_{b,Ca}}{2FV_i}+\frac{V_{up}(I_{up,leak}-I_{up})+I_{rel}V_{rel}}{V_i},\\
B2 &= 1+\frac{[Trpn]_{max}K_{m,Trpn}}{(Cai+K_{m,Trpn})^2}+\frac{[Cmdn]_{max}K_{m,Cmdn}}{(Cai+K_{m,Cmdn})^2},\\
\frac{\mathrm{d}Caup}{\mathrm{d}t} &= I_{up}-I_{up,leak}-I_{tr}\frac{V_{rel}}{V_{up}},\\
\frac{\mathrm{d}Carel}{\mathrm{d}t} &= (I_{tr}-I_{rel})\left(1+\frac{[Csqn]_{max}K_{m,Csqn}}{(Carel+K_{m,Csqn})^2}\right)^{-1},\\
\frac{\mathrm{d}y}{\mathrm{d}t} &= \frac{\overline{y}-y}{\tau_y}, \qquad y=m,h,j,o_a,o_i,u_a,u_i,x_r,x_s,d,f,f_{Ca},u,v,w.
\end{aligned}
$$

Table 2.4: The initial values for all the dynamic variables for Courtemanche et al's model.

State Variable	Resting Value	State Variable	Resting Value
E_{rest}	-81.2	m	$2.91 * 10^{-3}$
h	0.965	j	0.978
d	$1.37 * 10^{-4}$	f	0.999
u	0	v	1
w	0.999	x_r	$3.29 * 10^{-5}$
x_s	0.0187	Nai	11.2
Cai	$1.02 * 10^{-4}$	Ki	0.0139
$Caup$	1.49	$Carel$	1.49
o_a	0.0304	o_i	0.999
u_a	$4.96 * 10^{-3}$	u_i	0.999
f_{Ca}	0.775	$[Cmdn]_i - Cai$	$2.05 * 10^{-3}$
$[Csqn]_i - Cai$	6.51	$[Trpn]_i - Cai$	0.0118

Figure 2.6 shows the action potential of system (2.18) for the initial values in Table 2.4, which has a spike and dome shape and this is different from the Hodgkin-Huxley and Noble's action potentials.

The spike shows the sudden displacement of membrane potential from its resting state and then the recovery is a dome shape back to the equilibrium. The return to the equilibrium point is a smooth return here, as we can see from Fig. 2.6.

Figure 2.7 are the graphs of the currents of this system and they are drawn for the output from the twelfth action potential. All the graphs are drawn for I_{st}=0 for the times $[0, 100]$ and $[102, 600]$ and I_{st}=-2000 for the time $[100, 102]$.

Figure 2.7 is drawn using C_M=1 in the currents and C_M=12 in $\frac{\mathrm{d}E}{\mathrm{d}t}$ equation, i.e. the normalised currents.

2.1.5 Summary

In Section 2.1.1 for the Hodgkin-Huxley system, we can see from Fig. 2.2 that the curves h and n behave in a similar way and curves V and m behave in a similar way also. This is seen especially in Fig. 2.2(c) if we have a small voltage that is close to the threshold. So we can say that h and n are similar and V and m are similar. In Section 3.2, we will see that V and m are the fast variables

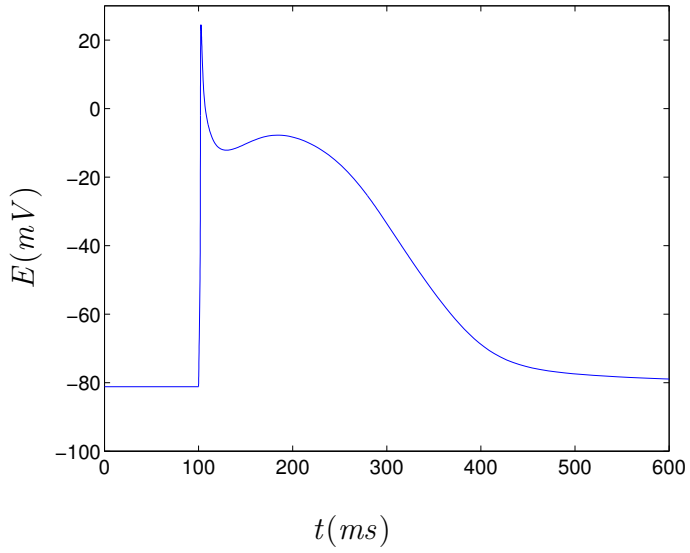

Figure 2.6: Action potential for CRN-21, system (2.18).

and h and n are the slow variables.

Hodgkin-Huxley, Noble and Courtemanche et al's models are all different in their own ways. Noble's model is for Purkinje fibres in mammals and is a modified version of the Hodgkin-Huxley model, which is for the nerve in a squid, and Courtemanche et al's model is for the human artial cell. Even though these three models are different, they also contain similar features, because they are excitable systems. From this we know that they display important features of excitable systems which are; a stable equilibrium, in Noble's model this is for the excitable system, which is in Chapter 5, threshold properties-above the threshold is where excitation occurs if the system is displaced from equilibrium, and below the threshold is where the system is slightly displaced from equilibrium, but not enough to cause excitation as it returns immediately to equilibrium. Also the action potentials display features of fast onset and slow return. They contain a physiological feature in their structure, where the sodium current I_{Na} has the same structure in all three models.

2.2 The FitzHugh System

FitzHugh suggested in his paper[4] that a modified version of the well-known van der Pol system of equations has qualitative properties similar to that of the Hodgkin-Huxley system. We look at this model because FitzHugh suggested

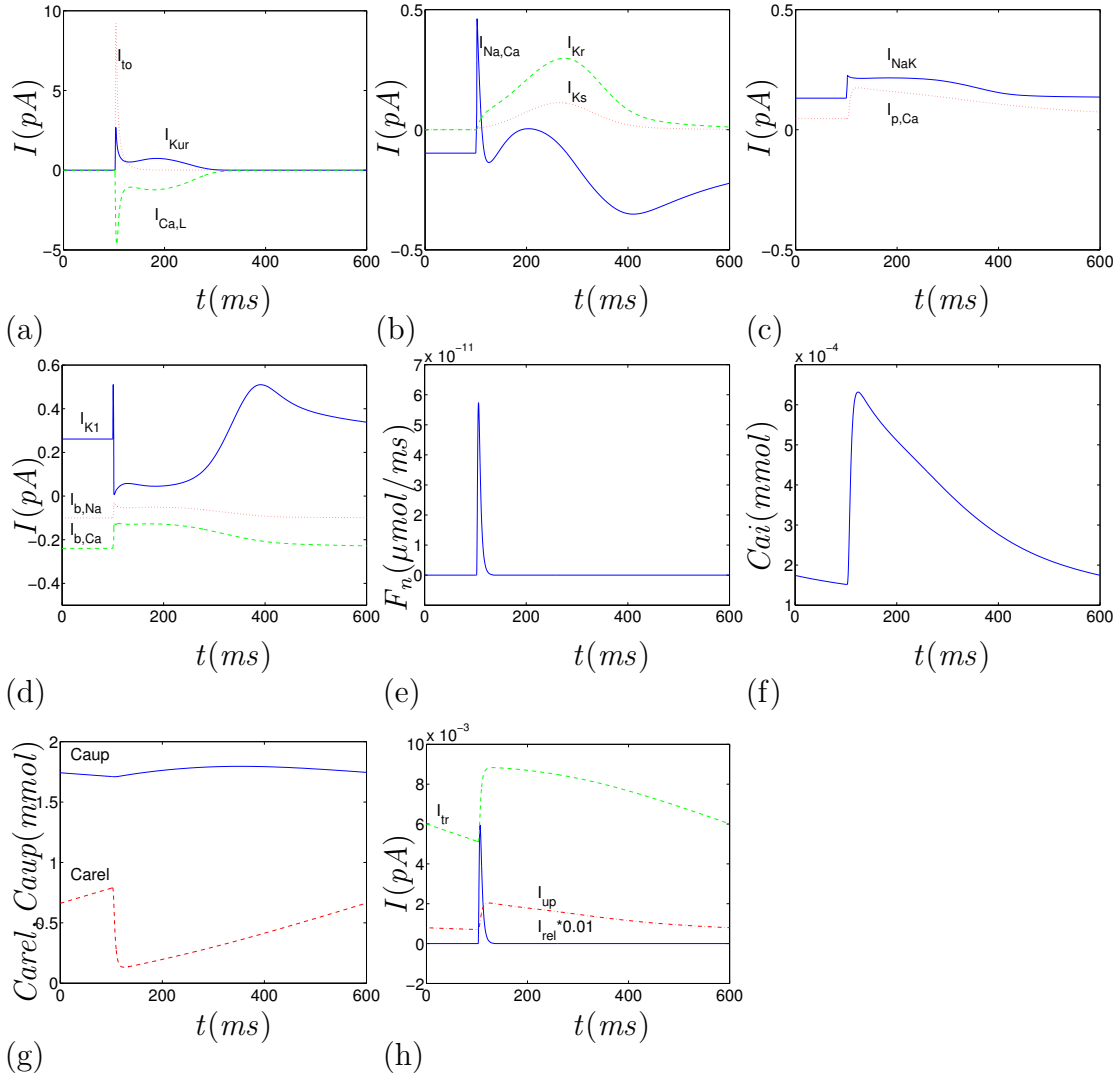

Figure 2.7: Graphs of the currents. (a) I_{Kur} (-), I_{to} (:), $I_{Ca,L}$ (- -), (b) I_{NaCa} (-), I_{Ks} (:), I_{Kr} (- -), (c) I_{NaK} (-), $I_{p,Ca}$ (:), (d) I_{K1} (-), $I_{b,Na}$ (:), $I_{b,Ca}$ (- -), (e) F_n (-), (f) Cai (-), (g) $Caup$ (-), $Carel$ (- -), and (h) $I_{rel} * 0.01$ (-), I_{up} (-.), I_{tr} (- -) drawn for the output from the twelfth action potential.

that the four-dimensional projection of the Hodgkin-Huxley phase portrait to a two-dimensional subspace gives a phase portrait, where the trajectories look similar to the trajectories of the FitzHugh phase portrait. So therefore this shows us that FitzHugh's two-dimensional model can be studied using the phase plane analysis, whereas Hodgkin-Huxley's model cannot.

Here we consider a concrete example of the FitzHugh System. We have the van der Pol system of equations in x and y.

$$\begin{aligned} \dot{x} &= c(y + x - x^3/3 + z), \\ \dot{y} &= -(x - a + by)/c. \end{aligned}$$

We can use different values of a, b, c and z to analyse this system of equations to find the nullclines, trajectories, singular point and the phase portrait.

The x-nullcline is:

$$y = x^3/3 - x - z.$$

This is a N-shaped cubic curve, which gives us the y-intercept (x, y)=$(0, -z)$, and the three x-intercepts satisfies the equation $x^3 - 3x - 3z$=0. The gradient of the slope at the three x intercepts are found using y'=$x^2 - 1$. The maximum and minimum points are (x, y)=$(1, -2/3 - z)$ and (x, y)=$(-1, 2/3 - z)$ respectively.

The y-nullcline is:

$$y = \frac{a - x}{b}.$$

This gives us a straight line with y intercept (x, y)=$(0, a/b)$ and x intercept (x, y)=$(a, 0)$. The gradient of the slope is y'=$-1/b$.

The equation for the singular point P is:

$$bx^3 + 3x(1 - b) - 3(a + bz) = 0.$$

Therefore there are three solutions to this equation. We consider two sets of values for a, b, c and z. One set is for an excitable system, (a, b, c, z)=$(3/4, 1/2, 3, 0)$, which gives two complex solutions and one real solution for the singular point. We only want the real root, P$\approx$ $(1.08, -0.66)$ to

two decimal places. The eigenvalues are complex conjugates with negative real part, so this is a stable spiral at the singular point P.

The other set of values is for an oscillatory system, where we just change z to 0.4 and keep a, b, and c the same. This gives two complex solutions and one real solution for the singular point again, where P$\approx (0.88, -0.25)$ to two decimal places. The eigenvalues are complex conjugates with positive real part, so this is an unstable spiral at the singular point P.

With all the information we have gathered we can now draw the phase portrait of our system.

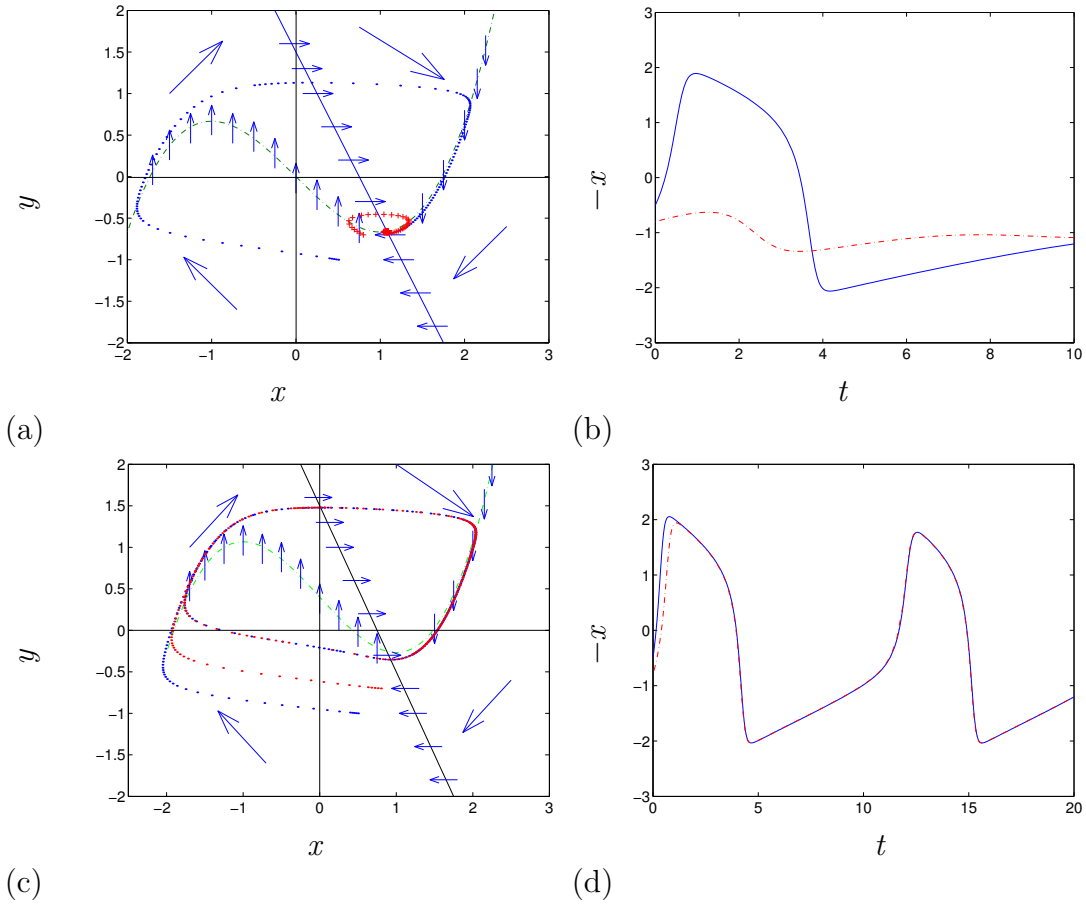

Figure 2.8: (a,c) The FitzHugh system with the x-nullcline (-.) and the y-nullcline (-) and the trajectories starting from different initial points, (x, y)=$(0.5, -1)$ (.) and (x, y)=$(0.8, -0.7)$ (+). (b,d) Action potential of $-x$ against time for the initial values (x, y)=$(0.5, -1)$ (-) and (x, y)=$(0.8, -0.7)$ (-.). (a,b) is for z=0, excitable system, and (c,d) is for z=-0.4, oscillatory system.

In Fig. 2.8(a), the arrows on the nullclines and in the four sections of the phase portrait show which direction the trajectories will travel at these points.

We can see that we have a stable singular point with a trajectory that spirals towards it. Figure 2.8(b) shows the action potentials for the two initial points that are used to draw the trajectories, (x, y)=$(0.5, -1)$ (-) and (x, y)=$(0.8, -0.7)$ (-.). Figures 2.8(c) and (d) show the FitzHugh system as an oscillatory system, which can be achieved by replacing z with a negative number. Therefore there is an unstable equilibrium point and the trajectories are limit cycles. The action potential is now a series of solutions and not one single solution, as we have for the excitable system.

FitzHugh used the van der Pol system of equations because it has qualitative properties similar to that of the Hodgkin-Huxley system. So we can say that the pair (V, m) corresponds to x as they are the fast variables and so they represent excitability. The pair (h, n) corresponds to y as they are the slow variables.

FitzHugh suggested a projection of the four-dimensional phase space of the Hodgkin-Huxley system to a two-dimensional subspace gives a phase portrait, where the trajectories look similar to the trajectories in this system. So we see from Fig. 2.9(a) that this is true. Using FitzHugh's replacements of the (V, m) and (h, n) variables, taken from his 1960 paper[34], we have x=$V - 36m$ and y=$(n - h)/2$. We see that the trajectories look similar to the trajectories in Fig. 2.8(a), so FitzHugh's suggestion is confirmed. Also Figs. 2.9(c) and (d) show that if z and I are negative, then the Hodgkin-Huxley system changes to an oscillatory system, just like FitzHugh's system did and Figs. 2.9(c) and (d) are similar to Figs. 2.8(c) and (d). Therefore the Hodgkin-Huxley model can be considered as belonging to the same general class of excitable-oscillatory systems as the FitzHugh system.

Figures 2.9(b) and (d) show the action potentials for the two initial points that are used to draw the trajectories and this is similar to what happens in Figs. 2.8(b) and (d) respectively for the FitzHugh system.

2.2.1 Summary

Van der Pol's system is generalized by the addition of terms to produce a pair of non-linear differential equations with either a stable singular point or a limit cycle.

FitzHugh considers the Hodgkin-Huxley model as a member of a large class of non-linear systems of equations showing excitable and oscillatory behaviour. Excitation occurs if the initial points, for the trajectories, are displaced from

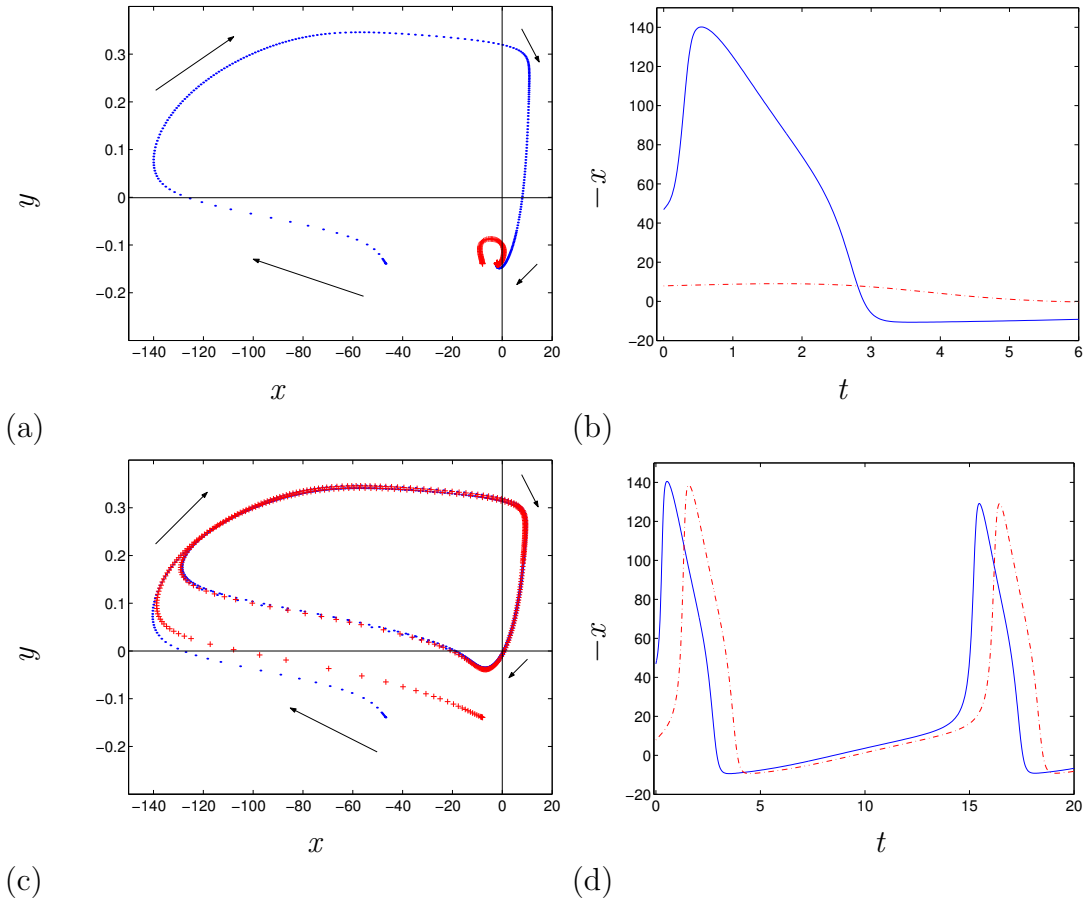

Figure 2.9: (a,c) Projection of the Hodgkin-Huxley system to a two-dimensional subspace with x=$V-36m$ and y=$(n-h)/2$, with trajectories starting from different initial points, (x, y)=$(-46.9080, -0.1392)$ (.) and (x, y)=$(-7.9080, -0.1392)$ (+). (b,d) Action potential of $-x$ against time for the initial values (x, y)=$(-46.9080, -0.1392)$ (-) and (x, y)=$(-7.9080, -0.1392)$ (-.). (a,b) is for z=0 and I=0, excitable system, and (c,d) is for z=-0.4 and I=-10, oscillatory system. The graphs can be compared with Fig. 2.8

right to left of the y-nullcline. So we have two responses, above the threshold and below the threshold. If we are above the threshold, then the action potential (-) in Fig. 2.8(b) has a long, non-monotonic return. If we are below the threshold, then the action potential (-.) in Fig. 2.8(b) has a fast, monotonic return.

This is also the same for Fig. 2.9(b) for the projection of the Hodgkin-Huxley system.

2.3 The Classical Perturbation Theory

All the definitions that are used throughout this work and two theorems on the perturbation theory by Tikhonov, that he published in 1952[5], and Pontryagin in 1957[35] are all contained in this section.

Tikhonov's theorem has since been used and explained in other books and papers, e.g. [36, 37].

Definition [*Manifold*]

A subset $X \subset \mathbb{R}^n$ is a K-dimensional manifold, $K \leq n$, if it is locally diffeomorphic to $\mathbb{R}^K$, that is for any $x \in X$ there exists a neighbourhood $v \subset X$ of x that is diffeomorphic to an open subset U of $\mathbb{R}^K$.

Definition [*Foliation and Leaves*]

A foliation is a partition of phase space to a set of manifolds of lesser dimension, such that for every point in the space there is exactly one manifold from that set that passes through that point. So these are called the leaves of the foliation. All leaves should be of the same dimension.

The above definition of foliation and leaves is a simple version of the definition in the book by Dubrovin et al[38]. Some authors[10] use the terms fibration and fibres to denote closely related concepts. There are some technical differences between both sets of definitions, which are not essential for our study and we will use the terms foliation and leaves, following Zeeman[6].

2.3.1 Tikhonov's theorem

Here we mostly follow notations used in Arnold et al[10]. We consider the system of $m+n$ autonomous first-order differential equations for $m+n$ dynamic variables, where m are slow variables and n are fast variables. Therefore the vector of slow

variables is $y \in \mathbb{R}^m$ and the vector of fast variables is $x \in \mathbb{R}^n$. The system of equations is:

$$\begin{aligned} \frac{\mathrm{d}x}{\mathrm{d}t} &= F(x, y, \epsilon), \\ \frac{\mathrm{d}y}{\mathrm{d}t} &= \epsilon G(x, y, \epsilon). \end{aligned} \tag{2.19}$$

All variables are real, the parameter $\epsilon > 0$ and t is an independent variable. We say this system has *asymptotic structure* (m, n).

We have the initial conditions,

$$x(0) = x_0, \qquad y(0) = y_0, \tag{2.20}$$

where x_0 and y_0 are constants, which don't depend on ϵ.

System (2.19) and the initial conditions (2.20) are called the *full problem* in the fast time.

Definition [*Asymptotic Stability Of Singular Points Of Differential Equations*]

Let

$$\frac{\mathrm{d}z}{\mathrm{d}t} = H(z, t),$$

be a vector system of real differential equations. A point $z{=}z_0$ is called a stable singular point of this system, as $t \to \infty$, if

1. $H(z_0, t){=}0$, for $t \geq 0$.

2. To every $\mu > 0$ there exists a $\delta(\mu) > 0$ with the properties that any solution $z(t)$ of the differential system for which $||z(0) - z_0|| < \delta(\mu)$ can be continued for all $t > 0$ and satisfies the inequality $||z(t) - z_0|| < \mu$.

A stable singular point is called asymptotically stable, if in addition,

$$\lim_{t \to \infty} z(t) = z_0,$$

for all solutions such that $||z(0) - z_0|| < \delta(\mu)$.

Function $\delta(\mu)$ is not uniquely defined here.

Definition

The following system of differential equations is obtained by putting $\epsilon{=}0$ in system (2.19), and this system is called the *fast system.*

$$\begin{aligned} \frac{\mathrm{d}x}{\mathrm{d}t} &= F(x,y,0), \\ \frac{\mathrm{d}y}{\mathrm{d}t} &= 0. \end{aligned} \tag{2.21}$$

For any solution of (2.21), y=constant. Geometrically, it means that all trajectories of (2.21) lie within leaves of the *fast foliation* defined by y=constant.

If ϵ is small, system (2.21) differs from system (2.19) only slightly, at every choice of variables x and y. That is, system (2.19) can be considered as a regularly perturbed version of system (2.21), which means that the solution of an initial value problem for system (2.19), for any fixed interval of time, converges to the solution of system (2.21) during that interval of time, as $\epsilon \to 0$, according to the theorem on the continuous dependence on parameters [39]. This is of course only valid as long as the interval of time is kept fixed as ϵ decreases. What we are also interested in, is what happens at long time intervals. Mathematically, this corresponds to time intervals that grow as ϵ decreases. To see the behaviour there, we use a change of variables $\tau = \epsilon t$ to system (2.19), where τ is the slow time.

$$\begin{aligned} \frac{\mathrm{d}x}{\mathrm{d}\tau} &= \frac{1}{\epsilon}F(x,y,\epsilon), \\ \frac{\mathrm{d}y}{\mathrm{d}\tau} &= G(x,y,\epsilon). \end{aligned} \tag{2.22}$$

System (2.22) with initial conditions (2.20) is the full problem in the slow time.

Definition

If $\epsilon \to 0$ we obtain the *slow system*:

$$\begin{aligned} \frac{\mathrm{d}y}{\mathrm{d}\tau} &= g(x,y), \\ f(x,y) &= 0, \end{aligned} \tag{2.23}$$

where $g(x,y)$=$G(x,y,0)$ and $f(x,y)$=$F(x,y,0)$.

This system is also called the "reduced system".

Assume that equation $f(x,y)$=0 defines at least one real solution for every y,

$$x = \phi(y).$$

This typically defines a manifold in the (x, y) space which is called the *slow manifold*. The slow manifold is a set of singular points of the fast equation $\frac{\mathrm{d}x}{\mathrm{d}t}$. We are interested in the solution $x{=}\phi(y)$, where x is a function of y.

We put this solution in the reduced system (2.23), then the reduced system becomes:

$$\begin{aligned} \frac{\mathrm{d}y}{\mathrm{d}\tau} &= g(\phi(y), y), \\ x &= \phi(y). \end{aligned} \tag{2.24}$$

This is the equation on the slow manifold. We note that if there is an equilibrium in the full system, then it always lies on the slow manifold.

We will consider the slow system (2.24) with initial conditions:

$$\begin{aligned} x(0) &= \phi(y_0), \\ y(0) &= y_0. \end{aligned} \tag{2.25}$$

System (2.24) and the initial conditions (2.25) are called the *reduced problem*.

We make the following assumptions:

Assumption 1 *The functions F and G in (2.19) are continuous.*

Assumption 2 *There is a n-dimensional continuous vector function $\phi(y)$ in $y \in \mathbb{D}$ such that $f(\phi(y), y) \equiv 0$, where $\mathbb{D} \subset \mathbb{R}^m$ is a domain.*

Assumption 3 *There exists a number $\eta > 0$, independent of y, such that the relations,*

$||x - \phi(y)|| < \eta, \qquad x \neq \phi(y) \qquad$ *for* $y \in \mathbb{D}$

imply

$f(x, y) \neq 0, \qquad$ *for* $y \in \mathbb{D}$.

A solution $\phi(y)$ that satisfies this condition will be called isolated in $y \in \mathbb{D}$.

Assumption 4 *The singular point $x{=}\phi(y)$ of the fast system (2.21) is asymptotically stable for all y in $y \in \mathbb{D}$.*

Assumption 5 *The full, as well as the reduced problem have unique solutions in an interval $0 \leq \tau \leq T$ for any ϵ.*

Theorem 1 (*Tikhonov*) *Let assumptions 1 to 5 be satisfied and let (x_0, y_0) be a point in the basin of attraction of the equilibrium $(\phi(y_0), y_0)$ of the fast system. Then the solution $x(\tau, \epsilon), y(\tau, \epsilon)$ of the full initial value problem (2.22), (2.20) is connected with the solution $y_s(\tau)$, $x_s(\tau){=}\phi(y_s(\tau))$ of the slow (reduced) problem (2.24) and (2.25), by the limit relations*

$$\begin{aligned} \lim_{\epsilon \to 0} x(\tau, \epsilon) = x_s(\tau) = \phi(y_s(\tau)), \qquad & 0 < \tau \leq T_0, \\ \lim_{\epsilon \to 0} y(\tau, \epsilon) = y_s(\tau), \qquad & 0 \leq \tau \leq T_0. \end{aligned}$$

Here $T_0 \leq T$ is any number such that $x{=}\phi(y_s(\tau))$ is an isolated stable root of $f(x, y_s(\tau)){=}0$ for $0 \leq t \leq T_0$. The convergence is uniform in $0 \leq \tau \leq T_0$, for $y(\tau, \epsilon)$, and in any interval $0 < t_1 \leq \tau \leq T_0$ for $x(\tau, \epsilon)$.

This says that as long as all the assumptions are satisfied then we can obtain the reduced system by putting $\epsilon{=}0$ in the $\frac{\mathrm{d}x}{\mathrm{d}t}$ equation and the solution of the reduced system is a good approximation of the original system, as long as ϵ is small enough for this to happen. Equation $x{=}\phi(y)$ says that a solution of $y{=}y_0$ of this will always move along the slow manifold $\phi(y)$. The solution for the full system will approach $\phi(y_s(t, 0))$ and then move along the slow manifold. At $t{=}0$, the two solutions are separated by finite distance. They will move closer for positive time, but not for $t{=}0$. No matter how small ϵ is they will never be the same at $t{=}0$.

This theorem will only hold as long as all the points on the slow manifold, through which the trajectories of the reduced system pass, are asymptotically stable equilibria of the fast system.

Tikhonov's theorem is stated for a two-speed system, but he also generalised his theorem for hierarchical systems that depend on more than one small parameter, e.g:

$$\frac{\mathrm{d}x}{\mathrm{d}t} \quad = \quad F(x, y, z, \epsilon_1, \epsilon_2), \qquad x \in \mathbb{R}^n,$$

$$\begin{aligned}\frac{\mathrm{d}y}{\mathrm{d}t} &= \epsilon_1 G(x,y,z,\epsilon_1,\epsilon_2), \qquad y \in \mathbb{R}^m,\\ \frac{\mathrm{d}z}{\mathrm{d}t} &= \epsilon_1\epsilon_2 H(x,y,z,\epsilon_1,\epsilon_2), \qquad z \in \mathbb{R}^l,\end{aligned}$$

where simultaneously $\epsilon_1 \to 0$ and $\epsilon_2 \to 0$. This is a system of $l+m+n$ first order differential equations for $l+m+n$ dynamic variables, where l are the super-slow variables, m are slow variables and n are fast variables.

All variables are real and ϵ_1, $\epsilon_2 > 0$ and t is an independent variable. So in this case, a typical trajectory would consist of:

1. fast motion where only x changes, while y and z remain constant during time $t \propto 1$, followed by,

2. a slow part where x and y changes, so that $F(x,y,z,\epsilon_1,0) \approx 0$, while z remains constant, lasting $t \propto \epsilon_1^{-1}$, followed by,

3. a super-slow part where all three sets of variables change with $F(x,y,z,0,0) \approx 0$ and $G(x,y,z,0,0) \approx 0$, on the time scale $t \propto \epsilon_1^{-1}\epsilon_2^{-1}$.

We say that this system has asymptotic structure (l,m,n).

2.3.2 Pontryagin's theorem

Pontryagin's theorem is obtained from Arnold et al[10] and it is as follows.

We consider the reduced system (2.23):

$$f(x,y) = 0, \qquad \frac{\mathrm{d}y}{\mathrm{d}\tau} = g(x,y),$$

where $f(x,y)$=$F(x,y,0)$ and $g(x,y)$=$G(x,y,0)$.

Definition [Fold Points]

Fold points are points on the slow manifold where the linearized equations for the fast variables have one zero eigenvalue. They represent the boundary between the stable (attractor) and unstable (repellor) parts of the slow manifold.

System (2.19) or (2.22) is a fast-slow system of equations where if $\epsilon \to 0$ we can study the asymptotic behaviour with respect to ϵ. In this system the singular (fixed) points of the equation of the fast foliation $\frac{\mathrm{d}y}{\mathrm{d}t}$ lose their stability as the slow variable y changes and this is due to one of the eigenvalues of the linearized fast

equations $\frac{\mathrm{d}x}{\mathrm{d}t}$ vanishing. Therefore the slow manifold will have stable (attractor) and unstable (repellor) parts, which are separated by fold points.

Definition [Regular and Degenerate Phase Curves]

The phase curves of the fast-slow system are subdivided into two kinds, the regular phase curves and degenerate duck-like curves called "degenerate ducks". The regular phase curves consist of trajectories flowing along the stable parts of the slow manifold and along the fast foliation. The degenerate ducks consists of trajectories flowing along the stable and unstable parts of the slow manifold and fast foliation. Therefore the trajectory will look like a duck.

Theorem 2 (*Mishchenko And Rozov (*1975*), Pontryagin (*1957*)*)
Suppose (x, y)=p is a fold point of the slow manifold of a fast-slow system of the form (2.22). Suppose that the vector $g(x, y)$ is transversal to the projection of the fold curve onto the phase space of the slow variables y along the axes of the fast variables x. Moreover, suppose that this vector is directed to the exterior, relative to the projection of the slow manifold on the phase plane of the slow variables. Then, there exists a neighbourhood U of the point p in the phase space such that for any point $q \in U$, the connected component of the intersection of the neighbourhood U with a positive semi-trajectory of the system (2.22) with initial point q converges, as $\epsilon \to 0$, to a regular phase curve of the fast-slow system.

The ducks existence were found for a two-dimensional fast-slow system of equations and is described in Guckenheimer and Ilyashenko 2001 paper[40]. They found an example where the ducks existence was a typical solution, but the ducks only exists for a small range of parameters in a system.

Theorem 2 says that if we have a point p on the slow manifold on the boundary between its stable and unstable pieces, and draw a trajectory that goes through this point, then it will follow the fast foliation to a stable piece of slow manifold, and then follow this until it reaches the point p, then it leaves the slow manifold by making a jump down the fast foliation to another piece of slow manifold. The regular phase curves correspond to having fixed initial conditions and the degenerate ducks correspond to different initial conditions for different values of ϵ.

2.3.3 Geometry of the slow manifold

Here we have some definitions to do with the geometry of two-dimensional slow manifolds. If a trajectory reaches a region on the slow manifold where the points are unstable equilibria, then the trajectory leaves the slow manifold and these points are called the threshold.

The boundary where the stable and unstable regions of the slow manifold meet are the fold curve.

These definitions only make sense for $x \in \mathbb{R}^1$. For more general definitions, see[41].

Definition [*The Fold Curve*]

The fold curve consists of fold points where the slow manifold is tangent to the fast foliation. This is defined by the equations $f{=}0$ and $\frac{\partial f}{\partial x}{=}0$.

Definition [*Threshold*]

The threshold is a point on the fold curve where a particular regular trajectory departs from the slow manifold.

Definition [*The Cusp Point*]

The cusp point occurs if the fold curve is tangent to the fast foliation. The fold curve is a smooth line that belongs to the slow manifold and the slow manifold is tangent to the fast foliation, but the projection of the fold curve will not be smooth at the cusp point. In addition to $f{=}0$ and $\frac{\mathrm{d}f}{\mathrm{d}x}{=}0$, we have $\frac{\partial^2 f}{\partial x^2}{=}0$ as well.

2.3.4 Parametric embedding

To apply Tikhonov and Pontryagin's theorems to our work, we need the models that we are studying to be in the same form as system (2.19). However, they do not depend explicitly on any parameters that can tend to zero, but only contain constants that have been measured experimentally.

So to apply Tikhonov and Pontryagin's theorems we need to define a parametric embedding, which is where we introduce the small parameter ϵ artificially.

Definition

We will call a system:

$$\frac{\mathrm{d}x}{\mathrm{d}t} = F(x;\epsilon), \qquad x \in \mathbb{R}^d,$$

depending on parameter ϵ, a *one-parametric embedding* of a system:

$$\frac{\mathrm{d}x}{\mathrm{d}t} = f(x), \qquad x \in \mathbb{R}^d,$$

if $f(x) \equiv F(x,1)$ for all $x \in \mathbb{R}^d$. Similarly, we define an *n-parametric embedding*, with right-hand sides in the form $F(x,\epsilon_1,\ldots,\epsilon_n)$ and $F(x,1,\ldots,1) \equiv f(x)$. If an n-parametric embedding has a form of a Tikhonov fast-slow system with asymptotic structure $(k_1,\ldots,k_n)$, we call it a (*Tikhonov*) $(k_1,\ldots,k_n)$-*asymptotic embedding.*

We use this procedure to replace a small dimensionless constant a with an artificial small parameter ϵa, where $\epsilon \ll 1$. The replacement ϵa constitutes a one-parametric embedding. We can consider the limit $\epsilon \to 0$ and observed what happens to the qualitative features that we are interested in. Namely, to see if they will converge satisfactorily, then the embedding is adequate for these features.

2.3.5 Summary

The classical perturbation theory, Tikhonov and Pontryagin's Theorems, describe the asymptotic behaviour of fast-slow systems of differential equations in $(m+n)$-dimensional space. This theory defines the slow manifold, fast foliation; fold curve, threshold and cusp.

Therefore we can say:

$$\begin{array}{rcrcl} Dim(SlowManifold) & + & Dim(FastFoliation) & = & Dim(PhaseSpace). \\ \#\text{ of slow variables} & + & \#\text{ of fast variables} & = & \text{total }\#\text{ of variables.} \end{array}$$

2.4 Two Excitable Systems by Zeeman

We study the methods Zeeman uses for his two "toy" models[6, 7]. The two models are simple equations, which describe solutions for the "heart", and "nerve", which are examples of fast-slow systems, where one equation is the fast equation and the other equation is the slow equation.

Zeeman built two simple mathematical models for "heart" and "nerve" because he wanted to demonstrate the fast onset and fast/slow return in the phase portraits and action potentials of the two models.

We have three dynamic qualities, which are displayed by the heart fibres and nerve axons and these are:

(1) stable equilibrium,

(2) threshold, for triggering an action, and

(3) return to equilibrium.

Quality (3) is split up into two more cases, depending on whether the return is smooth or not. These are:

(a) jump return ("heart"), as in Fig. 2.8(b) (-), and

(b) smooth return ("nerve"), as in Fig. 2.8(b) (-.).

2.4.1 The "heart" by Zeeman

We analyse the "heart" model first and show that the solutions satisfy "Theorem" 1.

"Theorem" 1 *There exists a dynamical system on* $\mathbb{R}^2$ *possessing the qualities* (1), (2) *and* (3), *where* (3) *is the jump return.*

Variables $x, b \in \mathbb{R}^2$ and ϵ is a small positive parameter, $\epsilon \ll 1$.

We call it "Theorem"1 as this is what Zeeman calls it, but it is not really a Theorem because there is no proof or even a rigorous formulation. This also applies to "Theorem"2 and the "Lemma".

Zeeman's "heart" model has asymptotic structure $(1, 1)$ which is written as follows:

$$\begin{aligned} \epsilon\dot{x} &= -(x^3 - x + b), \\ \dot{b} &= x - x_0. \end{aligned} \tag{2.26}$$

The fixed point is at x=x_0 and b=b_0. We want to find the stability of the fixed point and also how the trajectories act at this point, i.e. do they travel straight to the fixed point or is it a stable spiral like the FitzHugh system.

The x-nullcline is b=$-x^3 + x$ and this is a N-shaped cubic curve which gives b-intercept (b, x)=$(0, 0)$ and three x-intercepts (b, x)=$(0, 0)$ and $(0, \pm 1)$. The gradient of the slope at x=0 is b'=1 and at x=$\pm$1 it is b'=-2.

The maximum and minimum points are $(b,x)=(\frac{2}{3\sqrt{3}},\frac{1}{\sqrt{3}})$ and $(b,x)=(\frac{-2}{3\sqrt{3}},\frac{-1}{\sqrt{3}})$ respectively.

The b-nullcline is $x=x_0$ and for this we take the maximum point and have $x_0=\frac{1}{\sqrt{3}}$. We want $x_0 > \frac{1}{\sqrt{3}}$ so we can have a stable fixed point.

The eigenvalues are:

$$\lambda_{1,2} = \frac{(1-3x_0^2) \pm \sqrt{(1-3x_0^2)^2 - 4\epsilon}}{2\epsilon}.$$

We also obtain from the Jacobian matrix that the $\det(A)=\frac{1}{\epsilon} > 0$ as $\epsilon > 0$ and $\mathrm{Tr}(A)=\frac{1-3x_0^2}{\epsilon}$. If $\mathrm{Tr}(A) > 0$, then $3x_0^2 < 1$ and if $\mathrm{Tr}(A) < 0$, then $3x_0^2 > 1$. We know that $x_0 > \frac{1}{\sqrt{3}}$, then $\mathrm{Tr}(A) < 0$, so the fixed point is stable. So if $x_0 < \frac{1}{\sqrt{3}}$, we have an unstable fixed point.

Slow manifold and fast foliation

The slow manifold exists if $\epsilon=0$ and $f(b,x)=0$. The fast equation determines the slow manifold and the slow equation determines the behaviour on the slow manifold.

In our particular example, the fast foliation is a family of lines parallel to the x-axis, which are oriented towards x-positive if $f < 0$ and oriented towards x-negative if $f > 0$. If we say that the fast foliation is a tree, then the vertical lines b=constant are the leaves of that tree. They are the individual straight lines that make up the foliation.

Using Tikhonov's theorem we introduce a new variable $t=\epsilon T$ to system (2.26) to obtain another system of equations to find the fast foliation.

$$\begin{aligned} \frac{\mathrm{d}x}{\mathrm{d}T} &= -(x^3 - x + b), \\ \frac{\mathrm{d}b}{\mathrm{d}T} &= \epsilon(x - x_0). \end{aligned} \tag{2.27}$$

We take our two systems (2.26) and (2.27) and we use them to find the slow manifold and fast foliation in our phase plane.

System (2.26) gives us the slow manifold if $\epsilon=0$ and $f(b,x)=x^3 - x + b$.

$$\begin{aligned} b &= -x^3 + x, \\ \dot{b} &= x - x_0. \end{aligned}$$

System (2.27) gives us the fast foliation, if ϵ=0.

$$\begin{aligned} b &= \text{constant}, \\ \frac{\mathrm{d}x}{\mathrm{d}T} &= -(x^3 - x + b). \end{aligned}$$

The phase plane and action potential

We can now draw our phase portrait with the slow manifold and trajectories.

In our phase portrait, Fig. 2.10(a), T' and T are the thresholds and they are given by $3x^2$=1. The attracting branches of the slow manifold are $x^3 - x + b$=0 and $3x^2 \geq 1$ (-). The tangency at T is generic (quadratic), so therefore by continuity of the fast foliation, the slow manifold must change from attractor to repellor at T. Our fixed point here is stable, but if (x_0, b_0)=$(0, 0)$ then the fixed point would be unstable and if we take one of the trajectories on our phase plane and follow it round then it would never go near the fixed point, instead it would make a path around it and just keep going on this route without stopping. This is called a limit cycle. Points B and D are on the maximum and minimum of the curve. Paths T→B and T'→D are the instantaneous jumps that occur during the limit cycle TBT'D.

As we have a stable fixed point in our model then we do not have a limit cycle, instead our trajectories travel along the fast foliation until it reaches a point on the slow manifold and then it travels along the slow manifold to the equilibrium point.

In Fig. 2.10(a), we see that a trajectory starting from an initial point A in the phase plane will travel along the fast foliation to the piece of slow manifold, $x < 0$, (B). It travels along the slow manifold until it reaches T' and can't go any further as it has reached a piece of slow manifold that is a repellor (- -), and therefore has to make a jump from T' to D and travel back along the slow manifold to the equilibrium point (E). As the trajectory makes this jump at T' then we have a jump return and not a smooth return. For a smooth return to happen we would not have the repellor piece of the slow manifold.

Therefore Zeeman proposed the following:

"Lemma" 1 *In $\mathbb{R}^2$ a smooth return is not possible.*

Figure 2.10(b) is the action potential of the heart. It corresponds to the trajectory in Fig. 2.10(a) and as we can see from the action potential we can

follow the path of the trajectory starting at A and see which parts correspond to parts on the action potential. We can see that it has a jump return by the sharp corner at D. The return is not smooth as the return from T' to E in Fig. 2.10(b) is not smooth. If we compare the "heart" action potential to FitzHugh's action potentials in Fig. 2.8(b), then we see that Fig. 2.10(b) has a jump onset and a jump return, which is similar to Fig. 2.8(b) (-).

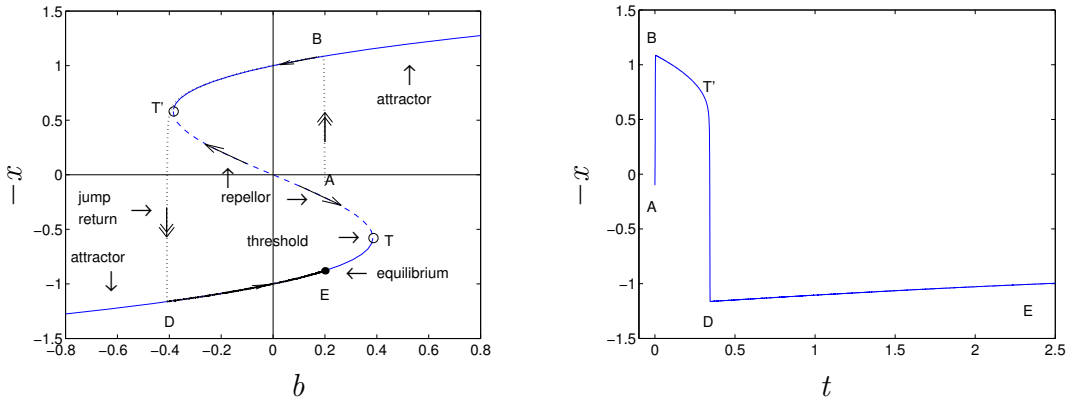

(a) (b)

Figure 2.10: (a) Phase portrait of Zeeman's "heart" model. The double arrows represent the flow on the fast foliation and the single arrows represent the flow on the slow manifold. A trajectory is shown for ϵ=10^{-3} at (b, x)=$(0.2, 0.1)$. Straight lines represent the stable parts of the slow manifold and the dashed lines represent the unstable part. (b) The "heart" action potential drawn against t corresponding to the trajectory in (a). Here the voltage is $-x$.

2.4.2 The "nerve" by Zeeman

We study the second of Zeeman's "toy" models and analyse the solutions to see if we obtain a smooth return, because we can't obtain a smooth return in $\mathbb{R}^2$.

We are now in three dimensions. Therefore we have one fast eigenvalue and two slow eigenvalues, which can either, be real or complex. As before the fast foliation will be a family of lines parallel to the x-axis. The slow manifold will be a surface cutting the fast foliation transversally near the equilibrium point. This means that the angle is non-zero if the slow manifold crosses the fast foliation.

We want to see if we obtain a cusp catastrophe in the "nerve" equation. A cusp catastrophe is if all three definitions of the fold curve, the threshold and the cusp point apply and the trajectories start from an initial point and travel smoothly around the cusp point to the stable equilibrium.

We analyse the "nerve" model to show that the solutions satisfy "Theorem" 2.

"Theorem" 2 *There exists a dynamical system on* $\mathbb{R}^3$ *possessing the qualities* (1), (2) *and* (3), *where* (3) *is a smooth return.*

Variables $x, a, b \in \mathbb{R}^3$ and $\epsilon \ll 1$.

Zeeman's "nerve" model has asymptotic structure $(2, 1)$ which is written as follows:

$$\epsilon\dot{x} = -(x^3 + ax + b), \tag{2.28}$$

$$\dot{a} = -2(a + x), \tag{2.29}$$

$$\dot{b} = -(a + 1). \tag{2.30}$$

Equation (2.28) is the fast equation and equations (2.29) and (2.30) are the slow equations. The slow equations determine the flow on the slow manifold. Therefore the fixed point is (x, a, b)=$(1, -1, 0)$.

Stability

We find the eigenvalues for this point by using the Jacobian matrix.

$$\mathrm{Jac}(1, -1, 0) = \begin{pmatrix} -\frac{2}{\epsilon} & -\frac{1}{\epsilon} & -\frac{1}{\epsilon} \\ -2 & -2 & 0 \\ 0 & -1 & 0 \end{pmatrix}.$$

The characteristic equation is:

$$\epsilon\lambda^3 + 2\lambda^2(1 + \epsilon) + 2\lambda + 2 = 0.$$

The eigenvalues are of two types, one type is if λ is finite and the other type is if λ is of the order ϵ^{-1} as $\epsilon \to 0$.

If λ is finite and ϵ=0, then the characteristic equation is:

$$\lambda^2 + \lambda + 1 = 0.$$

The solution to this is:

$$\lambda_{2,3} = \frac{-1 \pm \sqrt{3}i}{2}.$$

If λ is of order ϵ^{-1}, we say $\lambda \sim \frac{1}{\epsilon}$ as $\epsilon \to 0$ and λ=$\frac{1}{\epsilon}\Lambda$, where Λ is finite, $\Lambda \neq 0$.

Putting this in the characteristic equation we obtain:

$$\Lambda^3 + 2\Lambda^2(1+\epsilon) + 2\Lambda\epsilon + 2\epsilon^2 = 0.$$

As $\epsilon \to 0$:

$$\Lambda^3 + 2\Lambda^2 = 0.$$

So we have $\Lambda = 0$, which is a repeated root, and $\Lambda = -2$.

We have Λ finite, so we can't have the value Λ=0. Therefore $\lambda_1 = -\frac{2}{\epsilon}$.

Therefore the eigenvalues are:

$$\lambda_1 \approx -\frac{2}{\epsilon}, \qquad \lambda_{2,3} \approx \frac{-1 \pm \sqrt{3}i}{2}.$$

As $\epsilon \ll 1$, then $\lambda_1 \gg 1$.

All three eigenvalues have negative real part, $\lambda_1 < 0$ and $\mathrm{Re}(\lambda_{2,3}) < 0$, then we have a stable spiral of the transients, e.g. trajectories, that converges inwards at the point $(1, -1, 0)$. The equilibrium is stable.

Now $\left|-\frac{2}{\epsilon}\right| = \frac{2}{\epsilon}$ and,

$$\left|\frac{-1 \pm \sqrt{3}i}{2}\right| \quad = \quad 1.$$

If $\epsilon \ll 1$, then the first value is large, and the second value is small compared to $\frac{2}{\epsilon}$. So λ_1 is the fast eigenvalue and $\lambda_{2,3}$ are the slow eigenvalues.

For $\lambda_1 = -\frac{2}{\epsilon}$, we obtain the eigenvectors by multiplying the matrix by ϵ and then taking the limit as $\epsilon \to 0$. So we have x=0, a=0 and b=0. The eigenvector is:

$$\begin{pmatrix} 1 \\ 0 \\ 0 \end{pmatrix}.$$

This is the tangent to the fast foliation.

For $\lambda_2 = \frac{-1 \pm \sqrt{3}i}{2}$ we do the same thing again and the equation of the tangent plane is:

$$2x_1 + a_1 + b_1 = 0.$$

Where $x_1 = x - 1$, $a_1 = a + 1$ and $b_1 = b$. This plane is tangent to the slow manifold. This is also the plane that spans the two complex eigenvalues.

This is tangent to the slow manifold.

Slow manifold and fast foliation

Following Tikhonov's approach we introduce a new variable $t{=}\epsilon T$. This allows separate consideration of the processes. $x{=}x(T)$, $a{=}a(T)$, $b{=}b(T)$.

The slow system is:

$$\begin{aligned} \epsilon\dot{x} &= -(x^3 + ax + b), \\ \dot{a} &= -2(a + x), \\ \dot{b} &= -(a + 1). \end{aligned}$$

This gives us the slow manifold, if $\epsilon{=}0$, and $f(x, a, b){=}(x^3 + ax + b){=}0$. Therefore we obtain:

$$\begin{aligned} b &= -x^3 - ax, \\ \dot{a} &= -2(a + x), \\ \dot{b} &= -(a + 1). \end{aligned}$$

The fast system is:

$$\begin{aligned} \frac{\mathrm{d}x}{\mathrm{d}T} &= -(x^3 + ax + b), \\ \frac{\mathrm{d}a}{\mathrm{d}T} &= -2\epsilon(a + x), \\ \frac{\mathrm{d}b}{\mathrm{d}T} &= -\epsilon(a + 1). \end{aligned}$$

This gives us the fast foliation, if $\epsilon{=}0$.

$$\begin{aligned} a &= \text{constant}, \\ b &= \text{constant}, \\ \frac{\mathrm{d}x}{\mathrm{d}T} &= -(x^3 + ax + b). \end{aligned}$$

Finding the threshold at the equilibrium point

Our slow manifold is:

$$f(x, a, b) = x^3 + ax + b = 0.$$

This is the equation of the curved surface in $\mathbb{R}^3$. A solution of this is the equilibrium point. To find the threshold T we want to project the surface down along the x-axis to the (a, b) plane.

The direction of the projection is:

$$\begin{pmatrix} x \\ a \\ b \end{pmatrix} = \begin{pmatrix} 1 \\ 0 \\ 0 \end{pmatrix} = \underline{p}.$$

At every point we can define a normal vector $\underline{n}$. If $\underline{p}$ is tangent to a point on the slow manifold, then we have a normal to that point which is perpendicular to $\underline{p}$.

So we want to find the dot product of $\underline{n}$ and $\underline{p}$, where:

$$\underline{n} = \nabla f = \left(\frac{\partial f}{\partial x}, \frac{\partial f}{\partial a}, \frac{\partial f}{\partial b}\right) = (3x^2 + a, x, 1).$$

The dot product of $\underline{n}$ and $\underline{p}$ is:

$$\underline{n} \cdot \underline{p} = (3x^2 + a, x, 1) \begin{pmatrix} 1 \\ 0 \\ 0 \end{pmatrix} = 3x^2 + a = 0.$$

So the fold curve satisfies these two equations:

$$\begin{aligned} f = 0 : \quad & x^3 + ax + b = 0, \\ \frac{\partial f}{\partial x} = 0 : \quad & 3x^2 + a = 0. \end{aligned}$$

If we project the fold curves onto the (a, b) plane, then we obtain a cusp and to find the cusp we eliminate x from these two equations.

The second equation gives us:

$$x^2 = -\frac{a}{3}.$$

We put $x{=}\sqrt{-\frac{a}{3}}$ in $f{=}0$, to obtain:

$$4a^3 + 27b^2 = 0.$$

We see $f{=}0$ is a cubic equation in x, so if we project the fold curves onto the (a, b) plane we see that we obtain a cusp, which corresponds to the cubic

equation having three real roots and one of the roots is a repeated root. The assumption to find the threshold is that as we keep a constant and we take a point in the (x, a, b) space and draw a trajectory from this point. We allow x to follow the slow manifold, then the trajectory moves along the b-axis until it reaches the fold curve. The point where the trajectory reaches the fold curve is called the threshold T, and this point T is the intersection of the fold curve with the plane a=-1. The value a=-1 was taken from Zeeman's paper to obtain the value for b for the intersection of the fold curve and the plane a=-1.

So we rearrange $4a^3 + 27b^2$=0 to obtain:

$$b = -\frac{2a}{3}\sqrt{-\frac{a}{3}}.$$

Then the intersection of the fold curve and the plane a=-1 is b=$\frac{2}{3\sqrt{3}}$.

The phase portrait

Our phase portrait is now in three dimensions with the surface b=$-x^3 - ax$ as the slow manifold. We take a trajectory starting at the initial point (x, a, b) in the plane and see that it travels along the fast foliation to the nearest branch of the slow manifold. The trajectory then moves along the slow manifold around the cusp and back to the equilibrium point without making any jumps. As we have two complex eigenvalues then the trajectory travels smoothly around the cusp and we have a smooth return.

With having a threshold T we obtain a fold curve which separates a piece of slow attractor from a piece of slow repellor and as we have a return to equilibrium, then this means that there is another piece of slow attractor to catch the trajectory otherwise it won't return to the equilibrium. As we have a smooth return here and not a jump return, then this implies that the two pieces of slow attractor can be connected by an arc which doesn't cross any fold curves, in order to achieve the smooth return.

Figure 2.11(c) is the "nerve" model's action potential and it corresponds to the trajectory, (a, b, x)=$(-0.8, 0.25, -0.1)$, in Figs. 2.11(a) and (b). We can see here that it has a smooth return, as there is no sharp corner on the return. Figure 2.11(c) has a jump onset and a smooth return, which is similar to Fig. 2.8(b) (-.).

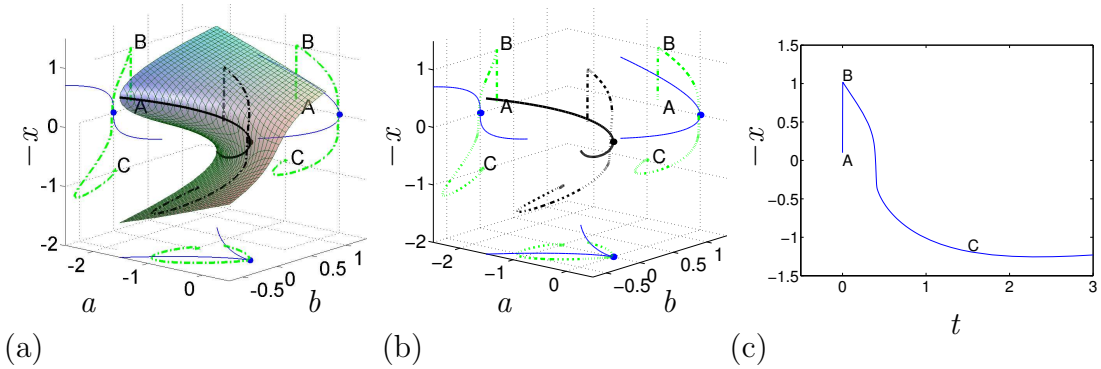

Figure 2.11: Phase portrait of Zeeman's "nerve" model. (a) Drawn are the slow manifold which is the semitransparent surface, a trajectory with ϵ=10^{-3} and its projections (-.) at (a, b, x)=$(-0.8, 0.25, -0.1)$, the fold curve (thick-) and its projections (thin-) and the cusp point $(0, 0, 0)$ and its projections (.). (b) Drawn are the trajectory, fold curve and their projections, and (c) the "nerve" action potential drawn against t corresponding to the trajectory, (a, b, x)=$(-0.8, 0.25, -0.1)$, in (a,b).

Projecting the slow manifold to the $(a, -x)$ plane

We want to project the slow manifold to the $(a, -x)$ plane, because the projection on that plane is unique and the projection on the (a, b) plane is not unique. We do this because we want to see what the projection looks like and this view was not in Zeeman's paper and therefore is part of our new research into this system. The slow manifold is:

$$b = -x^3 - ax,$$

for ϵ=0.

We differentiate b with respect to t and put $\dot{b}$=$-(a + 1)$ in to obtain:

$$\dot{x} = \frac{a + 1 - \dot{a}x}{3x^2 + a}.$$

Put $\dot{a}$=$-2(a + x)$ in here to obtain:

$$\begin{aligned} \dot{x} &= \frac{2x(a + x) + a + 1}{3x^2 + a}, \\ \dot{a} &= -2(a + x). \end{aligned}$$

This is our new system of equations.

The equilibrium point is (a, x)=$(-1, 1)$ and the eigenvalues are:

$$\lambda_{1,2} = \frac{-1 \pm \sqrt{3}i}{2}.$$

We have negative real part for each eigenvalue, therefore we have a stable spiral at the point $(-1, 1)$.

The x-nullcline is:

$$\dot{x} = 0 \Rightarrow a = \frac{-2x^2 - 1}{2x + 1}.$$

This is a curve which gives us two x intercepts (a, x)=$(0, \pm\sqrt{1/2}i)$ and the a intercept (a, x)=$(-1, 0)$. As the x-axis intersections are complex, then we are not interested in them as we can't see them in the real plane.

The a nullcline is:

$$\dot{a} = 0 \Rightarrow a = -x.$$

This gives us a straight line with a intercept (a, x)=$(0, 0)$ and x intercept (a, x)=$(0, 0)$. The gradient of the slope is a'=-1.

We find the trajectories by using different points on the phase plane and putting them into the differential equations. As we can see from the phase portrait we have two nullclines and the parabola a=$-3x^2$, from $\frac{\partial f}{\partial x}$=$0$ previously, which if you take a point inside the parabola the trajectory cannot cross it because we have $\dot{x}$=∞ on the parabola. Any trajectories taken near the parabola do not behave very well, so we only have points below and above the parabola that have trajectories that spiral towards the stable point as seen in the phase portrait, Fig. 2.12. Also, you can see that the parabola is the same as the projection of the fold curve on the (a, x) plane in Figs. 2.11(a) and (b).

The phase portrait shows us where the trajectories can travel on the slow manifold and we see that they can't travel inside the parabola a=$-3x^2$. On our phase portrait of the "nerve" model, a=$-3x^2$ are the threshold points and these points give us our fold curve which separates a piece of slow attractor from a piece of slow repellor. Therefore, the points inside the parabola a=$-3x^2$ are the points which make up the slow repellor piece of the slow manifold and the points outside the parabola make up the slow attractor piece of the slow manifold. Therefore this is why the trajectories cannot cross the parabola.

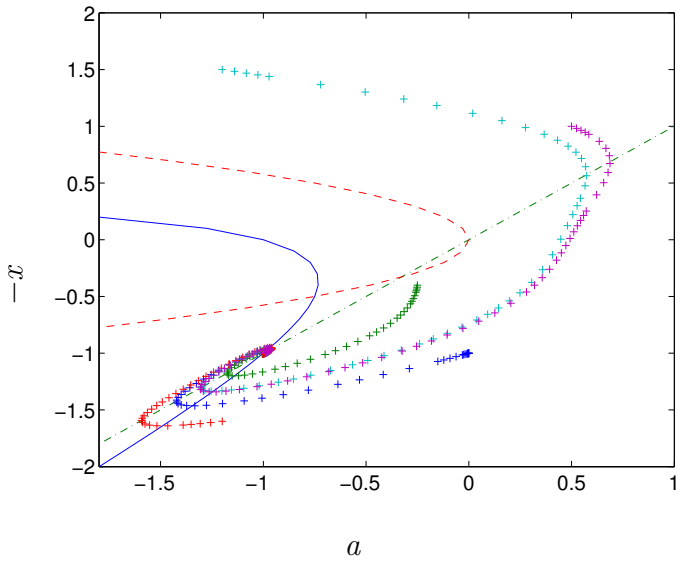

Figure 2.12: Projection of the slow manifold of Zeeman's "nerve" model, with the x nullcline (-), a nullcline (-.), projection of the fold curve (- -), and trajectories (+). Drawn as -x against t.

2.4.3 Applying Zeeman's method to the FitzHugh system

We wanted to see if Zeeman's methods would work for other systems, e.g. the FitzHugh system. To do this we transformed the FitzHugh system to look like Zeeman's "heart" model and then we used Zeeman's methods to find the slow manifold and fast foliation exactly as we did in Zeeman's "heart" model and we also draw two trajectories to see what path they take. We then compared the resulting phase portrait with Fig. 2.10(a) and Fig. 2.8(a).

If we compare our new phase portrait, Fig. 2.13, with FitzHugh's phase portrait, Fig. 2.8(a), we see that the two portraits look the same. Here the slow manifold is the same as the x-nullcline and the v and y nullclines are the same and we have the double arrows representing the flow on the fast foliation. Therefore FitzHugh's system is a particular example of Zeeman's system with a jump onset and a jump return. This is similar to the "heart" model.

2.4.4 Summary

Zeeman concludes that in a system with two equations, e.g. the "heart" model, we have a jump onset and a jump return, "Theorem" 1. In a system with three equations, e.g. the "nerve" model, we can have a jump onset and a smooth return, but only by having a cusp, "Theorem" 2. Also it is not possible to have

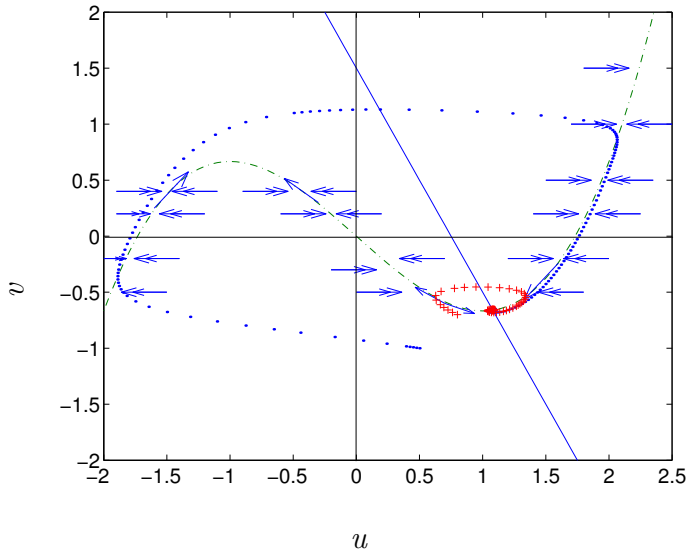

Figure 2.13: Phase portrait of the new FitzHugh system. The double arrows represent the flow on the fast foliation and the single arrows represent the flow on the slow manifold. In this case the slow manifold is the curve $v{=}\frac{u^3}{3} - u$ (-.). Also shown are trajectories starting from the initial points $(v, u){=}(0.5, -1)$ (.) and $(v, u){=}(0.8, -0.7)$ (+) and the v nullcline (-).

a jump onset and a smooth return in the system of two equations, "Lemma" 1.

2.5 Reduction of the Classical Models to a Second Order System by Krinsky and Kokoz

Krinsky and Kokoz wrote four papers on the analysis of the equations of excitable membranes. They wrote two papers[8, 9] on reducing the Hodgkin-Huxley equations to a system of two equations and they wrote two papers[42, 43] on reducing Noble's 1962 equations to a system of two equations.

Krinsky and Kokoz wanted to asymptotically reduce the Hodgkin-Huxley system to a system of two equations, so that they could analyse the second order system by qualitative methods without the use of a computer. They do this because it makes a convenient model for approximate evaluations of the solutions before calculations with a computer of the Hodgkin-Huxley system and also for analysing and planning electrophysiological experiments.

In their paper[8] Krinsky and Kokoz used the equations in Section 2.1.1 with a slight modification. They replaced V with $-E$ and $I{=}-I_b$. They did this with

the constants as well. So V_{Na} becomes $-E_{Na}$, V_K becomes $-E_K$ and V_l becomes $-E_l$. Therefore the equations become:

$$\begin{aligned}
\frac{\mathrm{d}E}{\mathrm{d}t} &= -(\overline{g}_K n^4(E-E_K) + \overline{g}_{Na} m^3 h(E-E_{Na}) + \overline{g}_l(E-E_l)) + I_b, \quad (2.31)\\
\frac{\mathrm{d}n}{\mathrm{d}t} &= \alpha_n(1-n) - \beta_n n,\\
\frac{\mathrm{d}m}{\mathrm{d}t} &= \alpha_m(1-m) - \beta_m m,\\
\frac{\mathrm{d}h}{\mathrm{d}t} &= \alpha_h(1-h) - \beta_h h,
\end{aligned}$$

$$\begin{aligned}
\alpha_n &= \frac{0.01(-E+10)}{e^{\frac{-E+10}{10}}-1}, \qquad \beta_n = 0.125e^{\frac{-E}{80}},\\
\alpha_m &= \frac{0.1(-E+25)}{e^{\frac{-E+25}{10}}-1}, \qquad \beta_m = 4e^{\frac{-E}{18}},\\
\alpha_h &= 0.07e^{\frac{-E}{20}}, \qquad \beta_h = \frac{1}{e^{\frac{-E+30}{10}}+1}.
\end{aligned}$$

Here we have E_K=-12, E_{Na}=115 and E_l=10.613. Following Krinsky and Kokoz we now use these equations to reduce the system to a second order system.

From Fig. 2.14 we obtain the relations:

$$\tau_m(E) \ll \tau_n(E), \tau_h(E), \tag{2.32}$$

$$\overline{n}(E) + \overline{h}(E) \approx \text{const}, \qquad \tau_h(E) \approx \tau_n(E). \tag{2.33}$$

Here we have:

$$\begin{aligned}
\overline{n} &= \frac{\alpha_n}{\alpha_n+\beta_n}, \qquad \overline{h} = \frac{\alpha_h}{\alpha_h+\beta_h},\\
\tau_n &= \frac{1}{\alpha_n+\beta_n}, \qquad \tau_h = \frac{1}{\alpha_h+\beta_h}.
\end{aligned}$$

This is so we can reduce the system to a second order system, by eliminating two equations.

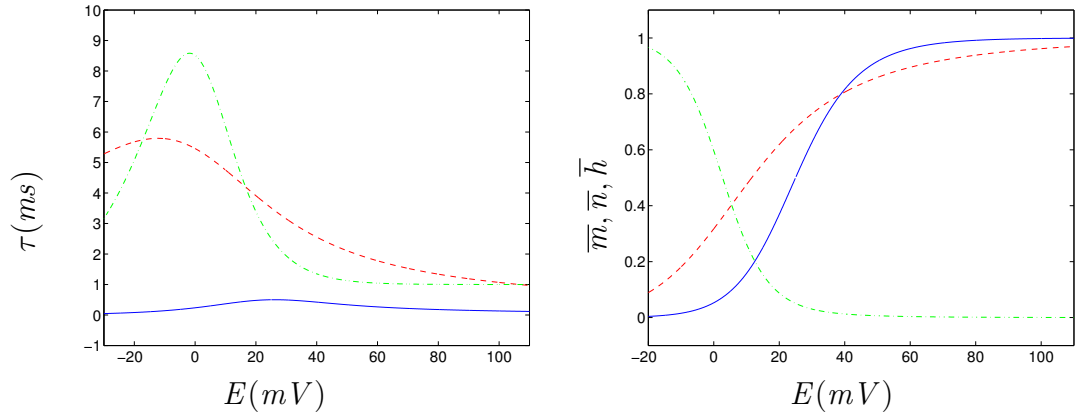

(a) (b)

Figure 2.14: (a) Graph of τ_n (- -), τ_m (-) and τ_h (-.) against E. (b) Graph of $\overline{n}$ (- -), $\overline{m}$ (-) and $\overline{h}$ (-.) against E.

2.5.1 Reduction of the Hodgkin-Huxley system to a third order system

We make relation (2.33) precise instead of approximate and use it in the original system to reduce it to a third order system.

$$\overline{n}(E) + \overline{h}(E) = G, \tag{2.34}$$

$$\tau_h(E) = \tau_n(E), \tag{2.35}$$

where G is a constant.

From now on we will take τ_n and discard τ_h according to equation (2.35).

So,

$$G = \frac{\alpha_n(\alpha_h + \beta_h) + \alpha_h(\alpha_n + \beta_n)}{(\alpha_n + \beta_n)(\alpha_h + \beta_h)}.$$

We can find G by drawing the graph of $\overline{n} + \overline{h}$ against voltage as shown in Fig. 2.15. We use G=1, 0.87 and 0.76 because Krinsky and Kokoz used G=0.87 and 0.76 to draw their phase portraits. We choose G=1 so we could compare our phase portraits with theirs.

Figure 2.15 is similar to Fig. 4 in Meunier's 1992 paper[44]. Meunier wrote a paper to assess the validity of Krinsky and Kokoz's reduction process, by studying the τ's and Krinsky and Kokoz's assumptions; m is a fast variable and $h+n$ can be replaced with a constant.

In the original system we have the arbitrary initial conditions:

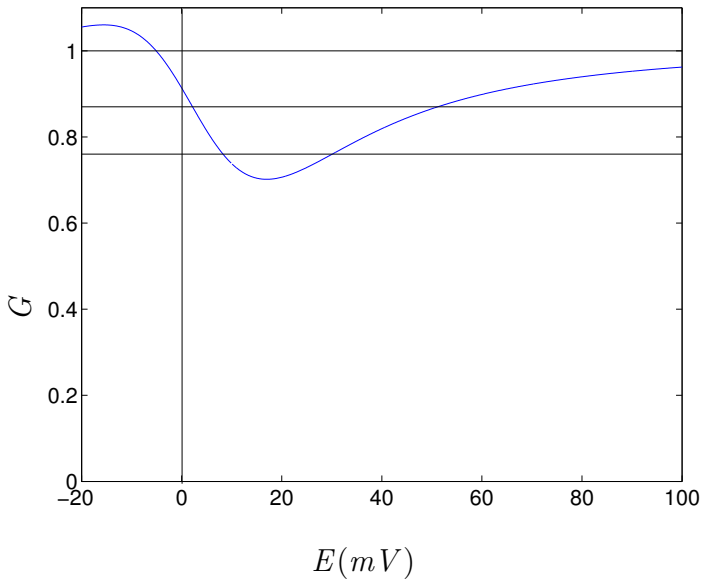

Figure 2.15: Graph of $G{=}\overline{n} + \overline{h}$ against E. The lines represent the values $G{=}1, 0.87, 0.76$.

$$E(0) = E_0, \quad m(0) = m_0, \quad n(0) = n_0, \qquad h(0) = h_0, \tag{2.36}$$

$$h_0 + n_0 = G. \tag{2.37}$$

By the law of conservation we have:

$$G \;=\; n(t) + h(t). \tag{2.38}$$

We use equation (2.38) to reduced the original system to a third order system. So the original system becomes:

$$\begin{aligned}
\frac{\mathrm{d}E}{\mathrm{d}t} &= -(\overline{g}_K n^4(E - E_K) + \overline{g}_{Na} m^3(G - n)(E - E_{Na}) + \overline{g}_l(E - E_l)) + I_b, \\
\frac{\mathrm{d}n}{\mathrm{d}t} &= \alpha_n(1 - n) - \beta_n n, \\
\frac{\mathrm{d}m}{\mathrm{d}t} &= \alpha_m(1 - m) - \beta_m m.
\end{aligned} \tag{2.39}$$

The original system now uses conditions (2.34) and (2.35), so the solutions of the original system comply with the solutions of a third order system for the initial values (2.36) and (2.37).

Krinsky and Kokoz gave a brief proof that it is always possible to reduce the original system to a third order system. We want to eliminate the h equation from the original system. So we use conditions (2.34) and (2.35) to obtain:

$$\dot{h} = \frac{G - \overline{n} - h}{\tau_n}.$$

We then introduce the new variable:

$$\eta = G - n - h,$$

then,

$$\dot{\eta} = -\dot{n} - \dot{h}.$$

We put this into the $\dot{h}$ equation to obtain:

$$\dot{\eta} = -\frac{\eta}{\tau_n}.$$

We replace h with η=$G - n - h$ in the original system and our new system is:

$$\begin{aligned}
\frac{\mathrm{d}E}{\mathrm{d}t} &= -(\overline{g}_K n^4 (E - E_K) + \overline{g}_{Na} m^3 (G - n - \eta)(E - E_{Na}) + \overline{g}_l (E - E_l)) \\
&\quad + I_b, \\
\dot{m} &= \alpha_m (1 - m) - \beta_m m, \\
\dot{n} &= \alpha_n (1 - n) - \beta_n n, \\
\dot{\eta} &= -\frac{\eta}{\tau_n(E)}.
\end{aligned} \tag{2.40}$$

So $\dot{\eta}$=0, η=0 is a solution, so η_0=0. Variable η monotonically approaches G as time goes on.

The new initial conditions are E_0, m_0, n_0 and η=0. Initial conditions E_0, m_0 and n_0 are arbitrary. So $\dot{\eta}$=$-\frac{\eta}{\tau_n}$ for fixed E=E_0 and initial condition η_0 has the solution:

$$\eta = \eta_0 e^{-\frac{t}{\tau_n(E_0)}}.$$

Also $\tau_n(E_0)$ is a limited function, so by putting,

$$\tau_n = \max_E \tau_n(E),$$

we obtain a solution of equation (2.40) that E satisfies the inequality:

$$|\eta(t)| \leq |\eta_0| e^{-\frac{t}{\tau_n}}.$$

From this $\eta(t) \rightarrow 0$ more rapidly then the exponent with the constant $\tau_n, \tau_n \approx$ 10ms. From the original system with the relations (2.32) and (2.33) we can consider $\eta(t)$=0 and that it is always possible to reduce the original system to the third order system.

2.5.2 Reduction of the third order system to a second order system

To reduce the third order system to a second order system we need to find which variable is the fastest and then eliminate this variable from the system. We do this by drawing the graph of τ_m, τ_n and τ_h against voltage to see which is the fastest. What we look for on the graph is which τ's are the smallest and these variables are considered as the fast variables, the largest τ's are consider as the slow variables. As we can see from Fig. 2.16, τ_m is the smallest and τ_n and τ_h are the largest variables. Therefore m is the fast variable and n and h are the slow variables. Now we have found this, we need to eliminate m from the system of equations.

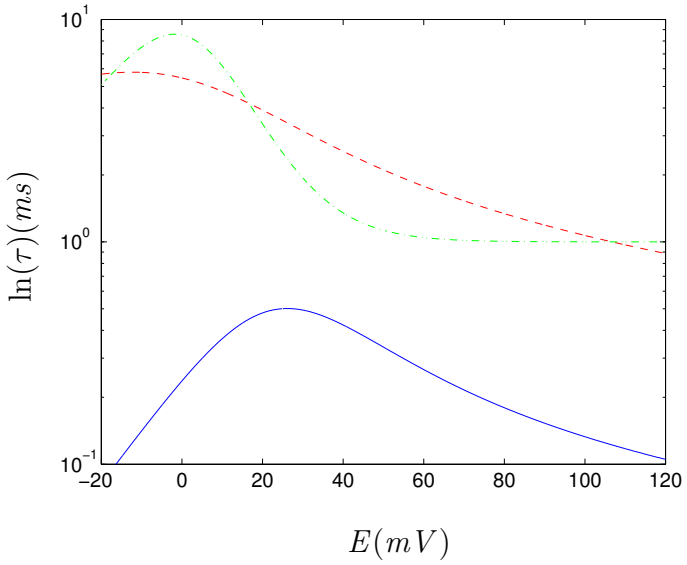

Figure 2.16: Graph of τ_n (- -), τ_m (-), τ_h (-.) against E drawn using a logarithmic scale on the vertical axis for the τ's.

To eliminate m we need to introduce a small parameter ϵ to the m equation because if we don't then Tikhonov's theorem and Zeeman's methods for finding the slow manifold and fast foliation can't be used. This is because Tikhonov's theorem will only work for a system of equations with an independent parameter,

as all our parameters are given constants of E. Therefore all the results are correct in the limit $\epsilon \to 0$.

So we introduce ϵ to the m equation as this is the fastest equation, where,

$$\epsilon = \max_E \left(\frac{\tau_m(E)}{\tau_n(E)} \right).$$

So equation (2.39) becomes:

$$\epsilon \frac{\mathrm{d}m}{\mathrm{d}t} = \frac{(\overline{m} - m)}{\tau_m}.$$

We use ϵ to find the slow manifold. So if $\epsilon \to 0$ the slow manifold is:

$$\overline{m} = m,$$

where,

$$\overline{m} = \frac{\alpha_m}{\alpha_m + \beta_m}, \tag{2.41}$$

and this is the stable equilibrium in the fast system.

The condition for the slow manifold is that both the fast and slow systems should contain the stable equilibrium. Parameter ϵ is small which enters the equation of the slow manifold, so we can exclude m to obtain a second order system of equations by using equation (2.41).

We know that the slow manifold of the third order system is $m{=}\overline{m}$, so we now want to find the fast foliation. To do this we introduce $t{=}\epsilon T$ to the third order system (2.39).

So the system becomes:

$$\begin{aligned}
\frac{\mathrm{d}E}{\mathrm{d}T} &= \epsilon(-(\overline{g}_K n^4 (E - E_K) + \overline{g}_{Na} m^3 (G - n)(E - E_{Na}) + \overline{g}_l (E - E_l)) + I_b), \\
\frac{\mathrm{d}m}{\mathrm{d}T} &= \frac{(\overline{m} - m)}{\tau_m}, \\
\frac{\mathrm{d}n}{\mathrm{d}T} &= \epsilon \frac{(\overline{n} - n)}{\tau_n}.
\end{aligned}$$

So the fast foliation, $\epsilon \to 0$, is:

$$\begin{aligned}
V &= \text{constant}, \\
n &= \text{constant}, \\
\dot{m} &= \frac{(\overline{m} - m)}{\tau_m}.
\end{aligned}$$

Now we can replace equation (2.39) with (2.41) in our third order system to exclude it. We can exclude it because it has an equilibrium point which is asymptotically stable for any fixed E. This is at $\dot{m}$=0. At $\epsilon \to 0$ the difference in the solutions of the second order system and the third order system tends to zero. We say that $\epsilon \ll 1$ and to prove this we need to draw the graph of $\frac{\tau_m}{\tau_n}$ and find the maximum. So,

$$\epsilon = \max_E \left(\frac{\frac{1}{\alpha_m+\beta_m}}{\frac{1}{\alpha_n+\beta_n}} \right),$$

$$\epsilon = \max_E \left(\frac{\alpha_n+\beta_n}{\alpha_m+\beta_m} \right) \ll 1.$$

From Fig. 2.17 we see that the maximum of the graph is at 0.1656. Therefore ϵ=0.1656 $\ll$ 1.

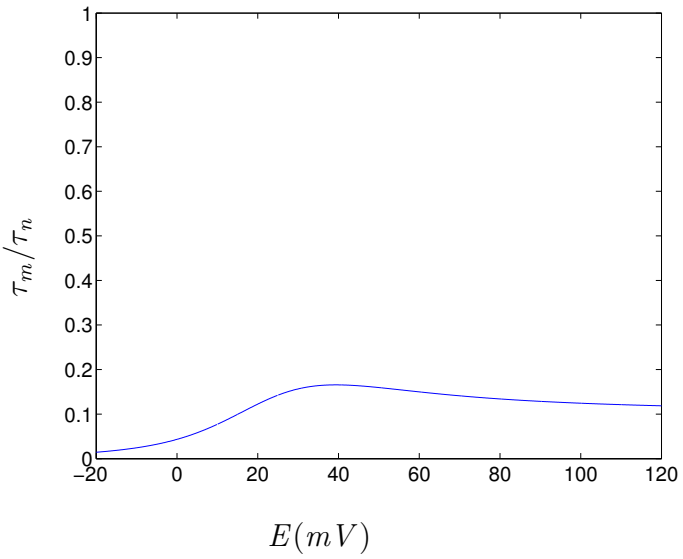

Figure 2.17: Graph of $\frac{\tau_m}{\tau_n}$ against voltage.

Now the second order system is:

$$\begin{aligned} \frac{\mathrm{d}E}{\mathrm{d}t} &= -(\overline{g}_K n^4(E-E_K) + \overline{g}_{Na}\overline{m}^3(G-n)(E-E_{Na}) + \overline{g}_l(E-E_l)) \\ &\quad +I_b, \qquad (2.42) \\ \frac{\mathrm{d}n}{\mathrm{d}t} &= \alpha_n(1-n) - \beta_n n = \frac{(\overline{n}-n)}{\tau_n}. \qquad (2.43) \end{aligned}$$

Therefore the original system has been reduced to a second order system of equations by conditions (2.38) and (2.41). Therefore, m and h are now functions of E.

As second order systems can be analysed by qualitative methods, we can see that by a simple coordinate transformation this second order system can be converted to a form similar to the van der Pol equations.

2.5.3 Phase portrait of the second order system

In the second order system E is the fast variable and n is the slow variable. We want to find the isoclines (nullclines).

The n isocline is:

$$n = \overline{n}.$$

The n intercept is (E, n)=$(0, 0.32)$ and the E intercept is (E, n)=$(10, 0)$.

The E isocline is:

$$\overline{g}_{Na}\overline{m}^3(G - n)(E - E_{Na}) + \overline{g}_K n^4(E - E_K) + \overline{g}_l(E - E_l) - I_b = 0.$$

The n intercept and the E intercept depends on the values of G and I_b. So the equation for E=0 is:

$$\overline{g}_{Na}\overline{m}^3(G - n)E_{Na} + \overline{g}_K n^4 E_K + \overline{g}_l E_l - I_b = 0.$$

This will give an N-shaped curve. For n=0 the equation is:

$$\overline{g}_{Na}\overline{m}^3 G(E - E_{Na}) + \overline{g}_l(E - E_l) - I_b = 0.$$

The singular point satisfies the following equation:

$$\overline{g}_K\overline{n}^4(E - E_K) - \overline{g}_{Na}(G - \overline{n})\overline{m}^3(E - E_{Na}) + \overline{g}_l(E - E_l) - I_b = 0.$$

Figure 2.18 shows the phase portraits for system (2.42) for different values of G and I_b. We see that for I_b=0 we have a stable equilibrium point and the trajectories for systems (2.42) and (2.31) travel to the equilibrium point for any value of G. For $I_b \neq 0$ we have an unstable equilibrium point and the trajectories form a limit cycle.

We can compare Fig. 2.18(a) to the FitzHugh system, Fig. 2.8(a) and we see that they are similar. In both systems we have isoclines that are similar to each

other. Also the trajectories don't always go monotonically to the equilibrium point, but some might have to take a longer path to get to it. This is similar to the trajectory in FitzHugh's phase portrait, Fig. 2.8(a) (-) as that doesn't go straight to the equilibrium point, so here excitation also occurs.

We can see that the two systems are similar by just looking at the equations, as the FitzHugh system is based on the van der Pol equations and Krinsky and Kokoz's second order system is similar to the generalised van der Pol system, so the phase portraits are going to be alike.

The difference between the FitzHugh and Krinsky and Kokoz systems is that Krinsky and Kokoz obtained results by the reduction of high order, complicated empirical systems of ordinary differential equations; and FitzHugh used the van der pol equations by ab initio construction of simplest nonlinear ordinary differential equations with required behaviour.

2.5.4 Reduction of Noble's 1962 model by Krinsky and Kokoz

In Krinsky and Kokoz's papers[42, 43] they obtained a second order system for Noble's 1962 model, by adiabatically eliminating the m variable and saying that:

$$\tau_m, \tau_h \ll \tau_n,$$

and that m and h are equally fast and much faster than E, based on the value of the membrane resistance outside the fast upstroke, which is determined mainly by the potassium conductance. Therefore the characteristic time of the charge of the membrane capacitance is large, $\tau_e \approx C_m/\overline{g}_K \approx 10^{-2}$sec, and m and h are replaced with their quasi-stationary values.

Once the second order system is found, due to these two findings, then the nullclines can be found and drawn. They use the method of nullclines to analyse the properties of excitable cells and the oscillatory behaviour of the second order system. They use this method, for example, to study the boundaries between oscillatory and excitable behaviour. From this the boundaries for the parameter regions, where the oscillatory behaviour can be observed, are found.

Therefore they found two new properties of Noble's equations, which are: the complete absence of accommodation and the easiness of repetitive responses. So the electrophysiological characteristics obtained from Noble's original system and the reduced system differ by no more than 1 to 3%.

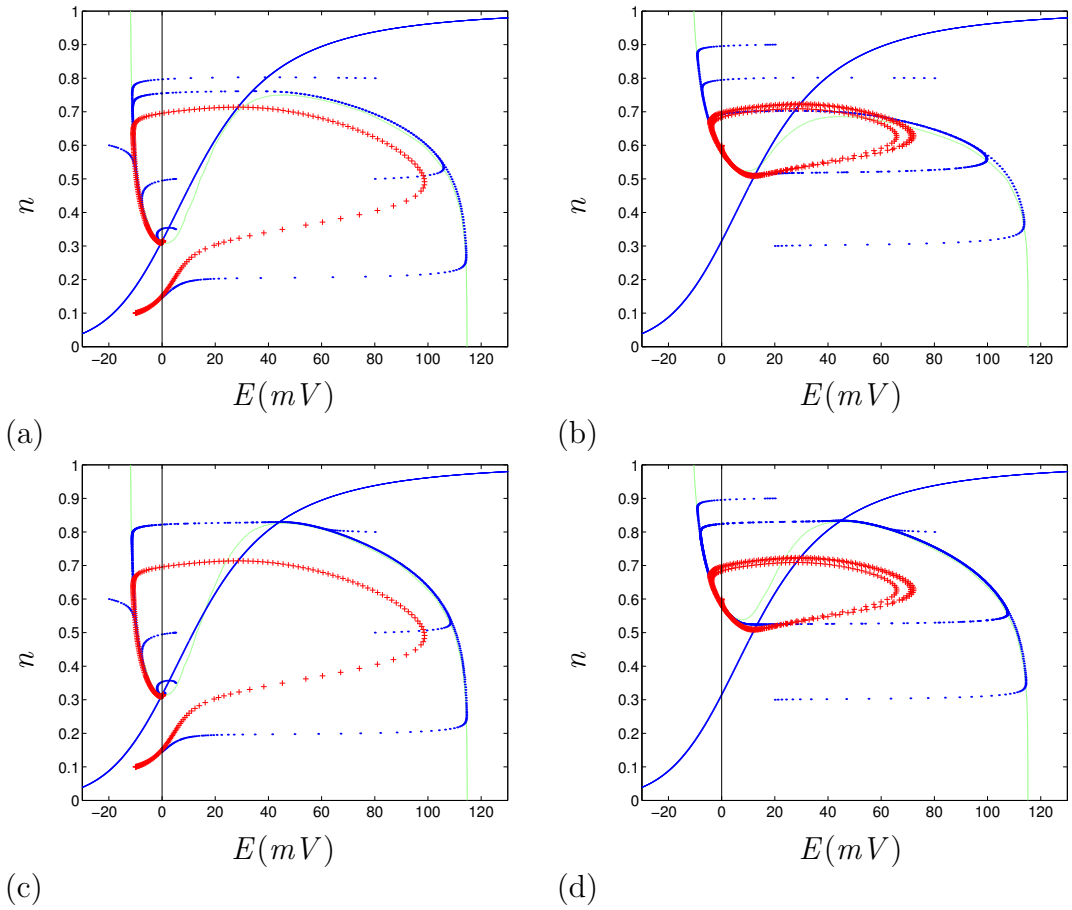

Figure 2.18: Phase portrait of the second order system (2.42) with two isoclines $\dot{n}$=0 (-) and $\dot{E}$=0 (:), and trajectories for system (2.42) (.) and the original system (2.31) (+) for (a) G=0.87 and I=0, (b) G=0.76 and I=50, (c) G=1 and I=0 and (d) G=1 and I=50.

Therefore the accuracy of Noble's equations is estimated and was found to be more accurate than the approximation for the Hodgkin-Huxley model, as the accuracy for the four-dimensional equations and the two-dimensional equations in the Hodgkin-Huxley model, differ by 10 to 15%.

Since these four papers, their methods have been used by others[45, 46] to study variations of the Hodgkin-Huxley model.

2.5.5 Further models using Krinsky and Kokoz's methods

Models concerning the development of membranes in the heart have been simplified using asymptotic methods similar to Krinsky and Kokoz's methods.

In 1994 Vinet and Roberge[47] wrote a paper using methods that were analogous to FitzHugh's[4, 34] and Krinsky and Kokoz's[8] work on reducing the Hodgkin-Huxley system of equations to a two-dimensional system. They used these methods on a variation of the Hodgkin-Huxley model (Beeler-Reuter model[20]) involving six voltage-dependent gating variables, to obtain a simplified model that would preserve the essential features of the action potential.

The action potential upstroke, plateau and repolarization phase in this model occur for different time stages, e.g. fast, intermediate and slow.

We will use similar methods to analyse Courtemanche et al's model in Chapter 6, as we split Courtemanche et al's model up into three time stages so that we can analyse each stage separately and reduce the system to a smaller number of variables.

First Vinet and Roberge adiabatically eliminate the m variable, which is super-fast, and then for the fast stage, where the upstroke occurs, they consider all other variables, except V, to be equal to their initial values. So therefore the system is reduced to one-dimension (V) and then they can draw the V nullcline for this equation to see how many equilibrium points there are and if they are stable or unstable.

For the intermediate stage they notice that h is only partially closed, so V and h are equally fast, similar to our reduction of Noble's model in Chapter 4, and therefore all other variables are equal to their initial values, so they obtain a two-dimensional system (V, h).

These two systems successfully reproduce the original systems main excitability properties.

For the slow stage they reduced the system to three variables, where V is

small compared to d, m and h, and I_{Na}=0 because of a small overlap between $\overline{m}$ and $\overline{h}$. As they cannot assume d reaches its steady state instantaneously due to faster repolarization then they approximate $x_1 \approx 1 - f$. So they have a three-dimensional model (V, d, f).

This was an efficient approach to simplifying a complicated model. However, they did not use explicit asymptotic analysis for their approximations, they did not formally identify different time scales and they did not use any phase plane analysis for the fast and slow stages.

Another example of using Krinsky's and Kokoz's methods is in work by Enns-Ruttan[48], where she uses the Kepler-Marder model[49] to study spontaneous secondary spiking in this Hodgkin-Huxley type system.

Enns-Ruttan studies and compares the results using two reductions, FitzHugh-Nagumo and Krinsky and Kokoz. She reduces the Kepler-Marder model to three equations instead of five, by using the FitzHugh-Nagumo reduction on the four Hodgkin-Huxley type equations (V, m, h, n) to two equations (V, U), and then using a Tikhonov style embedding of the slow system to see what happens to the action potential as $\epsilon \to 0$.

Then Enns-Ruttan compared these results with the reduction of the four Hodgkin-Huxley equations to two equations by using a Krinsky and Kokoz type reduction. This shows that Krinsky and Kokoz's methods can be used universally for different research.

Bernus et al[50] wrote a paper about the human ventricular cell by Priebe-Beuckelmann[51] in 2002. Bernus et al studied the Priebe-Beuckelmann model and then reduced this system to a six variable model using methods similar to what we used in our study of Courtemanche et al's model in Chapter 6, and also methods that would keep the numerical accuracy and stability of the reduced model, but they did not do any formal asymptotic analysis.

Their reduced model was 4.9 times faster for numerical computations and is more stable than the original model. It also retained all the properties and qualitative behaviour of the original model and was suitable for efficient and accurate studies of re-entrant phenomena in human ventricular tissue.

Papers have also been written studying high-order, non-linear systems, because these systems cannot be solved analytically and numerical study is complicated. So papers were written to solve this problem, by developing simple models, e.g. second order, to describe the integral characteristics of the propagation pulse,

the membrane potential and inward and outward currents[52, 53, 54, 55, 56].

2.5.6 Summary

Krinsky and Kokoz showed that it is possible to reduce the system of nerve equations to two equations, even though their theory of reducing the equations is not rigorously justified, e.g. $G=n+h$. Zeeman said that this was not possible for a system with small parameters, but Krinsky and Kokoz's reduced system doesn't contain any small parameters and this is why it was possible for them to reduce the Hodgkin-Huxley system to two equations and Zeeman's "nerve" model was in three dimensions.

We will use methods described here in the analysis of Courtemanche et al's model.

Chapter 3

Hodgkin-Huxley Model: Tikhonov's Approach

We have described Hodgkin-Huxley's model in Section 2.1.1, so now we want to use Tikhonov's approach and Zeeman's methods for finding the slow manifold, fast foliation and cusp to see what asymptotic structure this system has and the solutions we obtain from our analysis. We do this without assuming $n + h$ is constant. We don't use Krinsky and Kokoz's assumption because it is not rigorously justified and we want to use methods that can be used again on more complicated systems.

3.1 Looking For Small Parameters In The Hodgkin-Huxley Model

In this section we use the Hodgkin-Huxley system of equations to see if we can answer our question "Can we successfully reduce the system to a third order system of equations without causing too much change to the action potential?"

$$\begin{aligned}
\frac{\mathrm{d}V}{\mathrm{d}t} &= -(\overline{g}_K n^4(V - V_K) + \overline{g}_{Na} m^3 h(V - V_{Na}) + \overline{g}_l(V - V_l)),\\
\frac{\mathrm{d}n}{\mathrm{d}t} &= \alpha_n(1 - n) - \beta_n n = \frac{(\overline{n} - n)}{\tau_n},\\
\frac{\mathrm{d}m}{\mathrm{d}t} &= \alpha_m(1 - m) - \beta_m m = \frac{(\overline{m} - m)}{\tau_m},\\
\frac{\mathrm{d}h}{\mathrm{d}t} &= \alpha_h(1 - h) - \beta_h h = \frac{(\overline{h} - h)}{\tau_h}.
\end{aligned}$$

To reduce the system to three equations, we need to find which of these equations is the fastest, so we can solve it and exclude it from the system. We can use the same method as we used in Section 2.5, by drawing a graph of the τ's against V. As we don't have τ_V defined then we use a new definition to draw all the τ's. The definition is obtained from the equations of y where:

$$\frac{\mathrm{d}y}{\mathrm{d}t} = \frac{(\overline{y} - y)}{\tau_y},$$

as the gating variables contain the functions τ, and $\frac{\mathrm{d}V}{\mathrm{d}t}$ can be written in this form by rearranging its right-hand side.

Therefore we obtain the definition by differentiating the equation above:

$$\begin{aligned} \frac{\partial}{\partial y}\left(\frac{\mathrm{d}y}{\mathrm{d}t}\right) &= -\frac{1}{\tau_y}, \\ \tau_y &= \left|\frac{\partial}{\partial y}\left(\frac{\mathrm{d}y}{\mathrm{d}t}\right)\right|^{-1}. \end{aligned}$$

So this is the reason why we use this definition to find the τ's and it is the most reliable method to use.

We can see from Fig. 3.1 that τ_m is the fastest compared to τ_n and τ_h, but τ_V is faster than τ_m for large voltage and τ_m is faster than τ_V for small voltage. So V is a fast variable as well and V may be faster than m for a small time. Technically, we already knew this was true from Krinsky and Kokoz as they used the Hodgkin-Huxley equations with a slight modification, $E{=}{-}V$, which means that E is the reversal potential. Therefore the results should be the same except that Krinsky and Kokoz didn't draw τ_V, so the results are the same except that now we can treat V as a fast variable for a small amount of time. As V is only fast for a small moment of time then we will say that m is a super-fast variable and V is a fast variable.

For the original system we draw the graph of m against time and $\overline{m}$ against time to see the differences in the systems. This can be seen in Fig. 3.2. We see that they start from the same initial point and as we get closer to $m{=}\overline{m}{=}0$, and the voltage increases, then the graphs become the same. Both functions m and $\overline{m}$ for each value of V are similar, there is just a small difference between them.

This is why we can replace $\frac{\mathrm{d}m}{\mathrm{d}t}$ by zero, so m is a given function of V.

$$m = \overline{m} = \frac{\alpha_m}{\alpha_m + \beta_m}.$$

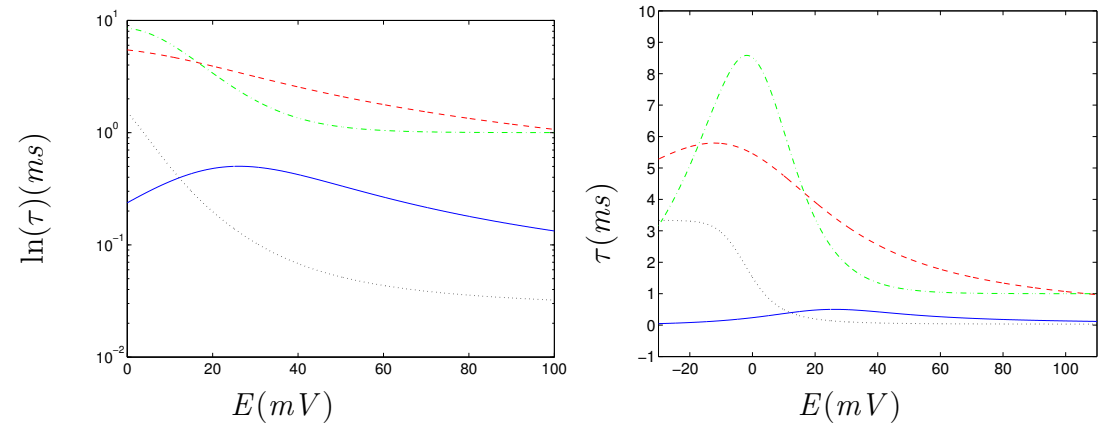

(a) (b)

Figure 3.1: Graph of τ_n (- -), τ_m (-), τ_h (-.) and τ_V (.) against V. (a) is drawn using a logarithmic scale on the vertical axis for the τ's and (b) is drawn using a real scale on the vertical axis for the τ's.

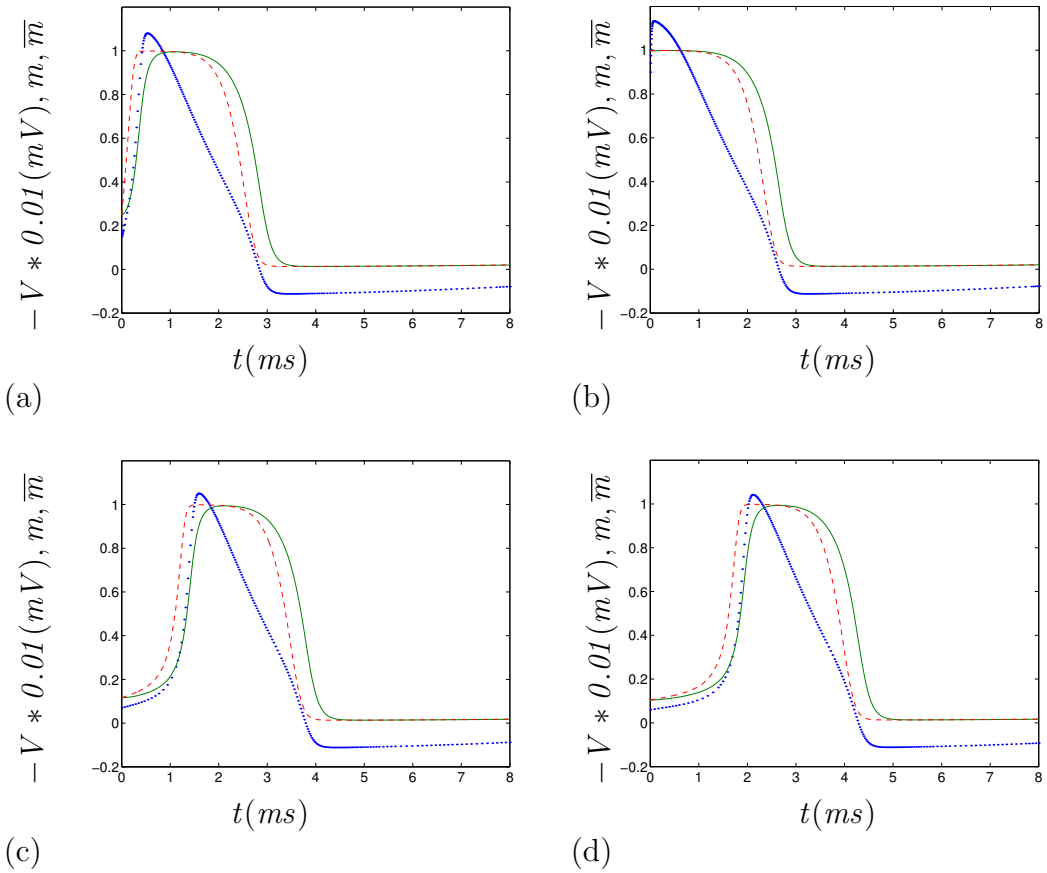

(a) (b) (c) (d)

Figure 3.2: Graphs of m (-), $\overline{m}$ (- -), $-V*0.01$ (.) against time for initial values (m_0, n_0, h_0)=$(0.0530, 0.3177, 0.5961)$ with T^o=6°C and (a) V_0=15, (b) V_0=90, (c) V_0=7 and (d) V_0=6.

3.1.1 The V, n, h reduced system

With m eliminated, the system becomes:

$$\begin{aligned}
\frac{\mathrm{d}V}{\mathrm{d}t} &= -(\overline{g}_K n^4(V - V_K) + \overline{g}_{Na}\overline{m}^3 h(V - V_{Na}) + \overline{g}_l(V - V_l)), \qquad (3.1)\\
\frac{\mathrm{d}h}{\mathrm{d}t} &= \alpha_h - (\alpha_h + \beta_h)h = \frac{(\overline{h} - h)}{\tau_h},\\
\frac{\mathrm{d}n}{\mathrm{d}t} &= \alpha_n - (\alpha_n + \beta_n)n = \frac{(\overline{n} - n)}{\tau_n}.
\end{aligned}$$

For the reduced system and the original system we drew the graphs of negative voltage against time to see how close the reduced system is to the original. We do this for different initial values of V, i.e. V_0. We see from Fig. 3.3 that the further away from the threshold we are the closer the graphs become, for example if the initial value is V_0=90; but the closer we are to the threshold the more the graphs are different. Therefore the latency for the rapid depolarisation of the action potential decreases as the initial V_0 increases.

3.1.2 Introducing a small parameter ϵ

We want to keep the qualitative behaviour of the reduced system the same as the original system, i.e. not much difference between them. So to do this we use the procedure of parametric embedding that we introduced in Section 2.3.4, where we introduce a small parameter $\epsilon \ll 1$ ($\epsilon \to 0$) to the $\dot{m}$ equation in the original system. We introduce it to the $\dot{m}$ equation as m is the fastest variable.

So the $\dot{m}$ equation becomes:

$$\frac{\mathrm{d}m}{\mathrm{d}t} = \frac{1}{\epsilon}(\alpha_m(1 - m) - \beta_m m).$$

Therefore all the results are correct in the limit $\epsilon \to 0$.

We can see in Fig. 3.4 that there is still a small difference between the two curves. If ϵ gets closer to zero then the difference becomes even smaller and almost impossible to see, so the two curves become identical. A small value of ϵ for V_0=15 and V_0=90, makes the difference small as we see in Figs. 3.4(a) and (b), but the value of ϵ doesn't work for V_0=7 and V_0=6 as we can see in Figs. 3.4(c) and (d), because we are close to the threshold, so we need an even smaller value of ϵ to make the difference smaller. Once we've done that then the two systems give identical curves.

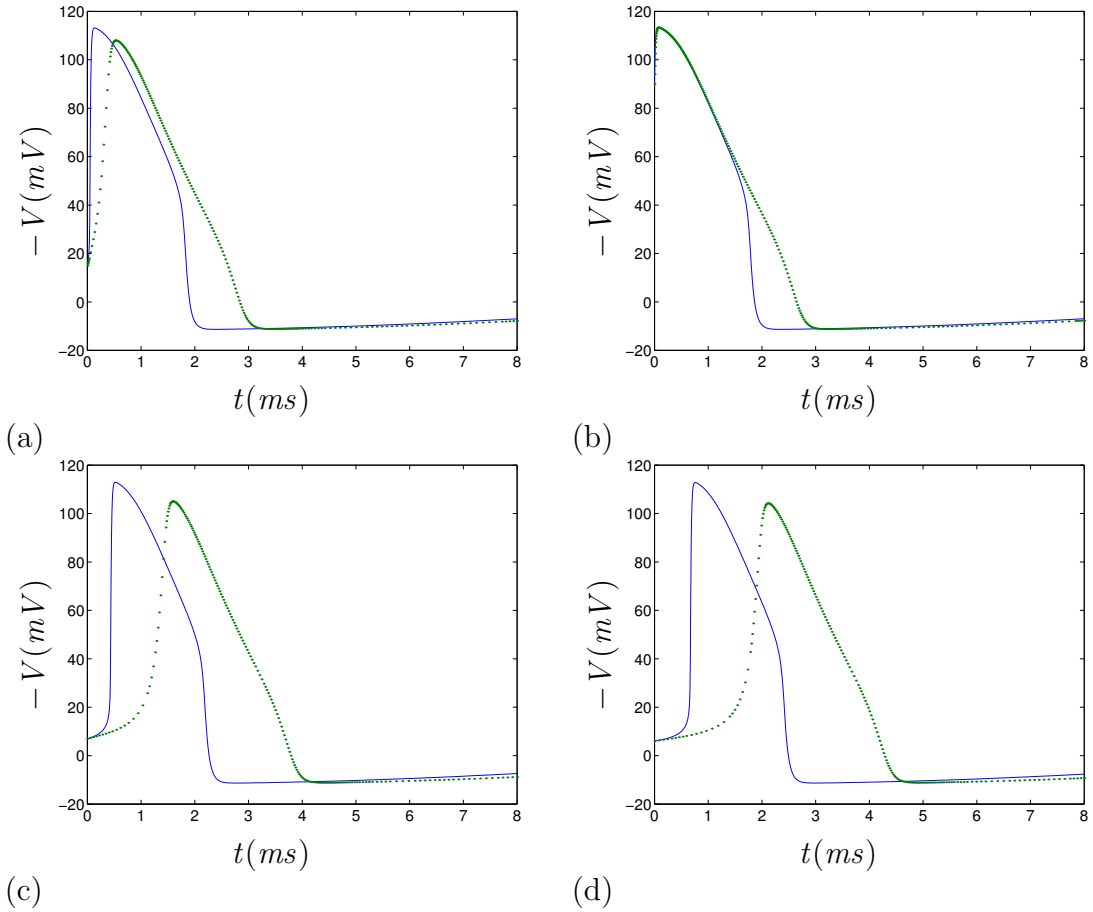

Figure 3.3: Graphs of $-V$ against t for T^o=6°C and different initial values of V_0, for the reduced system (3.1) (-) and the original Hodgkin-Huxley system (.). (a) V_0=15, (b) V_0=90, (c) V_0=7 and (d) V_0=6.

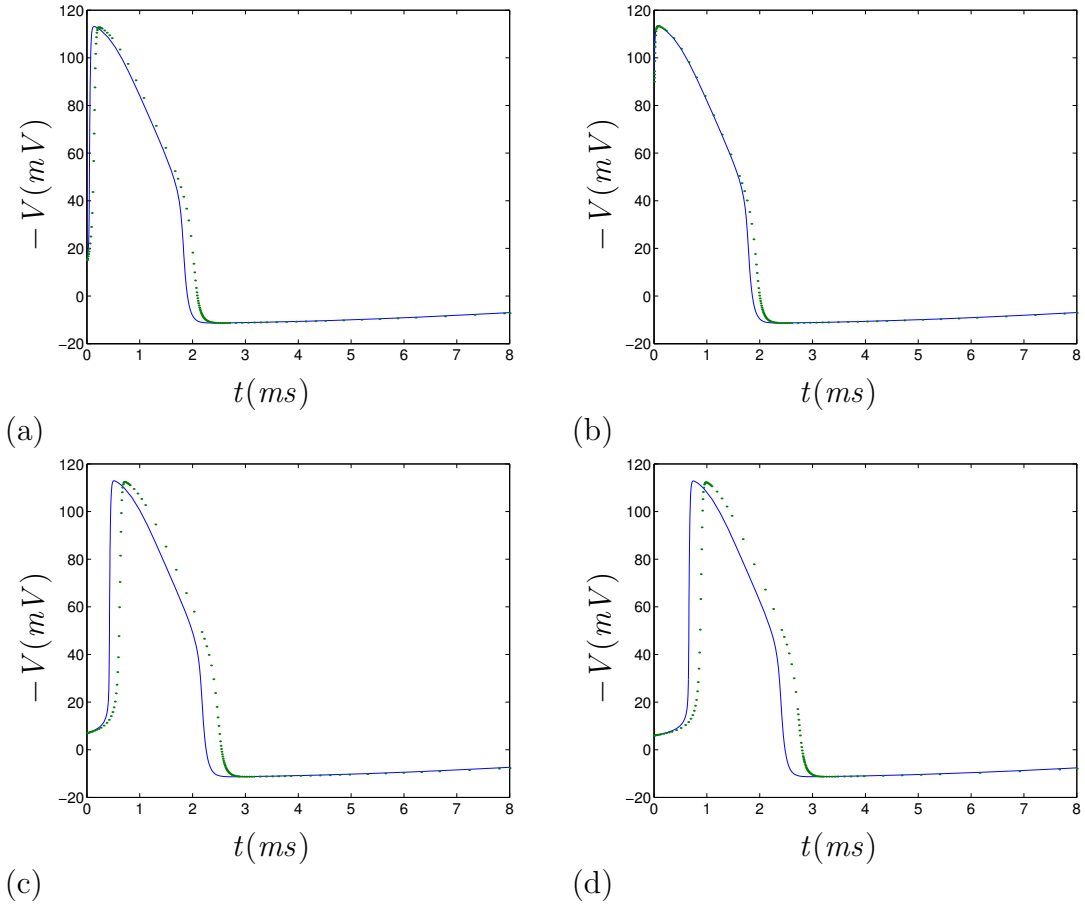

Figure 3.4: Graphs of $-V$ against t for the reduced system (3.1), $m(t)=\overline{m}(E(t))$, $\epsilon=0$, (-) and the original Hodgkin-Huxley system (.) with $T^o=6^oC$, $\epsilon=0.1$ and (a) $V_0=15$, (b) $V_0=90$, (c) $V_0=7$ and (d) $V_0=6$.

After seeing the differences in the two curves, we know that m is not always the fast variable, but from our speed analysis we know that V is the fast variable for small moments of time. So we draw the τ's for different initial V_0 to see what this does to the τ's.

In Fig. 3.5 we have τ_n, τ_m, τ_h and τ_V against time for the original system to see what happens to them. Functions τ_n, τ_m, τ_h and τ_V depend on time because V depends on time and as all four are functions of V then they all depend on time. If we get close to the threshold, as in Fig. 3.5 (c) and (d), then m becomes faster than V. If we are far away from the threshold, as in Fig. 3.5(b), then V is faster than m for a few milliseconds and then m is faster than V.

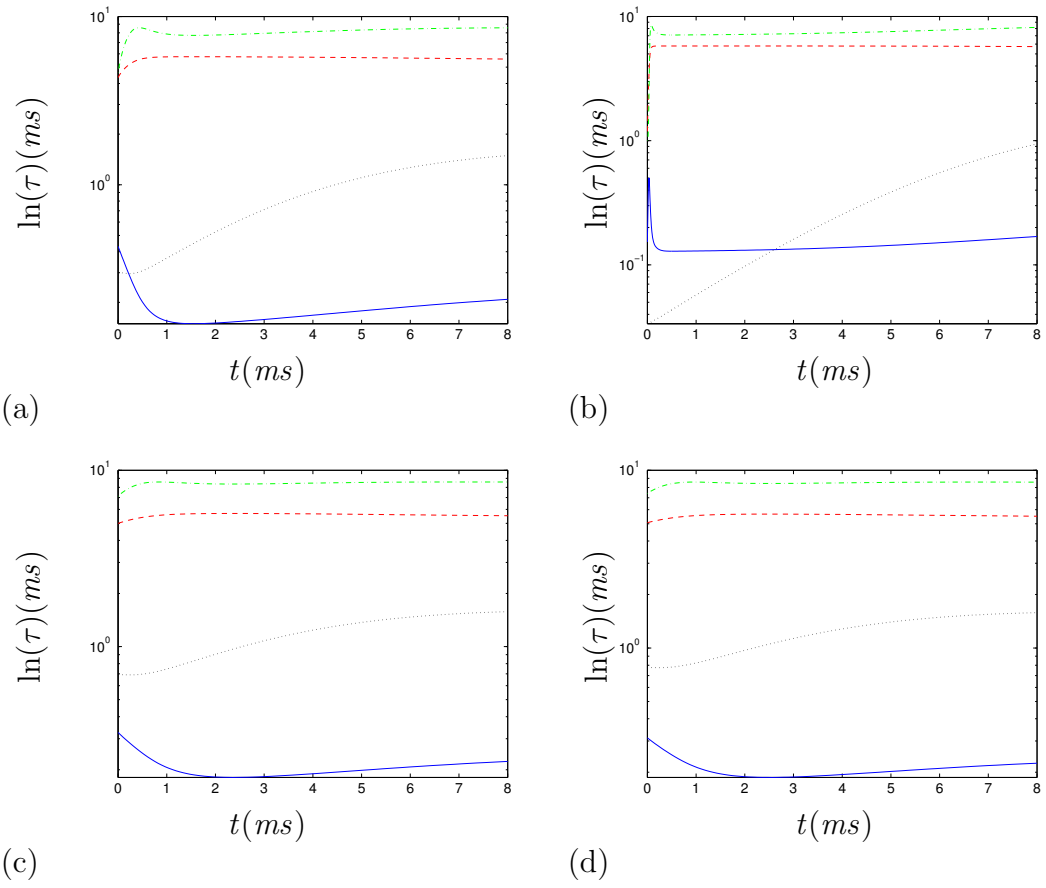

Figure 3.5: Graph of τ_n (–), τ_m (-), τ_h (-.) and τ_V (.) against time drawn using a logarithmic scale on the vertical axis for the τ's with T^o=6°C and (a) V_0=15, (b) V_0=90, (c) V_0=7 and (d) V_0=6.

Figure 3.5 is drawn for temperature being 6°C and we see that the further away from the threshold we are, then the more chance of τ_V being faster than τ_m. So if we change the temperature at the points furthest away from the threshold,

then τ_V and τ_m will interchange.

For other values of temperature we will now see if V can become consistently faster or consistently slower than m. For some moments in time we have $\tau_V > \tau_m$ and for other moments in time we have $\tau_V < \tau_m$.

As τ_V and τ_m depend on temperature in the original system we want to see for what temperature $\tau_V > \tau_m$ and $\tau_V < \tau_m$ for higher voltages, as τ_m is always greater than τ_V for any temperature if we are close to the threshold. We say that the ratio of the two τ's can either be greater than one or less than one for all times. So,

$$r(t) = \frac{\tau_m}{\tau_V}.$$

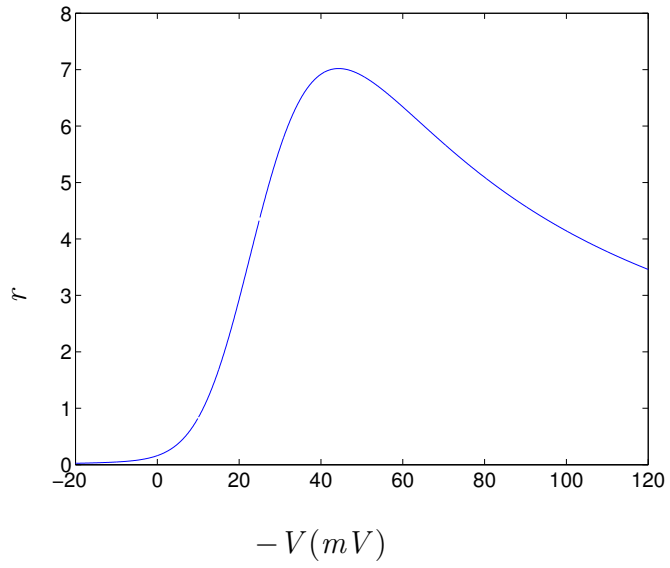

Figure 3.6: Graph of r against $-V$.

From Fig. 3.6 we see that the maximum of the graph is at 7.019. As we use the original system to draw the graphs of the τ's, then we have,

$$\phi C_M \sim \frac{\tau_V}{\tau_m}.$$

Here C_M=1 and ϕ depends on temperature. So,

$$\phi \sim \frac{\tau_V}{\tau_m} < 1.$$

This says for large ϕ, V is a slow variable and for small ϕ, V is a fast variable. So now τ_V is a fixed function of temperature and time. Therefore we can say that:

$$\tau_V(T^o, t) = \tau_V(T_0^o, t)\phi.$$

So the ratio becomes:

$$r(T^o, t) = \frac{\tau_m(t)}{\tau_V(T^o, t)} = \frac{\tau_m(t)}{\tau_V(T_0^o, t)\phi} \leq 1,$$

for all time. So,

$$\begin{aligned} 1 &\geq \max\left(\frac{\tau_m}{\tau_V}\right)\frac{1}{\phi}, \\ \phi &\geq \max\left(\frac{\tau_m}{\tau_V}\right), \\ \phi &\geq 7.0196, \\ 3^{(T^o-6.3)/10} &\geq 7.0196. \end{aligned}$$

We take logs of both sides to obtain:

$$T^o \geq 24.03^o\text{C}.$$

This says for temperatures above 24.03°C, $\tau_V > \tau_m$ throughout the action potential, and for temperatures below 24.03°C, $\tau_V > \tau_m$ in the beginning of the action potential and $\tau_V < \tau_m$ later.

From Fig. 3.6 we see that the minimum of the graph is at 0.0248. As we use the original system to draw the graphs of the τ's, then we have,

$$r(T^o, t) \geq 1,$$

for all time. So,

$$\begin{aligned} 1 &\leq \min\left(\frac{\tau_m}{\tau_V}\right)\frac{1}{\phi}, \\ \phi &\leq \min\left(\frac{\tau_m}{\tau_V}\right), \\ \phi &\leq 0.0248, \\ 3^{(T^o-6.3)/10} &\leq 0.0248. \end{aligned}$$

We take logs of both sides to obtain:

$$T^o \leq -27.35^o\text{C}.$$

This says for temperatures below −27.35°C, $\tau_V > \tau_m$ consistently, and for temperatures above −27.35°C, $\tau_V > \tau_m$ in the beginning of the action potential and $\tau_V < \tau_m$ later.

3.1.3 If the voltage was the fastest variable

We want to see if we can find m another way, for example by putting $\frac{\mathrm{d}V}{\mathrm{d}t}$=0. It is not possible to resolve $\frac{\mathrm{d}V}{\mathrm{d}t}$ with respect to V, so we resolve it with respect to m by projecting the slow manifold $\frac{\mathrm{d}V}{\mathrm{d}t}$=0 to the (V, n, h) space, rather than the (m, n, h) space.

$$m = \left(\frac{-(\overline{g}_K n^4 (V - V_K) + \overline{g}_l (V - V_l))}{\overline{g}_{Na} h (V - V_{Na})} \right)^{1/3}.$$

Substitute this into $\dot{m}$ to obtain:

$$\frac{\mathrm{d}m}{\mathrm{d}t} = \alpha_m - (\alpha_m + \beta_m) \left(\frac{-(\overline{g}_K n^4 (V - V_K) + \overline{g}_l (V - V_l))}{\overline{g}_{Na} h (V - V_{Na})} \right)^{1/3}.$$

Differentiate m with respect to time and equate it to the right hand side of the above equation.

$$\frac{\mathrm{d}m}{\mathrm{d}t} = \frac{\partial m}{\partial V}\dot{V} + \frac{\partial m}{\partial h}\dot{h} + \frac{\partial m}{\partial n}\dot{n}.$$

So after rearranging we obtain the final equation to be:

$$\begin{aligned} \dot{V} &= \frac{3\overline{g}_{Na} h m^2 (V - V_{Na})^2 (\alpha_m - (\alpha_m + \beta_m)m) - \dot{h}(V - V_{Na})(\overline{g}_K n^4 (V - V_K)}{h(\overline{g}_K n^4 (V_{Na} - V_K) + \overline{g}_l (V_{Na} - V_l))} \\ &\quad + \frac{\overline{g}_l (V - V_l)) + 4\dot{n}\overline{g}_K h n^3 (V - V_{Na})(V - V_K)}{h(\overline{g}_K n^4 (V_{Na} - V_K) + \overline{g}_l (V_{Na} - V_l))}. \end{aligned}$$

Therefore the reduced system of equations is:

$$\begin{aligned} \dot{V} &= \frac{3\overline{g}_{Na} h m^2 (V - V_{Na})^2 (\alpha_m - (\alpha_m + \beta_m)m) - \dot{h}(V - V_{Na})(\overline{g}_K n^4 (V - V_K)}{h(\overline{g}_K n^4 (V_{Na} - V_K) + \overline{g}_l (V_{Na} - V_l))} \\ &\quad + \frac{\overline{g}_l (V - V_l)) + 4\dot{n}\overline{g}_K h n^3 (V - V_{Na})(V - V_K)}{h(\overline{g}_K n^4 (V_{Na} - V_K) + \overline{g}_l (V_{Na} - V_l))}, \\ \dot{n} &= \alpha_n - (\alpha_n + \beta_n)n, \\ \dot{h} &= \alpha_h - (\alpha_h + \beta_h)h. \end{aligned}$$

With,

$$m = \left(\frac{-(\overline{g}_K n^4 (V - V_K) + \overline{g}_l (V - V_l))}{\overline{g}_{Na} h (V - V_{Na})} \right)^{1/3}.$$

The graphs of negative voltage against time, Fig. 3.7, can be seen for different initial values of V. We can see that the new reduced system is not at all close to the original system especially near the threshold, so this is not a good approximation for m and the original approximation we used is better.

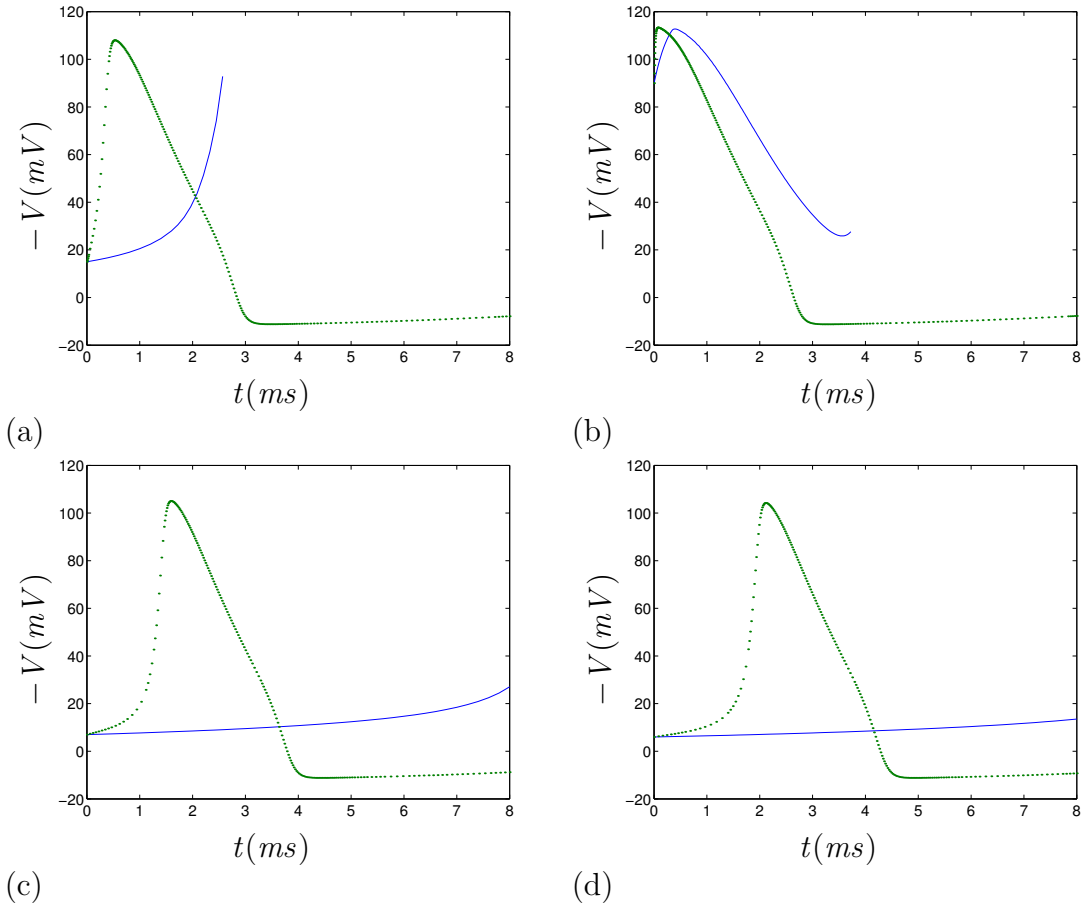

Figure 3.7: Graph of $-V$ against t for the new reduced system (-) and the original Hodgkin-Huxley system (.) for (a) V_0=15, (b) V_0=90, (c) V_0=7 and (d) V_0=6.

3.1.4 Summary

We've seen that we can reduce the original Hodgkin-Huxley system to a third order system, but as a result there is a change of shape in the action potentials of the third order system. We see this especially around the return. We therefore have a smooth return in the original system and this changes to a jump return in the reduced system. In answer to our question, we can say that yes we can successfully reduce the system of equations without causing too much change to the action potential for large initial values of V. The difference between the curves is large for values of V close to the threshold. We also see that by eliminating the other fast variable V instead of m doesn't make any sense, as the behaviour of the reduced system is completely different from the original system.

For our approximation, i.e. do we change m or V, we have two features:

1. excitable behaviour, and
2. the smooth return.

If we eliminate m, feature (1) is preserved, but feature (2) isn't. If we eliminate V we see that neither of them is preserved. So from this it is more logical to eliminate m as one feature is preserved and try to find other methods of preserving the second feature.

So therefore we have a $(2, 1, 1)$ asymptotic embedding where we have two slow variables n and h, one fast variable V and one super-fast variable m.

3.2 Properties of the Third Order Reduced Hodgkin-Huxley System

We want to test Zeeman's hypothesis of there being a cusp catastrophe in a three dimensional system. We take the third order Hodgkin-Huxley system, (3.1), that we obtained in Section 3.1 and we use Krinsky and Kokoz's notations, i.e. $E{=}{-}V$, and the methods we derived in Section 2.5, i.e. introducing ϵ to the fast equation, to see if we can obtain a cusp.

3.2.1 Hodgkin-Huxley's third order system

The Hodgkin-Huxley system is:

$$\begin{aligned}
\frac{\mathrm{d}E}{\mathrm{d}t} &= -(\overline{g}_K n^4(E-E_K)+\overline{g}_{Na}\overline{m}^3 h(E-E_{Na})+\overline{g}_l(E-E_l)),\\
\frac{\mathrm{d}n}{\mathrm{d}t} &= \alpha_n(1-n)-\beta_n n=\frac{(\overline{n}-n)}{\tau_n},\\
\frac{\mathrm{d}h}{\mathrm{d}t} &= \alpha_h(1-h)-\beta_h h=\frac{(\overline{h}-h)}{\tau_h}.
\end{aligned}$$

We have seen that after m, E is the fastest variable. So now we consider $\dot{E}$ as the fast equation and $\dot{n}$ and $\dot{h}$ as the slow equations. So we have reduced the $(2,1,1)$ asymptotic structure to a $(2,1)$ structure.

3.2.2 Slow manifold and fast foliation

We now use the theory in Section 2.5 to introduce a small parameter ϵ to the $\dot{E}$ equation, where $\epsilon \ll 1$ and this ϵ is not the same ϵ as in Section 3.1. We do this because we can't find the slow manifold and fast foliation without an independent parameter in the system as all the parameters depend on E. So the system becomes:

$$\begin{aligned}
\epsilon\frac{\mathrm{d}E}{\mathrm{d}t} &= -(\overline{g}_K n^4(E-E_K)+\overline{g}_{Na}\overline{m}^3 h(E-E_{Na})+\overline{g}_l(E-E_l)), \qquad (3.2)\\
\frac{\mathrm{d}n}{\mathrm{d}t} &= \alpha_n(1-n)-\beta_n n,\\
\frac{\mathrm{d}h}{\mathrm{d}t} &= \alpha_h(1-h)-\beta_h h.
\end{aligned}$$

This is the slow system and it gives the slow manifold.

We introduce the variable $t{=}\epsilon T$ to give us the fast system which we find the fast foliation from.

$$\begin{aligned}
\frac{\mathrm{d}E}{\mathrm{d}T} &= -(\overline{g}_K n^4(E-E_K)+\overline{g}_{Na}\overline{m}^3 h(E-E_{Na})+\overline{g}_l(E-E_l)), \qquad (3.3)\\
\frac{\mathrm{d}n}{\mathrm{d}T} &= \epsilon(\alpha_n(1-n)-\beta_n n),\\
\frac{\mathrm{d}h}{\mathrm{d}T} &= \epsilon(\alpha_h(1-h)-\beta_h h).
\end{aligned}$$

System (3.2) gives us the slow manifold, if $\epsilon{=}0$ and $f(E,n,h){=}(\overline{g}_K n^4(E-E_K)+\overline{g}_{Na}\overline{m}^3 h(E-E_{Na})+\overline{g}_l(E-E_l)){=}0$.

The slow manifold is:

$$
\begin{aligned}
h &= -\frac{(\overline{g}_K n^4(E-E_K)+\overline{g}_l(E-E_l))}{\overline{g}_{Na}\overline{m}^3(E-E_{Na})},\\
\dot{n} &= \alpha_n-(\alpha_n+\beta_n)n,\\
\dot{h} &= \alpha_h-(\alpha_h+\beta_h)h.
\end{aligned}
$$

System (3.3) gives us the fast foliation, if ϵ=0.

$$
\begin{aligned}
n &= \text{constant},\\
h &= \text{constant},\\
\frac{\mathrm{d}E}{\mathrm{d}T} &= -(\overline{g}_K n^4(E-E_K)+\overline{g}_{Na}\overline{m}^3 h(E-E_{Na})+\overline{g}_l(E-E_l)).
\end{aligned}
$$

3.2.3 Fold curve

Our slow manifold is:

$$f(E,n,h)=\overline{g}_K n^4(E-E_K)+\overline{g}_{Na}\overline{m}^3 h(E-E_{Na})+\overline{g}_l(E-E_l)=0.$$

This is the equation of the curved surface in $\mathbb{R}^3$. To find the fold curve we want to project the surface down along the fast foliation, i.e. along the E axis to the (n,h) plane.

The direction of the projection is:

$$\begin{pmatrix} E\\ n\\ h\end{pmatrix}=\begin{pmatrix}1\\0\\0\end{pmatrix}=\underline{p}.$$

At every point we can define a normal vector $\underline{n}$. If $\underline{p}$ is tangent to a point on the slow manifold, then we have a normal to that point which is perpendicular to $\underline{p}$. So we want to find the dot product of $\underline{n}$ and $\underline{p}$.

So,

$$\underline{n}=\left(\frac{\partial f}{\partial E},\frac{\partial f}{\partial n},\frac{\partial f}{\partial h}\right).$$

We want to differentiate f with respect to E. Therefore we obtain:

$$\frac{\partial f}{\partial E}=\overline{g}_K n^4+\overline{g}_l+\overline{g}_{Na}h[\overline{m}^3+3\overline{m}^2(E-E_{Na})\overline{m}'].$$

If we take the dot product of $\underline{n}$ and $\underline{p}$ we obtain:

$$\overline{g}_K n^4 + \overline{g}_l + \overline{g}_{Na} h(\overline{m}^3 + 3\overline{m}^2(E - E_{Na})\overline{m}') = 0.$$

So the fold curve satisfies the two equations:

$$\begin{aligned} f = 0: &\quad \overline{g}_K n^4(E - E_K) + \overline{g}_{Na}\overline{m}^3 h(E - E_{Na}) + \overline{g}_l(E - E_l) = 0, \\ \frac{\partial f}{\partial E} = 0: &\quad \overline{g}_K n^4 + \overline{g}_l + \overline{g}_{Na} h(\overline{m}^3 + 3\overline{m}^2(E - E_{Na})\overline{m}') = 0. \end{aligned}$$

From rearranging $\frac{\partial f}{\partial E}$=0, we obtain:

$$h = -\frac{(\overline{g}_K n^4 + \overline{g}_l)}{\overline{g}_{Na}(\overline{m}^3 + 3\overline{m}^2\overline{m}'(E - E_{Na}))}.$$

We obtain n^4 by putting h in f=0 and then obtaining a new equation for h without n^4. Therefore the two equations are:

$$n = \left(\frac{\overline{g}_l}{\overline{g}_K}\left(\frac{\overline{m}(E_{Na} - E_l) + 3\overline{m}'(E - E_{Na})(E - E_l)}{\overline{m}(E_K - E_{Na}) - 3\overline{m}'(E - E_{Na})(E - E_K)}\right)\right)^{1/4}, \tag{3.4}$$

$$h = \frac{\overline{g}_l(E_K - E_l)}{\overline{g}_{Na}(\overline{m}^3(E_{Na} - E_K) + 3\overline{m}^2\overline{m}'(E - E_{Na})(E - E_K))}. \tag{3.5}$$

This is only correct for $n^4 > 0$, as for $n^4 < 0$ we have complex roots. Since it is negative in an interval we obtain two disjoint branches of the fold curve. From Fig. 3.8(a) we see that $n^4 > 0$ for $E \in [-9.5, 15]$ and $E \in [41, 45.8]$. These are the two disjoint branches.

The projection of the fold curve onto the (n, h) plane in Fig. 3.8(b) gives two disjoint branches of the fold curve, not a cusp.

3.2.4 Finding the cusp point

A cusp corresponds to the case if f has three real roots and one of the roots is a repeated root. To find the threshold we take a point in the (E, n, h) plane and draw a trajectory from this point while keeping n constant. We allow E to follow the slow manifold, then the trajectory moves along the h axis until it reaches the fold curve. The point where we reach the fold curve is the threshold T.

We want to find the cusp point to compare with our graph. To do this we say:

$$f(E, n, h) = \overline{g}_K n^4(E - E_K) + F(E)h + \overline{g}_l(E - E_l),$$

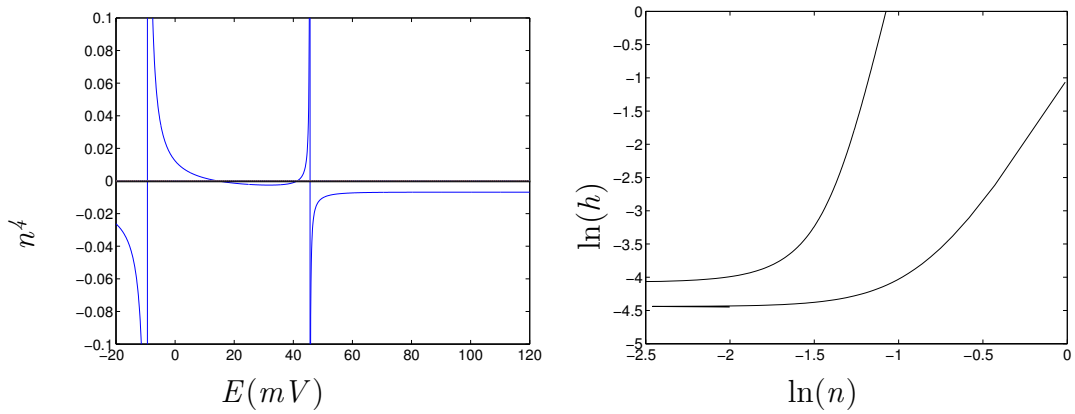

(a) (b)

Figure 3.8: (a) The graph of n^4 given by equation (3.5) plotted against E for the standard value E_l=10.613. (b) The projection of the fold curve in the (n, h) plane for E_l=10.613.

where,

$$F(E) = \overline{g}_{Na}\overline{m}^3(E - E_{Na}).$$

Then we differentiate f twice to obtain:

$$\frac{\partial^2 f}{\partial E^2} = F''(E)h.$$

The condition for the cusp point is $\frac{\partial^2 f}{\partial E^2}$=0, but $h \neq 0$, so $F''(E)$=0. We look for a solution E=E_2 say, where E_2 is a constant and does not depend on the values of the parameters, but it does depend on the function $\overline{m}(E)$ and parameter E_{Na}=115.

We rearrange $\frac{\partial f}{\partial E}$=0 and put in f=0. Therefore the system we have is:

$$\begin{aligned}(F(E) - F'(E)(E - E_K))h + \overline{g}_l(E_K - E_l) &= 0,\\ F''(E) &= 0,\end{aligned}$$

where $h \in [0, 1]$.

We now want to draw the graph of F'' plotted against E as for F''=0 we have our cusp point. As we can see from Fig. 3.9 the point is E_2=31.9 and n^4=−0.021 for this point. Therefore we have complex roots and there are no real solutions and no cusp points in the real space on this manifold.

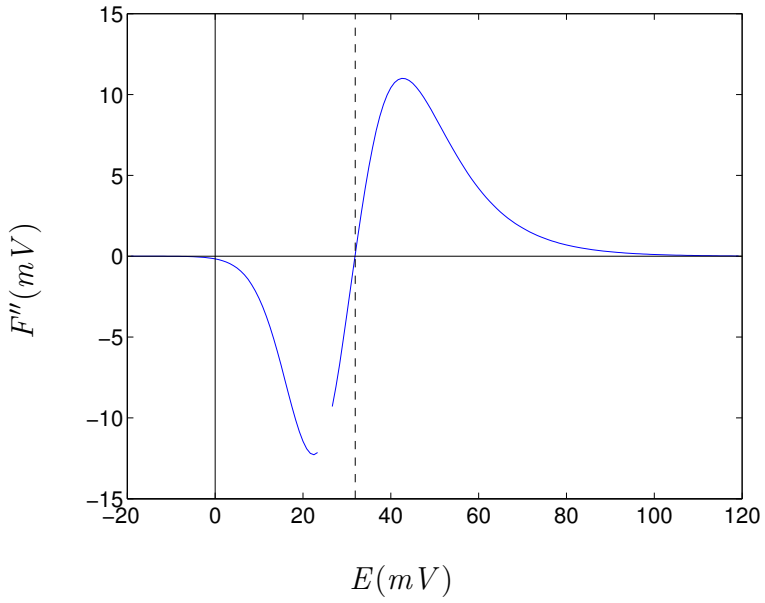

Figure 3.9: The graph of F'' plotted against E, where the dashed line represents E=31.9.

3.2.5 The phase portrait

Figures 3.10(a) and (b) show the slow manifold as the semitransparent surface, the fold curve is the thick solid lines and its projections are the thin solid lines and the trajectories and their projections are the dashed-dot lines. We use equations (3.4) and (3.5) to draw the fold curve and this can be seen by the thick black solid line in Figs. 3.10(a) and (b). The equilibrium values of n and h for E=0 were used as n and h's initial points for the trajectories. So the initial points are:

$$n_0 = 0.3177, \qquad h_0 = 0.5961, \qquad E_0 = 15.$$

We can see from Figs. 3.10(a) and (b) that the trajectory starts from a point and follows the fast foliation until it reaches a piece of the slow manifold. Then the trajectory moves along the slow manifold to the equilibrium point (h, n, E)=$(0.5961, 0.3177, 0)$.

We see that the trajectory travels to the equilibrium point, but from the action potential we see that for the reduced system we have a sharp corner at D, so therefore we have a jump return from C to D and the trajectory does not travel around the cusp point. Therefore we do not have a smooth return.

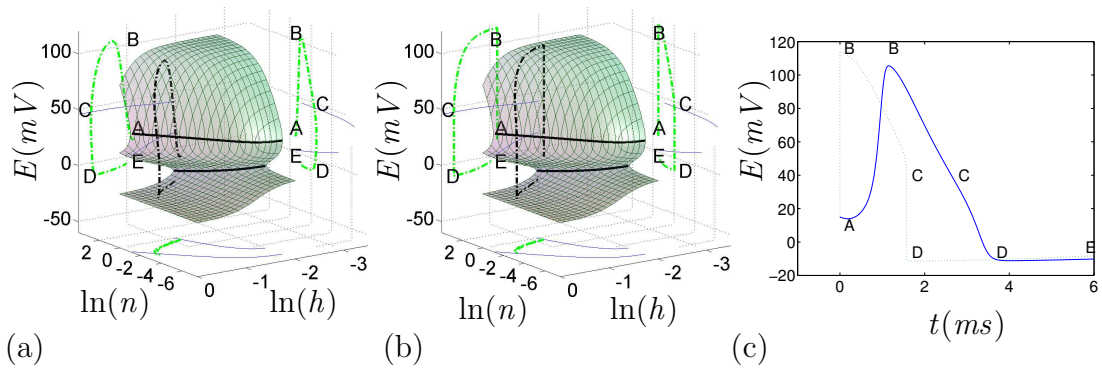

Figure 3.10: The phase portrait of the reduced system for E_l=10.613. Drawn are the slow manifold which is the semitransparent surface, a trajectory and its projections (:) at (E_0, h_0, m_0, n_0)=$(15, 0.5961, 0.0530, 0.3177)$ and the fold curve (thick-) and its projections (thin-). Labels A-E mark the feature points on the action potential in (c). The trajectory is drawn using (a) ϵ=1 and (b) ϵ=10^{-3} and (c) the action potential for this system where ϵ=1 (-) and ϵ=10^{-3} (:).

3.2.6 Finding where n^4 is positive

We want to find where $n^4 > 0$, so we can have the cusp point in the real plane. Say,

$$\begin{aligned} n &= \left(-\frac{\overline{g}_l}{\overline{g}_K}\left(\frac{q_1(E)-\mu(E)}{q_2(E)-\mu(E)}\right)\right)^{1/4}, \\ q_1(E) &= (E_{Na}-E)(E-E_l)(E_{Na}-E_l)^{-1}, \\ q_2(E) &= (E_{Na}-E)(E-E_K)(E_{Na}-E_K)^{-1}, \\ \mu(E) &= \frac{\overline{m}(E)}{3\overline{m}'(E)}. \end{aligned}$$

Figure 3.11(a) shows the graph of q_1, q_2 and μ drawn against E. We see from this figure that the closest curve to the intersection of μ with E=31.9 is q_1, and q_2 is the furthest away. We drew this graph because we wanted to see which curves are the closest to the intersection of μ and E=31.9 because we want to make $n^4 > 0$ at E=31.9. To do this we will have to change a parameter in equation (3.4), and from Fig. 3.11(b) we see that the parameter is E_l.

3.2.7 Changing the value of E_l

We want to change the value of E_l as this was chosen by Hodgkin and Huxley as they wanted the resting potential to be zero. The experimental value of E_l wasn't

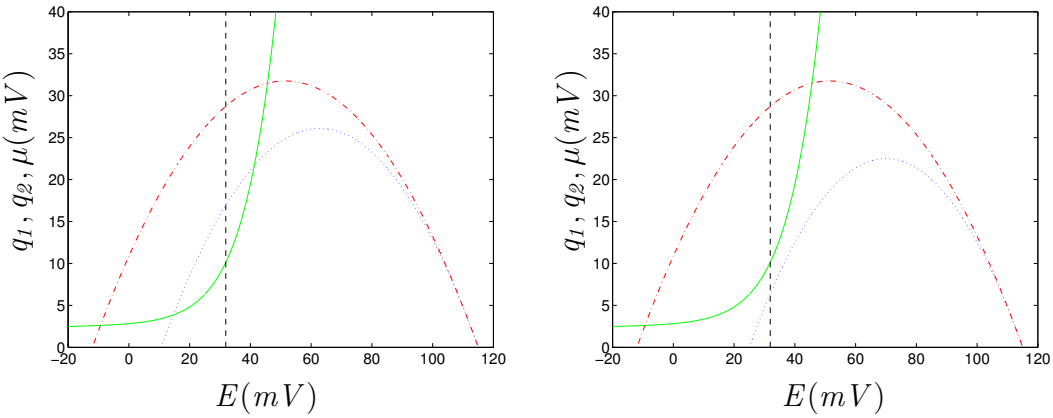

(a) (b)

Figure 3.11: Graph of $q_1(E)$ (:), $q_2(E)$ (-.) and $\mu(E)$ (-) for (a) E_l=10.613 and (b) E_l=25 with E=31.9 (- -) corresponding to the cusp point.

used as it wasn't to a high enough degree of precision. So we want to change this to a value that would give us n^4 positive. As we can see from Fig. 3.11(a) we want to change E_l so that q_1 moves to the right side of μ, Fig. 3.11(b), and therefore n^4 will be positive.

Therefore from experiments we found that for $E_l > 21$, we have $n^4 > 0$ and the two disjoint branches of the fold curve join together and a cusp is projected to the (n, h) plane. So we choose E_l=25 as this gives a clear phase portrait.

3.2.8 The phase portrait for E_l=25

The slow manifold is:

$$h = -\frac{(\overline{g}_K n^4(E - E_K) + \overline{g}_l(E - E_l))}{\overline{g}_{Na}\overline{m}^3(E - E_{Na})},$$

and our equations for the cusp point are:

$$\begin{aligned} f(E, n, h) &= \overline{g}_K n^4(E - E_K) + \overline{g}_{Na}\overline{m}^3 h(E - E_{Na}) + \overline{g}_l(E - E_l), \\ \frac{\partial f}{\partial E} &= \overline{g}_K n^4 + \overline{g}_l + \overline{g}_{Na} h(\overline{m}^3 + 3\overline{m}^2(E - E_{Na})\overline{m}'). \end{aligned}$$

So our h and n are:

$$n = \left(\frac{\overline{g}_l}{\overline{g}_K}\left(\frac{\overline{m}(E_{Na} - E_l) + 3\overline{m}'(E - E_{Na})(E - E_l)}{\overline{m}(E_K - E_{Na}) - 3\overline{m}'(E - E_{Na})(E - E_K)}\right)\right)^{1/4}, \tag{3.6}$$

$$h = -\frac{(\overline{g}_K n^4 + \overline{g}_l)}{\overline{g}_{Na}(\overline{m}^3(E_{Na} - E_K) + 3\overline{m}^2\overline{m}'(E - E_{Na})(E - E_K))}. \tag{3.7}$$

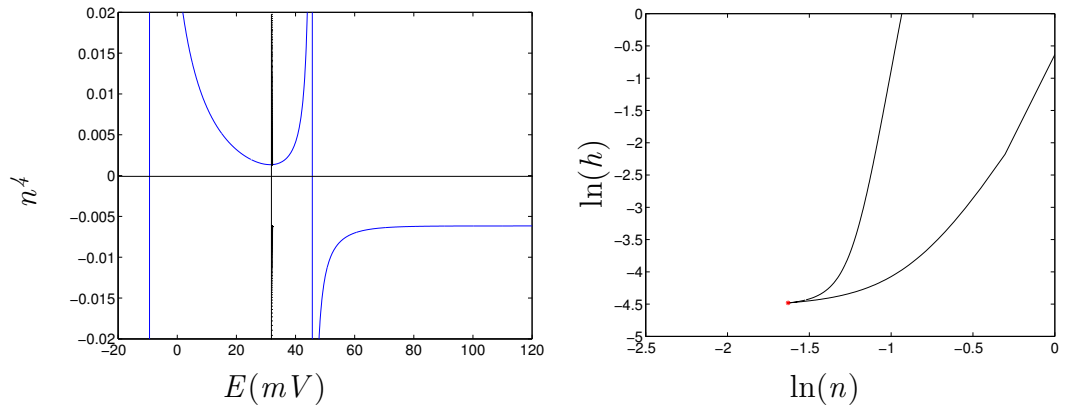

(a) (b)

Figure 3.12: (a) The graph of n^4 plotted against E with E_l=25. The black line represents E=31.9. (b) The projection of the fold curve in the (n, h) plane with E_l=25. The red star represents the cusp point (n, h)=(0.114, 0.0012).

Figure 3.12(a) shows n^4 plotted against E for E_l=25. We see that n^4 is positive between $45.8 > n^4 > -9$ and negative elsewhere.

We compare Fig. 3.12(a) to Fig. 3.8(a) and we see that the section of graph $45.8 > n^4 > -9$ is always positive as the curve does not cross the E axis, where in Fig. 3.8(a) it crosses the E axis in that domain. Here we see that $n^4 > 0$ at E=31.9.

Now we project the fold curves onto the (n, h) plane, using equations (3.6) and (3.7), and we see that we obtain a cusp in Fig. 3.12(b). This corresponds to f having three real roots and one of the roots is repeated.

We now want to find where the cusp point is. We put E=31.9 in equation (3.7) and we obtain:

$$n^4 = 0.00017,$$

where,

$$\overline{m} = 0.67, \qquad \overline{m}' = 0.02.$$

We see that n^4 is positive, so the cusp point is in the real plane. We put E in our new equations for h and n to obtain the point:

$$(E, n, h) = (31.9, 0.114, 0.0012).$$

As we can see from Fig. 3.13 we have the slow manifold as the semitransparent surface, the fold curve, its projections, the trajectory and its projections. We use

equations (3.6) and (3.7) to draw the fold curve. This can be seen by the thick black line in Fig. 3.13(a) and (b). We also see the cusp point, which is the filled circle on the plane. The equilibrium values of n and h at E=0 were used as n and h's initial points. So the initial points were:

$$n_0 = 0.3177, \qquad h_0 = 0.5961, \qquad E_0 = 15.$$

We can see from Figs. 3.13(a) and (b) that the trajectory starts from a point and moves along the E axis until it reaches the fast foliation, it then travels down the fast foliation to the slow manifold and along the slow manifold to the equilibrium point (h, n, E)=$(0.5961, 0.40, 0)$. As the trajectory doesn't travel around the cusp point, we have a jump return, and not a smooth return.

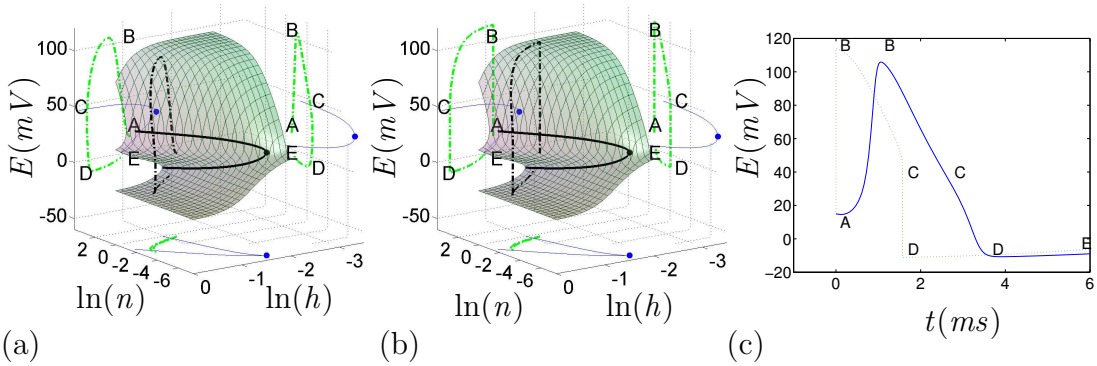

Figure 3.13: (a,b) The phase portrait of the reduced system for E_l=25. Drawn are the slow manifold which is the semitransparent surface, a trajectory and its projections (:) at (E_0, h_0, m_0, n_0)=$(15, 0.5961, 0.0530, 0.3177)$, the fold curve (thick-) and its projections (thin-) and the cusp point (E, h, m, n)=$(31.92, 0.0013, 0.6711, 0.1860)$ (.). Labels A-E mark the feature points on the action potential in (c). The trajectory is drawn using (a) ϵ=1 and (b) ϵ=10^{-3} and (c) the action potential for this system where ϵ=1 (-) and ϵ=10^{-3} (:).

3.2.9 Reducing the system by using the $\dot{E}$ and $\dot{m}$ equations

We saw that if we reduced the Hodgkin-Huxley equations to a third order system of equations, by using the m variable, we obtain a cusp, but the trajectory doesn't travel around the cusp point, so we have a jump return and not a smooth return.

Therefore we now consider m and E as equally fast, because we found from Figs. 3.1 and 3.5 that for some moments in time we have $\tau_V > \tau_m$ and for other

moments we have $\tau_m > \tau_V$. So far we have been considering that $\tau_m > \tau_V$, but there is a point where $\tau_V > \tau_m$. We want to see if the solutions are different if we consider m and E equally fast, and this will therefore give us a $(2,2)$ asymptotic structure.

We take the original Hodgkin-Huxley system.

$$\begin{aligned}
\dot{E} &= -(\overline{g}_K n^4(E-E_K) + \overline{g}_{Na} m^3 h(E-E_{Na}) + \overline{g}_l(E-E_l)),\\
\dot{m} &= \alpha_m(1-m) - \beta_m m = \frac{(\overline{m}-m)}{\tau_m},\\
\dot{n} &= \alpha_n(1-n) - \beta_n n = \frac{(\overline{n}-n)}{\tau_n},\\
\dot{h} &= \alpha_h(1-h) - \beta_h h = \frac{(\overline{h}-h)}{\tau_h}.
\end{aligned}$$

We want to find the slow manifold and the fast foliation, so we introduce a small parameter ϵ, where $\epsilon \ll 1$, to the $\dot{E}$ and $\dot{m}$ equations, so that the system becomes:

$$\begin{aligned}
\dot{E} &= -\frac{1}{\epsilon}(\overline{g}_K n^4(E-E_K) + \overline{g}_{Na} m^3 h(E-E_{Na}) + \overline{g}_l(E-E_l)), \qquad (3.8)\\
\dot{m} &= \frac{1}{\epsilon}\frac{(\overline{m}-m)}{\tau_m},\\
\dot{n} &= \frac{(\overline{n}-n)}{\tau_n},\\
\dot{h} &= \frac{(\overline{h}-h)}{\tau_h}.
\end{aligned}$$

For ϵ=0 we obtain the slow manifold:

$$\begin{aligned}
h &= -\frac{(\overline{g}_K n^4(E-E_K) + \overline{g}_l(E-E_l))}{\overline{g}_{Na}\overline{m}^3(E-E_{Na})}, \qquad (3.9)\\
m &= \overline{m}(E),
\end{aligned}$$

and the fast foliation, which is within the planes n=constant and h=constant.

The slow manifold is the set of equilibrium points of $\dot{E}$ and $\dot{m}$. The fast foliation will be along the trajectories of these equations.

We now want to find the fold curve; but instead of using the method we used earlier, which would give us the same answer as before, because our slow manifold is the same equation as we obtained by reducing the equations using

the m variable only. So we will only consider the $\dot{E}$ and $\dot{m}$ equations with n and h as constants.

$$\begin{aligned}\frac{\mathrm{d}E}{\mathrm{d}T} &= -(\overline{g}_K n^4(E-E_K)+\overline{g}_{Na}m^3h(E-E_{Na})+\overline{g}_l(E-E_l)),\\ \frac{\mathrm{d}m}{\mathrm{d}T} &= \frac{(\overline{m}-m)}{\tau_m}.\end{aligned}$$

We use the determinant of the Jacobian of these two equations, as one of the equations that satisfies the fold curve, the other equation that satisfies it is equation (3.9).

The Jacobian matrix is:

$$J_{Em}=\frac{\partial(\dot{E},\dot{m})}{\partial(E,m)}=\begin{pmatrix} -(\overline{g}_K n^4+\overline{g}_{Na}m^3h+\overline{g}_l) & -3\overline{g}_{Na}m^2h(E-E_{Na}) \\ \frac{\overline{m}'}{\tau_m}-\frac{(\overline{m}-m)(\tau_m')}{\tau_m^2} & -\frac{1}{\tau_m}\end{pmatrix}.$$

However, at an equilibrium m=$\overline{m}$, this reduces to:

$$J_{Em}=\frac{\partial(\dot{E},\dot{m})}{\partial(E,m)}=\begin{pmatrix} -(\overline{g}_K n^4+\overline{g}_{Na}\overline{m}^3h+\overline{g}_l) & -3\overline{g}_{Na}\overline{m}^2h(E-E_{Na}) \\ \frac{\overline{m}'}{\tau_m} & -\frac{1}{\tau_m}\end{pmatrix}.$$

An equilibrium is stable in linear approximation if and only if $\mathrm{Tr}(J_{Em})<0$ and $\det(J_{Em})>0$. We have :

$$\mathrm{Tr}(J_{Em})=-(\overline{g}_K n^4+\overline{g}_{Na}\overline{m}^3h+\overline{g}_l+\frac{1}{\tau_m})<0.$$

So $\mathrm{Tr}(J_{Em})<0$ is satisfied. The determinant is:

$$\det(J_{Em})=\frac{1}{\tau_m}(\overline{g}_K n^4+\overline{g}_{Na}\overline{m}^3h+\overline{g}_l+3\overline{g}_{Na}\overline{m}'\overline{m}^2h(E-E_{Na})).$$

The condition for the fold curve is $\det(J_{Em})$=0, which gives:

$$\overline{g}_K n^4+\overline{g}_{Na}\overline{m}^3h+\overline{g}_l+3\overline{g}_{Na}\overline{m}'\overline{m}^2h(E-E_{Na})=0.$$

Therefore:

$$h = -\frac{(\overline{g}_K n^4+\overline{g}_l)}{\overline{g}_{Na}\overline{m}^2(\overline{m}+3(E-E_{Na})\overline{m}')}. \tag{3.10}$$

So by solving the system $\dot{E}$=0, $\dot{m}$=0 and $\det(J_{Em})$=0, we can draw the fold curve, which is a parametric solution in terms of E.

Subtract equation (3.9) from equation (3.10) to obtain:

$$n = \left(\frac{\overline{g}_l}{\overline{g}_K} \left(\frac{\overline{m}(E_{Na} - E_l) + 3\overline{m}'(E - E_{Na})(E - E_l)}{\overline{m}(E_K - E_{Na}) - 3\overline{m}'(E - E_{Na})(E - E_K)} \right) \right)^{1/4}. \tag{3.11}$$

Put this in equation (3.10) to obtain:

$$h = \frac{\overline{g}_l(E_K - E_l)}{\overline{g}_{Na}(\overline{m}^3(E_{Na} - E_K) + 3\overline{m}^2\overline{m}'(E - E_{Na})(E - E_K))}. \tag{3.12}$$

These equations are exactly the same as equations (3.4) and (3.5). So therefore we will obtain the same answer as we did before. From this we can conclude that even if we treat the variables m and E as equally fast we still obtain the same answers as if we treat m as the fastest variable. Therefore the slow manifold and the fold curve do not change because of the condition $m{=}\overline{m}(E)$, which is satisfied on the slow manifold. So no matter which method we use we still obtain the same answer.

3.2.10 Summary

In this section we wanted to check Zeeman's hypothesis of there being a cusp catastrophe in Hodgkin-Huxley's system. We saw that there wasn't one for the standard values of parameters, because the equations for the cusp point only had complex solutions. As we changed E_l from the standard value of 10.613 to 25, we obtained a cusp point in the real plane and therefore the fold curves did form a cusp. So we've answered our question "What is the geometrical representation of the fold curve and does it form a cusp?

We didn't confirm the other part of Zeeman's hypothesis, because the trajectory did not go around the cusp point to the stable equilibrium, but it does jump from one part of the slow manifold to another while returning to the stable equilibrium point.

This is consistent with the behaviour of the reduced system as it produces a jump return, which is different to the original Hodgkin-Huxley system. Therefore the jump return must be produced by the reduction procedure. This procedure will need reviewing so we can construct a model containing a smooth return.

Chapter 4

Noble's 1962 Model Of The Purkinje Fibres: Tikhonov's Approach

We have described Noble's model in Section 2.1.2, so now we want to analyse this model so we can find its asymptotic structure and see if its structure is the same as Hodgkin-Huxley's as then it will give us a similar answer and we can test Zeeman's hypothesis to see if it gives a smooth return.

4.1 Reduction of Noble's Heart Equations

We want to reduce Noble's system of equations to a third order system, so we can verify Zeeman's hypothesis of there being a cusp catastrophe, like we did in Chapter 3 for Hodgkin-Huxley's model.

We have noticed from Fig. 2.5(a) that the pacemaker potential for the heart has a smooth return. It also has an unstable equilibrium as we have oscillations, so therefore the trajectories will be limit cycles. In Zeeman's paper, Zeeman said that for his "heart" model we have a jump return, but now it has been shown that this is incorrect. The heart can have a smooth return as well. Now we are modifying Zeeman's hypothesis to say that we want the reduced system to have an unstable equilibrium, a cusp and the trajectories make a limit cycle around the cusp point. Therefore we have a smooth return.

So we want to find which variable is the fastest variable by drawing a graph of the τ's, then reducing the system of equations by eliminating this variable.

4.2 Finding which Variable is the Fastest

We draw the graph of τ_m, τ_n, τ_h and τ_E against voltage to see which is the fastest variable.

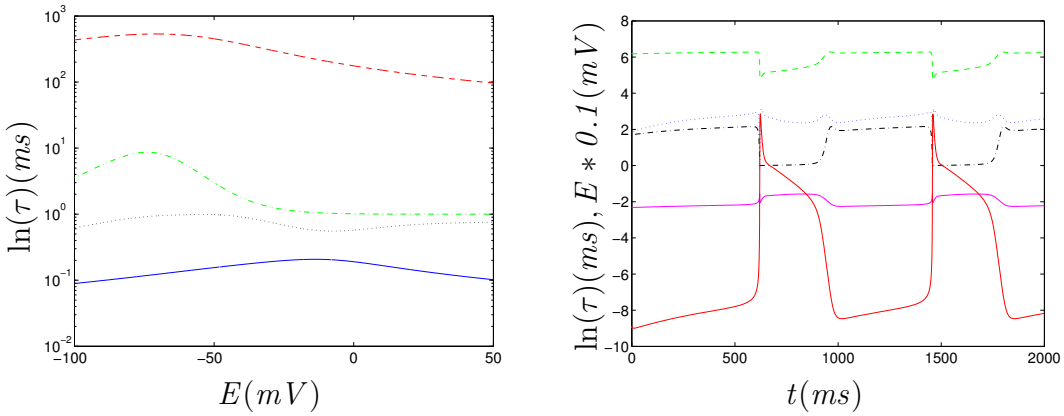

(a) (b)

Figure 4.1: Graph of τ_E (:), τ_m (-), τ_n (- -) and τ_h (-.) against (a) E drawn on a logarithmic scale and (b) t with the pacemaker potential of the original system (-).

We see from Fig. 4.1(a) that τ_m is always the fastest. Therefore m is the super-fast variable, n is the slow variable and τ_h and τ_E are very close together. In Fig. 4.1(b) τ_h and τ_E interchange at the spikes, so E and h are fast variables and must be treated as being equally fast. So we have one slow variable, two fast variables and one super-fast variable, therefore we have a $(1, 2, 1)$ asymptotic structure and this will give us a different structure for the slow manifold as the structure depends on how many slow variables there are.

4.3 Eliminating the m Variable

We have found out that m is the fastest variable, so we want to eliminate it from the system of equations. To do this we need to introduce a small parameter $\epsilon \ll 1$ to the $\dot{m}$ equation, but as we see we have a two-parametric embedding with two artificial small parameters ϵ_1 and ϵ_2. So our system becomes:

$$\begin{aligned}
\epsilon_1 \frac{\mathrm{d}E}{\mathrm{d}t} &= -\frac{1}{C_M}((m^3 h \overline{g}_{Na} + 0.14)(E - E_{Na}) + (g_{K_1} + g_{K_2})(E - E_K) \\
&\quad + g_l(E - E_l)), \\
\epsilon_2 \epsilon_1 \frac{\mathrm{d}m}{\mathrm{d}t} &= \alpha_m(1 - m) - \beta_m m = \frac{(\overline{m} - m)}{\tau_m},
\end{aligned}$$

$$\epsilon_1 \frac{\mathrm{d}h}{\mathrm{d}t} = \alpha_h(1-h) - \beta_h h = \frac{(\overline{h}-h)}{\tau_h},$$
$$\frac{\mathrm{d}n}{\mathrm{d}t} = \alpha_n(1-n) - \beta_n n = \frac{(\overline{n}-n)}{\tau_n}.$$

If we consider $\epsilon_2 \to 0$ in the above system, then we obtain the solution $m{=}\overline{m}$. We replace m in the $\dot{E}$ equation with $\overline{m}$. This means that we have a system of three equations without the m variable. We draw the pacemaker potentials of the reduced system and the original system for $\epsilon_1{=}1$ and then tend ϵ_2 to zero to see if the qualitative behaviour stays the same. We see from Fig. 4.2 that the pacemaker potentials for the original system and the reduced system are similar and as $\epsilon_2 \to 0$ the pacemaker potential for the original system does not change. Therefore this means that m is super-fast.

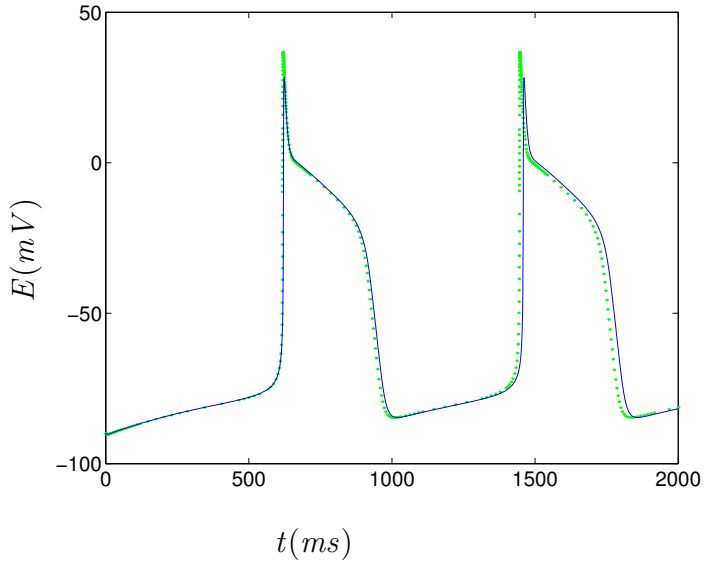

Figure 4.2: Graph of the original system (-) and the reduced system (4.1) (.), $m(t){=}\overline{m}(E(t))$, for $E_0{=}{-}90$.

The reduced system is:

$$\begin{aligned}
\frac{\mathrm{d}E}{\mathrm{d}t} &= -\frac{1}{C_M}((\overline{m}^3 h \overline{g}_{Na} + 0.14)(E - E_{Na}) + (g_{K_1} + g_{K_2})(E - E_K) \quad (4.1)\\
&\quad + g_l(E - E_l)),\\
\frac{\mathrm{d}h}{\mathrm{d}t} &= \alpha_h(1-h) - \beta_h h,\\
\frac{\mathrm{d}n}{\mathrm{d}t} &= \alpha_n(1-n) - \beta_n n.
\end{aligned}$$

We now consider that the E and h variables are the fast variables from

Fig. 4.1. So $\dot{n}$ is the slow equation and $\dot{E}$ and $\dot{h}$ are the fast equations. The equilibrium point for these equations is for $\dot{E}$=$\dot{n}$=$\dot{h}$=0 being satisfied.

4.4 The Slow Manifold and Fast Foliation

As we have found E and h are equally fast, then we have two fast variables and one slow variable. So therefore we will have a one-dimensional curve for the slow manifold and a two-dimensional plane for the fast foliation. So we cannot use Zeeman's hypothesis, as we do not obtain a cusp in this reduced system instead we will have a phase portrait similar to the FitzHugh system. We can still find out if the trajectories make a limit cycle and how they travel along the slow manifold. Therefore we have a jump return because of this result. So our system is:

$$\begin{aligned}
\epsilon_1 \frac{\mathrm{d}E}{\mathrm{d}t} &= -\frac{1}{C_M}((\overline{m}^3 h \overline{g}_{Na} + 0.14)(E - E_{Na}) + (g_{K_1} + g_{K_2})(E - E_K) \\
&\quad + g_l(E - E_l)), \qquad (4.2) \\
\epsilon_1 \frac{\mathrm{d}h}{\mathrm{d}t} &= \alpha_h(1 - h) - \beta_h h, \\
\frac{\mathrm{d}n}{\mathrm{d}t} &= \alpha_n(1 - n) - \beta_n n.
\end{aligned}$$

This is the slow system.

We want to see what happens to the shape of the pacemaker potential as we tend $\epsilon_1 \to 0$. Figure 4.3 shows the pacemaker potentials of the reduced system for ϵ_1=1 (-) and the reduced system as we tend $\epsilon_1 \to 0$ (.).

We see from Fig. 4.3 that the period of oscillations is shortening. So the period has a limit as $\epsilon_1 \to 0$. This is called the normal limit. We see from the shape of the pacemaker potentials that as we tend $\epsilon_1 \to 0$ we obtain a fast onset and a sharp return. As $\epsilon_1 \to 0$ we see that this furthers the quickening of the fast onsets. So therefore we have a jump return here and not a smooth return. Figure 4.3(a) is the same as the FitzHugh system, as we have the fast onset. So the smooth returns are now changed to jump returns and this will give us a phase portrait that is similar to Zeeman's "heart" model.

Now we introduce a new variable t=$\epsilon_1 T$ to obtain the fast system.

$$\begin{aligned}
\frac{\mathrm{d}E}{\mathrm{d}T} &= -\frac{1}{C_M}((\overline{m}^3 h \overline{g}_{Na} + 0.14)(E - E_{Na}) + (g_{K_1} + g_{K_2})(E - E_K)
\end{aligned}$$

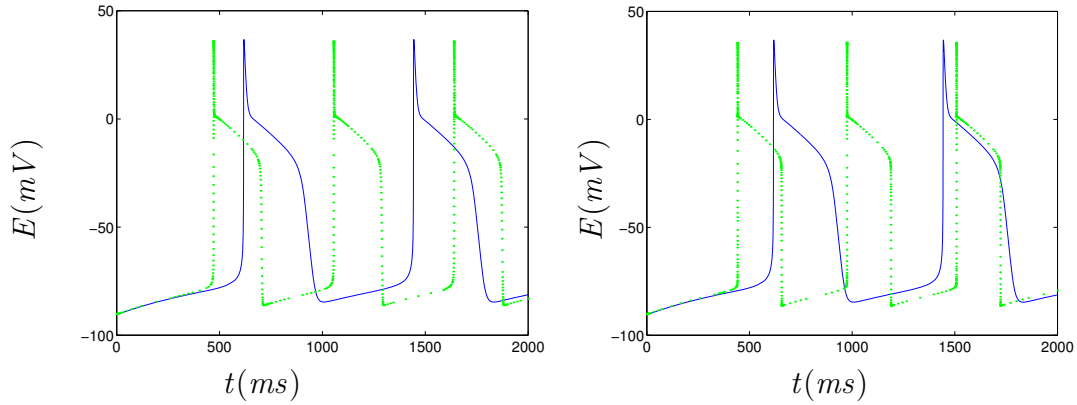

(a) (b)

Figure 4.3: Pacemaker potentials for the reduced system (4.2) with ϵ_1 in front of the $\dot{E}$ and $\dot{h}$ equations. Reduced system with ϵ_1=1 (-) and (a) ϵ_1=0.1 (.) and (b) ϵ_1=0.01 (.).

$$
\begin{aligned}
& +g_l(E-E_l)), && (4.3)\\
\frac{\mathrm{d}h}{\mathrm{d}T} &= \alpha_h(1-h)-\beta_h h,\\
\frac{\mathrm{d}n}{\mathrm{d}T} &= \epsilon_1(\alpha_n(1-n)-\beta_n n).
\end{aligned}
$$

System (4.2) gives us the slow manifold, if ϵ_1=0.

$$
\begin{aligned}
h &= \frac{\alpha_h}{(\alpha_h+\beta_h)} = \overline{h},\\
f(E,n) &= (\overline{m}^3\overline{h}\overline{g}_{Na}+0.14)(E-E_{Na})+(g_{K_1}+g_{K_2})(E-E_K)+g_l(E-E_l)\\
&= 0.
\end{aligned}
$$

Therefore the slow manifold is:

$$
\begin{aligned}
n &= \left(\frac{(\overline{m}^3\overline{h}\overline{g}_{Na}+0.14)(E_{Na}-E)+g_{K_1}(E_K-E)+g_l(E_l-E)}{1.2(E-E_K)}\right)^{1/4},\\
\dot{n} &= \alpha_n-(\alpha_n+\beta_n)n.
\end{aligned}
$$

The slow manifold is a one-dimensional curve as it only has one slow variable. The $\dot{n}$ equation is the projection of the slow manifold to the (h,E) plane.

System (4.3) gives us the fast foliation, if ϵ_1=0.

$$
n = \text{constant},
$$

$$\begin{aligned}\frac{\mathrm{d}E}{\mathrm{d}T} &= -\frac{1}{C_M}((\overline{m}^3 h\overline{g}_{Na}+0.14)(E-E_{Na})+(g_{K_1}+g_{K_2})(E-E_K)\\ &\quad +g_l(E-E_l)),\\ \frac{\mathrm{d}h}{\mathrm{d}T} &= \alpha_h(1-h)-\beta_h h.\end{aligned}$$

So the slow manifold is a curve and the fast foliation is a two-dimensional plane in the (h, E) plane, as there are two fast variables consisting of planes n=constant. Therefore, we won't obtain a three-dimensional phase portrait, as the slow manifold is a curve not a surface. Instead we are going to obtain a two-dimensional phase portrait.

Figure 4.4 shows the graph of $\overline{h}$, where $\overline{h}$ is a function of E.

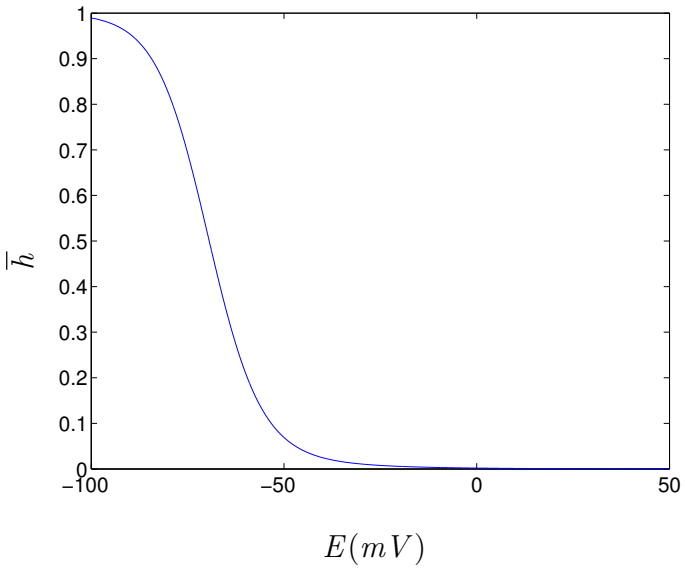

Figure 4.4: The graph of $\overline{h}$.

4.5 Phase Portraits

As we are choosing to study a two-dimensional phase portrait not three-dimensional, then we need to find the nullclines of the system. We find the nullclines because we want to draw the four leaves of the fast foliation, so we can see which parts of the slow manifold are stable and which parts are unstable.

We find the nullclines and trajectories of the following system.

$$\frac{\mathrm{d}E}{\mathrm{d}T} = -\frac{1}{C_M}((\overline{m}^3 h\overline{g}_{Na}+0.14)(E-E_{Na})+(g_{K_1}+1.2n^4)(E-E_K)$$

$$
\begin{aligned}
& +g_l(E-E_l)), \qquad (4.4)\\
\frac{\mathrm{d}h}{\mathrm{d}T} &= \alpha_h(1-h)-\beta_h h,
\end{aligned}
$$

where we assume that n is a constant parameter defining the leaf.

We select four different values of n to draw portraits of four leaves of the fast foliation. To draw the leaves we need to find the nullclines and the equilibria on those nullclines by drawing trajectories of system (4.4).

The h nullcline is:

$$h = \frac{\alpha_h}{(\alpha_h+\beta_h)} = \overline{h}(E). \qquad (4.5)$$

The E nullcline is:

$$h = \frac{0.14(E_{Na}-E)+(g_{K_1}+g_{K_2})(E_K-E)+g_l(E_l-E)}{\overline{m}^3\overline{g}_{Na}(E-E_{Na})}. \qquad (4.6)$$

The slow manifold is the set of equilibrium points of $\dot{E}$ and $\dot{h}$. We want to study the Jacobian matrix of this system to check to see which branches on the slow manifold are stable and which are unstable. We also want to find the fold curve.

The stability of an equilibrium in system (4.4) is determined by the Jacobian of the right hand sides of the equations. We use the determinant of the Jacobian of these two equations as one of the equations that satisfies the fold curve, the other equations that satisfies it are:

$$\dot{E}=0, \qquad \dot{h}=0,$$

which gives the slow manifold,

$$
\begin{aligned}
n &= \left(\frac{(\overline{m}^3\overline{h}\overline{g}_{Na}+0.14)(E_{Na}-E)+g_{K_1}(E_K-E)+g_l(E_l-E)}{1.2(E-E_K)}\right)^{1/4},\\
\dot{n} &= \alpha_n-(\alpha_n+\beta_n)n.
\end{aligned}
$$

The Jacobian matrix is:

$$J_{Eh} = \frac{\partial(\dot{E},\dot{h})}{\partial(E,h)}$$

$$= \begin{pmatrix} -C_M^{-1}(\overline{m}^2 h\overline{g}_{Na}(\overline{m}+3\overline{m}^{'}(E-E_{Na})) & -C_M^{-1}\overline{m}^3\overline{g}_{Na}(E-E_{Na}) \\ +g_{K_1}^{'}(E-E_K)+g_l+g_{K_1} & \\ +1.2n^4+0.14) & \\ \\ \frac{\overline{h}^{'}}{\tau_h}-\frac{(\overline{h}-h)\tau_h^{'}}{\tau_h^2} & -\frac{1}{\tau_h} \end{pmatrix}.$$

However, at an equilibrium $h{=}\overline{h}(E)$, the Jacobian becomes:

$$J_{Eh} = \begin{pmatrix} -C_M^{-1}(\overline{m}^2\overline{h}\overline{g}_{Na}(\overline{m}+3\overline{m}^{'}(E-E_{Na})) & -C_M^{-1}\overline{m}^3\overline{g}_{Na}(E-E_{Na}) \\ +g_{K_1}^{'}(E-E_K)+g_l+g_{K_1} & \\ +1.2n^4+0.14) & \\ \\ \frac{\overline{h}^{'}}{\tau_h} & -\frac{1}{\tau_h} \end{pmatrix}.$$

An equilibrium is stable in linear approximation if and only if $\mathrm{Tr}(J_{Eh}) < 0$ and $\det(J_{Eh}) > 0$. So we have:

$$\begin{aligned} \mathrm{Tr}(J_{Eh}) &= -C_M^{-1}(g_l+g_{K_1}+1.2n^4+0.14+g_{K_1}^{'}(E-E_K) \\ &\quad +\overline{m}^2 h\overline{g}_{Na}(\overline{m}+3\overline{m}^{'}(E-E_{Na}))) - \frac{1}{\tau_h}, \\ \det(J_{Eh}) &= C_M^{-1}\tau_h^{-1}(\overline{m}^2 h\overline{g}_{Na}(\overline{m}+3\overline{m}^{'}(E-E_{Na}))+g_l+g_{K_1}+1.2n^4 \\ &\quad +0.14+g_{K_1}^{'}(E-E_K)+\overline{m}^3\overline{g}_{Na}(E-E_{Na})\overline{h}^{'}). \end{aligned}$$

We draw the graphs of the $\det(J_{Eh})$ and $\mathrm{Tr}(J_{Eh})$ against E to check that we have the condition $\mathrm{Tr}(J_{Eh}) < 0$ and $\det(J_{Eh}) > 0$. We see from Fig. 4.5 that the stability condition for $\mathrm{Tr}(J_{Eh}) < 0$ is violated in the range of $E{=}(-68.25, -57.01)$ and that the condition for $\det(J_{Eh}) < 0$ is satisfied in the intervals $E{=}(-\infty, -77.37), (-55.54, -47.24), (-20.27, +\infty)$.

We see that the interval of stability due to positive trace, lies in the interval $(-77.37, -55.54)$ of the determinant and here the equilibria are unstable due to negative determinant. Therefore we have found that the slow manifold has attractive (stable) and repelling (unstable) pieces, which are determined by the sign of the determinant only. We can deduce the sign of the determinant and the stability of the slow manifold from the slope of its (n, E) projection. The slow manifold defines this projection.

We differentiate the slow manifold to find the slope of its projection as:

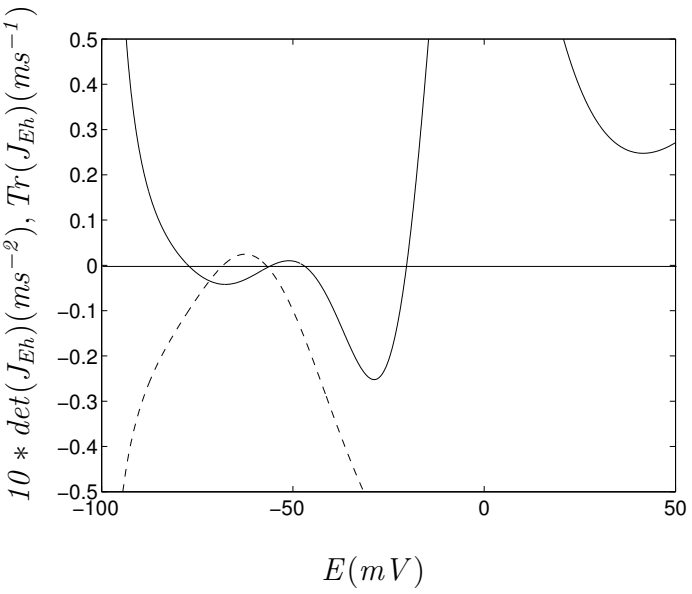

Figure 4.5: Graph of $\mathrm{Tr}(J_{Eh})$ (- -) and $10 * \det(J_{Eh})$ (-).

$$\begin{aligned}\frac{\mathrm{d}n}{\mathrm{d}E} &= -\frac{1}{4n^3(E_K-E)1.2}\frac{(g_l(E_K-E_l)+(\overline{m}^3\overline{h}\overline{g}_{Na}+0.14)(E_K-E_{Na})}{(E-E_K)} \\ &\quad +\frac{\overline{m}^2\overline{g}_{Na}(E_{Na}-E)(E-E_K)(3\overline{h}\overline{m}'+\overline{m}\overline{h}')-\overline{g}'_{K_1}(E_K-E)^2)}{(E-E_K)}.\end{aligned}$$

We can rewrite this as:

$$\frac{\mathrm{d}n}{\mathrm{d}E} = -\left(\frac{\partial\overline{f}_E(n)}{\partial n}\right)^{-1}\left(\frac{\partial\overline{f}_E}{\partial E}+\frac{\partial\overline{f}_E}{\partial h}\frac{\mathrm{d}\overline{h}}{\mathrm{d}E}\right),$$

where $\left(\frac{\partial\overline{f}_E(n)}{\partial n}\right)^{-1}=\frac{1}{4n^3(E_K-E)1.2}$ and $\overline{f}_E(E,\overline{h},n(E))=(\overline{m}^3\overline{h}\overline{g}_{Na}+0.14)(E-E_{Na})+(\overline{g}_{K_1}+1.2n^4(E))(E-E_K)+g_l(E-E_l)$.

We compare this with the $\det(J_{Eh})$ which can be rewritten as:

$$\det(J_{Eh}) = -C_M^{-1}\tau_h^{-1}\left(\frac{\partial\overline{f}_E}{\partial E}+\frac{\partial\overline{f}_E}{\partial h}\frac{\mathrm{d}\overline{h}}{\mathrm{d}E}\right).$$

We see that $\det(J_{Eh})$ has the opposite sign to $\frac{\mathrm{d}n}{\mathrm{d}E}$ as long as $E > E_K$, i.e. during any physiologically sensible pacemaker potential. Therefore, the stable points of the slow manifold are those where the slope of the projection of the slow manifold to the (E,n) plane is negative.

The condition for the fold curve is $\det(J_{Eh})$=0, which gives:

$$\begin{aligned}&g_l+g_{K_1}+1.2n^4+0.14+g'_{K_1}(E-E_K)+\overline{m}^2\overline{h}\overline{g}_{Na}(\overline{m}+3\overline{m}'(E-E_{Na})) \\ &+\overline{h}'(\overline{m}^3\overline{g}_{Na}(E-E_{Na}))=0.\end{aligned}$$

Therefore,

$$n^4 = -\frac{(g_l + g_{K_1} + 0.14 + g'_{K_1}(E - E_K) + \overline{m}^2\overline{h}\overline{g}_{Na}(\overline{m} + 3\overline{m}'(E - E_{Na})))}{1.2} - \frac{(\overline{h}'(\overline{m}^3\overline{g}_{Na}(E - E_{Na})))}{1.2}.$$

We subtract the equation for the slow manifold from the equation above to obtain:

$$g_l(E_K - E_l) - g'_{K_1}(E_m - E_K)^2 + (\overline{m}^3\overline{h}\overline{g}_{Na} + 0.14)(E_K - E_{Na}) + \overline{m}^2\overline{g}_{Na}(E_{Na} - E_m)(E_m - E_K)(\overline{m}\overline{h}' + 3\overline{m}'\overline{h}) = 0.$$

This is the equation for the fold points and is the same as $\frac{\mathrm{d}n}{\mathrm{d}E}$=0.

We draw the phase portraits of the fast leaves at specified values of n and this shows us that the top branch and the bottom branch are stable and the middle branch is split up into two unstable and one stable piece.

Figure 4.7 shows the phase portrait for the reduced system for two values of ϵ_1 for the trajectory. So Fig. 4.7(a) has the trajectory for ϵ_1=1 and Fig. 4.7(b) has the trajectory for the reduced system for ϵ_1=10^{-3} which corresponds to $\epsilon_1 \to 0$.

We see that the trajectory starting from an initial point (E_0, n_0, h_0)=$(-81.5, 0.5, 0.0019)$ will travel along the slow manifold until it reaches the repellor piece; then it makes a jump up the fast foliation to the attractor piece. The trajectory travels along the same path like this because we have an unstable equilibrium point, and therefore we have a limit cycle. Here A and D are our fold points (threshold).

Figure 4.7(c) is the pacemaker potential of the original system, which is the same as Fig. 2.5(a). We can compare this pacemaker potential with the slow manifold. We have labelled parts of the pacemaker potential and the slow manifold so we can see which parts of the two graphs correspond to each other.

The pacemaker potential starts at A which corresponds to the trajectory in Fig. 4.7. The trajectory jumps up the fast foliation to the point B as we have a repellor piece on the slow manifold. This corresponds to the jump onset (AB) on the pacemaker potential. Point B is the overshot and this can be seen on the pacemaker potential as well. This corresponds to the time independent potassium current g_{K_1}, and the value 0.14 is a small component of g_{Na}, which is also a time independent variable. These two-time independent variables cause

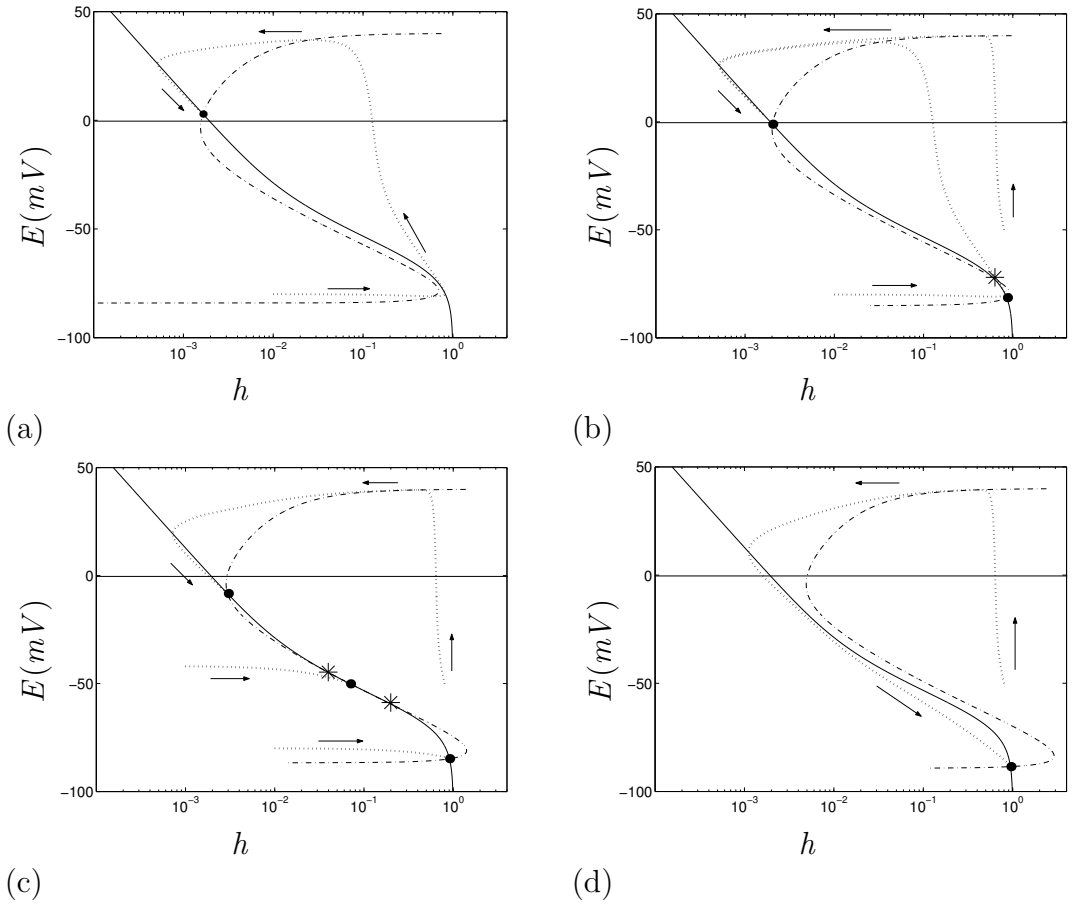

Figure 4.6: Phase portraits of the fast leaves at the specified values of n with the $\dot{E}$=0 isoclines (- -), $\dot{h}$=0 isoclines (-), selected trajectories (:), stable equilibria (.) and saddle points (*). (a) n=0.3, (b) n=0.5, (c) n=0.636 and (d) n=0.8.

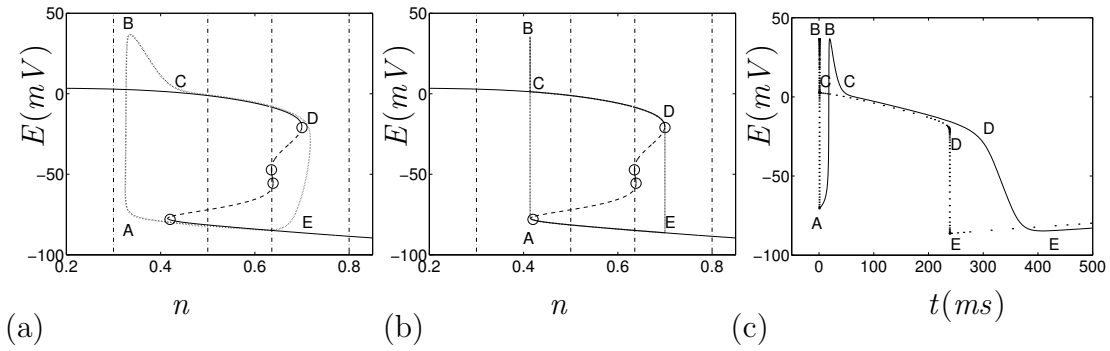

Figure 4.7: (a) The projection of the phase portrait of Noble's system onto the (n, E) plane with the slow manifold (-) and (- -), a selected "pacemaker potential" trajectory (:) and the positions of the selected fast leaves shown in figure 4.6 (-.). (b) Same as (a), with the trajectory of the embedded system at ϵ_1=10^{-3}. (c) The pacemaker potentials of the original (-) and embedded (.) systems. Letters A-E mark feature points on the pacemaker potential trajectory.

the overshot. The Hodgkin-Huxley model doesn't have an overshot as it only has g_{K_2} in its equation.

At B the trajectory travels to C, which is an attractor piece of the slow manifold and then travels along it to the point D, this corresponds to the path CD on the pacemaker potential, then the trajectory makes another jump down the fast foliation to E and then travels along the slow manifold to A, which is where it started from, and follows the same path around again. The path BE corresponds to the smooth return on the pacemaker potential. Then EA on the pacemaker potential shows the start of the limit cycle as the trajectory moves along the slow manifold to start its journey again and it goes on like this forever.

4.6 Using Tikhonov's Approach for an Excitable Version of Noble's Model

We want to make Noble's model excitable, because other systems in the heart are excitable, e.g. human atrial cell, and we want to see what results we will achieve if we use Tikhonov's method to find the phase portrait.

We decide to modify the parameter E_K from -100 to -110 to obtain an excitable system, and therefore we will have one action potential solution not an infinite series of solutions. So we cut the time period down to $[0, 600]$, so that we can see what happens during this one action potential solution. Therefore we have a stable equilibrium point.

We decided to modify E_K instead of the constant in front of the first exponential in g_{K_1}, e.g. change value from 1.2 to 1.3, even though Krinsky and Kokoz said that you can obtain an excitable system by modifying g_{K_1}[42].

We are not really interested in which parameter we change, as we want an excitable system. We chose E_K, because it is physiologically more feasible than changing g_{K_1}, as g_{K_1} is harder to change if we want to find the result using laboratory experiments, whereas E_K can be changed with ease.

Also we compared the results from both modifications and preferred the accuracy we achieved using E_K, but there are still different ways that Noble's model can be made excitable.

So we use Tikhonov's method, equations and results from the previous four sections and changed the parameter E_K to -110 and redrew most of the graphs. We also have to change the initial values to:

$$E_0 = -10, \qquad n_0 = 0, \qquad h_0 = 1.$$

We found that if we did this, the results are different, but still qualitatively the same with the non-excitable model, and we still obtain a jump return, which is a feature of Tikhonov's method. This can be seen from Figs. 4.8, 4.9, and 4.10.

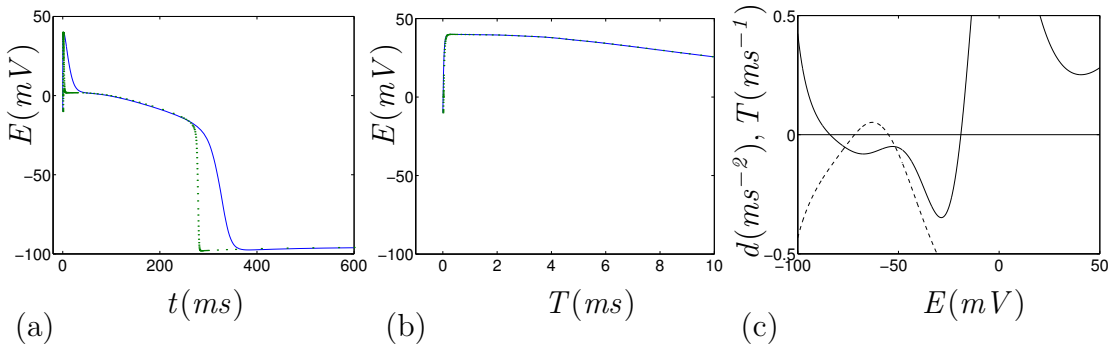

Figure 4.8: Action potentials for the reduced system with ϵ_1 in front of the $\dot{E}$ and $\dot{h}$ equations. ϵ_1=1 (-) and ϵ_1=0.1 (.). (a) The slow time scale, system (4.2). (b) The fast time scale T, system (4.3). (c) Graph of T=Tr(J_{Eh}) (- -) and d=10 $*$ det(J_{Eh}) (-). Same as Fig. 4.3(a) and Fig. 4.5 with E_K=−110.

We see that if we change the system to an excitable system, we have two disjoint branches of the slow manifold, Fig. 4.10, as one piece is in the complex plane. The trajectory travels along the slow manifold to the equilibrium point, which is different to the non-excitable model as we have limit cycles there.

4.7 Summary

Even though Krinsky and Kokoz[42] found that they could reduce Noble's 1962 model to a system of two equations by asymptotic methods, we have found that we can reduce Noble's system to a three-dimensional system of equations consisting of (2+1) equations, i.e. two fast and one slow.

This is because Krinsky and Kokoz said that m and h are equally fast and can be replaced with their quasi-stationary values, but from our analysis we have found that this is not true. From our speed analysis of the original system, we have found that m is super-fast, E and h equally fast and n is slow. Therefore m can be replaced with its quasi-stationary value, but h can not, as h and E must be considered fast at the same time.

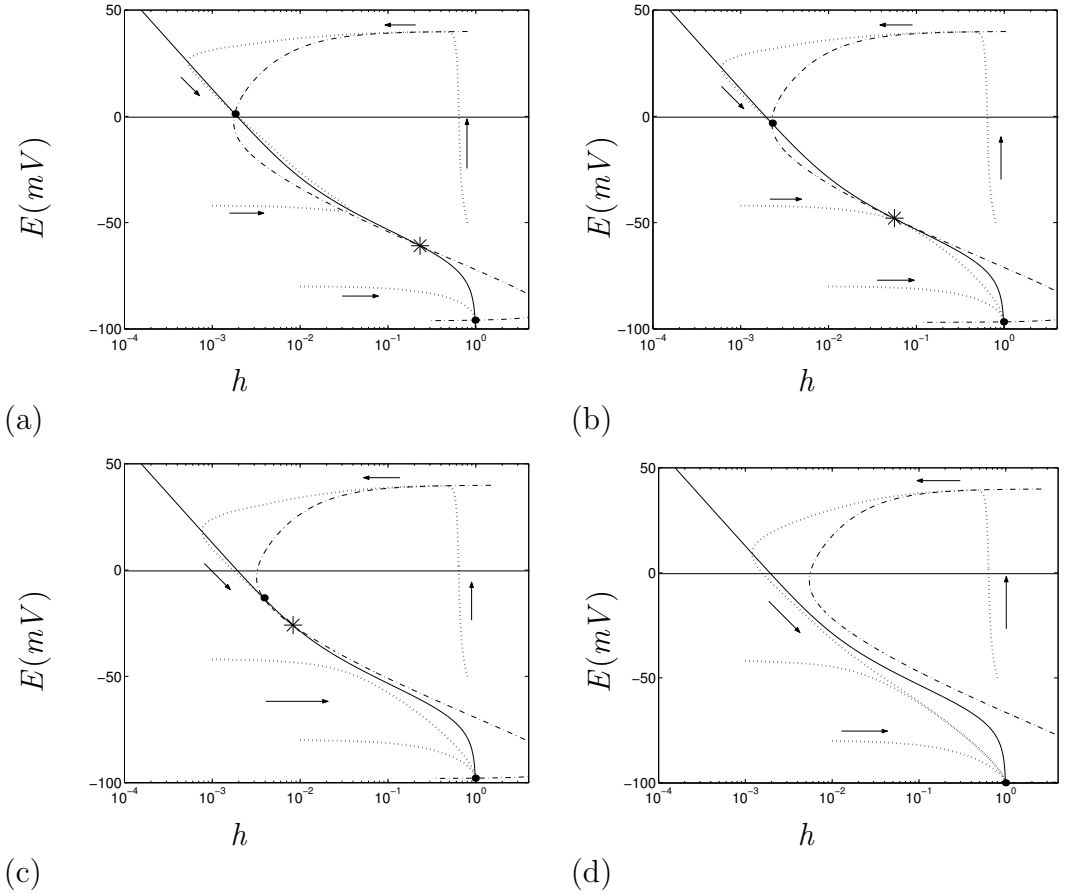

Figure 4.9: Phase portraits of the fast leaves at the specified values of n with the $\dot{E}$=0 isoclines (- -), $\dot{h}$=0 isoclines (-), selected trajectories (:), stable equilibria (.) and saddle points (*). (a) n=0.3, (b) n=0.5, (c) n=0.636 and (d) n=0.8. Same as Fig. 4.6 with E_K=−110.

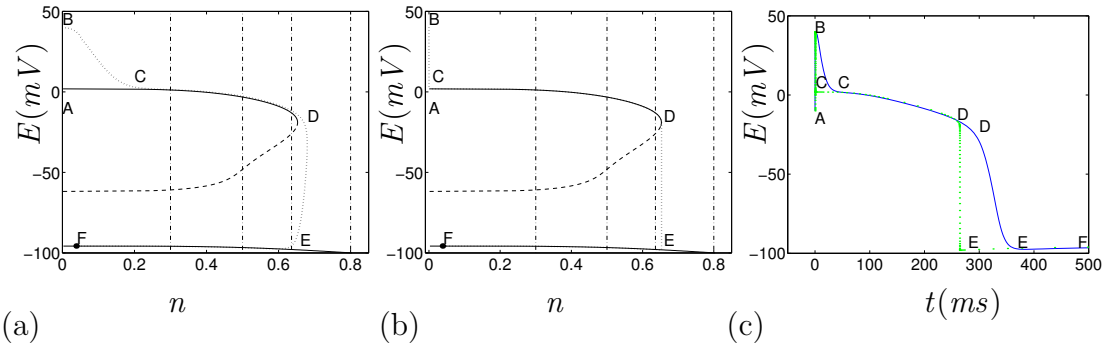

Figure 4.10: (a) The projection of the phase portrait of Noble's system onto the (n, E) plane with the slow manifold (-) and (- -), a selected "action potential" trajectory (:) and the positions of the selected fast leaves shown in figure 4.9 (-.). (b) Same as (a), with the trajectory of the embedded system at ϵ_1=10^{-3}. (c) The action potentials of the original (-) and embedded (.) systems. Letters A-E mark feature points on the action potential trajectory. Same as Fig. 4.7 with E_K=−110.

Krinsky and Kokoz also said that their two-dimensional system describes the slow processes in Noble's system and is not applicable for the description of the onset of the action potential, which is the fast process. As we are interested in studying both fast and slow processes of the system, then this method used by Krinsky and Kokoz is not sufficient to us, even though the equation for the $\dot{E}$=0 nullcline is the same equation as our slow manifold.

We have found that here we have one super-fast variable, m, two fast variables h and E, and one slow variable, n, where the Hodgkin-Huxley system had two fast variables, m and E and two slow variables, h and n. From this we have seen that we have a one-dimensional slow manifold and a two-dimensional fast foliation, this results in there not being a cusp. Therefore this gives us a FitzHugh like phase portrait. Also, we cannot obtain a smooth return; instead we obtain a jump return with limit cycles.

We have found that with there being two fast variables, we can't test Zeeman's hypothesis on this model; but we have seen that it gives us a jump return which corresponds with Zeeman's "heart" model in Section 2.4.1. The phase portrait also corresponds with Zeeman's "heart" model except that we have a limit cycle here and in Zeeman's model we have the trajectories going straight to the stable equilibrium. We can obtain a limit cycle with Zeeman's model if we have $x_0 < \frac{1}{\sqrt{3}}$.

We also found from analysing Tikhonov's method for Noble's oscillatory and excitable systems that with using this method we still obtain a jump return.

So to obtain more accurate results for excitable systems we need to introduce a non-Tikhonov embedding.

We also see that there is the possibility of fast oscillatory instability, as this is theoretically possible in systems with two fast variables, but not in systems with one fast variable.

This is characterized by the change of sign in the trace of the Jacobian at the equilibrium with a positive determinant, i.e. a Hopf bifurcation. This possibility is not realised here because we have the change of sign in the trace, but a negative determinant. However, because there exists a change of sign in the trace, doesn't say that this can't happen for different parameter values, or in other models of similar nature.

This would correspond to bursts of high frequency oscillations at the plateau of the action potential, which can be seen in other models[57, 48].

Chapter 5

Noble's 1962 Model: Non-Tikhonov Approach

In Chapter 4 we studied Noble's model using Tikhonov's method for fast-slow systems of equations and found that we had a one-dimensional slow manifold and a two-dimensional fast foliation. This was because we had a $(1, 2, 1)$ asymptotic structure. We saw from Fig. 4.3 that if we let $\epsilon_1 \to 0$, then we obtained a fast onset and a sharp return, so this is a jump return and not a smooth return.

We also saw from Section 4.6 that if we change the oscillatory system to an excitable system, by modifying the parameter E_K, and then using Tikhonov's method, we still obtain a fast onset and sharp (jump) return. This is therefore a feature of Tikhonov's method. The results for this are accurate, but we want to obtain a smooth return. So to do this we will have to use a non-Tikhonov embedding method.

We use a non-Tikhonov embedding method to obtain a non-Tikhonov system of equations and therefore retain the fast onset and smooth return, instead of a jump return. This will then confirm that we can reduce a fast-slow system of equations and retain the smooth return, which we haven't been able to do with Hodgkin-Huxley's model or Noble's model, using Tikhonov's method.

5.1 Non-Tikhonov Embedding of Noble's Model

We still have a $(1, 2, 1)$ asymptotic structure for Noble's model and a two-parametric embedding, so we take Noble's model once we have adiabatically

eliminated the m variable:

$$\begin{aligned}
\frac{\mathrm{d}E}{\mathrm{d}t} &= -\frac{1}{C_M}((\overline{g}_{Na}\overline{m}^3 h + 0.14)(E - E_{Na}) + (g_{K_1} + g_{K_2})(E - E_K) \\
&\quad + g_l(E - E_l)), \\
\frac{\mathrm{d}h}{\mathrm{d}t} &= \frac{(\overline{h} - h)}{\tau_h}, \\
\frac{\mathrm{d}n}{\mathrm{d}t} &= \frac{(\overline{n} - n)}{\tau_n}.
\end{aligned} \tag{5.1}$$

We know from Chapter 4 that if we just introduce an artificial small parameter ϵ to system (5.1) in a Tikhonov way, then we will obtain Fig. 4.3 again. So this time we introduce ϵ to the h equation, and for the E equation we just introduce ϵ to the large current only, as $\dot{E}$ contains large and small currents. The large current in $\dot{E}$ is I_{Na}, so we introduce $\frac{1}{\epsilon}$ in front of $\overline{g}_{Na}\overline{m}^3 h(E - E_{Na})$ only.

We also changed the E_K parameter from -100 to -110 and this changed the system from being oscillatory to excitable. Therefore we obtain one action potential solution and not an infinite series of solutions. So we then cut the time period down to $[0, 600]$, so that we can see what happens during this one action potential solution. Therefore a stable equilibrium exists, where the oscillatory model had an unstable equilibrium, and the trajectories will travel to the equilibrium point and not be limit cycles. We have a two-dimensional slow manifold and a two-dimensional fast foliation here, whereas with Tikhonov's method we obtain a one-dimensional slow manifold and a two-dimensional fast foliation.

Figure 5.1 shows the action potential of system (5.1) with graphs for h and n and we see that the action potential looks similar to Noble's original pacemaker potential, Fig. 4.3, except that we have one action potential here.

5.2 Replacing $\overline{m}^3$ and $\overline{h}$ with Heaviside Functions

From Fig. 5.2(a) we observed that we could replace $\overline{m}^3$ and $\overline{h}$ with Heaviside functions:

$$\overline{m}^3 \approx \theta(E - E_m), \qquad \overline{h} \approx \theta(E_h - E), \tag{5.2}$$

where E_m=-14 and E_h=-69.

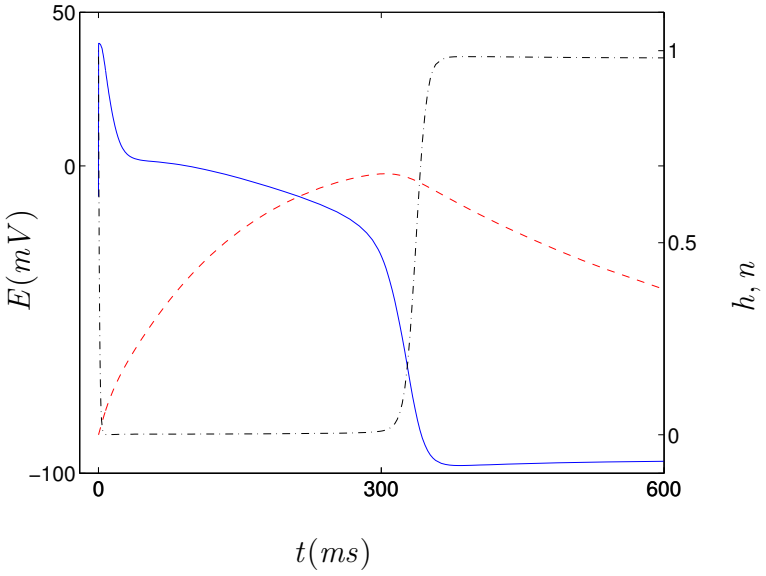

Figure 5.1: Action potential of system (5.1) (-), with h (-.) and n (- -).

This method was obtained from Biktashev's papers[58, 59] on the dissipation of excitation wave fronts, where in these papers this method was used for the Hodgkin-Huxley and Courtemanche et al's models.

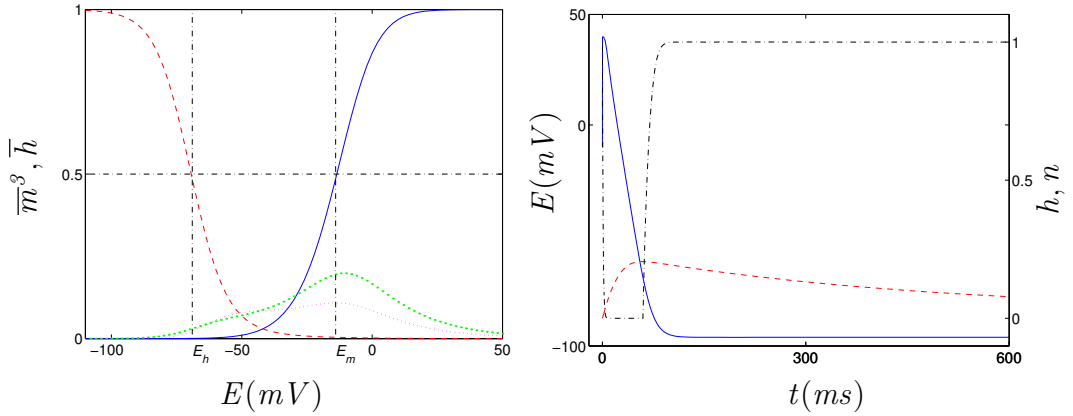

Figure 5.2: (a) Graph of $\overline{m}^3$ (-) and $\overline{h}$ (- -) with the products of $100\overline{m}^3\overline{h}$ (.) and $1000\overline{m}^3\overline{h}'$ (:). (b) Action potential of system (5.1) (-) with approximations (5.2) and h (-.) and n (- -).

Once we've done this we draw the action potential and graphs for n and h, system (5.1), with the approximations (5.2) to see what happens to the action potential. We see from Fig. 5.2(b) that with this approximation we shorten the fast onset of the action potential and therefore shorten the return by making the action potential return immediately to the resting state. This was not what we

wanted to do, as we wanted to replace $\overline{m}^3$ and $\overline{h}$ and still retain the qualitative properties of the system.

We can see why this happens by drawing the currents for the reduced system (5.1), and the reduced system with the approximations (5.2). Figure 5.3(a) shows the currents for the reduced system without the approximations, where I_{Na}=$\overline{g}_{Na}\overline{m}^3 h(E - E_{Na})$ (- -), I_{out}=$(g_{K_2} + g_{K_1})(E - E_K)$ (:) and I_{in}=$g_l(E - E_l) + 0.14(E - E_{Na})$ (-.) and Fig. 5.3(b) shows the currents for the reduced system with the approximations.

We see that if we compare both graphs, the reason for the shortening of the action potential is that I_{Na} closes very quickly. So instead of closing at t about 350ms, it closes near enough immediately and therefore we have the voltage returning to the resting state. This is because the m and h gates remain close to their quasi-stationary values as voltage slowly decreases, and therefore their product with the approximation is zero.

In the reduced model, without the approximations, the product of $\overline{m}^3\overline{h}$ remains non-zero and therefore plays a significant role in returning the action potential to its resting state. This product plays a significant role because if it is multiplied by $\overline{g}_{Na}$, which is a large number, it makes the sodium current large and therefore comparable to the potassium and leakage current. This sodium current is called the "window" sodium current because it runs in the region $[E_h, E_m]$, where the product of the gates is very small and therefore almost closed. This feature of Noble's model of Purkinje cells is not observed in models of other types of cells, e.g. Courtemanche's model, which can be seen in Fig. 5.3(c).

A study of the "window" sodium current was done in 1979 by Attwell et al[60], where he found that the sodium current was large and I_{Na_∞} will not be zero if both $\overline{m}^3$ and $\overline{h}$ are non-zero. I_{Na} is only zero if $\overline{m}^3 \to 0$ at negative potentials and if $\overline{h} \to 0$ at positive potentials.

We also see in Fig. 5.3(a) that the potassium current counteracts the sodium current for most of the plateau phase.

5.3 Axiomatic Approach

From Fig. 5.2(b) we found that if we replace $\overline{m}^3$ and $\overline{h}$ with Heaviside functions, then we shorten the action potential, therefore this is not a good approximation, as we don't want to do this. So we need to find another approximation that will

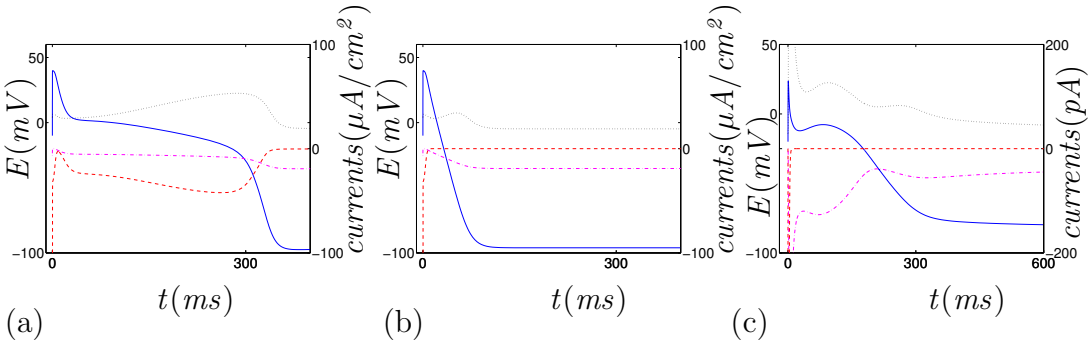

Figure 5.3: Graph of the currents I_{Na} (- -), I_{out} (:) and I_{in} (-.), and action potential (-) for (a) the reduced system (5.1) without the approximations (5.2) and (b) system (5.1) with the approximations (5.2) and (c) for Courtemanche's system (2.18).

allow us to retain the shape of the action potential.

To do this we use an axiomatic approach and obtain some axioms from observations of the properties of system (5.1). Then once we do this we can obtain a more accurate approximation and perform the embedding on the system to find the slow manifold, fast foliation and the phase portraits.

The axioms are:

A1 constant $\overline{g}_{Na}$=400 is large compared to similar constants 0.14 in I_{Na}, $\overline{g}_K$=1.2, and g_l=0. So we can describe $\overline{g}_{Na}$ by a small parameter ϵ, because the value of associated small constants $\overline{g}_K/\overline{g}_{Na}$ etc are of the order of 10^{-2}. Therefore we replace $\overline{g}_{Na}$ with:

$$\underline{\overline{g}_{Na}}(\epsilon) = \epsilon^{-1}\overline{g}_{Na}.$$

A2 Function $\frac{1}{\tau_h}$ is large, so h is a fast variable. Also the speed of h is comparable to E during the upstroke and they both are faster than n. Therefore, we characterise this speed by the same small parameter ϵ, so that:

$$\underline{\tau_h}(E;\epsilon) = \epsilon\tau_h(E).$$

A3 Function $\overline{m}^3(E)$ is finite, in fact mostly close to unity, for $E > E_m$ and small below it, Fig. 5.2(a). The value of the switch voltage E_m can be chosen at around the solution of $\overline{m}(E)$=1/2, which is -14. Therefore we replace $\overline{m}(E)$ with $\underline{\overline{m}}(E;\epsilon)$ so that:

$$\lim_{\epsilon\to 0}\left(\underline{\overline{m}}(E;\epsilon)^3\right) = M(E)\theta(E-E_m).$$

A4 Function $\overline{h}(E)$ is finite, mostly close to unity, for $E < E_h$ and small above it, Fig. 5.2(a). The value of the switch voltage E_h can be chosen at around the solution of $\overline{h}(E)$=1/2, which is -69. So we replace $\overline{h}(E)$ with $\underline{\overline{h}}(E;\epsilon)$ where:

$$\lim_{\epsilon\to 0} \underline{\overline{h}}(E;\epsilon) = H(E)\theta(E_h - E).$$

A5 The switch voltages obey the inequality:

$$E_m > E_h.$$

This is obviously satisfied from Fig. 5.2(a). A consequence of A3, A4 and A5 is that $\lim_{\epsilon\to 0}\left[\overline{\underline{m}}^3\overline{\underline{h}}\right]$=0.

A6 The product of $W(E)$=$\overline{\underline{m}}^3(E)\overline{\underline{h}}(E)$ is small, which can be seen in Fig. 5.2(a), and is of the order of ϵ. We assume, therefore, that:

$$\lim_{\epsilon\to 0}\left[\epsilon^{-1}\overline{\underline{m}}^3(E;\epsilon)\overline{\underline{h}}(E;\epsilon)\right] = \tilde{W}(E) > 0,$$

where $\tilde{W}(E)$ is in some sense close to $W(E)$.

A7 In addition to A5, we will also assume that:

$$\lim_{\epsilon\to 0}\left[\overline{\underline{m}}^3\frac{\partial}{\partial E}\overline{\underline{h}}\right] = 0.$$

So these axioms allow us to do our asymptotic embedding of system (5.1), where they say that we can introduce ϵ^{-1} in front of $\overline{g}_{Na}\overline{m}^3 h(E - E_{Na})$ and $\dot{h}$ only. Then we obtain a more accurate approximation for $\overline{m}^3$ and $\overline{h}$ and also add the product $W(E)$ to $\dot{E}$ as we need this for our approximations to work. Therefore we won't be shortening the action potential.

The reason we obtain $W(E)$ (A6) is because $\overline{h}$ is small, but $\overline{m}$ is not, which can be seen from Fig. 5.2(a). So with $\overline{m}$ not being small, if we tend $\epsilon \to 0$ to study the embedding, we have a small parameter ϵ multiplied by a large parameter $\overline{g}_{Na}\overline{m}^3$ and therefore we can't neglect $\overline{g}_{Na}\overline{m}^3\overline{h}(E - E_{Na})$. In Chapter 6 later on, we study the embedding for the fast time stage for Courtemanche's model where we see that $\overline{m}$ is small and if $\epsilon \to 0$ we can neglect the I_{Na} current, and therefore we don't need to introduce the term $W(E)$.

So if we study our embedding, $\epsilon \to 0$, we obtain a finite function of E, $W(E)$, which is positive and not smaller than ϵ. So $\epsilon^{-1}W(E)$ will leave a finite function as $\epsilon \to 0$.

A7 is included to assure that $\overline{h}^{'}$ is small as well.

Therefore we obtain our asymptotic embedding of system (5.1):

$$\begin{aligned}
\frac{\mathrm{d}E}{\mathrm{d}t} &= -\frac{1}{C_M}((\epsilon^{-1}\overline{g}_{Na}\overline{\underline{m}}^3(E;\epsilon)h + 0.14)(E - E_{Na}) \\
&\quad +(g_{K_1} + g_{K_2})(E - E_K) + g_l(E - E_l)), \\
\frac{\mathrm{d}h}{\mathrm{d}t} &= \epsilon^{-1}\frac{(\overline{\underline{h}}(E;\epsilon) - h)}{\tau_h}, \\
\frac{\mathrm{d}n}{\mathrm{d}t} &= \frac{(\overline{n} - n)}{\tau_n},
\end{aligned} \tag{5.3}$$

where A1-A5 is taken into account.

Now we consider system (5.3):

$$\begin{aligned}
\frac{\mathrm{d}E}{\mathrm{d}t} &= -\frac{1}{C_M}((\epsilon^{-1}\overline{g}_{Na}\overline{\underline{m}}^3(E;\epsilon)\overline{\underline{h}}(E;\epsilon) + 0.14)(E - E_{Na}) + (g_{K_1} + g_{K_2})(E - E_K) \\
&\quad +g_l(E - E_l)) + o(1), \\
O(\epsilon) &= \overline{\underline{h}}(E;\epsilon) - h, \\
\frac{\mathrm{d}n}{\mathrm{d}t} &= \frac{(\overline{n} - n)}{\tau_n},
\end{aligned}$$

where the $o(1)$ term in the first equation is due to the small deviation of h and $\overline{\underline{h}}$. As $\epsilon \to 0$ and taking into account A6 and A7, we have:

$$\begin{aligned}
\frac{\mathrm{d}E}{\mathrm{d}t} &= -\frac{1}{C_M}((\overline{g}_{Na}\tilde{W}(E) + 0.14)(E - E_{Na}) + (g_{K_1} + g_{K_2})(E - E_K) \\
&\quad +g_l(E - E_l)), \\
h &= H(E)\theta(E_h - E), \\
\frac{\mathrm{d}n}{\mathrm{d}t} &= \frac{(\overline{n} - n)}{\tau_n}.
\end{aligned} \tag{5.4}$$

System (5.4) defines the slow manifold which is two-dimensional because we have two slow variables. Variables E and n are the slow variables and therefore E is both a fast and slow variable, which is a non-Tikhonov feature.

Variable E is a fast variable because if we use the change of variable $t{=}\epsilon T$ and $\epsilon \to 0$ we obtain the fast system:

$$\begin{aligned}
\frac{\mathrm{d}E}{\mathrm{d}T} &= -\frac{1}{C_M}(\overline{g}_{Na}M(E)\theta(E-E_m)h(E-E_{Na})), \qquad (5.5)\\
\frac{\mathrm{d}h}{\mathrm{d}T} &= \frac{(H(E)\theta(E_h-E)-h)}{\tau_h},\\
n &= \text{constant.}
\end{aligned}$$

From system (5.5) we see that we have two fast variables E and h. The slow manifold is the set of equilibria of this system and is defined by the set of finite equations:

$$M(E)\theta(E-E_m)h = 0, \qquad (5.6)$$

$$H(E)\theta(E_h-E)-h = 0. \qquad (5.7)$$

With the substitution of (5.7) into (5.6) taking into account that A5 makes (5.6) an identity due to the product of the two Heaviside functions. Therefore we have a co-dimension one slow manifold that is defined by (5.7), as we have a three-dimensional system and a two-dimensional slow manifold, it therefore has co-dimension one. This is a non-Tikhonov feature, because in a Tikhonov system the co-dimension of the slow manifold is equal to the number of fast variables. This feature is the consequence of (5.6) becoming an identity if (5.7) is satisfied, which in turn is a consequence of a near-perfect switch behaviour of $\overline{h}(E)$ and $\overline{m}(E)$.

A consequence of this feature is that all equilibria of the fast system are not isolated, and therefore we cannot use Tikhonov's method here, as it requires asymptotic stability of equilibria of the fast system.

5.4 Modifying System (5.1)

From our axioms we can modify the reduced system (5.1) and analyse the asymptotics to see if we obtain an action potential that looks similar to Fig. 5.1. Therefore our modified system is:

$$\begin{aligned}
\frac{\mathrm{d}E}{\mathrm{d}t} &= -\frac{1}{C_M}((\overline{g}_{Na}M\theta(E-E_m)h+\overline{g}_{Na}W+0.14)(E-E_{Na}) \qquad (5.8)\\
&\quad +(g_{K_1}+g_{K_2})(E-E_K)+g_l(E-E_l)),\\
\frac{\mathrm{d}h}{\mathrm{d}t} &= \frac{(H\theta(E_h-E)-h)}{\tau_h},
\end{aligned}$$

$$\frac{\mathrm{d}n}{\mathrm{d}t} = \frac{(\overline{n}-n)}{\tau_n},$$

where $M{=}\overline{m}^3$, $H{=}\overline{h}$ and $W{=}\overline{m}^3\overline{h}$.

Here we add to the $\dot{E}$ equation another time-independent variable W, which is separate from the sodium current.

Figure 5.4 shows the action potential, the h and n graphs for systems (5.8) and (5.1). We see that the two graphs are similar, but there is a slight difference in the return due to $\overline{m}$ and $\overline{h}$ being replaced by Heaviside functions, as h now has a fracture point instead of a round point as $\overline{h}$ changes from $\overline{h}$ to 0.

Therefore the modified system has the same asymptotic properties as the original system, but now the modified system produces them constructively via a smooth explicit embedding, rather than axiomatically or via discontinuous embedding. So now the action potential has a fast onset and a smooth return, not a fast onset and a jump return like Fig. 4.3. This is now similar to Zeeman's "nerve" model where Zeeman had a fast onset and a smooth return, Fig. 2.11(c).

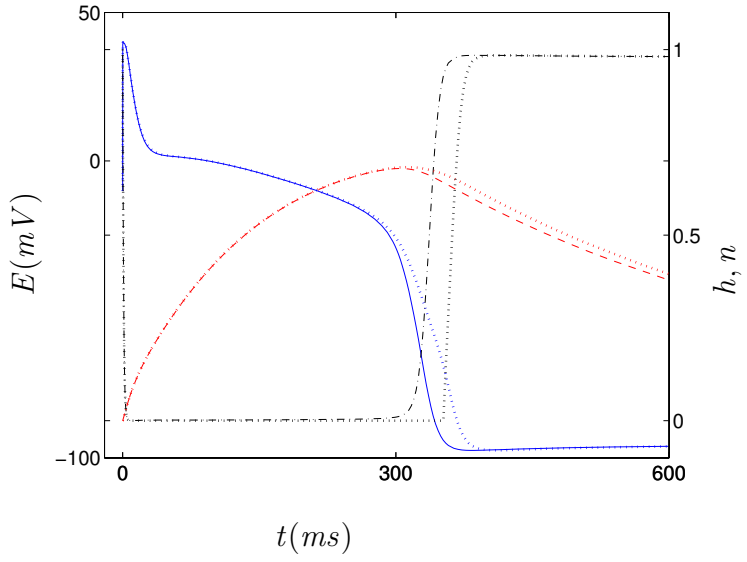

Figure 5.4: Action potential of system (5.8) (blue:), h (black:) and n (red:) with the curves for E (-), n (- -) and h (-.) from the original system (5.1).

System (5.8)'s simplest asymptotic embedding, agreeing with axioms A1-A7, is:

$$\begin{aligned}\frac{\mathrm{d}E}{\mathrm{d}t} = & -\frac{1}{C_M}((\epsilon^{-1}\overline{g}_{Na}M\theta(E-E_m)h+\overline{g}_{Na}W+0.14)(E-E_{Na}) \\ & +(g_{K_1}+g_{K_2})(E-E_K)+g_l(E-E_l)),\end{aligned} \tag{5.9}$$

$$\begin{aligned}\frac{\mathrm{d}h}{\mathrm{d}t} &= \epsilon^{-1}\frac{(H\theta(E_h-E)-h)}{\tau_h},\\ \frac{\mathrm{d}n}{\mathrm{d}t} &= \frac{(\overline{n}-n)}{\tau_n}.\end{aligned}$$

We use the change of variable $t{=}\epsilon T$ to obtain the fast system:

$$\begin{aligned}\frac{\mathrm{d}E}{\mathrm{d}T} &= -C_M^{-1}(\overline{g}_{Na}M\theta(E-E_m)h(E-E_{Na})+ \\ &\quad \epsilon((\overline{g}_{Na}W+0.14)(E-E_{Na})+(g_{K_1}+g_{K_2})(E-E_K)+g_l(E-E_l))), \\ \frac{\mathrm{d}h}{\mathrm{d}T} &= \frac{(H\theta(E_h-E)-h)}{\tau_h}, \\ \frac{\mathrm{d}n}{\mathrm{d}T} &= \epsilon\frac{(\overline{n}-n)}{\tau_n}.\end{aligned} \tag{5.10}$$

For $\epsilon \to 0$, the slow system is:

$$\begin{aligned}\frac{\mathrm{d}E}{\mathrm{d}t} &= -C_M^{-1}((\overline{g}_{Na}W+0.14)(E-E_{Na})+(g_{K_1}+g_{K_2})(E-E_K) \\ &\quad +g_l(E-E_l)), \\ h &= H\theta(E_h-E), \\ \frac{\mathrm{d}n}{\mathrm{d}t} &= \frac{(\overline{n}-n)}{\tau_n}.\end{aligned} \tag{5.11}$$

This gives us the slow manifold, defined by h, which is a two-dimensional surface as we have two slow variables.

The fast system, for $\epsilon \to 0$, is:

$$\begin{aligned}\frac{\mathrm{d}E}{\mathrm{d}T} &= -C_M^{-1}\overline{g}_{Na}M\theta(E-E_m)h(E-E_{Na}), \\ \frac{\mathrm{d}h}{\mathrm{d}T} &= \frac{(H\theta(E_h-E)-h)}{\tau_h}, \\ n &= \text{constant}.\end{aligned} \tag{5.12}$$

This gives us the fast foliation, which is n=constant, and it is a two-dimensional plane in the (h, E) plane, as there are two fast variables consisting of planes n=constant.

Figure 5.5 shows the embedding for systems (5.9) and (5.10) for two values of ϵ. We see that as $\epsilon \to 0$ the fast onset on the action potential becomes sharper and this shows the onset getting quicker. We don't see much more change to the action potential, so this shows that the modified embedding is accurate.

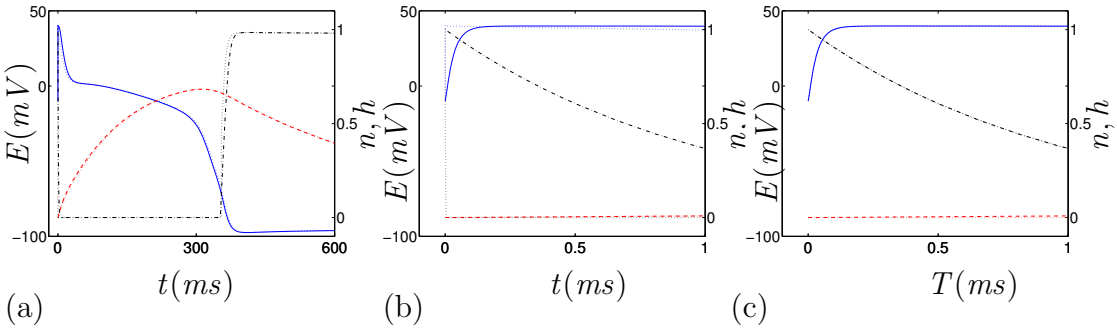

Figure 5.5: Action potential (-) with n (- -) and h (-.) for different values of ϵ for (a,b) system (5.9) and (c) system (5.10). ϵ=0.001 (:).

5.5 Slow System

Our phase portrait is going to be two-dimensional like in Chapter 4, so we take system (5.11) and analyse it so that we can draw the phase portrait. We want to find the nullclines, equilibrium points and their stability and trajectories for this system.

The n nullcline is:

$$n = \overline{n}(E),$$

and the E nullcline is:

$$\begin{aligned} 0 &= (\overline{g}_{Na}W + 0.14)(E - E_{Na}) + (g_{K_1} + g_{K_2})(E - E_K) + g_l(E - E_l), \\ n^4 &= \left(\frac{(\overline{g}_{Na}W + 0.14)(E_{Na} - E) + g_l(E_l - E) + g_{K_1}(E_K - E))}{1.2(E - E_K)} \right). \end{aligned}$$

The equation for n^4 is the same equation as the slow manifold in the Tikhonov embedding, except that here E_K=−110.

To find the stability of the three points where the n and E nullclines intersect, (n, E)=(0.281, −61.09), (0.51, −46.09), and (0.02366, −95.7453), we find the Jacobian of the system (5.11). We use the determinant of the Jacobian of $\dot{E}$ and $\dot{h}$ as one of the equations that satisfies the fold curve, the other equations that satisfies it are:

$$\dot{E} = 0, \qquad \dot{h} = 0.$$

The Jacobian matrix is:

$$J_{En} = \frac{\partial(\dot{E}, \dot{n})}{\partial(E, n)}$$

$$= \begin{pmatrix} -C_M^{-1}(g_l + g_{K_1} + 1.2n^4 + 0.14 & -4C_M^{-1}n^3 1.2(E - E_K) \\ \overline{g}_{Na}\overline{m}^3\overline{h} + g_{K_1}^{'}(E - E_K) & \\ +\overline{m}^2\overline{g}_{Na}(E_{Na} - E)(\overline{m}\overline{h}^{'} + 3\overline{m}^{'}\overline{h})) & \\ \\ \frac{\overline{n}^{'}}{\tau_n} - \frac{(\overline{n}-n)\tau_n^{'}}{\tau_n^2} & -\frac{1}{\tau_n} \end{pmatrix}.$$

However, at an equilibrium $n{=}\overline{n}(E)$, the Jacobian becomes:

$$J_{Eh} = \begin{pmatrix} -C_M^{-1}(g_l + g_{K_1} + 1.2\overline{n}^4 + 0.14 & -4C_M^{-1}\overline{n}^3 1.2(E - E_K) \\ \overline{g}_{Na}\overline{m}^3\overline{h} + g_{K_1}^{'}(E - E_K) & \\ +\overline{m}^2\overline{g}_{Na}(E_{Na} - E)(\overline{m}\overline{h}^{'} + 3\overline{m}^{'}\overline{h})) & \\ \\ \frac{\overline{n}^{'}}{\tau_n} & -\frac{1}{\tau_n} \end{pmatrix}.$$

An equilibrium is stable in linear approximation if and only if $\mathrm{Tr}(J_{En}) < 0$ and $\det(J_{En}) > 0$. So we have:

$$\begin{aligned} \mathrm{Tr}(J_{En}) &= -C_M^{-1}(g_l + g_{K_1} + 1.2\overline{n}^4 + 0.14 + g_{K_1}^{'}(E - E_K) + \overline{g}_{Na}\overline{m}^3\overline{h} \\ &\quad +\overline{m}^2\overline{g}_{Na}(E - E_{Na})(\overline{m}\overline{h}^{'} + 3\overline{m}^{'}\overline{h})) - \frac{1}{\tau_n}, \\ \det(J_{En}) &= C_M^{-1}\tau_n^{-1}(g_l + g_{K_1} + 1.2\overline{n}^4 + 0.14 + \overline{g}_{Na}\overline{m}^3\overline{h} + g_{K_1}^{'}(E - E_K) \\ &\quad +\overline{m}^2\overline{g}_{Na}(E - E_{Na})(\overline{m}\overline{h}^{'} + 3\overline{m}^{'}\overline{h}) + 4\overline{n}^3 1.2(E - E_K)\overline{n}^{'}). \end{aligned}$$

We draw the graphs of the $\det(J_{En})$ and $\mathrm{Tr}(J_{En})$ against E to check where our points lie and if they are stable ($\mathrm{Tr}(J_{En}) < 0$ and $\det(J_{En}) > 0$), unstable ($\mathrm{Tr}(J_{En}) > 0$ and $\det(J_{En}) > 0$) or a saddle ($\mathrm{Tr}(J_{En}) < 0$ and $\det(J_{En}) < 0$). We see from Fig. 5.6 that $(n, E){=}(0.0236, -95.7453)$ (F) is a stable point, $(n, E){=}(0.281, -61.09)$ (G) is a saddle point and $(n, E){=}(0.51, -46.09)$ (H) is an unstable point. So therefore the slow manifold has attractive and repelling pieces, which are determined by the sign of the determinant.

From studying the stability, we found that G is an unstable spiral as $\mathrm{Tr}(J_{En})^2 - 4\det(J_{En}) < 0$. The eigenvalues for all three points are:

$$\begin{aligned} \mathrm{F}: &\quad \lambda_1 = 0.0408, \qquad \lambda_2 = -0.00165, \\ \mathrm{G}: &\quad \lambda_{1,2} = 0.0084 \pm 0.0019i, \\ \mathrm{H}: &\quad \lambda_1 = -0.0022, \qquad \lambda_2 = -0.088. \end{aligned}$$

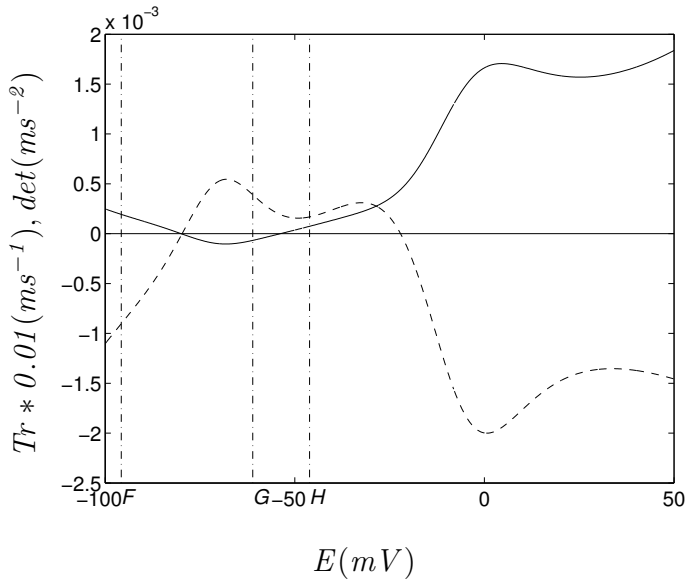

Figure 5.6: Graph of Tr(J_{En})∗0.01 (- -) and det(J_{En}) (-), where F, G and E correspond to Fig. 5.7.

Figure 5.7(a) and (b) show the phase portraits for the slow system with a trajectory (thick dotted line) for system (5.9) with (a) ϵ=1 and (b) ϵ=0.001. Also we see that for $\epsilon \to 0$ the onset becomes sharper. So the trajectory will start at point B and travel along the slow manifold until it reaches the repellor piece of the slow manifold (D), this is our fold point (threshold), then it jumps down the fast foliation to the point (E) and travels along the stable piece of the slow manifold until it reaches the equilibrium point (F).

The phase portrait is similar to Fig. 4.7, except here our slow manifold has a section that is in the complex plane, and therefore cannot be seen, and we have a stable equilibrium point instead of an unstable one. Also here the two points that are a saddle and unstable points can be seen more clearly.

The action potential in Fig. 5.8 can be compared with the trajectories to see what happens to the onset and the return.

5.6 Fast System

We take system (5.12) and analyse it so that we can draw its phase portrait. We want to find the isoclines, equilibrium points and trajectories.

The h isocline is:

$$h = H\theta(E_h - E),$$

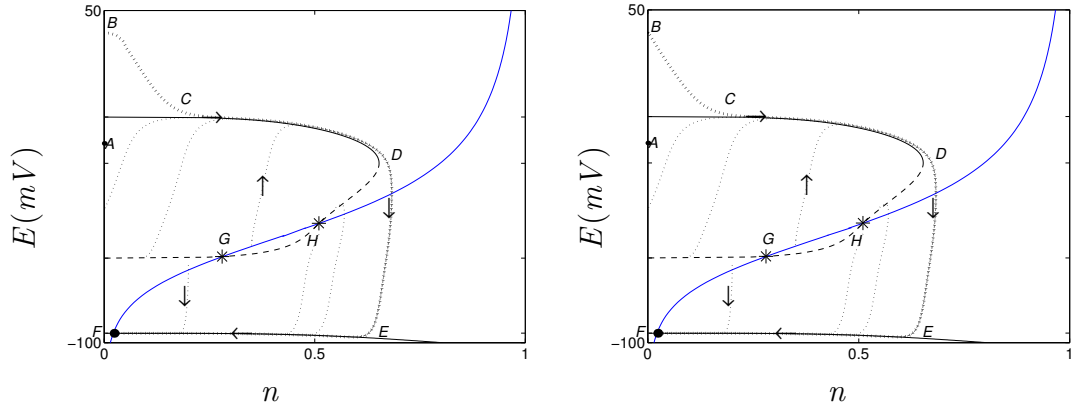

Figure 5.7: Phase portrait for the slow system with n nullcline (-), E nullcline (- -) and numerical trajectories, system (5.11), for (a) ϵ=1 and (b) ϵ=0.001 (:). The thick dotted line is the trajectory corresponding to system (5.9). The arrows represent the flow of the trajectory. A-F mark feature points of the action potential trajectory. G=$(0.281, -61.09)$ and H=$(0.51, -46.09)$.

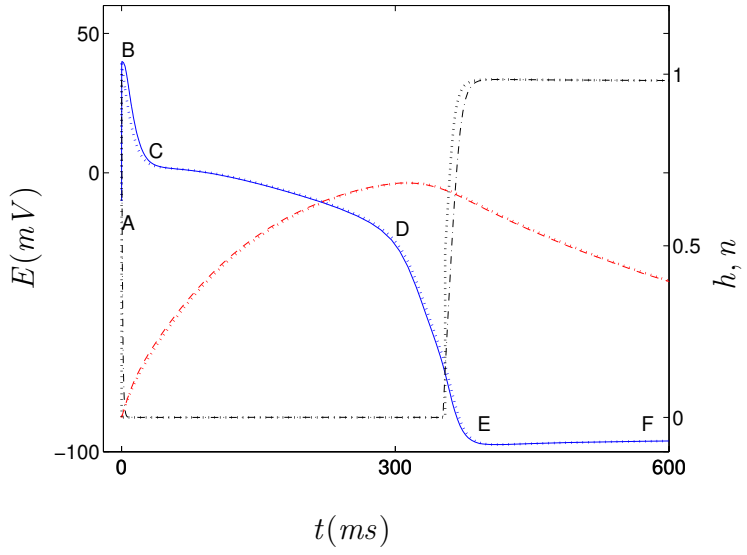

Figure 5.8: Action potential for system (5.9) (-) with h (-.) and n (- -), for ϵ=1 and ϵ=0.001 (:).

and the E isocline is defined by equation:

$$\overline{g}_{Na}M(E)\theta(E-E_m)h(E-E_{Na})=0.$$

From this the solutions are:

$$\begin{cases} E & \in & [-\infty, E_m], \\ h & \in & [0,1], \end{cases}$$

$$\begin{cases} E & \in & [-\infty, +\infty], \\ h & = & 0, \end{cases}$$

and

$$\begin{cases} E & = & E_{Na}, \\ h & \in & [0,1]. \end{cases}$$

The equation for the equilibrium points satisfies $\frac{\mathrm{d}h}{\mathrm{d}T}$=0 and $\frac{\mathrm{d}E}{\mathrm{d}T}$=0. We know that for $\frac{\mathrm{d}h}{\mathrm{d}T}$=0 we obtain h=$H\theta(E_h-E)$, so we put this into the equation for $\frac{\mathrm{d}E}{\mathrm{d}T}$=0 to obtain:

$$\overline{g}_{Na}M\theta(E-E_m)H\theta(E_h-E)(E-E_{Na})=0.$$

The solution from this equation is:

$$\begin{cases} E & \in & [-\infty, \infty], \\ h & = & H\theta(E_h-E). \end{cases}$$

Figure 5.9(a) and (b) shows the phase portraits for the fast system with a trajectory (thick dotted line) for system (5.10) with (a) ϵ=1 and (b) ϵ=0.001.

5.6.1 If we consider τ_h as a constant

We replace τ_h with a constant to obtain an analytical solution for the trajectories of system (5.10).

We choose the value for τ_h at E=E_{Na}. We used E_{Na} because we are only interested in the region $[E_m, E_{Na}]$ and this is the maximum value of E in this range.

If $E < E_m$, the trajectories are straight lines as we have:

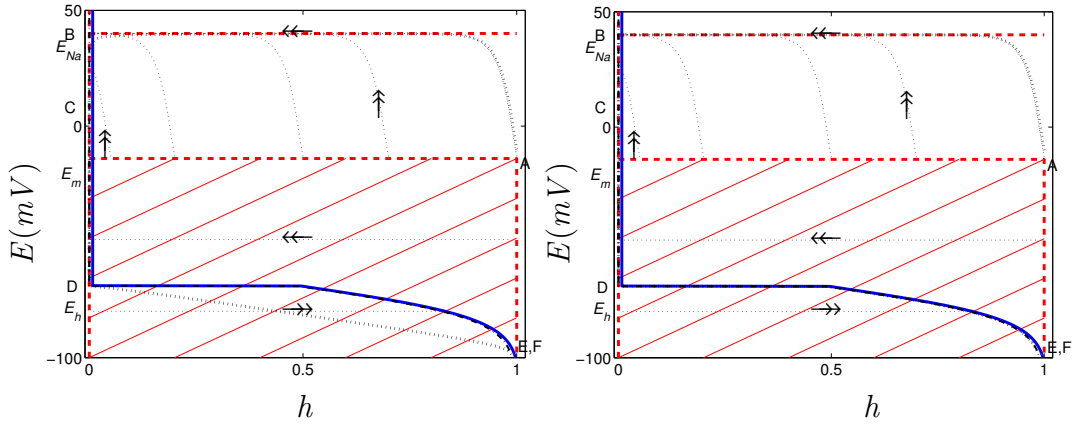

Figure 5.9: Phase portrait for the fast system with h isocline (-), E isocline (- -) and the dashed region, equilibrium points (-.), numerical trajectories, fast system (5.12), (:) for (a) ϵ=1 and (b) ϵ=0.001. The thick dotted trajectory corresponds to the full system (5.10). The arrows represent the flow of the trajectories.

$$\begin{aligned}\frac{\mathrm{d}E}{\mathrm{d}T} &= 0,\\ \frac{\mathrm{d}h}{\mathrm{d}T} &= \frac{H\theta(E_h-E)-h}{\tau_h},\end{aligned}$$

as $M\theta(E-E_m)$=0. Therefore E=constant and

$$h = H\theta(E_h-E)+(h_0-H\theta(E_h-E))e^{-(T-T_0)/\tau_h(E)}.$$

If $E > E_m$, $H\theta(E_h-E)=0$ and $M\theta(E_m-E)=\overline{m}^3$.

$$\begin{aligned}\frac{\mathrm{d}h}{\mathrm{d}E} &= \frac{\frac{\mathrm{d}h}{\mathrm{d}T}}{\frac{\mathrm{d}E}{\mathrm{d}T}} = \frac{C_m}{\tau_h(E_{Na})\overline{g}_{Na}\overline{m}^3(E)(E-E_{Na})},\\ \int_{h_0}^{h}\mathrm{d}h &= \frac{C_m}{\tau_h(E_{Na})\overline{g}_{Na}}\int_{E_0}^{E}\frac{1}{\overline{m}^3(E)(E-E_{Na})}\mathrm{d}E,\\ h &= h_0+\frac{C_m}{\tau_h(E_{Na})\overline{g}_{Na}}\int_{E_0}^{E}\frac{1}{\overline{m}^3(E)(E-E_{Na})}\mathrm{d}E. \qquad (5.13)\end{aligned}$$

We obtain our answer for the analytical trajectories in quadratures because $\overline{m}^3$ is a function containing exponentials and therefore equation (5.13) cannot be integrated easily.

5.7 Summary

We have found a non-Tikhonov embedding that retains the qualitative properties of Noble's system, fast onset and smooth return. We kept the asymptotic structure of Noble's system, but found that if we tend $\epsilon \to 0$ in the three-dimensional system, including the approximations for $\overline{m}$ and $\overline{h}$, that we didn't obtain a one-dimensional slow manifold, like in Chapter 4, instead we have a two-dimensional slow manifold.

To be able to do the asymptotic embedding of Noble's reduced system (5.1), we needed to modify this system so that we could retain the asymptotic properties of the system. So we formulated seven axioms that described the properties of the three-dimensional reduced system (5.1) and from these we could obtain our modified model (5.8), then we could do our asymptotic embedding on this system to obtain the phase portraits in the fast and slow time scales.

We found from our analysis that the simple asymptotic embedding, replacing $\overline{m}$ and $\overline{h}$ with Heaviside functions, didn't retain the qualitative features of the system, whereas the embedding for the modified model did. So from the phase portraits for the fast and slow embedding we found that the trajectories travelled to the equilibrium point of system (5.8).

We compared the two phase portraits of the slow time scale with Fig. 4.7 and saw that the E nullcline had the same equation as the slow manifold using Tikhonov's embedding in Chapter 4.

In the fast system we don't have different fast leaves as before for different values of n, instead here n doesn't enter our equations. So we have the same fast phase portrait for all n with nullclines, sets of equlilbria points and trajectories that follow the nullclines to the equilibrium point.

Therefore the main features of the non-Tikhonov embedding are:

1. that it preserves the smooth return of the original four-dimensional system,

2. E is both a fast and slow variable,

3. the fast subsystem is extremely unusual because it gives a whole line of equilibria which are neither asymptotically stable or isolated, and

4. the slow manifold has co-dimension one, despite having two slow variables.

Chapter 6

The Human Atrial Cell Action Potential-Courtemanche et al Model

In this chapter we analyse the Courtemanche et al model[1], with a view to reduce it to a simpler form using asymptotic methods, and then perform qualitative analysis wherever possible. As the model is much more complicated than the models considered previously, we deliberately restrict our attention to approximating one selected action potential solution.

We choose to study one solution for a certain initial condition and not a series of solutions for different initial conditions, as this would be too complicated. We only use one solution to see how accurate our methods are, and if they will work for a complicated model for one solution.

We want to demonstrate that the asymptotic techniques are applicable in principle to detailed contemporary models.

6.1 Time Scales and Time Stages

We want to analyse the Courtemanche system, so we can reduce it to a combination of simpler systems, which don't contain small parameters.

6.1.1 The action potential solution

In their paper[1] Courtemanche et al uses two different values for I_{st}, where I_{st} is the stimulus current, which is a function that depends on time. I_{st} takes two

values depending on time which is written as:

$$I_{st}(t) = I_{st(max)}\theta(t-100)\theta(102-t),$$

where $I_{st(max)}$=−2000pA and time t is measured in ms.

From this we can see that for the first 100ms, I_{st}=0 and there is a balance of membrane currents in diastole. Courtemanche et al says that during the diastole phase, the relaxed state of the heart, the steady state involves a balance between the pump and exchanger currents $I_{Na,K}$, $I_{p,Ca}$ and $I_{Na,Ca}$, the background currents $I_{b,Na}$ and $I_{b,Ca}$, and I_{K_1}.

Then at 100ms a 2ms pulse of I_{st}=$I_{st(max)}$, twice the diastolic threshold, is introduced to the system of equations and this causes the overshot to happen in the action potential. This pulse is over at 102ms, so I_{st}=0 again and the voltage returns back to its resting state. This gives us a spike and dome shaped action potential as seen in Fig. 6.1(a).

We want to treat system (6.1) without external stimulus current, I_{st}, so we put I_{st} always equal to zero and therefore we don't have the 100ms diastole state, instead we'll start our action potential at t=0.

To be able to do this we need to find the threshold value of E_0 that will let us keep the shape of the action potential for I_{st}=0. From our numerical experiments we have found that any value between $[-50, 0]$ will do this, so we choose the value E_0=−20 so that we can see the overshot happening. So Fig. 6.1(b) shows the action potential for our new values of E_0=−20 and I_{st}=0.

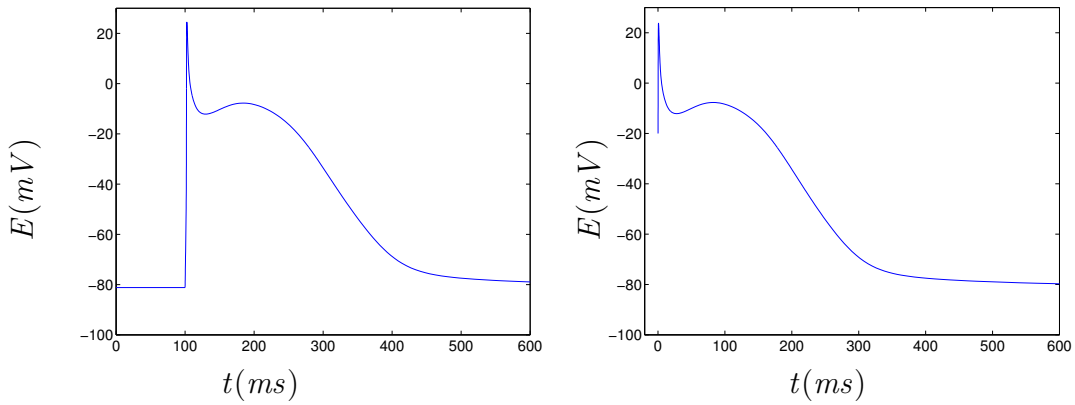

(a) (b)

Figure 6.1: Action potential of CRN-21 with (a) I_{st}=−2000, E_0=−81.18 and (b) I_{st}=0, E_0=−20.

Our CRN-21 system is:

$$
\begin{aligned}
\frac{\mathrm{d}E}{\mathrm{d}t} &= -\frac{I_{ion}}{C_M}, \qquad (6.1)\\
I_{ion} &= I_{Na}(E,m,h,j) + I_{K1}(E,Ki) + I_{to}(E,Ki,o_a,o_i)\\
&\quad + I_{Kur}(E,Ki,u_a,u_i) + I_{Kr}(E,Ki,x_r) + I_{Ks}(E,Ki,x_s)\\
&\quad + I_{Ca,L}(E,d,f,f_{Ca}) + I_{p,Ca}(Cai) + I_{Na,K}(E,Nai)\\
&\quad + I_{NaCa}(E,Nai,Cai) + I_{b,Na}(E,Nai) + I_{b,Ca}(E,Cai),\\
\frac{\mathrm{d}y}{\mathrm{d}t} &= \frac{\overline{y}-y}{\tau_y}, \qquad y = m,h,j,o_a,o_i,u_a,u_i,x_r,x_s,d,f,f_{Ca},u,v,w,\\
\frac{\mathrm{d}Nai}{\mathrm{d}t} &= (FV_i)^{(-1)}(-3I_{NaK}(E,Nai) + 3I_{NaCa}(E,Nai,Cai)\\
&\quad + I_{b,Na}(E,Nai) + I_{Na}(E,m,h,j)),\\
\frac{\mathrm{d}Ki}{\mathrm{d}t} &= (FV_i)^{(-1)}(2I_{NaK}(E,Nai) - I_{K1}(E,Ki) - I_{to}(E,Ki,o_a,o_i)\\
&\quad - I_{Kur}(E,Ki,u_a,u_i) - I_{Kr}(E,Ki,x_r) - I_{Ks}(E,Ki,x_s)\\
&\quad - I_{b,K}(E,Ki)),\\
\frac{\mathrm{d}Cai}{\mathrm{d}t} &= \frac{B1}{B2},\\
B1 &= (2FV_i)^{(-1)}(2I_{NaCa}(E,Nai,Cai) - I_{p,Ca}(Cai)\\
&\quad - I_{Ca,L}(E,d,f,f_{Ca}) - I_{b,Ca}(E,Cai))\\
&\quad + (V_i)^{(-1)}(V_{up}(I_{up,leak}(Caup) - I_{up}(Cai))\\
&\quad + I_{rel}(Cai,Carel,u,v,w)V_{rel}),\\
B2 &= 1 + \frac{[Trpn]_{max}K_{m,Trpn}}{(Cai+K_{m,Trpn})^2} + \frac{[Cmdn]_{max}K_{m,Cmdn}}{(Cai+K_{m,Cmdn})^2},\\
\frac{\mathrm{d}Caup}{\mathrm{d}t} &= I_{up}(Cai) - I_{up,leak}(Caup) - I_{tr}(Caup,Carel)\frac{V_{rel}}{V_{up}},\\
\frac{\mathrm{d}Carel}{\mathrm{d}t} &= \frac{(I_{tr}(Caup,Carel) - I_{rel}(Cai,Carel,u,v,w))}{\left(1 + \frac{[Csqn]_{max}K_{m,Csqn}}{(Carel+K_{m,Csqn})^2}\right)},
\end{aligned}
$$

and the initial conditions are:

$$
\begin{aligned}
y_0 &= (E_0, Nai_0, Ki_0, Cai_0, Caup_0, Carel_0, m_0, h_0, j_0, o_{a_0}, o_{i_0}, u_{a_0}, u_{i_0}, x_{r_0}, x_{s_0}, d_0,\\
&\quad f_0, f_{Ca_0}, u_0, v_0, w_0),\\
&= (-20, 11.17, 0.0139, 1.013 * 10^{-4}, 1.488, 1.488, 2.908 * 10^{-3}, 0.9649, 0.9775,\\
&\quad 0.03043, 0.9992, 4.966 * 10^{-3}, 0.9986, 3.296 * 10^{-5}, 0.01869, 1.367 * 10^{-4},\\
&\quad 0.9996, 0.7755, 2.350 * 10^{-112}, 1, 0.9992).
\end{aligned}
$$

6.1.2 Speed analysis

We first want to be able to put the variables into two categories, super-fast and super-slow. There are also fast and slow variables as well, but we are only interested at the moment in determining which are super-fast and which are super-slow. To do this we use Tikhonov's method for fast-slow systems to find which variables are super-fast and which are super-slow. We draw the graph of the τ's for the 21 variables in this system.

To obtain the graphs of the τ's against time we use the definition:

$$\tau_y = -\left|\frac{\partial}{\partial y}\left(\frac{\mathrm{d}y}{\mathrm{d}t}\right)\right|^{-1}, \tag{6.2}$$

where y=$E, Cai, Nai, Ki, Caup, Carel, m, h, j, o_a, o_i, u_a, u_i, x_r$, x_s, d, f, f_{Ca}, u, v and w.

Figure 6.2 shows us the graph of the τ's and from this we can see that the variables with the smaller τ will be called super-fast and fast variables, the variables with the larger τ will be called super-slow and slow variables. This helps us to obtain an asymptotic embedding of the system using the super-fast, super-slow, fast and slow variables.

As we see from Fig. 6.2, the τ's intersect each other for the time period $[0, 600]$, but we are able to see clearly that the m variable is a super-fast variable and the Ki and Nai variables are the super-slow variables.

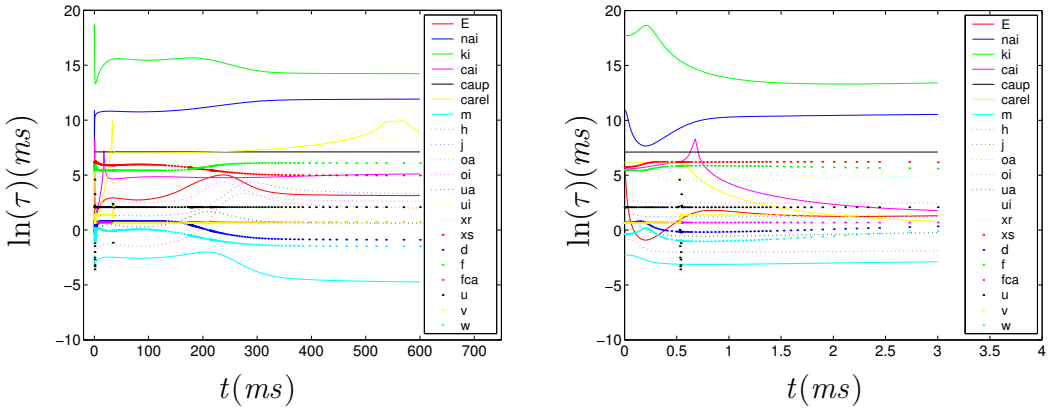

(a) (b)

Figure 6.2: Graph of the ln(τ)'s for CRN-21, system (6.1), for I_{st}=0, E_0=−20, and (a) t=[0, 600] and (b) t=[0, 3].

6.1.3 Elimination of the super-slow variables

We start eliminating the super-slow variables from CRN-21. We consider Nai, Ki, $Caup$ and u_i as the super-slow variables as these are the largest τ's, from Fig. 6.2.

We want to check that the super-slow variables are actually super-slow variables. So we take CRN-21 and we introduce ϵ to the right-hand sides of Nai, Ki, $Caup$ and u_i. We then tend ϵ to zero to see what happens to the shape of the action potential. We also check this by putting ϵ=0 in system (6.3). So we replace system (6.1) with:

$$
\begin{aligned}
\frac{\mathrm{d}E}{\mathrm{d}t} &= -\frac{I_{ion}}{C_M}, \qquad (6.3)\\
I_{ion} &= I_{Na}(E,m,h,j) + I_{K1}(E,Ki) + I_{to}(E,Ki,o_a,o_i) + I_{Kur}(E,Ki,u_a,u_i)\\
&\quad + I_{Kr}(E,Ki,x_r) + I_{Ks}(E,Ki,x_s) + I_{Ca,L}(E,d,f,f_{Ca}) + I_{p,Ca}(Cai)\\
&\quad + I_{Na,K}(E,Nai) + I_{NaCa}(E,Nai,Cai) + I_{b,Na}(E,Nai) + I_{b,Ca}(E,Cai),\\
\frac{\mathrm{d}y}{\mathrm{d}t} &= \frac{\overline{y}-y}{\tau_y}, \qquad y = m,h,j,o_a,o_i,u_a,x_r,x_s,d,f,f_{Ca},u,v,w,\\
\dot{u_i} &= \epsilon\frac{(\overline{u}_i - u_i)}{\tau_{u_i}},\\
\frac{\mathrm{d}Nai}{\mathrm{d}t} &= \epsilon(FV_i)^{(-1)}(-3I_{NaK}(E,Nai) + 3I_{NaCa}(E,Nai,Cai) + I_{b,Na}(E,Nai)\\
&\quad + I_{Na}(E,m,h,j)),\\
\frac{\mathrm{d}Ki}{\mathrm{d}t} &= \epsilon(FV_i)^{(-1)}(2I_{NaK}(E,Nai) - I_{K1}(E,Ki) - I_{to}(E,Ki,o_a,o_i)\\
&\quad - I_{Kur}(E,Ki,u_a,u_i) - I_{Kr}(E,Ki,x_r) - I_{Ks}(E,Ki,x_s) - I_{b,K}(E,Ki)),\\
\frac{\mathrm{d}Cai}{\mathrm{d}t} &= \frac{B1}{B2},\\
B1 &= (2FV_i)^{(-1)}(2I_{NaCa}(E,Nai,Cai) - I_{p,Ca}(Cai) - I_{Ca,L}(E,d,f,f_{Ca})\\
&\quad - I_{b,Ca}(E,Cai)) + (V_i)^{(-1)}(V_{up}(I_{up,leak}(Caup) - I_{up}(Cai))\\
&\quad + I_{rel}(Cai,Carel,u,v,w)V_{rel}),\\
B2 &= 1 + \frac{[Trpn]_{max}K_{m,Trpn}}{(Cai+K_{m,Trpn})^2} + \frac{[Cmdn]_{max}K_{m,Cmdn}}{(Cai+K_{m,Cmdn})^2},\\
\frac{\mathrm{d}Carel}{\mathrm{d}t} &= \frac{(I_{tr}(Caup,Carel) - I_{rel}(Cai,Carel,u,v,w))}{\left(1+\frac{[Csqn]_{max}K_{m,Csqn}}{(Carel+K_{m,Csqn})^2}\right)},\\
\frac{\mathrm{d}Caup}{\mathrm{d}t} &= \epsilon\left(I_{up}(Cai) - I_{up,leak}(Caup) - I_{tr}(Caup,Carel)\frac{V_{rel}}{V_{up}}\right).
\end{aligned}
$$

If we put ϵ=0 we see that the resulting action potential doesn't change compared to the CRN-21 action potential and this can be seen in Fig. 6.3(a).

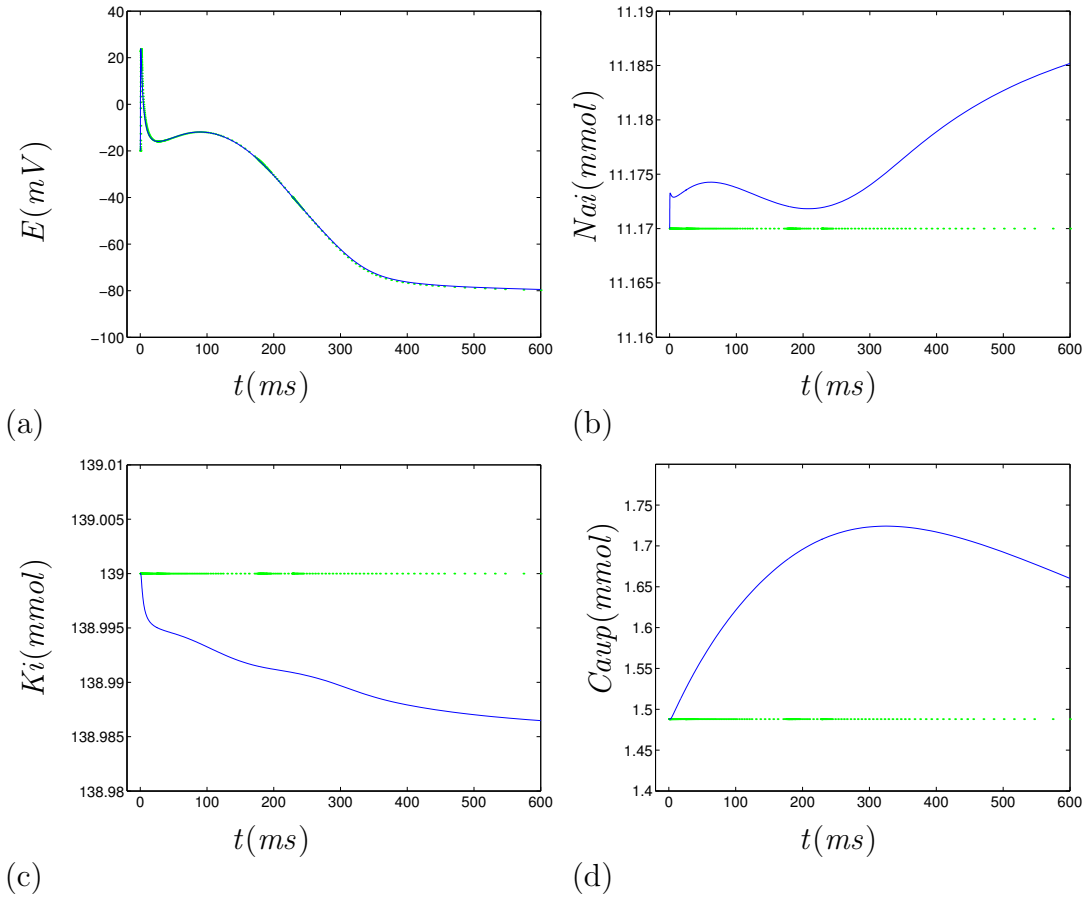

Figure 6.3: Graphs of CRN-21, system (6.1), (-) and CRN-21, system (6.3), (.) with the super-slow variables frozen, Nai, Ki, $Caup$ and u_i. (a) E, (b) Nai, (c) Ki, (d) $Caup$, and (e) u_i.

We also see from Fig. 6.3(b), (c) and (d) that if ϵ=0 Nai, Ki, $Caup$ and u_i can be treated as their initial values. So therefore the variables can be replaced with their initial values, as they are super-slow variables. Now we have a system of 17 equations, CRN-17:

$$\begin{aligned}
\frac{\mathrm{d}E}{\mathrm{d}t} &= -\frac{I_{ion}}{C_M}, \qquad (6.4)\\
I_{ion} &= I_{Na}(E,m,h,j) + I_{K1}(E) + I_{to}(E,o_a,o_i) + I_{Kur}(E,u_a) + I_{Kr}(E,x_r)\\
&\quad + I_{Ks}(E,x_s) + I_{Ca,L}(E,d,f,f_{Ca}) + I_{p,Ca}(Cai) + I_{Na,K}(E) + I_{b,Na}(E)\\
&\quad + I_{NaCa}(E,Cai) + I_{b,Ca}(E,Cai),\\
\frac{\mathrm{d}y}{\mathrm{d}t} &= \frac{\overline{y}-y}{\tau_y}, \qquad y = m,h,j,o_a,o_i,u_a,x_r,x_s,d,f,f_{Ca},u,v,w,\\
\frac{\mathrm{d}Cai}{\mathrm{d}t} &= \frac{B1}{B2},\\
B1 &= (2FV_i)^{(-1)}(2I_{NaCa}(E,Cai) - I_{p,Ca}(Cai) - I_{Ca,L}(E,d,f,f_{Ca})\\
&\quad - I_{b,Ca}(E,Cai)) + (V_i)^{(-1)}(V_{up}(I_{up,leak} - I_{up}(Cai))\\
&\quad + I_{rel}(Cai,Carel,u,v,w)V_{rel}),\\
B2 &= 1 + \frac{[Trpn]_{max}K_{m,Trpn}}{(Cai+K_{m,Trpn})^2} + \frac{[Cmdn]_{max}K_{m,Cmdn}}{(Cai+K_{m,Cmdn})^2},\\
\frac{\mathrm{d}Carel}{\mathrm{d}t} &= \frac{(I_{tr}(Carel) - I_{rel}(Cai,Carel,u,v,w))}{\left(1+\frac{[Csqn]_{max}K_{m,Csqn}}{(Carel+K_{m,Csqn})^2}\right)}.
\end{aligned}$$

6.1.4 Adiabatical elimination of the super-fast variables

Now that we have eliminated the super-slow variables, we can eliminate the super-fast variables. We see that m, u_a and w have the smallest τ's, so we check this by introducing $1/\epsilon$ to the right-hand sides of their equations:

$$\dot{x} = \frac{1}{\epsilon}\frac{(\overline{x}-x)}{\tau_x}, \qquad x = m,u_a,w. \qquad (6.5)$$

If we tend ϵ to zero, we obtain the solution x=$\overline{x}$ and we can adiabatically eliminate these variables from system (6.4) by replacing them with their quasi-stationary values in the system. Where,

$$\overline{x} = \frac{\alpha_x}{\alpha_x+\beta_x},$$

for all gating variables.

As we want to replace x with $\overline{x}$, then we want to see what difference there is between x and $\overline{x}$ for these variables and this shows us how accurate the replacement is. We draw the graphs for each variable in the long and short time scales to see the differences, Fig. 6.4. For the short time scale we can see where the differences are and they are mostly at the spike.

We see that m is close to its quasi-stationary value. So this gives us the result that m is a super-fast variable and is also responsible for the excitability at the spike.

We see that there are changes in u_a and w. These variables correspond to the height of the spike being higher than for CRN-21 in the time scale t=$[0, 600]$, but we can still consider them a good replacement.

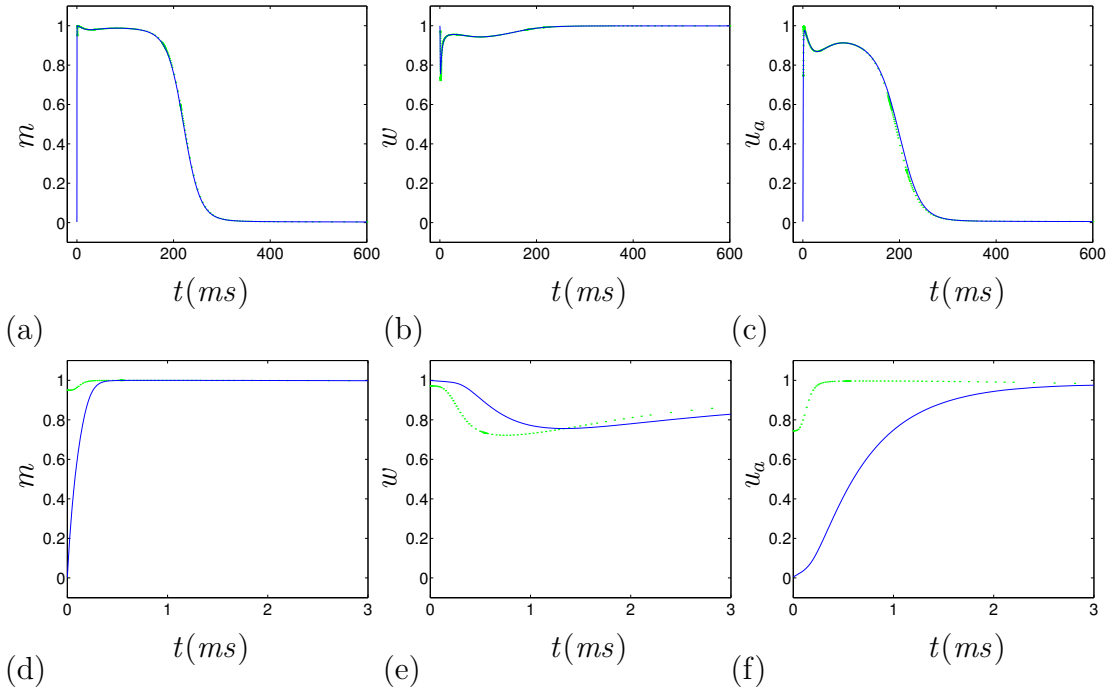

Figure 6.4: Graphs of the super-fast variables (-) and their quasi-stationary values (.) for CRN-17, system (6.4), (a) m, t=$[0, 600]$, (b) w, t=$[0, 600]$, (c) u_a, t=$[0, 600]$, (d) m, t=$[0, 3]$, (e) w, t=$[0, 3]$ and (f) u_a, t=$[0, 3]$.

So we now know that this is a good replacement, therefore we put ϵ=0 in CRN-17 and replace x=$\overline{x}$ to give us a new system CRN-14:

$$\begin{aligned} \frac{\mathrm{d}E}{\mathrm{d}t} &= -\frac{I_{ion}}{C_M}, \qquad (6.6) \\ I_{ion} &= I_{Na}(E, \overline{m}, h, j) + I_{K1}(E) + I_{to}(E, o_a, o_i) + I_{Kur}(E, \overline{u}_a) + I_{Kr}(E, x_r) \\ &\quad + I_{Ks}(E, x_s) + I_{Ca,L}(E, d, f, f_{Ca}) + I_{p,Ca}(Cai) + I_{Na,K}(E) + I_{b,Na}(E) \end{aligned}$$

$$
\begin{aligned}
& +I_{NaCa}(E,Cai)+I_{b,Ca}(E,Cai),\\
\frac{\mathrm{d}y}{\mathrm{d}t} &= \frac{\overline{y}-y}{\tau_y}, \qquad y=h,j,o_a,o_i,x_r,x_s,d,f,f_{Ca},u,v,\\
\frac{\mathrm{d}Cai}{\mathrm{d}t} &= \frac{B1}{B2},\\
B1 &= (2FV_i)^{(-1)}(2I_{NaCa}(E,Cai)-I_{p,Ca}(Cai)-I_{Ca,L}(E,d,f,f_{Ca})\\
& -I_{b,Ca}(E,Cai))+(V_i)^{(-1)}(V_{up}(0.000496-I_{up}(Cai))\\
& +I_{rel}(Cai,Carel,u,v,\overline{w})V_{rel}),\\
B2 &= 1+\frac{[Trpn]_{max}K_{m,Trpn}}{(Cai+K_{m,Trpn})^2}+\frac{[Cmdn]_{max}K_{m,Cmdn}}{(Cai+K_{m,Cmdn})^2},\\
\frac{\mathrm{d}Carel}{\mathrm{d}t} &= \frac{(I_{tr}(Carel)-I_{rel}(Cai,Carel,u,v,\overline{w}))}{\left(1+\frac{[Csqn]_{max}K_{m,Csqn}}{(Carel+K_{m,Csqn})^2}\right)},
\end{aligned}
$$

and the initial conditions are:

$$
\begin{aligned}
y_0 &= (E_0,Nai_0,Ki_0,Cai_0,Caup_0,Carel_0,m_0,h_0,j_0,o_{a_0},o_{i_0},u_{a_0},u_{i_0},x_{r_0},x_{s_0},d_0,f_0,\\
& f_{Ca_0},u_0,v_0,w_0),\\
&= (-20,11.17,0.0139,1.013*10^{-4},1.488,1.488,2.908*10^{-3},0.9649,0.9775,\\
& 0.03043,0.9992,4.966*10^{-3},0.9986,3.296*10^{-5},0.01869,1.367*10^{-4},\\
& 0.9996,0.7755,2.350*10^{-112},1,0.9992).
\end{aligned}
$$

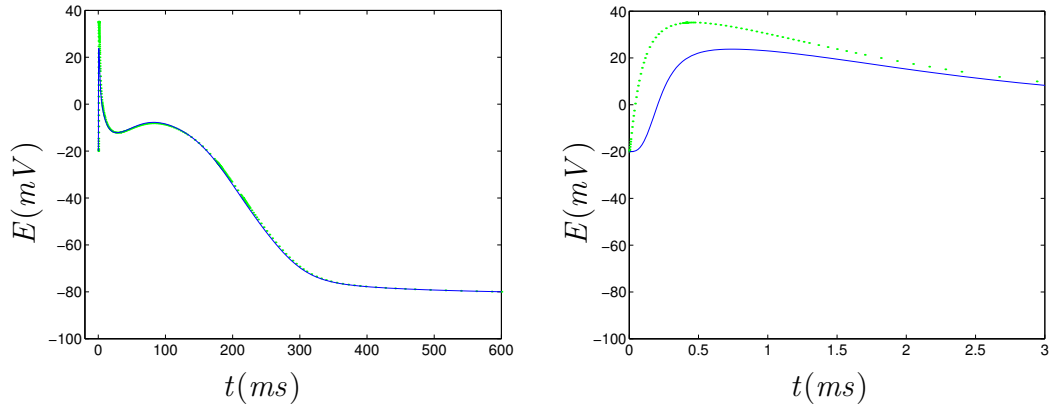

(a) (b)

Figure 6.5: Action potential of CRN-17, system (6.4), (-) and CRN-14, system (6.6), (.) for the time periods (a) $[0,600]$ and (b) $[0,3]$.

We draw the action potential for CRN-17 and CRN-14 for two time periods, Fig. 6.5, to see what difference it makes to the action potential. The difference is that the spike is higher for CRN-14. So we want to check which variable causes

this. To do this we take CRN-17, and use the time period $[0, 3]$ to obtain a better look, Fig. 6.6. We then adiabatically eliminate each variable separately to see which causes the spike. Figure 6.6(a) shows that the m variable is responsible for the change, so m plays the essential role at the spike. As the change is only in the spike of the action potential for a small moment of time, we can say that the qualitative behaviour of the system hasn't been modified and that the change is such a small percentage of the whole that we can carry on analysing CRN-14. All the other variables make no or little change here.

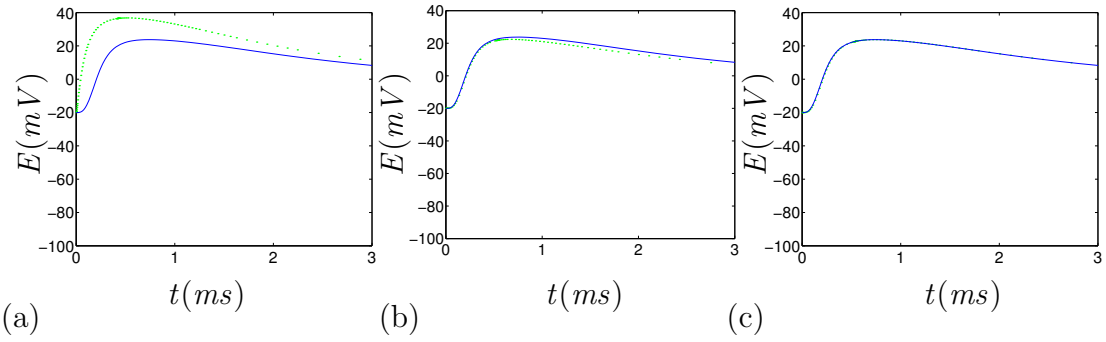

Figure 6.6: (a) Action potential for CRN-17, system (6.4), (-) for the time period $[0, 3]$ with the following variables adiabatically eliminated (a) m (.), (b) u_a (.) and (c) w (.).

6.1.5 Definition of the fast, intermediate and slow time stages

We have found from our numerical experiments that the sodium current is only open for a short period of time, which is approximately $[t_0, t_1]$=$[0, 1.2]$ and then it is over and can be treated as zero after that. So we can split CRN-14 into three different time stages, fast, intermediate and slow.

In the fast stage we have I_{Na} active. In the intermediate stage the sodium current is over, $I_{Na} \approx 0$, and therefore h, d and o_a are fast variables and therefore can be put to their quasi-stationary values.

The same can be done for other variables in the intermediate and slow stages, where in the intermediate stage we take CRN-11 and find which are the fast variables here. We see that u and v are the fast variables and can be replaced with functions of t, and not their quasi-stationary value. We found that they are fast in the slow stage, and can therefore be replaced with their quasi-stationary

Super Fast< 1ms	Fast≈ 1ms	Intermediate≈ 10ms	Slow≈ 100ms	Super Slow> 100ms
m	h	u	x_r	Nai
u_a	o_a	v	x_s	Ki
w	d	j	f	$Caup$
		f_{Ca}		u_i
		o_i		
Non-Tikhonov variables: E, Cai and $Carel$.				

Table 6.1: Defining the different time stages and corresponding variables for Courtemanche et al's model.

values there.

Even though u and v are fast in both the intermediate and slow stages, we have two time stages and not one because u and v are taken as different values in each time stage. This is because the intermediate stage finishes if τ_v and $\overline{u}$ switches from one value to another. The reason they switch is due to the Ca^{2+} flux variable, F_n, as at this moment of time F_n reaches its threshold. Therefore the intermediate stage finishes here and this is also where the slow stage begins.

For the slow stage we take CRN-11 again and replace u and v with their quasi-stationary values, as well as the fast variables that are in this system; j, f_{Ca} and o_i.

Variables can be considered as fast and slow for different time stages, this helps us to reduce this system further. We cannot further reduce the system using Tikhonov's method and therefore have to use a non-Tikhonov embedding method. The time scale is split into three sections, fast, intermediate and slow. Table 6.1 shows which variables are considered as fast or slow variables in these time stages, where E, Cai and $Carel$ are the variables spread across different time stages.

6.1.6 Summary

We chose to study one solution of Courtemanche et al's model for a certain initial condition and not a series of solutions for different initial conditions, as this would be too complicated. We only use one solution to show how accurate our methods

are, and that they will work for a complicated model for one solution. Some of the approximations that we do are specific to keeping the qualitative behaviour of this single solution. So the elimination of the super-slow and super-fast variables does not change the systems action potential for our analysis, but the changes may appear in a series of action potentials, or sub-threshold responses, i.e. anything different from a single action potential.

Therefore we wanted to demonstrate that the asymptotic techniques are applicable in principle to detailed contemporary models.

6.2 The Fast Stage $[t_0, t_1]$

We are only interested in the fast time stage $[t_0, t_1]$=[0, 1.2] for CRN-14 as this is where I_{Na} enters into this system. After t_1=1.2, sodium current is over and can be treated as zero, so we look at CRN-14 and concentrate on the E, h, o_a, and d variables and the I_{Na} current. We are only interested in h, o_a and d as we see from Fig. 6.7 that for this time stage, the τ's for these variables are the smallest and therefore they are the fast variables. This can also be seen from Fig. 6.8, as we draw these variables against their quasi-stationary values for this time period and we see that there is no difference. Also we know that I_{Na} is a large current, as this current is the largest compared to all the other currents.

We also notice from Fig. 6.7 that τ_u has a discrepancy around t=0.4, this is because at this point the equation for τ_u becomes zero, i.e. $\frac{\partial}{\partial u}\left(\frac{\mathrm{d}u}{\mathrm{d}t}\right)$=0, so if we draw $\ln(\tau_u)$ the discrepancy occurs because we obtain infinity at this point. This is the reason this happens and not because the u variable is fast or slow at this moment of t.

We now use a non-Tikhonov embedding here to analyse system (6.6), which is the same non-Tikhonov embedding that we used in Chapter 5 for Noble's model. So we still introduce ϵ to the fast variables, and the large currents in the $\dot{E}$ equation, as $\dot{E}$ contains small and large currents.

Now that we know that h, d and o_a are fast variables and I_{Na} is a large current, we make the variables even faster by introducing $1/\epsilon$ to the right-hand sides of their equations in system (6.6), and we make I_{Na} even larger by introducing $1/\epsilon$ in front of I_{Na} to obtain system (6.7):

$$\frac{\mathrm{d}E}{\mathrm{d}t} = -\frac{I_{ion}}{C_M}, \tag{6.7}$$

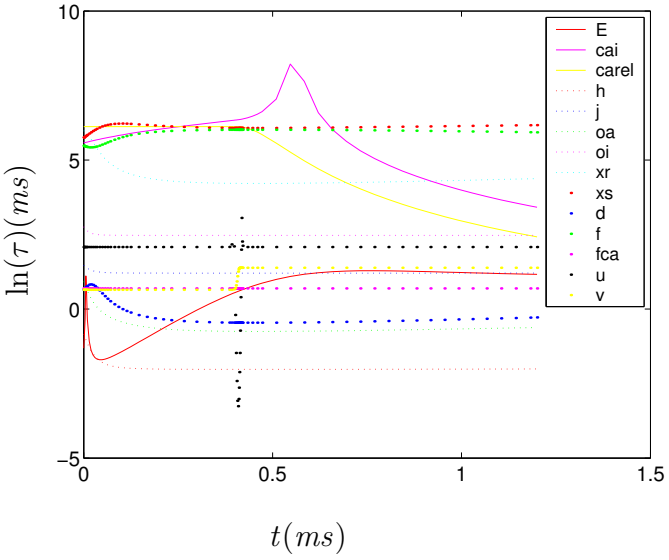

Figure 6.7: Graph of the τ's for CRN-14, system (6.6), for the time scale $[0, 1.2]$.

$$
\begin{aligned}
I_{ion} &= I_{Na}(E,\overline{m},h,j)/\epsilon + I_{K1}(E) + I_{to}(E,o_a,o_i) + I_{Kur}(E,\overline{u}_a) + I_{Kr}(E,x_r) \\
&\quad + I_{Ks}(E,x_s) + I_{Ca,L}(E,d,f,f_{Ca}) + I_{p,Ca}(Cai) + I_{Na,K}(E) + I_{b,Na}(E) \\
&\quad + I_{NaCa}(E,Cai) + I_{b,Ca}(E,Cai), \\
\frac{\mathrm{d}y}{\mathrm{d}t} &= \frac{\overline{y}-y}{\tau_y}, \qquad y = j, o_i, x_r, x_s, f, f_{Ca}, u, v, \\
\frac{\mathrm{d}x}{\mathrm{d}t} &= \frac{1}{\epsilon}\frac{\overline{x}-x}{\tau_x}, \qquad x = h, o_a, d, \\
\frac{\mathrm{d}Cai}{\mathrm{d}t} &= \frac{B1}{B2}, \\
B1 &= (2FV_i)^{(-1)}(2I_{NaCa}(E,Cai) - I_{p,Ca}(Cai) - I_{Ca,L}(E,d,f,f_{Ca}) \\
&\quad - I_{b,Ca}(E,Cai)) + (V_i)^{(-1)}(V_{up}(0.000496 - I_{up}(Cai)) \\
&\quad + I_{rel}(Cai,Carel,u,v,\overline{w})V_{rel}), \\
B2 &= 1 + \frac{[Trpn]_{max}K_{m,Trpn}}{(Cai+K_{m,Trpn})^2} + \frac{[Cmdn]_{max}K_{m,Cmdn}}{(Cai+K_{m,Cmdn})^2}, \\
\frac{\mathrm{d}Carel}{\mathrm{d}t} &= \frac{(I_{tr}(Carel) - I_{rel}(Cai,Carel,u,v,\overline{w}))}{\left(1 + \frac{[Csqn]_{max}K_{m,Csqn}}{(Carel+K_{m,Csqn})^2}\right)}.
\end{aligned}
$$

Figures 6.9 and 6.10 show what happens to E, h, o_a and d if we tend ϵ to zero in system (6.7). We see that the spike becomes higher and starts earlier.

We then use the change of variable $t{=}\epsilon T$ to system (6.7) to see what happens to all the other variables.

$$
\frac{\mathrm{d}E}{\mathrm{d}T} = -\frac{I_{ion}}{C_M}, \tag{6.8}
$$

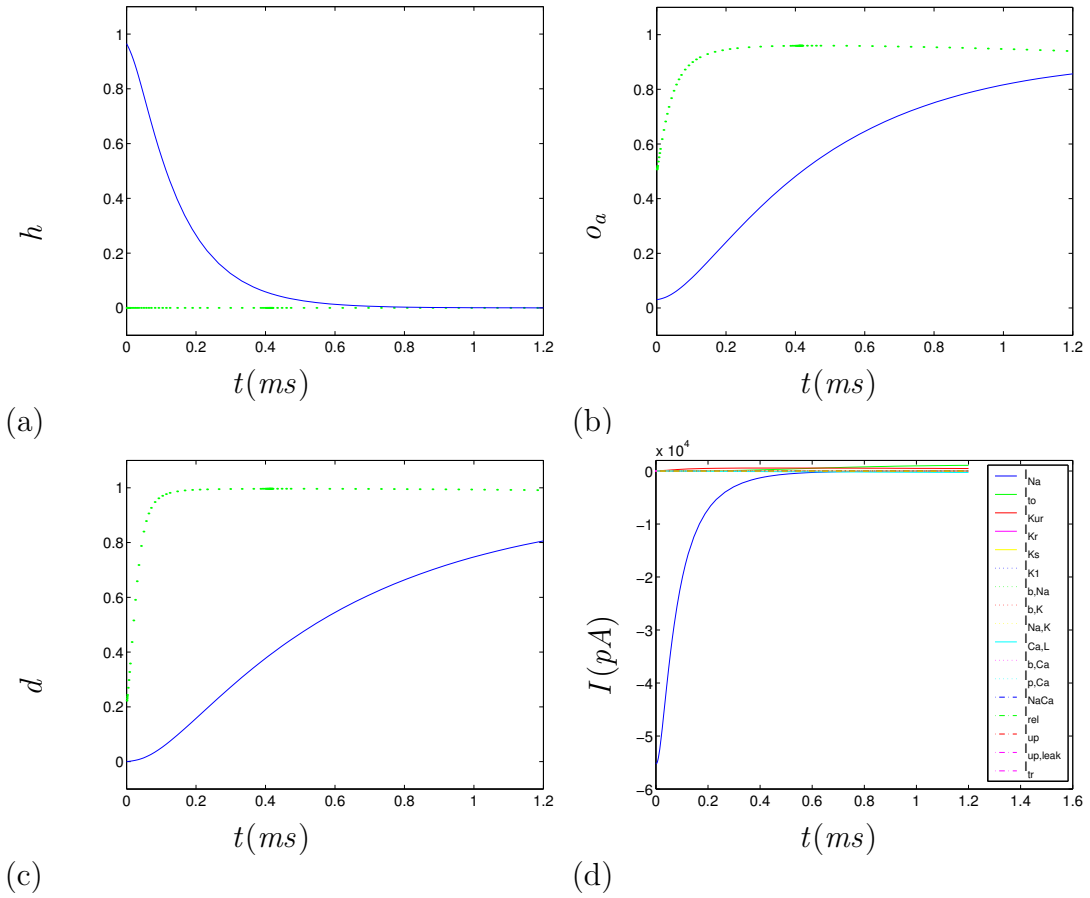

Figure 6.8: Graphs of the fast variables (-) and their quasi-stationary values (.) for CRN-14, system (6.6), t=$[0, 1.2]$. (a) h, (b) o_a, (c) d and (d) graph of the currents for CRN-14, where the solid blue line represents I_{Na} which is larger than any other currents.

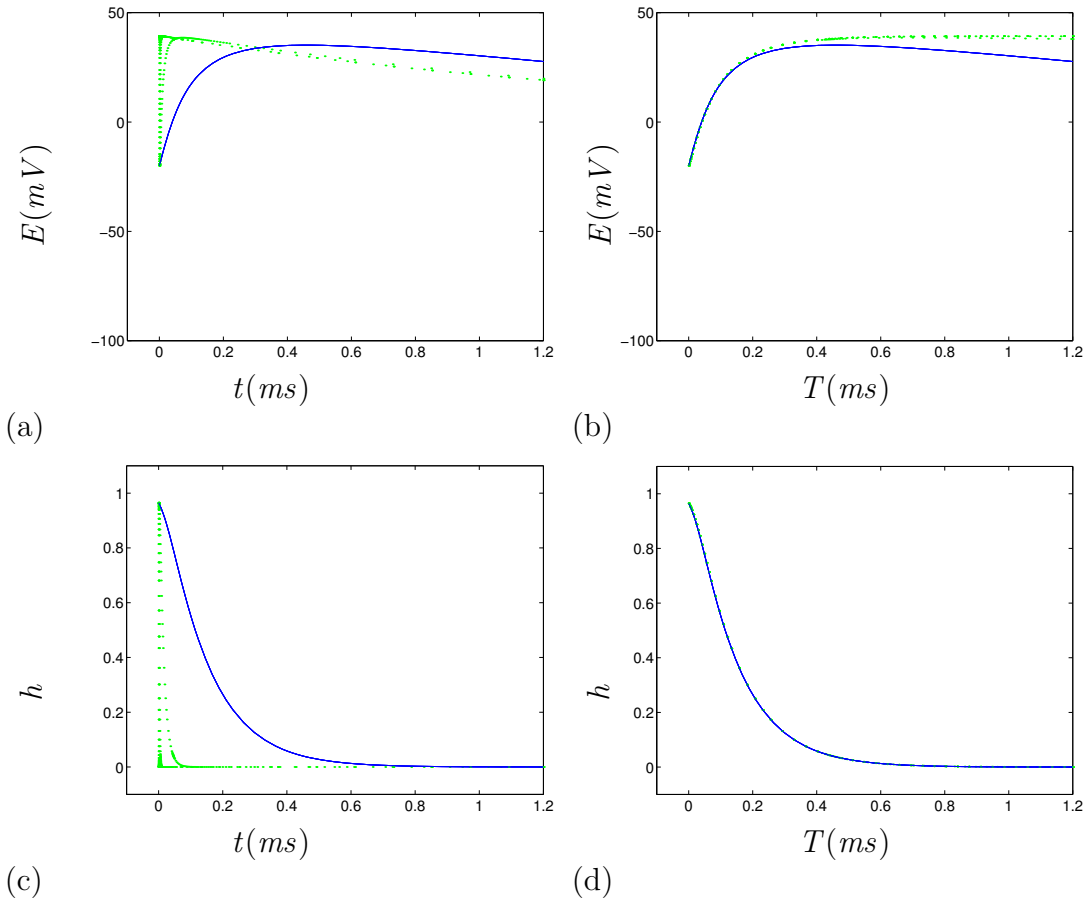

Figure 6.9: Graph of CRN-14, system (6.6) ϵ=1, (-) and CRN-14, system (6.7) $\epsilon \to 0$, (.) for t=[0, 1.2] for the variables (a) E and (c) h. Graph of CRN-14, system (6.6) ϵ=1, (-) and CRN-14, system (6.8) $\epsilon \to 0$, (.) for T=[0, 1.2] for the variables (b) E and (d) h.

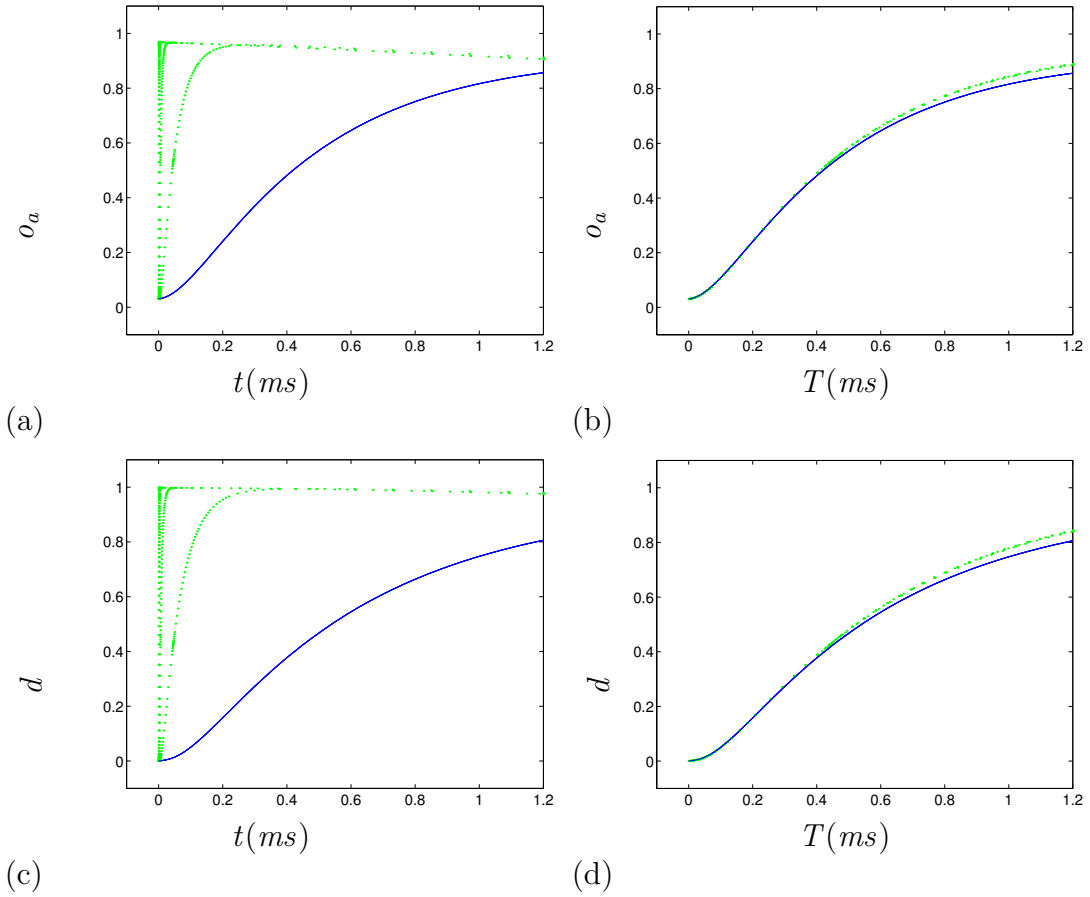

Figure 6.10: Graph of CRN-14, system (6.6) ϵ=1, (-) and CRN-14, system (6.7) $\epsilon \to 0$, (.) for t=[0, 1.2] for the variables (a) o_a and (c) d. Graph of CRN-14, system (6.6) ϵ=1, (-) and CRN-14, system (6.8) $\epsilon \to 0$, (.) for T=[0, 1.2] for the variables (b) o_a and (d) d.

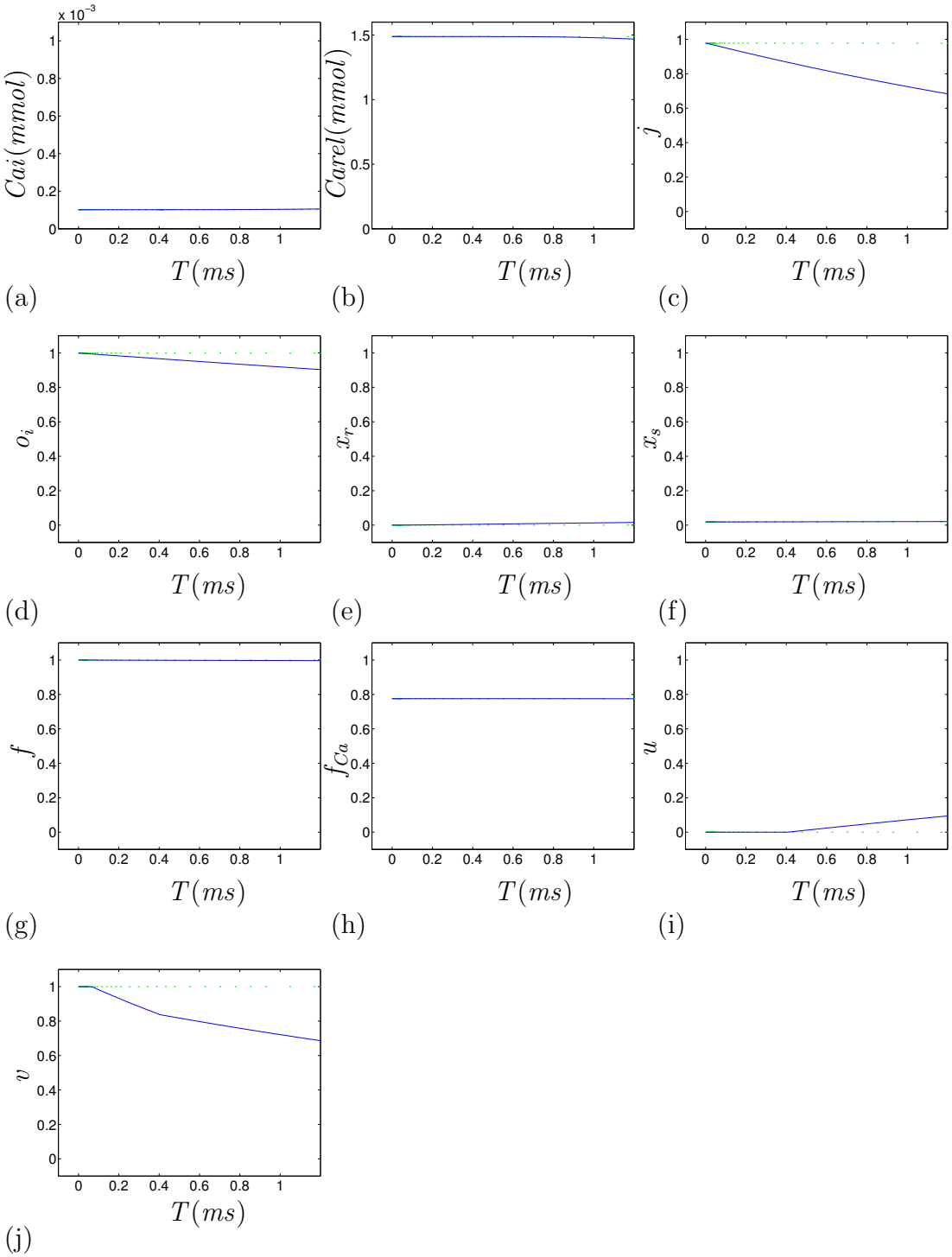

Figure 6.11: Graph of CRN-14, system (6.6) ϵ=1, (-) and CRN-14, system (6.8) ϵ=0, (.) for the variables (a) Cai, (b) $Carel$, (c) j, (d) o_i, (e) x_r, (f) x_s, (g) f, (h) f_{Ca}, (i) u and (j) v.

$$
\begin{aligned}
I_{ion} &= I_{Na}(E,\overline{m},h,j)+\epsilon(I_{K1}(E)+I_{to}(E,o_a,o_i)+I_{Kur}(E,\overline{u}_a)+I_{Kr}(E,x_r)\\
&\quad +I_{Ks}(E,x_s)+I_{Ca,L}(E,d,f,f_{Ca})+I_{p,Ca}(Cai)+I_{Na,K}(E)+I_{b,Na}(E)\\
&\quad +I_{NaCa}(E,Cai)+I_{b,Ca}(E,Cai)),\\
\frac{\mathrm{d}y}{\mathrm{d}T} &= \epsilon\frac{\overline{y}-y}{\tau_y}, \qquad y=j,o_i,x_r,x_s,f,f_{Ca},u,v,\\
\frac{\mathrm{d}x}{\mathrm{d}T} &= \frac{\overline{x}-x}{\tau_x}, \qquad x=h,o_a,d,\\
\frac{\mathrm{d}Cai}{\mathrm{d}T} &= \epsilon\frac{B1}{B2},\\
B1 &= (2FV_i)^{(-1)}(2I_{NaCa}(E,Cai)-I_{p,Ca}(Cai)-I_{Ca,L}(E,d,f,f_{Ca})\\
&\quad -I_{b,Ca}(E,Cai))+(V_i)^{(-1)}(V_{up}(0.000496-I_{up}(Cai))\\
&\quad +I_{rel}(Cai,Carel,u,v,\overline{w})V_{rel}),\\
B2 &= 1+\frac{[Trpn]_{max}K_{m,Trpn}}{(Cai+K_{m,Trpn})^2}+\frac{[Cmdn]_{max}K_{m,Cmdn}}{(Cai+K_{m,Cmdn})^2},\\
\frac{\mathrm{d}Carel}{\mathrm{d}T} &= \epsilon\frac{(I_{tr}(Carel)-I_{rel}(Cai,Carel,u,v,\overline{w}))}{\left(1+\frac{[Csqn]_{max}K_{m,Csqn}}{(Carel+K_{m,Csqn})^2}\right)}.
\end{aligned}
$$

If we put ϵ=0 in system (6.8), Fig. 6.11, we see that all the other variables, Cai, $Carel$, j, o_i, x_r, x_s, f, f_{Ca}, u and v, become their initial values. So we can replace them with their initial values to obtain a new system, CRN-4, that just contains E, h, d and o_a. Also Fig. 6.9(b), (d), (f) and (h) shows what happens to E, h, o_a and d if $\epsilon \to 0$ in system (6.8). There is little change in E, o_a and d and no change in h.

$$
\begin{aligned}
\frac{\mathrm{d}E}{\mathrm{d}T} &= -\frac{C_M\overline{g}_{Na}\overline{m}^3(E)hj(E-E_{Na})}{C_M},\\
\frac{\mathrm{d}h}{\mathrm{d}T} &= \frac{\overline{h}(E)-h}{\tau_h(E)},\\
\frac{\mathrm{d}o_a}{\mathrm{d}T} &= \frac{\overline{o}_a(E)-o_a}{\tau_{o_a}(E)},\\
\frac{\mathrm{d}d}{\mathrm{d}T} &= \frac{\overline{d}(E)-d}{\tau_d(E)}.
\end{aligned}
\tag{6.9}
$$

Figure 6.12 shows that if we compare CRN-4 with CRN-14 there is no change in h and little change in E, o_a and d. We see that making h, d and o_a fast, and I_{Na} large for $[0, 1.2]$ is a good approximation. So we now have a system of four equations for the fast stage. After this time stage I_{Na}=0 and x=$\overline{x}$, where x=h, d and o_a.

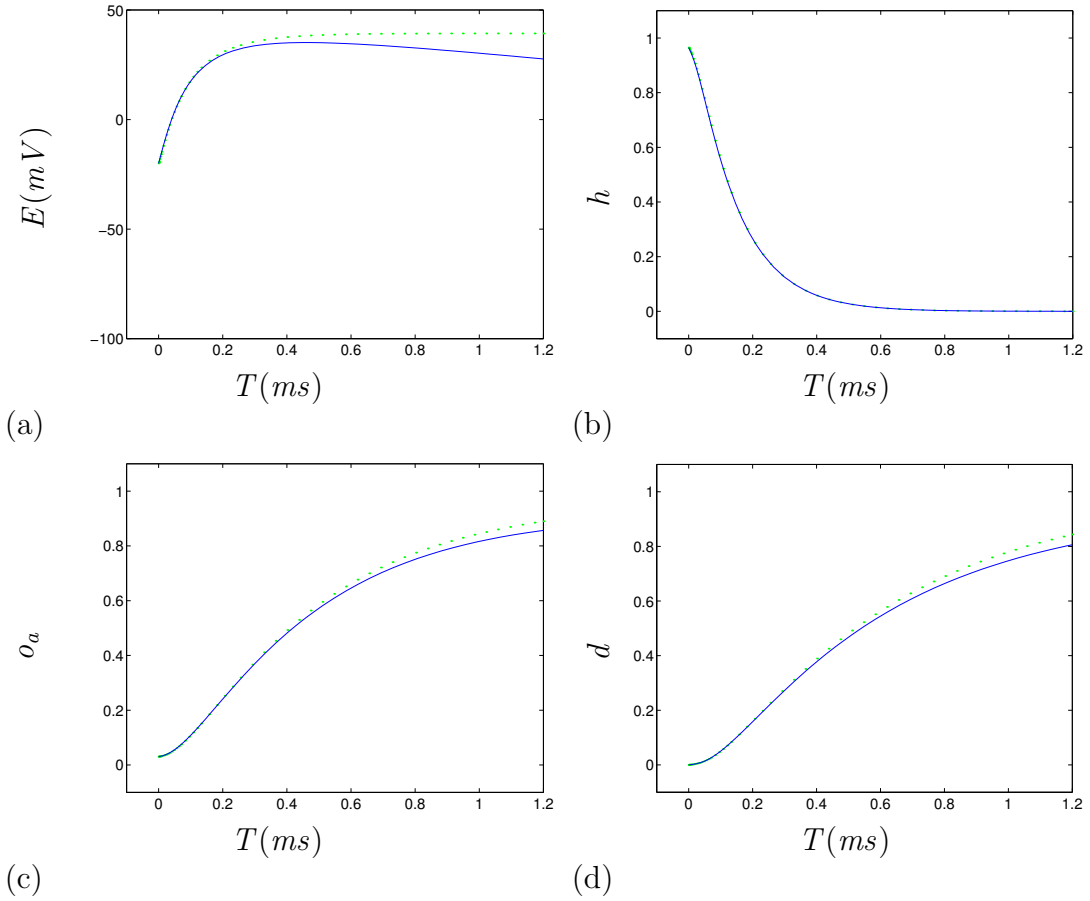

Figure 6.12: Graph of CRN-14, system (6.6), (-) and CRN-4, system (6.9), (.) for T=$[0, 1.2]$ for the variables (a) E, (b) h, (c) o_a and (d) d.

6.2.1 Phase portrait for sodium embedding

We have the following system of equations, same as the first two equations of system (6.9), T=$[t_0, t_1]$:

$$\begin{aligned} \frac{\mathrm{d}h}{\mathrm{d}T} &= \frac{(\overline{h}(E) - h)}{\tau_h(E)}, \\ \frac{\mathrm{d}E}{\mathrm{d}T} &= -\frac{I_{Na}(E, \overline{m}, h, j)}{C_M} = -A\overline{m}^3(E)h(E - E_{Na}), \end{aligned} \tag{6.10}$$

where

$$\begin{aligned} A = g_{Na}j = 7.6245, &\qquad E_{Na} = 67.5339, \\ \tau_h = \frac{1}{\alpha_h + \beta_h}, &\qquad Cai = \text{const}, Carel = \text{const}, j = \text{const}, \\ o_i = \text{const}, x_r = \text{const}, x_s = \text{const}, &\qquad f = \text{const}, u = \text{const}, v = \text{const}. \end{aligned}$$

We are only interested in the E and h equations at the moment so that we can find an analytical solution for h and E, and then we can find a solution for o_a and d in quadratures. This is because the two equations are separate from the E and h equations. What we mean by this is that o_a and d are not contained in $\dot{E}$ and $\dot{h}$, but E is contained in $\dot{o_a}$ and $\dot{d}$. As o_a and d don't affect the action potential then we only study the sodium embedding of E and h.

We have found that $\overline{m}$ and $\overline{h}$ can be replaced by Heaviside functions, which is what we found in Section 5.6 for Noble's non-Tikhonov embedding, and this will help make our embedding easier. Therefore the Heaviside functions are:

$$\overline{h} = \theta(-E + E_h), \qquad \overline{m} = \theta(E - E_m),$$

where E_h=-66.6 and E_m=-32.7.

We find the isoclines and equilibrium points for system (6.10).

The h isocline is:

$$h = \overline{h} = \theta(-E + E_h).$$

This is a step function.

The E isocline is:

$$\begin{aligned} I_{Na} &= 0 \Rightarrow A\overline{m}^3 h(E - E_{Na}) = 0, \\ A &\neq 0, \\ \overline{m}^3 h(E - E_{Na}) &= 0. \end{aligned}$$

From this the solutions are:

$$\begin{cases} E & \in & [-\infty, E_m], \\ h & \in & [0,1], \\ \overline{m}^3 & = & \theta(E - E_m) = 0, \end{cases}$$

$$\begin{cases} E & \in & [-\infty, \infty], \\ h & = & 0, \\ \overline{m}^3 & = & \theta(E - E_m), \end{cases}$$

and

$$\begin{cases} E & \in & E_{Na}, \\ h & \in & [0,1], \\ \overline{m}^3 & = & \theta(E - E_m) = 1. \end{cases}$$

The equation for the equilibrium points satisfies $\frac{\mathrm{d}h}{\mathrm{d}T}$=0 and $\frac{\mathrm{d}E}{\mathrm{d}T}$=0. So we know that for $\frac{\mathrm{d}h}{\mathrm{d}T}$=0 we obtain h=$\overline{h}$, so we put this into the equation for $\frac{\mathrm{d}E}{\mathrm{d}T}$=0 to obtain:

$$A\overline{m}^3\overline{h}(E - E_{Na}) = 0.$$

From this we have the solution:

$$\begin{cases} E & \in & [-\infty, \infty], \\ h & = & \overline{h}(E), \end{cases}$$

which represents a continuum of equilibrium points, or line of equilibria, which is the same as in Section 5.6.

6.2.2 Replacing τ_h with a constant or a function of E

We replace τ_h with a constant to obtain an analytical solution for the trajectories of system (6.10), and then compare them with the numerical answer to see how accurate they are.

$$\begin{aligned} \frac{\mathrm{d}h}{\mathrm{d}T} &= \frac{(\overline{h}(E) - h)}{\tau_h(E)}, \\ \frac{\mathrm{d}E}{\mathrm{d}T} &= -A\overline{m}^3(E)h(E - E_{Na}). \end{aligned}$$

We are only interested in the region $[E_m, E_{Na}]$, which is the same region that we were interested in for finding the analytical solutions for the trajectories in Chapter 5 for Noble's non-Tikhonov embedding. For $E < E_m$, the trajectories are straight lines and they have the same equation as we obtained in Chapter 5, except here $\overline{h}$=$\theta(E_h - E)$.

In the range $[E_m, E_{Na}]$, for $E > E_m$, $\overline{h}$=0 and $\overline{m}^3$=1 and the equation for the trajectories in this range will be:

$$\begin{aligned}
\frac{\mathrm{d}h}{\mathrm{d}E} &= \frac{\frac{\mathrm{d}h}{\mathrm{d}T}}{\frac{\mathrm{d}E}{\mathrm{d}T}} = \frac{h}{\tau_h(E)Ah(E - E_{Na})}, \\
\int_{h_0}^{h} \mathrm{d}h &= \frac{1}{A}\int_{E_0}^{E} \frac{1}{\tau_h(E)(E - E_{Na})}\mathrm{d}E, \\
h - h_0 &= \frac{1}{A}\int_{E_0}^{E} \frac{1}{\tau_h(E)(E - E_{Na})}\mathrm{d}E.
\end{aligned}$$

We found the value, for τ_h to be a constant, at E=E_{Na}. We used E_{Na} because we are only interested in the region $[E_m, E_{Na}]$ and E_{Na} is the maximum value of E in this region. Therefore the equation for E is:

$$E = (E_0 - E_{Na})e^{(h-h_0)/B} + E_{Na},$$

where,

$$B = \frac{1}{\tau_h(E_{Na})A}, \qquad A = g_{Na}j = 7.6245, \qquad \tau_h(E_{Na}) = 0.1301.$$

This solution is drawn on the phase portrait, Fig. 6.13, and is represented by magenta (thick :). This can be compared with Fig. 5.9 from Noble's non-Tikhonov analysis, and we can see that the graphs are similar, where we have the h and E isoclines, where the E isocline also has a rectangle region as well, and the numerical trajectories travel to the equilibrium points, which consists of a line of equilibria.

If we consider τ_h as a function of E in our region, then we approximate τ_h so it is easily integrated. We say that $\epsilon(E)$=$\frac{1}{\tau_h(E)(E-E_{Na})}$. As $E \to E_{Na}$, the singularity, we have:

$$\epsilon(E) \approx \frac{1}{\tau_h(E_{Na})(E - E_{Na})}.$$

Therefore $\epsilon(E)$ can be written as follows:

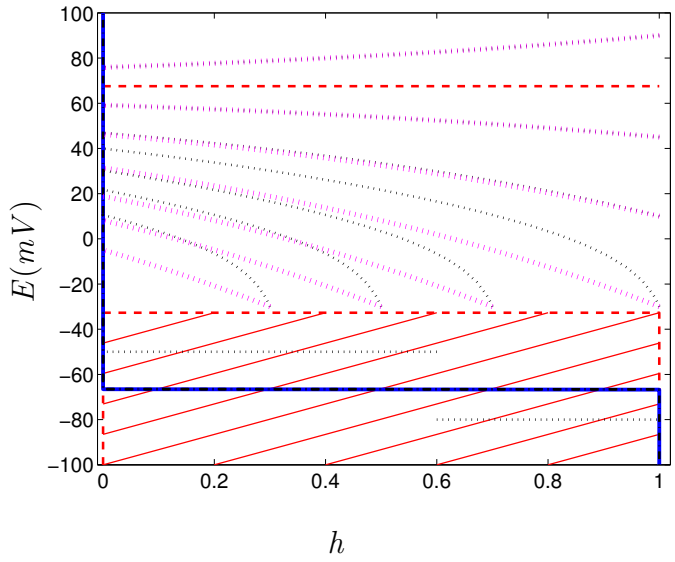

Figure 6.13: Phase portrait for the sodium embedding with h isocline (-), E isocline (- -) and the dashed region, equilibrium points (-.), numerical trajectories, system (6.10), (black:) and analytical trajectories for τ_h=const (magenta, thick :).

$$\begin{aligned}
\epsilon(E) &= \frac{1}{\tau_h(E_{Na})(E-E_{Na})} + \frac{1}{(E-E_{Na})}\left(\frac{1}{\tau_h(E)} - \frac{1}{\tau_h(E_{Na})}\right), \\
&= \frac{1}{\tau_h(E_{Na})(E-E_{Na})} + \frac{\tau_h(E_{Na}) - \tau_h(E)}{(E-E_{Na})\tau_h(E)\tau_h(E_{Na})}, \\
&= \frac{1}{\tau_h(E_{Na})(E-E_{Na})} + \mu(E),
\end{aligned}$$

where $\mu(E)$ is continuous at E=E_m.

6.2.3 Representing μ as an exponential function

We draw the graph of $\ln(\mu)$ first to see if we can approximate this with a straight line and then we can find a linear approximation for $\mu(E)$. We obtain $\mu(E) \approx e^{(mE+c)} \approx Ke^{mE}$, where m=−0.0471, c=−4.2321 and K=e^c=0.1452. We obtain this from Fig. 6.14, by ensuring the approximation is exact at E=E_m and E=E_{Na}.

So,

$$\epsilon(E) = \frac{1}{\tau_h(E_{Na})(E-E_{Na})} + Ke^{mE}.$$

Therefore,

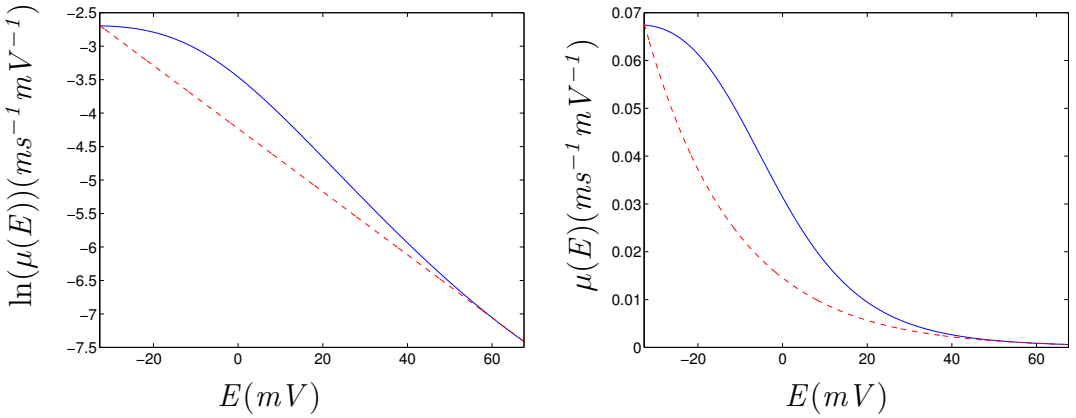

(a) (b)

Figure 6.14: (a) Graph of $\ln(\mu)$ (-) and its approximation $\ln(\mu)$=$-0.0471E - 4.2321$ (- -). (b) Graph of μ (-) and its approximation μ=$0.1452e^{-0.0471E}$ (- -).

$$\begin{aligned} \frac{\mathrm{d}h}{\mathrm{d}E} &= \frac{\epsilon(E)}{A}, \\ h &= B\ln\left(\frac{|E-E_{Na}|}{|E_0-E_{Na}|}\right) + G(e^{mE}-e^{mE_0}) + h_0, \end{aligned}$$

with initial conditions $h(E_0)$=h_0 and

$$B = \frac{1}{\tau_h(E_{Na})A}, \qquad G = \frac{K}{Am}.$$

The analytical solutions are drawn on the phase portrait, Fig. 6.15, as blue (thick :) lines, and we can see that the solutions are not close to the numerical solutions (black :).

If we put K=0 and G=0, then we obtain the same solution as τ_h=const.

$$\begin{aligned} h &= B\ln\left(\frac{|E-E_{Na}|}{|E_0-E_{Na}|}\right) + G(e^{mE}-e^{mE_0}) + h_0, \\ h &= B\ln\left(\frac{|E-E_{Na}|}{|E_0-E_{Na}|}\right) + h_0, \\ E &= (E_0-E_{Na})e^{(h-h_0)/B} + E_{Na}. \end{aligned}$$

6.2.4 Approximating μ by a quasi-polynomial using the Marquardt-Levenberg procedure (best fit)

In Fig. 6.15 the analytical trajectories are not close enough for our satisfaction to the numerical trajectories, as we want to see if we can get them exactly the

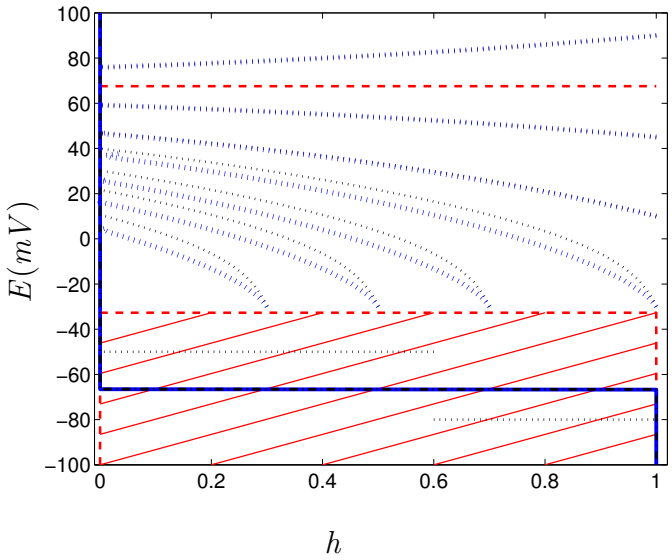

Figure 6.15: Phase portrait for the sodium embedding with h isocline (-), E isocline (- -) and the dashed region, equilibrium points (-.), numerical trajectories, system (6.10), (black:) and analytical trajectories for μ=Ke^{mE} (blue, thick :).

same or only slightly displaced. So we try again with another approximation, and we use the Marquardt-Levenberg procedure for best fit.

This time we have $\mu(E)$=$(a+bE)e^{-cE}$, where a=0.0304031, b=$-$0.000597257 and c=0.0145176, which is the best fit for our interval of E, $[E_m, E_{Na}]$. For any other interval we would have to use this procedure again and obtain another solution. Figure 6.16 shows our new μ (- -) drawn against our old μ (-) and it shows the difference between them.

Therefore,

$$\begin{aligned}\frac{\mathrm{d}h}{\mathrm{d}E} &= \frac{\epsilon(E)}{A},\\ h &= B\ln\left(\frac{|E-E_{Na}|}{|E_0-E_{Na}|}\right)+H(c(a+bE_0)e^{-cE_0}+be^{-cE_0}-c(a+bE)e^{-cE}-be^{-cE})\\ &\quad +h_0,\end{aligned}$$

with initial conditions $h(E_0)$=h_0 and

$$H=\frac{1}{Ac^2},\qquad B=\frac{1}{\tau_h(E_{Na})A}.$$

The analytical solutions are drawn on the phase portrait, Fig. 6.17, as blue (thick :) lines and we can see that they are the same as the numerical solutions (black :). Therefore we have found a good approximation.

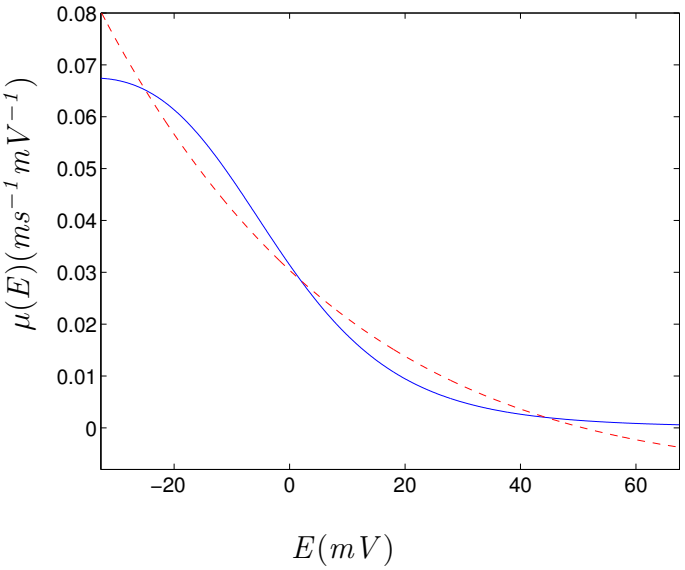

Figure 6.16: Graph of μ (-) and μ=$(a+bE)e^{-cE}$ (- -).

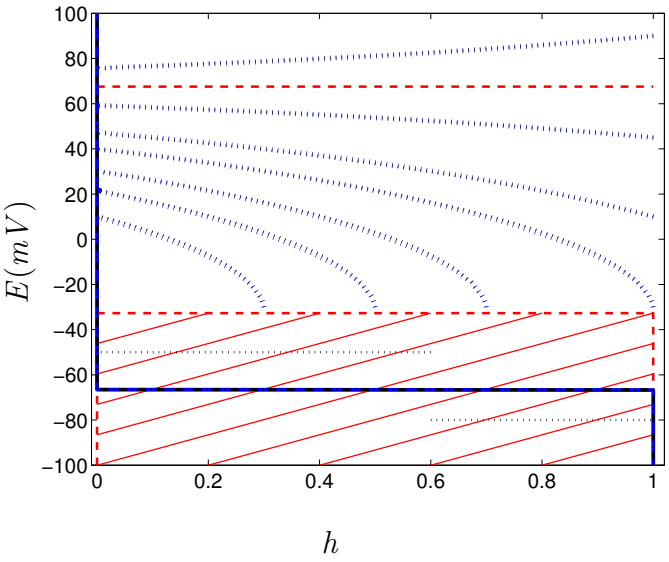

Figure 6.17: Phase portrait for the sodium embedding with h isocline (-), E isocline (- -) and the dashed region, equilibrium points (-.), numerical trajectories, system (6.10), (black:) and analytical trajectories for $\mu(E)$=$(a+bE)e^{-cE}$ (blue, thick:). Here they practically coincide.

6.2.5 Obtaining $E(T)$ using the solution from τ_h=constant

We want to obtain a solution for $E(T)$ because the beginning of the intermediate stage is the final stage of the fast stage. We can't deduce the final stage for E, unlike all other three variables, from qualitative analysis, since there is a whole line of equilibria at different values of E, and the system may end up in any of them, depending on initial conditions. So we need to find the dependence of $E_\infty(E_0)$, where E_∞ is $\lim_{T\to+\infty} E(T)$ and E_0=$E(0)$.

The solution from τ_h=constant is:

$$h(E) = \frac{1}{\tau_h(E_{Na})A} \ln\left(\frac{|E - E_{Na}|}{|E_0 - E_{Na}|}\right) + h_0.$$

We put this solution in system (6.10) to obtain a differential equation, that can be separated and integrated to find the solution $E(T)$. So by using initial conditions (E_0, T_0)= $(-20, 0)$ we obtain:

$$E(T) = (E_0 - E_{Na})e^{-(A\tau_h(E_{Na})h_0(1-e^{-\frac{(T-T_0)}{\tau_h(E_{Na})}})} + E_{Na}.$$

For $T \to \infty$ we obtain the equation $E_\infty(E_0)$:

$$E_\infty(E_0) \;=\; (E_0 - E_{Na})e^{-A\tau_h(E_{Na})h_0} + E_{Na} \approx 33.9247, \qquad (6.11)$$

for E_0=-20 and h_0=0.965.

In Fig. 6.18 we draw the graph of $E(T)$ against T for two different time periods to make sure that this answer is correct and it looks similar to the original $E(T)$, Fig. 6.12(a) (.).

We draw $E(T)$ against E_0, for $T \to \infty$, to see what values we obtain for E_∞ for different values of E_0, this can be seen from equation (6.11), and we see from Fig. 6.19 that we obtain a straight line. So for every new value of E_0, the function E_∞ grows as a linear function.

If E=$E(T)$ is known we can obtain an analytical solution for o_a and d in quadratures:

$$\begin{aligned} o_a &= o_{a_0} + \int_{T_0}^{T} \frac{\overline{o}_a(T)}{\tau_{o_a}(T)} \mathrm{d}T, \\ d &= d_0 + \int_{T_0}^{T} \frac{\overline{d}(T)}{\tau_{o_a}(T)} \mathrm{d}T. \end{aligned}$$

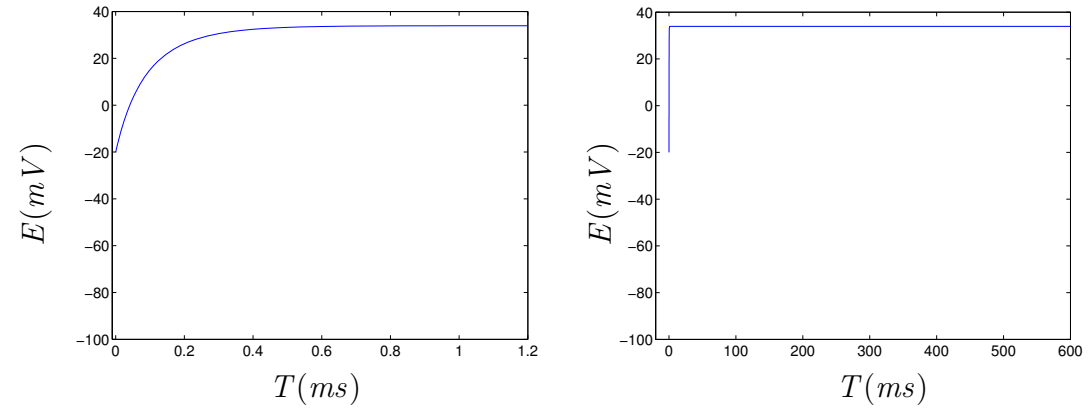

(a) (b)

Figure 6.18: Graph of $E(T)$ against T for the time periods (a) $[0, 1.2]$ and (b) $[0, 600]$.

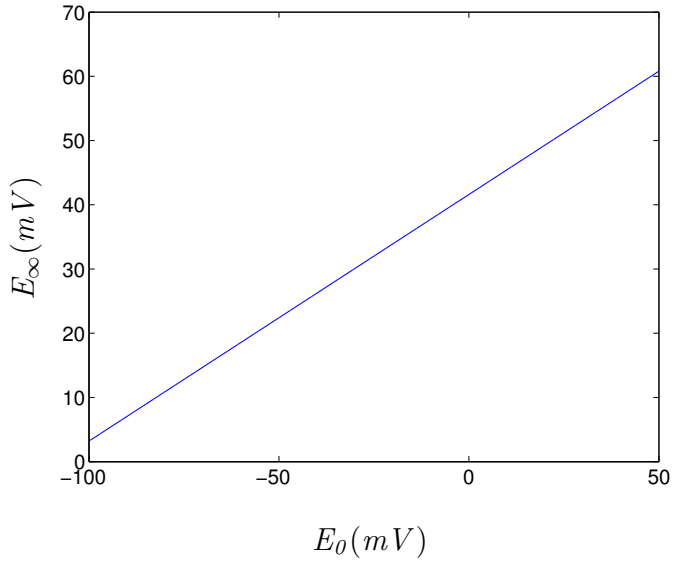

Figure 6.19: Graph of peak voltage E_∞, (6.11), against the initial voltage E_0 for the approximation τ_h=constant.

We can also find the solutions for o_a and d by using the value of E_∞, from equation (6.11), for E in $\overline{o}_a$, $\overline{d}$, τ_{o_a} and τ_d. Therefore these functions of E can be replaced with a constant for $E{=}E_\infty$.

$$\begin{aligned} \overline{o}_a &= 0.9569, & \tau_{o_a} &= 1.4467, \\ \overline{d} &= 0.9959, & \tau_d &= 0.6493. \end{aligned}$$

From our analysis we found that we can replace $\overline{o}_a$, $\overline{d}$, τ_{o_a} and τ_d with constants for short and long periods of time. For a short period of time the approximations are not as accurate and therefore we just replace $\overline{o}_a$ and $\overline{d}$ with constants.

For the time period $[t_0, 0.12]$ we have the solutions:

$$\begin{aligned} o_a &= \overline{o}_a + (o_{a_0} - \overline{o}_a)e^{\int_{T_0}^{T} 1/\tau_{o_a}(T)\mathrm{d}T}, \\ d &= \overline{d} + (d_0 - \overline{d})e^{\int_{T_0}^{T} 1/\tau_d(T)\mathrm{d}T}, \end{aligned}$$

and for the time period $[0.12, t_1]$ we have the solutions:

$$\begin{aligned} o_a &= \overline{o}_a + (o_{a_0} - \overline{o}_a)e^{-(T-T_0)/\tau_{o_a}}, \\ d &= \overline{d} + (d_0 - \overline{d})e^{-(T-T_0)/\tau_d}. \end{aligned}$$

6.2.6 Summary

For the fast stage we have found that I_{Na} is a fast current during the time period $[0, 1.2]$, and after this sodium doesn't enter the system or if it does then it is very small and can be ignored. We also found from the speed analysis that the fast gating variables are h, o_a and d. So by using a Tikhonov and non-Tikhonov embedding we obtained CRN-4 in the fast time T. Variables E and h are described by a system of equations similar to the fast system in Chapter 5.

With this result we were able to study the graphs of h and E and obtain a two-dimensional phase portrait with nullclines, stable equilibria and trajectories. We also tested approximations for τ_h and found a suitable approximation that gave explicit answers for the analytical trajectories. From this an equation for $E(T)$ was found that gave the same solution for E that we obtained from the system of equations.

Therefore if $E(T)$ is known, then explicit equations are found for o_a and d. As we saw from Fig. 6.18, we did obtain an action potential that looked the same as the action potential for the system of four equations (6.9), the dotted line in Fig. 6.12(a). So this confirmed that our embedding for the sodium subsystem and the approximations for τ_h, to find an equation for $E(T)$, are correct.

6.3 Calcium Subsystem in the Intermediate Stage

We know that I_{Na}=0 after the fast stage, so we now have the intermediate stage, where I_{Na}=0, h=$\overline{h}$, o_a=$\overline{o}_a$ and d=$\overline{d}$.

We have noticed that $\overline{u}$ and $\overline{v}$ can be written in the form of the Heaviside function of F_n, as they contain a very small parameter a and as this parameter tends to zero we obtain the Heaviside function. This small parameter a and the equation for F_n were obtained by Courtemanche et al from a master thesis by Friedman[61] and a paper also by Friedman[62]. In the thesis Friedman introduces these equations to the calcium system for the human atrium.

$$\begin{aligned}
\overline{u} &= \left(1+e^{-\frac{(F_n-3.4175*10^{-13})}{13.67*10^{-16}}}\right)^{-1}, \Rightarrow \overline{u}=(1+He^{-F_n/a})^{-1},\\
\overline{v} &= 1-\left(1+e^{-\frac{(F_n-6.835*10^{-14})}{13.67*10^{-16}}}\right)^{-1} \Rightarrow \overline{v}=1-(1+Ge^{-F_n/a})^{-1},
\end{aligned}$$

where

$$H=3.7465*10^{108}, \qquad a=13.67*10^{-16}, \qquad G=5.1847*10^{21}.$$

Here a is small compared to typical variations of F_n.

Therefore from the limit:

$$\lim_{a\to+0}(1+e^{-(F_n-F_*)/a})^{-1}=\theta(F_n-F_*),$$

we obtain:

$$\overline{u}=\theta(F_n-F_1), \qquad \overline{v}=\theta(F_n-F_2),$$

where

$$F_1=a\ln H=3.4175*10^{-13}, \qquad F_2=a\ln G=6.8350*10^{-14}.$$

So therefore we have a piecewise solution for $\overline{u}$ and $\overline{v}$ where $a \gg F_1, F_2$.

So we use the time scale $[1.2, 33]$ for the intermediate stage because at t_2=33, $\overline{u}$ and τ_v switch their values. This is because $\overline{u}$ and τ_v are Heaviside functions that depend on F_n, and at t_2=33, F_n exceeds its threshold F_1=$3.4175 * 10^{-13}$, and therefore $\overline{u}$ switches from 1 to 0 and τ_v switches from 4 to 1.91. So for this time period $\overline{u}$ and τ_v can be kept at one value and then after t_2=33 they can be kept at another value. So we have a new system, CRN-11:

$$
\begin{aligned}
\frac{\mathrm{d}E}{\mathrm{d}t} &= -\frac{I_{ion}}{C_M}, \qquad (6.12)\\
I_{ion} &= I_{K1}(E) + I_{to}(E, \overline{o}_a, o_i) + I_{Kur}(E, \overline{u}_a) + I_{Kr}(E, x_r) + I_{Ks}(E, x_s)\\
&\quad + I_{Ca,L}(E, \overline{d}, f, f_{Ca}) + I_{p,Ca}(Cai) + I_{Na,K}(E) + I_{NaCa}(E, Cai)\\
&\quad + I_{b,Na}(E) + I_{b,Ca}(E, Cai),\\
\frac{\mathrm{d}y}{\mathrm{d}t} &= \frac{\overline{y} - y}{\tau_y}, \qquad y = j, o_i, x_r, x_s, f, f_{Ca}, u, v,\\
\frac{\mathrm{d}Cai}{\mathrm{d}t} &= \frac{B1}{B2},\\
B1 &= (2FV_i)^{(-1)}(2I_{NaCa}(E, Cai) - I_{p,Ca}(Cai) - I_{Ca,L}(E, \overline{d}, f, f_{Ca})\\
&\quad - I_{b,Ca}(E, Cai)) + (V_i)^{(-1)}(V_{up}(0.000496 - I_{up}(Cai))\\
&\quad + I_{rel}(Cai, Carel, u, v, \overline{w})V_{rel}),\\
B2 &= 1 + \frac{[Trpn]_{max}K_{m,Trpn}}{(Cai + K_{m,Trpn})^2} + \frac{[Cmdn]_{max}K_{m,Cmdn}}{(Cai + K_{m,Cmdn})^2},\\
\frac{\mathrm{d}Carel}{\mathrm{d}t} &= \frac{(I_{tr}(Carel) - I_{rel}(Cai, Carel, u, v, \overline{w}))}{\left(1 + \frac{[Csqn]_{max}K_{m,Csqn}}{(Carel + K_{m,Csqn})^2}\right)}.
\end{aligned}
$$

We consider from the τ's that j, o_i, f_{Ca}, u and v are the fast variables here and f, x_r and x_s are the slow variables. Even though we know that I_{Na}=0, so j doesn't affect the action potential at all, j must still be part of the system, because E affects j and a solution for j can still be found. This is similar to o_a and d in the fast stage.

6.3.1 Considering u as a fast variable

We know that u is fast in this time stage from the graph of the τ's, Fig. 6.20(c). So we want to look at system (6.12) for t=$[1.2, 600]$, because u is fast in both the intermediate and slow stages, therefore we use t=$[1.2, 600]$. We want to see what exactly happens to the u equation if we consider it as fast. If we replace u with $\overline{u}$ we will obtain a system of ten equations. So if we consider this we end

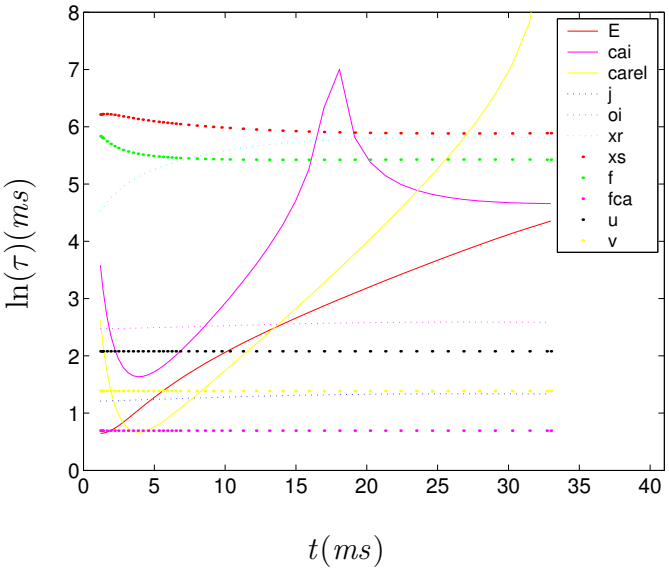

Figure 6.20: Graph of the τ's for CRN-11, system (6.12), for the time scale $[1.2, 33]$.

up with a loop because I_{rel} contains $\overline{u}$, $\overline{u}$ contains F_n and F_n contains I_{rel}. So we have a non-linear system of three equations:

$$\begin{aligned} I_{rel} &= K_{rel}\overline{u}^2 v\overline{w}(E)(Carel - Cai), \\ \overline{u} &= \left(1 + e^{-\frac{(F_n - 3.4175*10^{-13})}{13.67*10^{-16}}}\right)^{-1}, \\ F_n &= 10^{-12} V_{rel} I_{rel}(E, Cai, Carel, \overline{u}, v, \overline{w}) \\ &\quad -\frac{5*10^{-13}}{F}\left(\frac{1}{2}I_{Ca,L}(E, \overline{d}, f, f_{Ca}) - \frac{1}{5}I_{NaCa}(E, Cai)\right). \end{aligned} \tag{6.13}$$

So,

$$\begin{aligned} I_{rel} &= K\overline{u}^2, \\ \overline{u} &= (1 + He^{-F_n/a})^{-1}, \\ F_n &= CI_{rel}(E, Cai, Carel, \overline{u}, v, \overline{w}) - D, \end{aligned} \tag{6.14}$$

where,

$$\begin{aligned} K(E, Cai, Carel, v) &= K_{rel} v\overline{w}(E)(Carel - Cai), \\ C &= 10^{(-12)} V_{rel}, \\ D(E, Cai, f, f_{Ca}) &= \frac{5*10^{(-13)}}{F}(\frac{1}{2}I_{Ca,L}(E, \overline{d}, f, f_{Ca}) - \frac{1}{5}I_{Na,Ca}(E, Cai)), \end{aligned}$$

$$
\begin{aligned}
E &= 3.7465 * 10^{108}, \\
a &= 13.67 * 10^{-16}.
\end{aligned}
$$

We know that $\overline{u}$ is between $[0, 1]$, but we still want to find an equation for $\overline{u}$ so we can show that the solutions are between $[0, 1]$.

We eliminate F_n and I_{rel} from system (6.14) by replacing $\overline{u}$ with $(1 + e^{-(F_n - F_1)/a})^{-1}$, where $F_1{=}a \ln H$ and rearranging $\overline{u}$ to have $F_n(\overline{u})$ and replacing F_n with this:

$$
F_n = F_1 - a \ln \left(\frac{1 - \overline{u}}{\overline{u}} \right).
$$

So we obtain the following equation:

$$
F_1 + D - a \ln \left(\frac{1 - \overline{u}}{\overline{u}} \right) = CK\overline{u}^2. \tag{6.15}
$$

This can't be resolved with respect to $\overline{u}$ easily, so we will find solutions of $\overline{u}$ by drawing both sides of this equation and see where the solutions are.

$$
\begin{aligned}
y_1 &= F_1 + D - a \ln \left(\frac{1 - \overline{u}}{\overline{u}} \right), && (6.16) \\
y_2 &= CK\overline{u}^2. && (6.17)
\end{aligned}
$$

If we draw y_1 we see that it is a step function on the y-axis between $[0, 1]$ for $\overline{u}$, because we know that $\overline{u}$ is between $[0, 1]$. We see that y_1 goes from being a vertical line downwards at $\overline{u}{=}0$ to a vertical line upwards at $\overline{u}{=}1$, in-between it is a horizontal line at $y_1{=}F_1 + D$. Equation y_2 is a parabola and for $\overline{u}$ between $[0, 1]$ we obtain the positive section of the parabola, where it touches the $\overline{u}$ axis at zero.

So to find for what value of $\overline{u}$ these two cross we put them equal to each other. We know from Fig. 6.21 that they cross three times for $y_1{=}0$, $F_1 + D$ and 1. So the y_2 values corresponding to this are 0, $+\sqrt{\frac{F_1+D}{CK}}$ and CK. We are only interested in the positive root as the negative root is not in the region we are looking at.

Therefore we find that we have one or three solutions:

$$
t = 1.2 - 14.9761, \qquad \text{one solution},
$$

$$
\begin{aligned}
t &= 15.9053 - 33.8085, \qquad \text{three solutions,} \\
t &= 34.1751 - 171.9058, \qquad \text{one solution,} \\
t &= 172.2015 - 600, \qquad \text{three solutions.}
\end{aligned}
$$

We also see that if we use the original E_0=−81.18 we have three solutions and if we use E_0=−20 we have one solution, at t=0. Even though we are drawing the graphs for the time period $[1.2, 600]$, we draw the two graphs for different E_0 to show that if we use the original E_0 we obtain three solutions and if we use our modified value we obtain one solution. Therefore for different time periods of the action potential we have either one or three solutions of equations (6.16) and (6.17). In Fig. 6.21, we see that for E_0=−81.18 we have the solution on the lower branch of y_1 and for E_0=−20 we have the solution on the top branch of y_1.

We use different values from the action potential to draw the graphs to show how many solutions we have for different points on the action potential. Figure 6.21 shows six graphs of equations (6.16) (- -) and (6.17) (-) that are drawn for the following points of the action potential:

$$
\begin{aligned}
(a) \qquad & (t, E_0) = (0, -81.18), \\
(b) \qquad & (t, E_0) = (0, -20), \\
(c) \qquad & (t, E) = (6.5215, -1.9925), \\
(d) \qquad & (t, E) = (29.0419, -12.5132), \\
(e) \qquad & (t, E) = (83.8959, -7.3251), \\
(f) \qquad & (t, E) = (172.9342, -24.7021).
\end{aligned}
$$

Graphs (a) and (b) are drawn using the resting values of all the variables for different E_0, where also I_{st}=−2000 for (a) and I_{st}=0 for (b), (c), (d), (e) and (f). Graphs (c), (d), (e) and (f) are drawn using the results after one action potential for different values of t and E. The dots represent the equilibrium (true solution) of the fast subsystem CRN-11 and the stars represent the other solutions.

Therefore we see that for different time periods of the action potential we have the solutions of equations (6.16) and (6.17) alternating between one and three solutions. For E_0=−81.18 we have three solutions and for E_0=−20 we have one solution. So we see that if we change the initial value of E we obtain

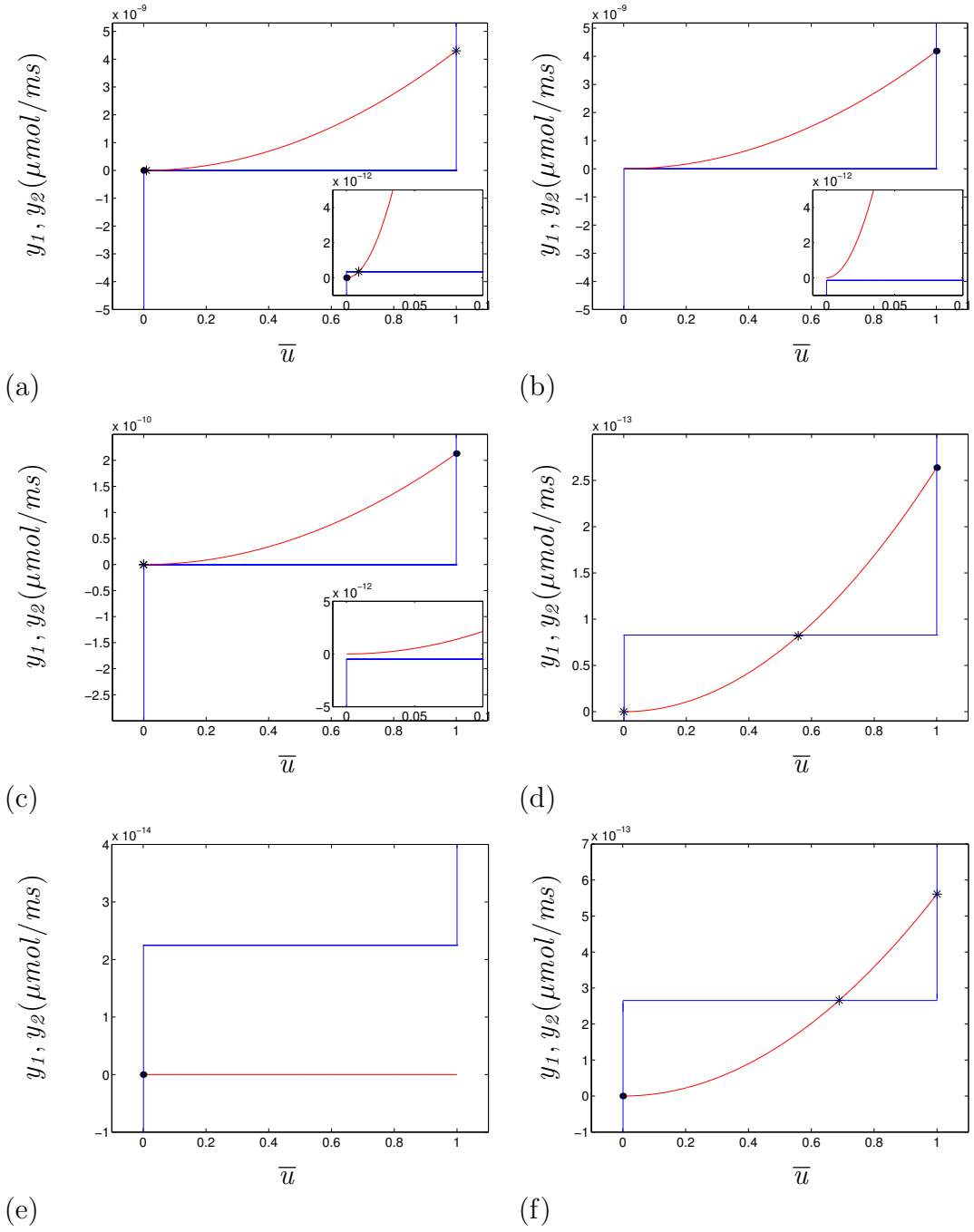

Figure 6.21: Graphs of equations (6.16) (- -) and (6.17) (-) for the resting values with (a) E_0=−81.18, (b) E_0=−20 and after one action potential for (c) (t, E)=(6.5215, −1.9925), (d) (t, E)=(29.0419, −12.5132), (e) (t, E)=(83.8959, −7.3251) and (f) (t, E)=(172.9342, −24.7021).

different results and the true solution for E_0=−81.18 is on the lower branch, and for E_0=−20 the true solution is on the top branch of equation (6.16). For the upstroke and overshot of the action potential we have one solution, (c), and then if the action potential comes down for the return we have three solutions, (d), then back to one solution, (e), and then three solutions again, (f).

Therefore we see that the solutions for equations (6.16) and (6.17) start at the lower branch of equation (6.16) for E_0=−81.18, then at E_0=−20 it moves to the top branch and stays there until we have one solution at t=34.1751 where it moves to the lower branch and it stays on the lower branch. Therefore we have a jump return from the top branch to the lower branch.

So the solutions jump from one bistability region of the slow manifold to another bistability region, completely avoiding the monostability region. This is just like the Hodgkin-Huxley, FitzHugh and Noble 1962 systems. We have a jump return because we don't have a monostability region where the upper and lower solutions coincide to make one true solution, which would be in between these two solutions. So therefore we don't have a cusp catastrophe like in Zeeman's "nerve" system.

Therefore the three solutions are:

$$\begin{aligned} F_{n_1} &\approx -D, & \overline{u}_1 &\approx 0, \\ F_{n_2} &\approx F_1, & \overline{u}_2 &\approx +\sqrt{\frac{F_1 + D}{CK}}, \\ F_{n_3} &\approx CK - D, & \overline{u}_3 &\approx 1. \end{aligned}$$

We obtain F_n by putting the values for $\overline{u}$ in equation (6.14), where $\overline{u}_1$ corresponds to the lower branch/solution of equation (6.16), $\overline{u}_2$ corresponds to the middle branch/solution of equation (6.16) and $\overline{u}_3$ corresponds to the upper branch /solution of equation (6.16).

Function $\overline{u}_2$ depends on what values you take from the solution of the action potential, as D=$D(E, Cai, f, f_{Ca})$, C=const, K=$K(E, Cai, Carel, v)$ and F_1=const.

Figure 6.22 shows a typical solution of equations (6.16) and (6.17). We use the same graph as Fig. 6.21(d), except here we have marked the three solutions, $\overline{u}_1$, $\overline{u}_2$ and $\overline{u}_3$

Figures 6.23(c) and (d) shows the graphs of the absolute values of $\overline{u}_1$, $\overline{u}_2$, $\overline{u}_3$ and $\overline{u}$, the true solution from CRN-11, for two time periods. We see that $\overline{u}$ is a

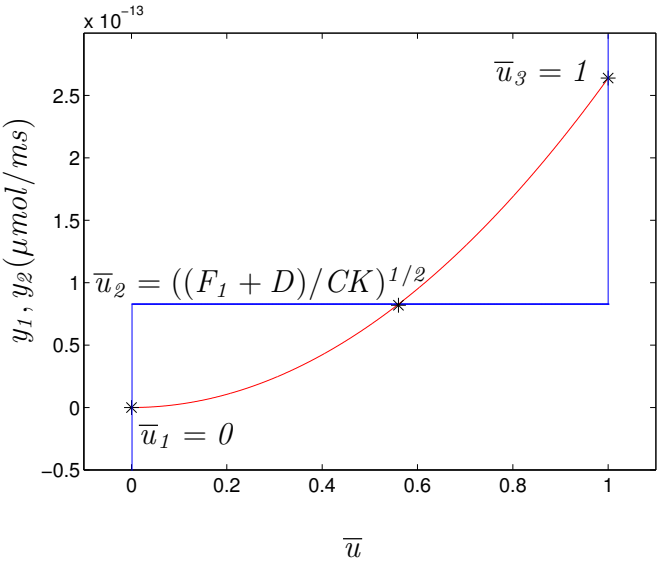

Figure 6.22: Graph of y_1 (6.16) (- -) and y_2 (6.17) (-) for t=29.05132, Fig. 6.21(d), with $\overline{u}_1, \overline{u}_2$ and $\overline{u}_3$.

step function that follows the path of $\overline{u}_3$ at the very beginning and then changes to follow $\overline{u}_1$.

From Figs. 6.22 and 6.23(c) we are able to formulate three algorithms to give us values for $\overline{u}$. We see from Fig. 6.22 that we can't have $\overline{u}_3 < \overline{u}_2$ and $\overline{u}_1 > \overline{u}_2$ as this is not possible. So if this happens we have $\overline{u}$=$\overline{u}_1$ and $\overline{u}_3$ respectively. We use Fig. 6.23(c) to see for what time period this happens. Inequality $\overline{u}_1 > \overline{u}_2$ never happens for our time period t=$[1.2, 600]$, it might happen before t=1.2, but we are not interested in that time period here. Inequality $\overline{u}_3 < \overline{u}_2$ happens for t=$[33.92, 172.61]$. For the remaining time we have $\overline{u}_1 < \overline{u}_2 < \overline{u}_3$, we can't say exactly what $\overline{u}$ is, so we have to use an algorithm that takes a previous value of $\overline{u}$, calculates if it is closer to $\overline{u}_1$ or $\overline{u}_3$ and which ever one it is closer to is our new $\overline{u}$. From this we see that for t=$[1.2, 33.92]$, $\overline{u}$=$\overline{u}_3$ and for t=$[172.61, 600]$, $\overline{u}$=$\overline{u}_1$.

Therefore for any point on the action potential we can say that $\overline{u}$ is either $\overline{u}_1$ or $\overline{u}_3$. We are now able to replace the $\overline{u}$ equation in system (6.12) with either $\overline{u}_1$ or $\overline{u}_3$ for different moments in time. This confirms that the Heaviside equation for $\overline{u}$ is a correct assumption. Therefore we keep $\overline{u}$ as the Heaviside function:

$$\overline{u} = \theta(F_n - F_1),$$

where F_1=$3.4175 * 10^{-13}$.

Function $\overline{u}$ can also be written in the following form without F_n:

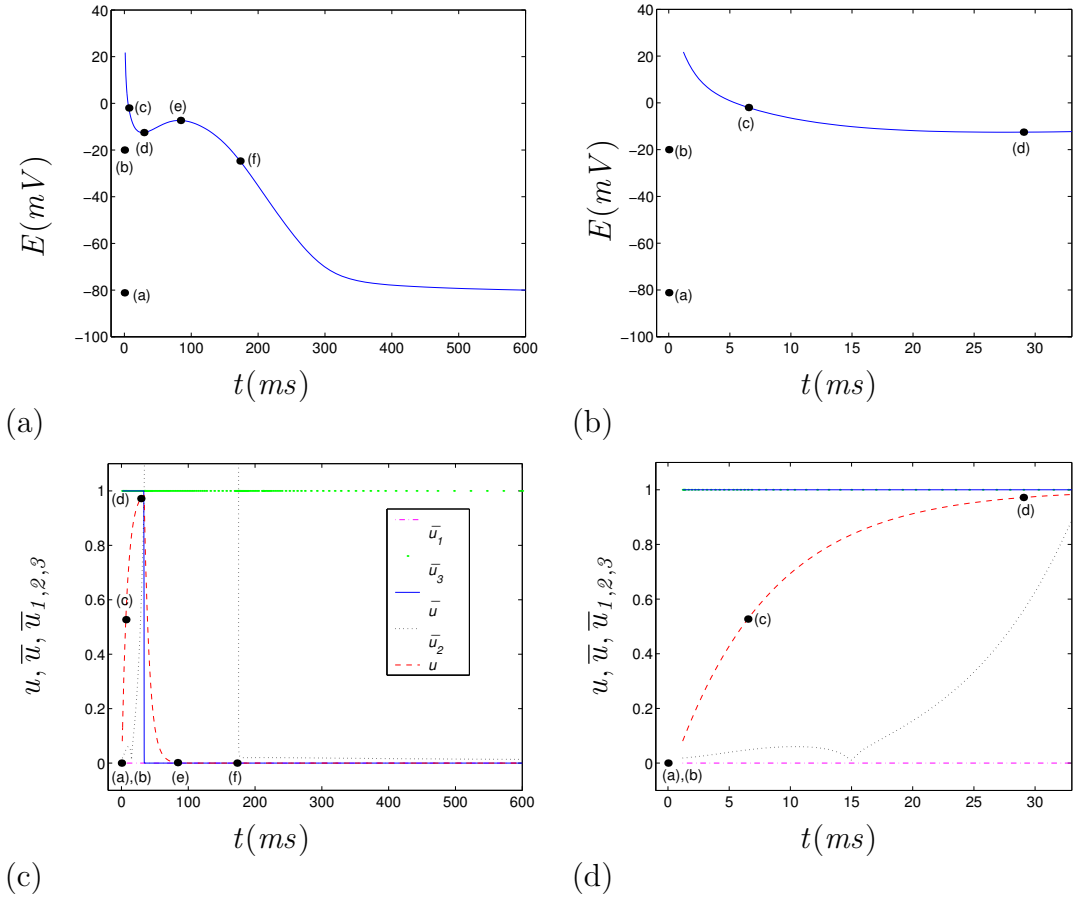

Figure 6.23: (a) and (b) are the action potentials of CRN-11, system (6.12), and (c) and (d) are the graphs of u (- -) and the absolute values of $\overline{u}$ (-),$\overline{u}_1$ (-.), $\overline{u}_2$ (:) and $\overline{u}_3$ (.) for E_0=-20. (a) and (c) are for the time period $[1.2, 600]$ and (b) and (d) are for the time period $[1.2, 33]$ with the points (a) E_0=-81.18, (b) E_0=-20, (c) (t, E)=$(6.5215, -1.9925)$, (d) (t, E)=$(29.0419, -12.5132)$, (e) (t, E)=$(83.8959, -7.3251)$ and (f) (t, E)=$(172.9342, -24.7021)$.

$$\overline{u} = \begin{cases} 0 & \text{if} \quad \overline{u}_1 \geq \overline{u}_2, \\ & \text{if} \quad \overline{u}_1 < \overline{u}_2 < \overline{u}_3 \quad \text{and} \quad \overline{u} - \overline{u}_1 < \overline{u}_3 - \overline{u}, \\ 1 & \text{if} \quad \overline{u}_3 \leq \overline{u}_2, \\ & \text{if} \quad \overline{u}_1 < \overline{u}_2 < \overline{u}_3 \quad \text{and} \quad \overline{u} - \overline{u}_1 > \overline{u}_3 - \overline{u}. \end{cases}$$

Therefore we now have a new system of ten variables, CRN-10:

$$\begin{aligned} \frac{\mathrm{d}E}{\mathrm{d}t} &= -\frac{I_{ion}}{C_M}, \qquad (6.18) \\ I_{ion} &= I_{Na}(E, \overline{m}, h, j) + I_{K1}(E) + I_{to}(E, \overline{o}_a, o_i) + I_{Kur}(E, \overline{u}_a) + I_{Kr}(E, x_r) \\ &\quad + I_{Ks}(E, x_s) + I_{Ca,L}(E, \overline{d}, f, f_{Ca}) + I_{p,Ca}(Cai) + I_{Na,K}(E) + I_{b,Na}(E) \\ &\quad + I_{NaCa}(E, Cai) + I_{b,Ca}(E, Cai), \\ \frac{\mathrm{d}y}{\mathrm{d}t} &= \frac{\overline{y} - y}{\tau_y}, \qquad y = h, j, o_i, x_r, x_s, f, v, \\ \frac{\mathrm{d}Cai}{\mathrm{d}t} &= \frac{B1}{B2}, \\ B1 &= (2FV_i)^{(-1)}(2I_{NaCa}(E, Cai) - I_{p,Ca}(Cai) \\ &\quad - I_{Ca,L}(E, \overline{d}, f, f_{Ca}) - I_{b,Ca}(E, Cai)) \\ &\quad + (V_i)^{(-1)}(V_{up}(0.000496 - I_{up}(Cai)) \\ &\quad + I_{rel}(Cai, Carel, \overline{u}_n, v, \overline{w})V_{rel}), \\ B2 &= 1 + \frac{[Trpn]_{max}K_{m,Trpn}}{(Cai + K_{m,Trpn})^2} + \frac{[Cmdn]_{max}K_{m,Cmdn}}{(Cai + K_{m,Cmdn})^2}, \\ \frac{\mathrm{d}Carel}{\mathrm{d}t} &= \frac{(I_{tr}(Carel) - I_{rel}(Cai, Carel, \overline{u}_n, v, \overline{w}))}{\left(1 + \frac{[Csqn]_{max}K_{m,Csqn}}{(Carel + K_{m,Csqn})^2}\right)}. \end{aligned}$$

Figure 6.24 shows the action potential of CRN-11 and CRN-10 and we see that the spike is the same, but there is a slight change on the return. The new system, CRN-10, still looks like the old system, CRN-11.

6.3.2 Comparing u and $\overline{u}$

From the graph of u and $\overline{u}$, Fig. 6.25, we see that the quasi-stationary value is now a rectangular shape, but is still a perfect switch for the u variable. We also see that for various moments in time u is not close to $\overline{u}$.

Also we see that u comes into action during the intermediate stage $[1.2, 33]$ as after this it is close to zero. So this confirms our assumption that u can be considered a fast variable during this time period. Also we see that for this time

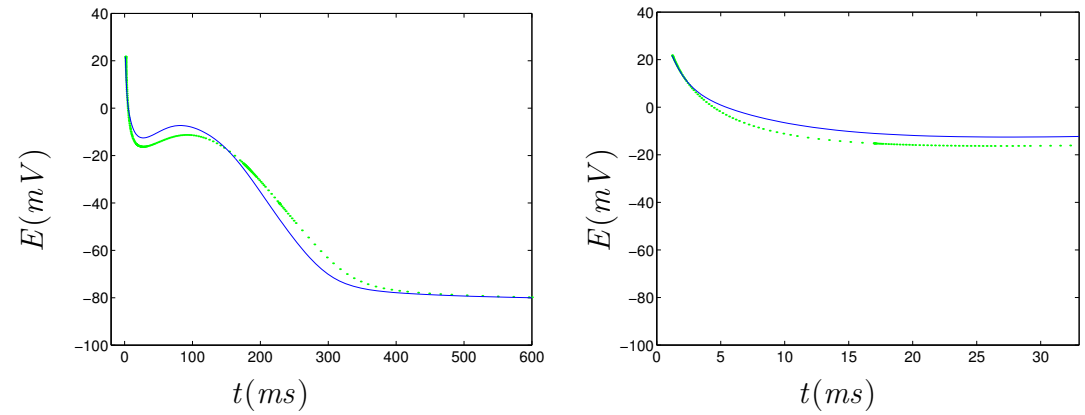

(a) (b)

Figure 6.24: Action potential for CRN-11, system (6.12), (-) and CRN-10, system (6.18), (.) for E_0=−20 for the time periods (a) $[1.2, 600]$ and (b) $[1.2, 33]$.

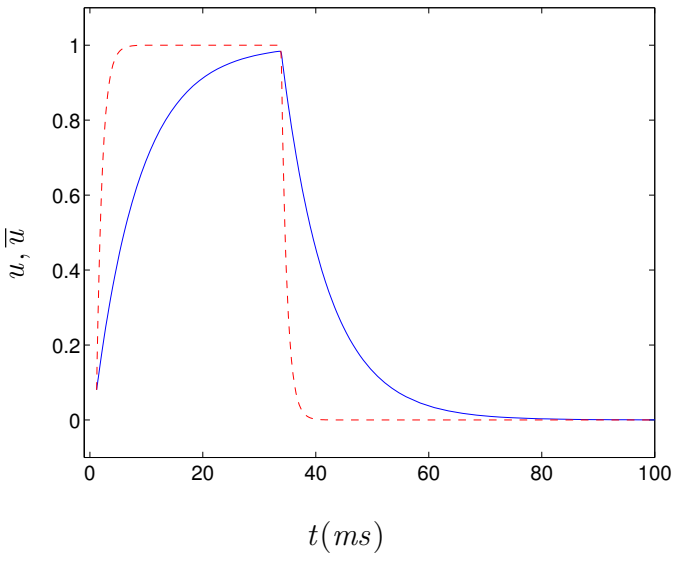

Figure 6.25: Graph of u (-) and its quasi-stationary value $\overline{u}$ (- -) for CRN-11 for the time period $[1.2, 100]$.

period u can be replaced with an exponential function of time. We go into more detail on replacing u with an exponential function later.

Variable u=$\overline{u}$ in principle, but introduces noticeable errors. On the other hand, this suggests a more accurate way to treat u, which is considered later.

6.3.3 Finding the threshold for E where the intersections change from three to one in Fig. 6.21, lower equilibrium disappears

We have equation (6.15) for $\overline{u}$ and to find how many intersections this has we draw equations (6.16) and (6.17), Fig. 6.21. We found that for the initial conditions and different values of E_0 we obtained one or three intersections, so we want to find for what value of E_0 this change happens. We use equation (6.15) to do this:

$$F_1 + D - a \ln\left(\frac{1-\overline{u}}{\overline{u}}\right) \;=\; CK\overline{u}^2.$$

We know that we have three solutions to this equation, $\overline{u}_1$, $\overline{u}_2$ and $\overline{u}_3$:

1. $\overline{u} < +\sqrt{\frac{F_1+D}{CK}}$; $\overline{u}_1$=0 iff $+\sqrt{\frac{F_1+D}{CK}} > 0$,
2. $\overline{u}$=$+\sqrt{\frac{F_1+D}{CK}}$; $\overline{u}_2 = +\sqrt{\frac{F_1+D}{CK}}$ iff $1 > +\sqrt{\frac{F_1+D}{CK}} > 0$,
3. $\overline{u} > +\sqrt{\frac{F_1+D}{CK}}$; $\overline{u}_1$=1 iff $+\sqrt{\frac{F_1+D}{CK}} < 1$.

So we have two conditions here:

$$\begin{aligned} \text{Condition} \quad 1: \quad & +\sqrt{\frac{F_1+D}{CK}} > 0, \\ \text{Condition} \quad 2: \quad & +\sqrt{\frac{F_1+D}{CK}} < 1. \end{aligned}$$

$$\begin{aligned} \text{Condition} \quad 1 \;&\Leftrightarrow\; \text{S1} : \overline{u}_1 = 0, \\ \text{Conditions} \quad 1,2 \;&\Leftrightarrow\; \text{S2} : \overline{u}_2 = +\sqrt{\frac{F_1+D}{CK}}, \\ \text{Condition} \quad 2 \;&\Leftrightarrow\; \text{S3} : \overline{u}_3 = 1. \end{aligned}$$

So we are looking for the threshold where S1 and S2 cease to exist. This is for $\overline{u}_1 \geq \overline{u}_2 \Rightarrow 0 \geq +\sqrt{\frac{F_1+D}{CK}}$. Therefore the threshold is at $+\sqrt{\frac{F_1+D}{CK}}$=0.

$$\begin{aligned}\frac{F_1+D}{CK} &= 0,\\ F_1 &= -D.\end{aligned}$$

Therefore if we put the initial conditions in $D{=}-F_1$ we obtain:

$$\frac{A}{F}\left(\frac{1}{2}I_{Ca,L}(E,\overline{d}(E)) - \frac{1}{5}I_{Na,Ca}(E)\right) + F_1 = 0,$$

where

$$\begin{aligned}A = 5*10^{(-13)}, &\qquad F = 96.4867,\\ g_{Ca,L} = 0.12375, &\qquad \overline{d} = (1+e^{-(E+10)/8})^{-1} = (1+e^{-(E+E_d)/b},\\ \overline{f}_{Ca} = 0.7749, &\qquad f = 0.9959,\\ Cai = 0.0001, &\qquad C_M = 100,\\ I_{Na,Ca}(max) = 1600, &\qquad K_{sat} = 0.1,\\ \gamma = 0.35, &\qquad R = 8.3143,\\ T = 310, &\qquad Nai = 11.17,\\ \mathrm{Cao} = 1.8, &\qquad \mathrm{Nao} = 140,\\ K_{m,Na} = 87.5, &\qquad K_{M,Ca} = 1.38,\\ I_{Ca,L} = C_M g_{Ca,L}\overline{d}f f_{Ca}(E-65) &= 9.55\overline{d}(E-E_{Ca,L}).\end{aligned}$$

$$\begin{aligned}I_{Na,Ca} &= \frac{C_M I_{Na,Ca}(max)\{e^{(\gamma FE/RT)}Nai^3\mathrm{Cao} - e^{(\gamma-1)FE/RT}\mathrm{Nao}^3 Cai\}}{(K^3_{m,Na}+\mathrm{Nao}^3)(K_{M,Ca}+\mathrm{Cao})(1+K_{sat}e^{(\gamma-1)FE/RT})},\\ &= \frac{0.01\{2508.7e^{0.0131E} - 274.4e^{-0.0243E}\}}{1+0.1e^{-0.0243E}}.\end{aligned}$$

Now we say that:

$$\begin{aligned}y &= \frac{1}{2}I_{Ca,L}(E,\overline{d}(E)) - \frac{1}{5}I_{Na,Ca}(E) + \frac{F_1F}{A} = 0,\\ y &= \frac{1}{2}B\overline{d}(E)(E-E_{Ca,L}) - \frac{1}{5}\frac{G\{He^{IE} - Je^{LE}\}}{1+K_{sat}e^{LE}} + \frac{F_1F}{A} = 0,\end{aligned}$$

where

$$\overline{d} = (1 + e^{-(E+E_d)/b})^{-1}, \qquad E_{Ca,L} = 65,$$
$$B = C_M g_{Ca,L} f f_{Ca} = 9.55, \qquad H = Nai^3\mathrm{Cao} = 2508.7,$$
$$I = (\gamma F/RT) = 0.0131, \qquad J = \mathrm{Nao}^3 Cai = 274.4,$$
$$L = (\gamma - 1)F/RT = -0.0243, \qquad \frac{F_1 F}{A} = 5.9487,$$
$$G = \frac{C_M I_{Na,Ca}(max)}{(K^3_{m,Na} + \mathrm{Nao}^3)(K_{M,Ca} + \mathrm{Cao})} = 0.01, \qquad K_{sat} = 0.1,$$

and we draw y against voltage, Fig. 6.26(a), as this equation is too complicated to resolve with respect to E, and we see that the curve crosses y=0 at E=−24.09.

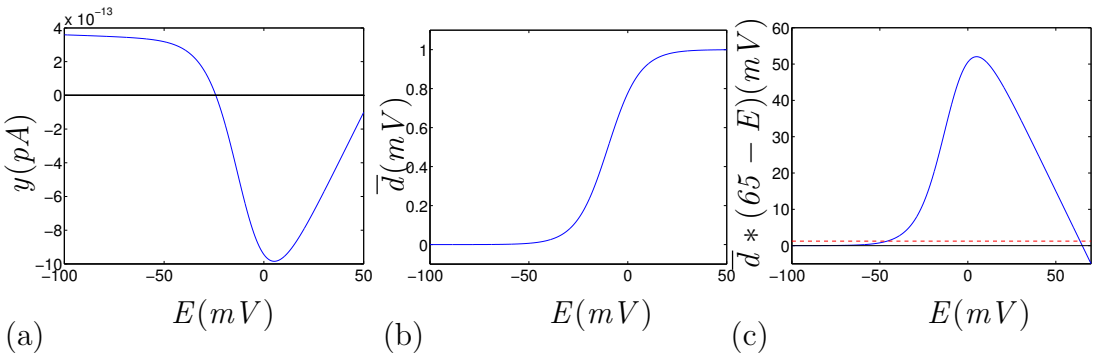

Figure 6.26: (a) Graph of y against E. (b) Graph of $\overline{d}$ against E. (c) Graph of $\overline{d}(E_{Ca,L} - E)$ (-) and q (- -) against E.

We want to approximate analytically the solution to $y(E)$=0. So we take y=0 and we know that $I_{Na,Ca}$ is small compared to $I_{Ca,L}$, so we can ignore this term. Therefore y=0 becomes:

$$\begin{aligned} B\overline{d}(E)(E - E_{Ca,L}) &= -2\frac{F_1 F}{A}, \\ \overline{d}(E)(E_{Ca,L} - E) &= q, \end{aligned}$$

where,

$$q = 2\frac{F_1 F}{AB} = 2\frac{a\ln(H)F}{AC_M g_{Ca,L} f f_{Ca}} = 1.246.$$

Then we use the definition of $\overline{d}(E)$, to obtain:

$$E = -E_d - b\ln\left(\frac{E_{Ca,L} - E - q}{q}\right).$$

From this equation we can take iterations for E, but to do this we need an initial point, E_0, for the iterations. We choose E_0=$-E_d$, because if we draw $\overline{d}$ against E, Fig. 6.26(b), we see that $\overline{d}$ changes from 0 to 1 at around E=$-E_d$. Also from Fig. 6.26(c), graph of q=$\overline{d}(65-E)$, we see that we have two solutions, one is q=$\frac{2F_1F}{AB}$=1.246 (- -), and the other is $\overline{d}(65-E)$ (-). We see that we have a fast raising $\overline{d}$ which occurs at E=$-E_d$. So we use E_0=$-E_d$ and take iterations of E and see if this will give us the same value of E, as we obtained with the numerical method.

$$E_{n+1} = -E_d - b\ln\left(\frac{E_{Ca,L} - E_n - q}{q}\right).$$

We take E_0=$-E_d$ as our initial value for E_0 in the iterations. So the iterations give us the following values:

$$\begin{aligned} E_0 &= -10, & E_1 &= -21.9079, \\ E_2 &= -23.3305, & E_3 &= -23.4847, \\ E_4 &= -23.5012, & E_5 &= -23.5030, \\ E_6 &= -23.5032, & E_7 &= -23.5032. \end{aligned}$$

We see that the values of the iterations tend to E=-23.5032 which is close to the value of the numerical answer, E=-24.09. So the iteration method gives an answer close to the numerical answer and therefore this method can be used to find the threshold of E, without having to find it numerically.

Therefore E_1 gives a good approximation so we can say:

$$E \approx E_1 = -E_d - b\ln\left(\frac{E_{Ca,L} + E_d - q}{q}\right).$$

6.3.4 Finding the threshold for E where the intersections change from three to one in Fig. 6.21, upper equilibrium disappears

Now that we have found the threshold where the lower equilibrium disappears, then we want to find the threshold where the upper equilibrium disappears. This happens if S2 and S3 ceases to exist. This happens at the following values:

$$(E, Cai, Carel, j, o_i, x_r, x_s, f, f_{ca}, u, v) = (-12.1869, 0.0008, 0.1485, 0.0001,$$

$$0.0719, 0.0935, 0.0445, 0.8732,$$
$$0.2965, 0.9535, 0.0002),$$

and t=34.1751. So this is for $F_2 > F_3 \Rightarrow F_1 > CK - D$. Therefore the threshold is at F_1=$CK - D$.

This happens if S2 and S3 ceases to exist. So this is for $\overline{u}_2 > \overline{u}_3 \Rightarrow +\sqrt{\frac{F_1+D}{CK}} > 1$. Therefore the threshold is at $+\sqrt{\frac{F_1+D}{CK}}$=1.

$$\begin{aligned} +\sqrt{\frac{F_1+D}{CK}} &= 1, \\ F_1 &= CK - D. \end{aligned}$$

$$\begin{aligned} CK - D &= CK - \frac{A}{F}\left(\frac{1}{2} I_{Ca,L}(E, \overline{d}, f, f_{Ca})\right), \\ K(E, Cai, Carel, v) &= K_{rel} v \overline{w}(E)(Carel - Cai), \\ C &= V_{rel} * 10^{(-12)} = 96.48 * 10^{(-12)}, \\ F_1 &= 3.4175 * 10^{(-13)}, \\ K_{rel} &= 30. \end{aligned}$$

Therefore if $CK - D$=F_1 we obtain:

$$c\overline{w}(E) - e\overline{d}(E)(E - E_{Ca,L}) - F_1 = 0,$$

where

$$\begin{aligned} \overline{w} = 1 - (1 + e^{-(E-40)/17})^{-1} &= 1 - (1 + e^{-(E-E_w)/d})^{-1}, \\ \overline{d} = (1 + e^{-(E+10)/8})^{-1} = (1 + e^{-(E+E_d)/b})^{-1}, & \quad e = \frac{AB}{2F}, \\ c = CK_{rel} v(Carel - Cai), & \quad A = 5 * 10^{(-13)}, \\ F = 96.4867, & \quad B = C_M g_{Ca,L} f f_{Ca}, \\ E_{Ca,L} = 65, & \quad F_* = 3.4175 * 10^{(-13)}. \end{aligned}$$

Now we say that:

$$y = c\overline{w}(E) - e\overline{d}(E)(E - E_{Ca,L}) - F_1 = 0,$$

and draw y against voltage for the values of Cai, $Carel$, f, f_{Ca} and v at t=34.1751 where the solutions change from three to one intersections. We see from Fig. 6.27

that the curve crosses the y-axis in two places at E=−13.24 and 30.01. So this equation has two values of E, but going from Fig. 6.21 E=−13.24 is relevant and E=30.01 isn't.

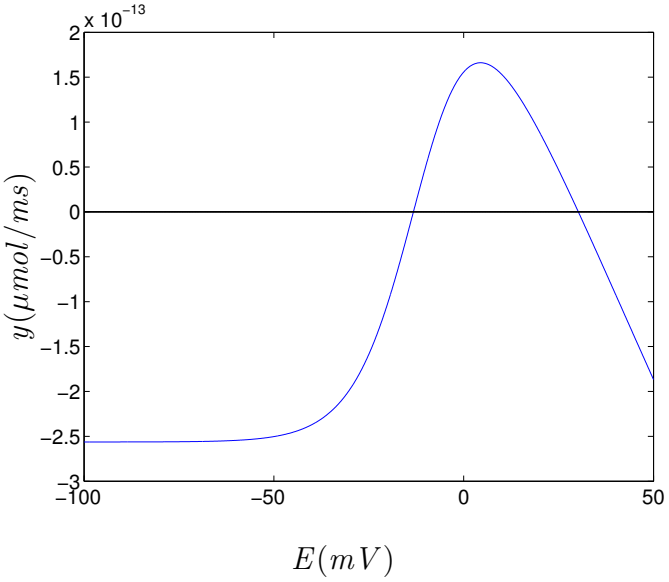

Figure 6.27: Graph of y against E.

We want to approximate analytically $y(E)$=0, therefore take y=0:

$$\begin{aligned} c\overline{w}(E) - e\overline{d}(E)(E - E_{Ca,L}) - F_1 &= 0, \\ \overline{d}(E) &= \frac{p}{(E_{Ca,L} - E)}, \\ p &= \frac{F_1 - c\overline{w}(E)}{e}, \\ E &= -E_d - b\ln\left(\frac{E_{Ca,L} - E - p}{p}\right), \\ E_{n+1} &= -E_d - b\ln\left(\frac{E_{Ca,L} - E_n - p}{p}\right), \end{aligned}$$

where

$$\begin{aligned} \overline{w}(E_0) &= 1 - (1 + e^{-(E_0-40)/17})^{-1}, & c &= 8.5501 * 10^{-14}, \\ e &= 8.3015 * 10^{-15}, & F_1 &= 3.4175 * 10^{-13}, \\ Cai &= 0.0008, & Carel &= 0.1485, \\ f &= 0.8732, & f_{Ca} &= 0.2965, \\ v &= 0.0002. \end{aligned}$$

We take E_0=$-E_d$ as our initial value for E_0 in the iterations. So the iterations give us the following values:

$$\begin{aligned} E_0 &= -10, & E_1 &= -12.6328, \\ E_2 &= -13.1321, & E_3 &= -13.2231, \\ E_4 &= -13.2396, & E_5 &= -13.2426, \\ E_6 &= -13.2431, & E_7 &= -13.2432, \\ E_8 &= -13.2432. \end{aligned}$$

So we see that the analytical value is the same as the numerical value to two decimal places.

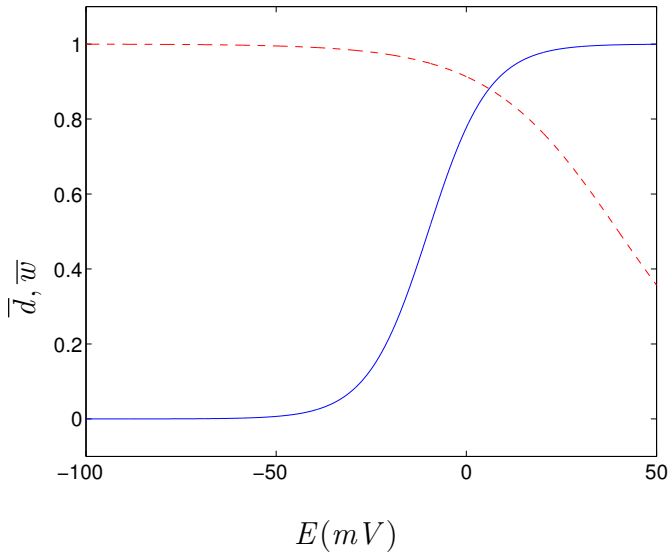

Figure 6.28: Graph of $\overline{w}$ (- -) and $\overline{d}$ (-) against E.

From Fig. 6.28 we could also take $\overline{w}$=1, if $\overline{d}$ changes from 0 to 1 at E=$-E_d$ as we see that if d is open then w is closed and vice versa, but d opens at a faster rate than w is closing at. So we can take iterations of E and see if this will give us an answer similar to the numerical answer.

We see that the values of the iterations tend to E=-13.4643 which is close to the value of the numerical answer E=-13.24, but is not the same value as we obtained above with the other iterations. So the iteration method gives an answer close to or the same as the numerical answer, therefore this method can be used to find the threshold of E without having to find it numerically.

We can say again that E_1 gives a good approximation, so:

$$E \approx E_1 = -E_d - b \ln \left(\frac{E_{Ca,L} + E_d - p}{p} \right).$$

6.3.5 Summary

We can summarize this section and see that the main results are:

1. we know that $\overline{u}$ can be written as follows,

$$\overline{u} \approx \theta(F_n - F_1),$$

in the limit $a \to 0$ where $F_1 = a \ln E = 3.4175 * 10^{-13}$,

2. we found that u can be considered as a fast variable during the intermediate and slow stage $[1.2, 600]$ because τ_u is small. Variable u is close to $\overline{u}$ most of the time, but we were studying u mainly for the intermediate stage and found that it can be treated as fast in the slow stage as well,

3. function $\overline{u}$ is a solution of the following equation:

$$F_1 + D - a \ln \left(\frac{1 - \overline{u}}{\overline{u}} \right) = CK\overline{u}^2, \tag{6.19}$$

4. during the time period $t = [1.2, 600]$ we have,

$$\begin{aligned} t &= 1.2 - 14.9761, && \text{one solution of (6.19)}, \\ t &= 15.9053 - 33.8085, && \text{three solutions of (6.19)}, \\ t &= 34.1751 - 171.9058, && \text{one solution of (6.19)}, \\ t &= 172.2015 - 600, && \text{three solutions of (6.19)}, \end{aligned}$$

5. the three solutions for $\overline{u}$ and F_n from (6.19) and $F_n = CK\overline{u}^2 - D$ are,

$$\begin{aligned} F_{n_1} \approx -D, \quad & \overline{u}_1 \approx 0, \\ F_{n_2} \approx F_1, \quad & \overline{u}_2 \approx +\sqrt{\frac{F_1 + D}{CK}}, \\ F_{n_3} \approx CK - D, \quad & \overline{u}_3 \approx 1, \end{aligned}$$

provided that $\overline{u}_1 \leq \overline{u}_2 \leq \overline{u}_3$,

6. we found that the equation for the bifurcation of merging the lower and middle solutions is,

$$\overline{u}_1 > \overline{u}_2,$$
$$\frac{A}{F}\left(\frac{1}{2}I_{Ca,L}(E,\overline{d}(E))\right) + F_1 = 0,$$

and,

$$E \approx E_1 = -E_d - b\ln\left(\frac{E_{Ca,L}+E_d-q}{q}\right) = -21.9079,$$

7. we found that the equation for the bifurcation of merging the upper and middle solutions is,

$$\overline{u}_2 > \overline{u}_3,$$
$$c\overline{w}(E) - e\overline{d}(E)(E-E_{Ca,L}) - F_1 = 0,$$

and

$$E \approx E_1 = -E_d - b\ln\left(\frac{E_{Ca,L}+E_d-p}{p}\right) = -12.6328.$$

We want to draw the parametric plane for our solution of $\overline{u}$. So we take the two equations for the bifurcations, leaving the variables as their initial values for the whole of the action potential and not just at the start of it. So we use the following two equations:

$$\begin{aligned} \frac{1}{2}I_{Ca,L}(E,\overline{d}(E),f,f_{Ca}) + \frac{F_1F}{A} &= 0, \\ CK(E,Cai,Carel) - \frac{A}{2F}I_{Ca,L}(E,\overline{d}(E),f,f_{Ca}) - F_1 &= 0, \end{aligned}$$

and find two common parameters in them and then draw the plane of these two parameters. We see from the two equations that K and $I_{Ca,L}$ are the common parameters. We rearrange these two equations to obtain the following two equations:

$$\begin{aligned} I_{Ca,L} &= -\frac{2F_1F}{A}, \\ I_{Ca,L} &= \frac{2F(F_1-CK)}{A}. \end{aligned}$$

Figure 6.29(a) shows the graph of these two equations and we see that they cross and give us a quadrant. If we draw the trajectory corresponding to the

action potential of the system we see that the trajectory only touches three parts of the quadrant. The trajectory is colour and line coded to show which part corresponds to the lower solution $\overline{u}_1$ (*) and which corresponds to the upper solution $\overline{u}_3$ (.). The quadrant is also marked with which section corresponds to how many solutions of the action potential there are and which solutions they are. We see that the lower left quadrant corresponds to the solutions for $\overline{u}_2$, but we can say that if we change the initial values for the action potential, then the trajectory would enter this quadrant and the solution here would be three solutions with $\overline{u}_3$ (upper) solution being the true solution.

We draw the phase portrait for the calcium subsystem to show where all three solutions for $\overline{u}$ exist. We use equation (6.19) equal to zero to draw the three-dimensional surface, where (x, y, z)=$(K, I_{Ca,L}, \overline{u})$. So the equation for the surface is:

$$f = 0 : \qquad F_1 + D - a \ln\left(\frac{1-\overline{u}}{\overline{u}}\right) - CK\overline{u}^2 = 0,$$

where D=$\frac{AI_{Ca,L}}{2F}$ as we considered $I_{Na,Ca}$=0 earlier.

So we can say that f=0 is our slow manifold for the calcium subsystem. We also want to find the fold curve, and draw a trajectory to see if the projections of the fold curve and trajectory onto the $(K, I_{Ca,L})$ plane looks exactly like Fig. 6.29(a). The fold curve satisfies the following two equations:

$$\begin{aligned} f = 0 : \qquad & F_1 + D - a \ln\left(\frac{1-\overline{u}}{\overline{u}}\right) - CK\overline{u}^2 = 0, \\ \frac{\partial f}{\partial \overline{u}} = 0 : \qquad & -2CK\overline{u} + a\left(\frac{1}{1-\overline{u}} + \frac{1}{\overline{u}}\right) = 0. \end{aligned}$$

If we rearrange $\frac{\partial f}{\partial \overline{u}}$=0 and put the answer in f=0, we obtain the following two equations:

$$\begin{aligned} K &= \frac{a}{2C\overline{u}^2(1-\overline{u})}, \\ I_{Ca,L} &= \frac{2F}{A}\left(a \ln\left(\frac{1-\overline{u}}{\overline{u}}\right) + \frac{a}{2(1-\overline{u})} - F_1\right). \end{aligned}$$

If we project the fold curve to the $(K, I_{Ca,L})$ plane we obtain a right angled curve, where the right angle is our cusp point. So the projection doesn't look like a cusp, this is because the fold curve is not smooth around the cusp point and we see what is projected if the fold curve is travelling along the $\overline{u}$ axis.

To find the cusp point we use the equation $\frac{\partial^2 f}{\partial \overline{u}^2}$=0, which gives us the solution $(K, I_{Ca,L}, \overline{u})$=$(4.7819 * 10^{-5}, -131.4716, 2/3)$.

We drew three graphs corresponding to f=0, where two are using approximations for $\overline{u}$, so that we have a good view of the surface and can see all the solutions for $\overline{u}$. Figure 6.29(b) is drawn for z=$\overline{u}$, Fig. 6.29(c) is drawn for z=$\ln(\frac{1-\overline{u}}{\overline{u}})$, where the fold curve satisfies:

$$\begin{aligned} K &= \frac{a(e^z+1)^3}{2Ce^z}, \\ I_{Ca,L} &= \frac{2F}{A}\left(az + \frac{a(e^z+1)}{2e^z} - F_1\right), \end{aligned}$$

and the cusp point is $(K, I_{Ca,L}, \overline{u})$=$(4.7819 * 10^{-5}, -131.4716, -0.6931)$.

Figure 6.29(d) is drawn for z=$\frac{1}{\overline{u}}$, where the fold curve satisfies:

$$\begin{aligned} K &= \frac{az^3}{2C(z-1)}, \\ I_{Ca,L} &= \frac{2F}{A}\left(a(z-1) + \frac{az}{2(z-1)} - F_1\right), \end{aligned}$$

and the cusp point is $(K, I_{Ca,L}, \overline{u})$=$(4.7819 * 10^{-5}, -131.4716, 3/2)$.

So we see from all three graphs that the projection to the $(K, I_{Ca,L})$ plane is the same as Fig. 6.29(a), and therefore the surface further proves which quadrant the solutions lie in, i.e. $\overline{u}_1$, $\overline{u}_2$ and $\overline{u}_3$.

We also see from Fig. 6.29(b) that the trajectory doesn't start near the slow manifold and doesn't at first travel along it. This is because the beginning of the trajectory corresponds to the time period $[1.2, 20]$, where u is actually not fast, as it is not close to its quasi-stationary value, which can be seen from Fig. 6.25.

Also, if you look at Fig. 6.29(c), you'll see that the projection of the trajectory to the $(I_{Ca,L}, \ln(\frac{1-\overline{u}}{\overline{u}}))$ axis is a straight line, whereas the trajectory is actually not straight at this point, this is because the projection has squashed the trajectory so that it looks like a straight line.

Figure 6.30 shows two enlarged graphs of the projection of the fold curve to the $(K, I_{Ca,L})$ plane from Fig. 6.29(b), from two different viewpoints. This is to show that even though the projection is a right angle, if viewed in this scale, it is actually still a cusp. So by enlarging the scale we can see that a cusp is projected down the z-axis. This then corresponds with the theory from Zeeman that we used to draw the phase portraits for the Hodgkin-Huxley system.

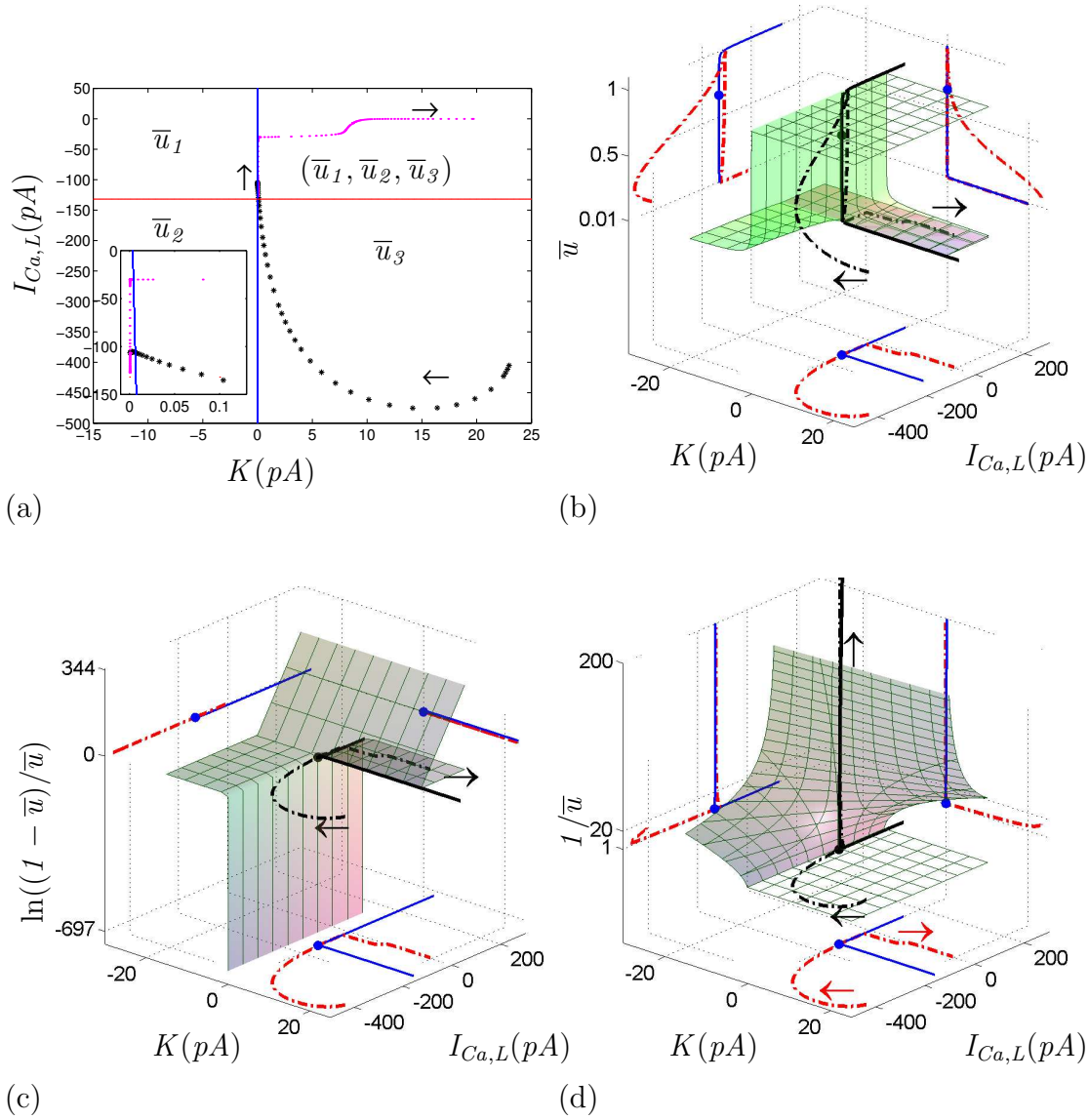

Figure 6.29: (a) Graph of $I_{Ca,L}$ against K with a trajectory that corresponds to the action potential representing the lower solution (*) and the upper solution (.). Phase portrait of the calcium subsystem with the semi-transparent surface as the slow manifold (6.19), fold curve and its projections (-) and trajectory and its projections (-.) for (x, y, z)=$(K, I_{Ca,L}, z)$, where (b) z=$\overline{u}$, (c) z=$\ln(\frac{1-\overline{u}}{\overline{u}})$ and (d) z=$\frac{1}{\overline{u}}$. The arrows represent the flow on the slow manifold.

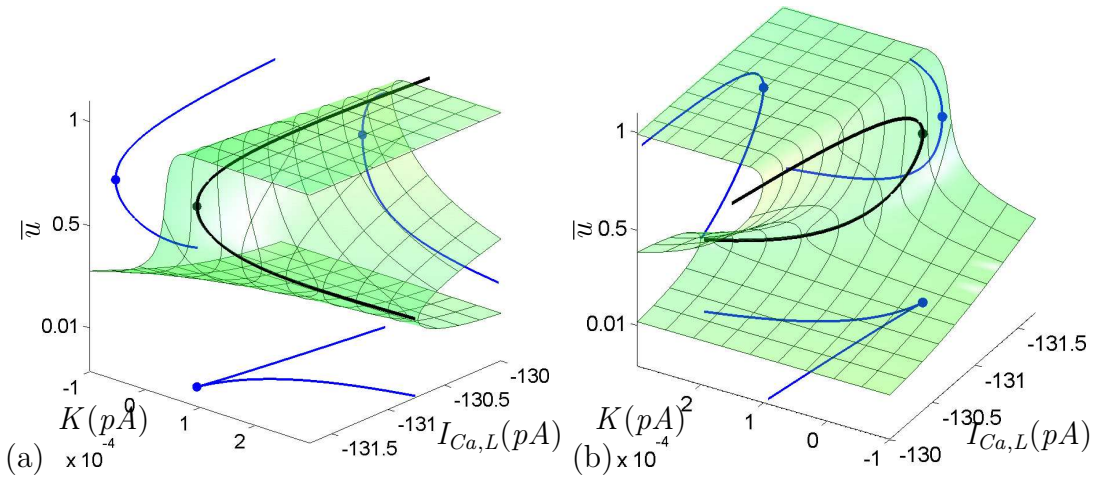

Figure 6.30: Phase portrait of the calcium subsystem with the semi-transparent surface as the slow manifold (6.19), fold curve and its projections (-) and trajectory and its projections (-.) for (x, y, z)=$(K, I_{Ca,L}, \overline{u})$, which corresponds to Fig. 6.29(b), from two viewpoints and different ranges of variables.

6.4 Other Variables in the Intermediate Stage $[t_1, t_2]$

In the intermediate stage we have CRN-11 (6.12), which is a problem in a finite interval and therefore we have regular perturbation and not singular perturbation, because if ϵ=0 we don't have zeros in the denominator.

We know that f, x_r and x_s were slow variables in the fast stage, and we assume from their τ's that they are slow variables here and can be replaced with their initial values. To show this we take CRN-11 and introduce ϵ to the right-hand sides of f, x_r and x_s. We then tend ϵ to zero to see what happens to the shape of the action potential. So CRN-11 looks like this:

$$
\begin{aligned}
\frac{\mathrm{d}E}{\mathrm{d}t} &= -\frac{I_{ion}}{C_M}, \qquad (6.20)\\
I_{ion} &= I_{K1}(E) + I_{to}(E, \overline{o}_a, o_i) + I_{Kur}(E, \overline{u}_a) + I_{Kr}(E, x_r) + I_{Ks}(E, x_s)\\
&\quad + I_{Ca,L}(E, \overline{d}, f, f_{Ca}) + I_{p,Ca}(Cai) + I_{Na,K}(E) + I_{NaCa}(E, Cai)\\
&\quad + I_{b,Na}(E) + I_{b,Ca}(E, Cai),\\
\frac{\mathrm{d}y}{\mathrm{d}t} &= \frac{\overline{y} - y}{\tau_y}, \qquad y = j, o_i, f_{Ca}, u, v,\\
\frac{\mathrm{d}x}{\mathrm{d}t} &= \epsilon\frac{\overline{x} - x}{\tau_x}, \qquad y = x_r, x_s, f,\\
\frac{\mathrm{d}Cai}{\mathrm{d}t} &= \frac{B1}{B2},
\end{aligned}
$$

$$
\begin{aligned}
B1 &= (2FV_i)^{(-1)}(2I_{NaCa}(E,Cai) - I_{p,Ca}(Cai) - I_{Ca,L}(E,\overline{d},f,f_{Ca}) \\
&\quad -I_{b,Ca}(E,Cai)) + (V_i)^{(-1)}(V_{up}(0.000496 - I_{up}(Cai)) \\
&\quad +I_{rel}(Cai,Carel,u,v,\overline{w})V_{rel}), \\
B2 &= 1 + \frac{[Trpn]_{max}K_{m,Trpn}}{(Cai+K_{m,Trpn})^2} + \frac{[Cmdn]_{max}K_{m,Cmdn}}{(Cai+K_{m,Cmdn})^2}, \\
\frac{\mathrm{d}Carel}{\mathrm{d}t} &= \frac{(I_{tr}(Carel) - I_{rel}(Cai,Carel,u,v,\overline{w}))}{\left(1 + \frac{[Csqn]_{max}K_{m,Csqn}}{(Carel+K_{m,Csqn})^2}\right)}.
\end{aligned}
$$

Figure 6.31 is draw using the new initial conditions, y_1, for the intermediate stage.

$$
\begin{aligned}
y_1 &= (E, Cai, Carel, j, o_i, x_r, x_s, f, f_{Ca}, u, v) \\
&= (21.7785, 0.0001, 1.4735, 0.6892, 0.9054, 0.0107, 0.0202, 0.9959, 0.7749, \\
&\quad 0.0804, 0.6972).
\end{aligned}
$$

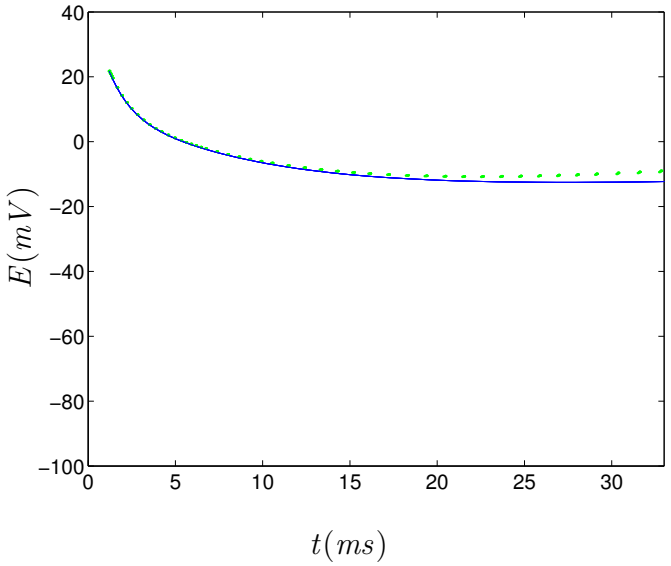

Figure 6.31: Action potential for CRN-11, system (6.20) ϵ=1, (-) and system (6.20) $\epsilon \to 0$, (.) for t=[1.2, 33].

We see from Fig. 6.31 that there is little change on the action potential, so we can replace f, x_r and x_s with their initial values and obtain a system of eight variables, CRN-8:

$$
\frac{\mathrm{d}E}{\mathrm{d}t} = -\frac{I_{ion}}{C_M}, \tag{6.21}
$$

$$
\begin{aligned}
I_{ion} &= I_{K1}(E) + I_{to}(E\overline{o}_a, o_i) + I_{Kur}(E, \overline{u}_a) + I_{Kr}(E) + I_{Ks}(E) \\
&\quad + I_{Ca,L}(E, \overline{d}, f_{Ca}) + I_{p,Ca}(Cai) + I_{Na,K}(E) + I_{NaCa}(E, Cai) \\
&\quad + I_{b,Na}(E) + I_{b,Ca}(E, Cai), \\
\frac{\mathrm{d}y}{\mathrm{d}t} &= \frac{\overline{y} - y}{\tau_y}, \qquad y = j, o_i, f_{Ca}, u, v, \\
\frac{\mathrm{d}Cai}{\mathrm{d}t} &= \frac{B1}{B2}, \\
B1 &= (2FV_i)^{(-1)}(2I_{NaCa}(E, Cai) - I_{p,Ca}(Cai) - I_{Ca,L}(E, \overline{d}, f_{Ca}) \\
&\quad - I_{b,Ca}(E, Cai)) + (V_i)^{(-1)}(V_{up}(0.000496 - I_{up}(Cai)) \\
&\quad + I_{rel}(Cai, Carel, u, v, \overline{w})V_{rel}), \\
B2 &= 1 + \frac{[Trpn]_{max}K_{m,Trpn}}{(Cai + K_{m,Trpn})^2} + \frac{[Cmdn]_{max}K_{m,Cmdn}}{(Cai + K_{m,Cmdn})^2}, \\
\frac{\mathrm{d}Carel}{\mathrm{d}t} &= \frac{(I_{tr}(Carel) - I_{rel}(Cai, Carel, u, v, \overline{w}))}{\left(1 + \frac{[Csqn]_{max}K_{m,Csqn}}{(Carel + K_{m,Csqn})^2}\right)}.
\end{aligned}
$$

Figure 6.32 shows the action potential for CRN-11 and CRN-8 to show that if we replace x_r, x_s and f with their initial values that it makes little difference to the action potential, no more than 3.6414mV.

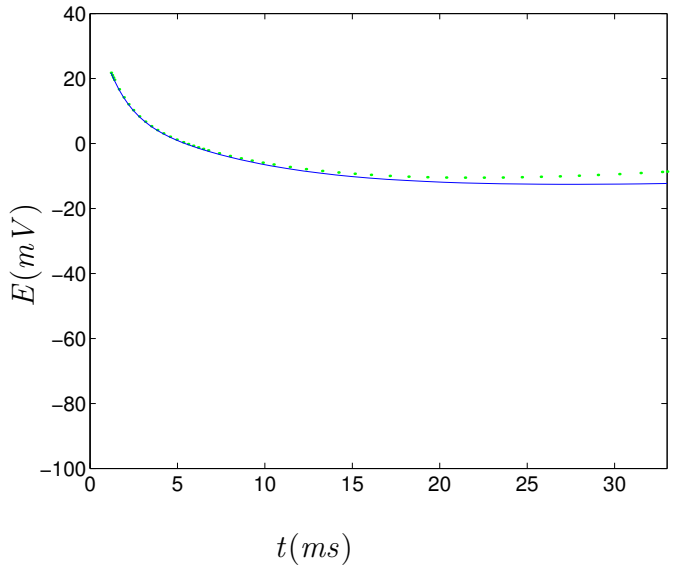

Figure 6.32: Action potential for CRN-11, system (6.20) ϵ=1, (-) and CRN-8, system (6.21), (.) for $[1.2, 33]$.

6.4.1 Neglecting dependence of I_{rel} on Cai

We see from Fig. 6.33 that $Carel$ is greater than Cai so therefore we can replace $(Carel - Cai) \approx Carel$ in I_{rel}, then I_{rel} will depend on fewer variables. So

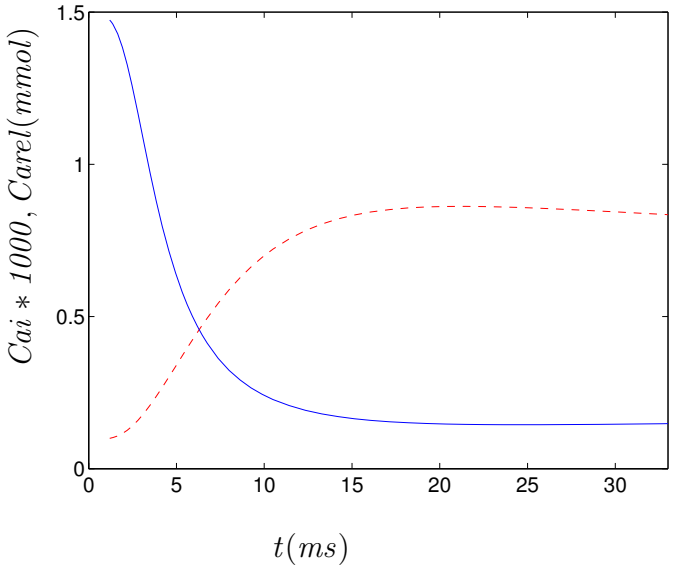

Figure 6.33: Graph of $Cai * 1000$ (- -) and $Carel$ (-) for CRN-8, system (6.21), for $[1.2, 33]$.

we draw the variables and currents that I_{rel} becomes involved with and see that with this replacement there is no difference, Fig. 6.34. We even drew the graphs for $[0, 600]$ and found that there was no change either. So we can replace $(Carel - Cai) \approx Carel$ in I_{rel}.

6.4.2 Explicit solution for u and v in the intermediate stage

We found earlier that u could be replaced with $\overline{u}$ which is either 0 or 1, and this introduced notable error, but from Fig. 6.34(d) we see that u can be written as a function of t which is a more accurate way of writing u. Also from Fig. 6.34(e) we see that we can rewrite v as a function of t, for this time scale $[1.2, 33]$. This is because we know that τ_u=8 and from looking at τ_v against t we found that the graph looked like the Heaviside function and also this is in the same limit as $\overline{u}$ if $a \to 0$, so we can treat τ_v as a Heaviside function and it can be written as follows:

$$\begin{aligned} \tau_v &= 2 + 2\theta(F_n - F_1), \\ &= 4 - 2\theta(t - t_3). \end{aligned}$$

If F_n reaches its threshold $\overline{u}$ and τ_v switch from one value to another. So τ_v

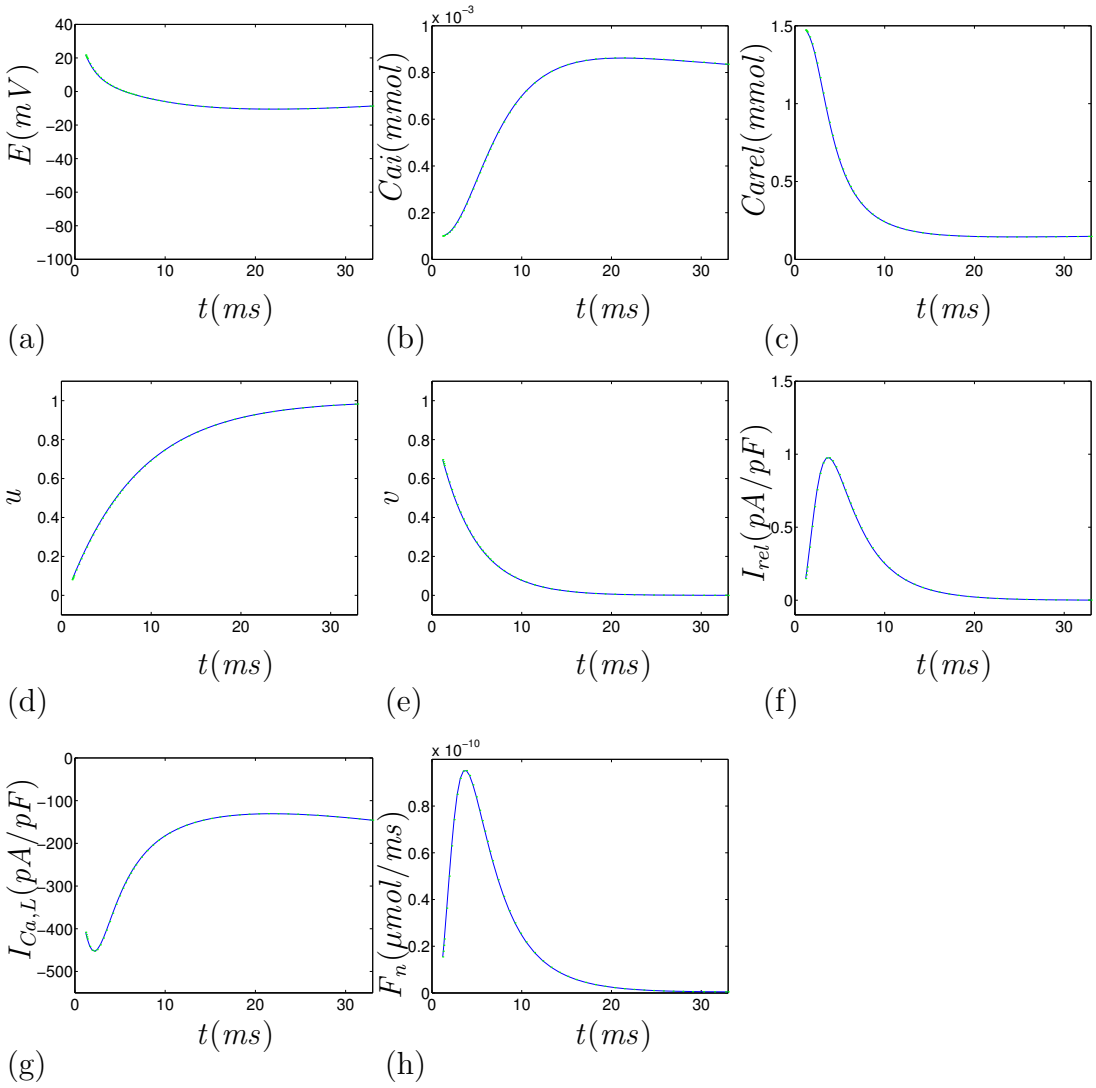

Figure 6.34: Graph of CRN-8, system (6.21), (-) and CRN-8 with $(Carel - Cai) \approx Carel$ in I_{rel} (.) for t=[1.2, 33] for the variables (a) E, (b) Cai, (c) $Carel$, (d) u, (e) v, (f) I_{rel}, (g) $I_{Ca,L}$ and (h) f_n.

remains constant for the whole of the intermediate stage.

Therefore u and v can be rewritten as functions of time:

$$u(t) = 1 - e^{-t/\tau_u}, \qquad v(t) = e^{-t/\tau_v}.$$

So we finally have a system of six equations, CRN-6:

$$\begin{aligned}
\frac{\mathrm{d}E}{\mathrm{d}t} &= -\frac{I_{ion}}{C_M}, \\
I_{ion} &= I_{K1}(E) + I_{to}(E, \overline{o}_a, o_i) + I_{Kur}(E, \overline{u}_a) + I_{Kr}(E) + I_{Ks}(E) \\
&\quad + I_{Ca,L}(E, \overline{d}, f_{Ca}) + I_{p,Ca}(Cai) + I_{Na,K}(E) + I_{NaCa}(E, Cai) \\
&\quad + I_{b,Na}(E) + I_{b,Ca}(E, Cai), \\
\frac{\mathrm{d}j}{\mathrm{d}t} &= \frac{\overline{j}(E) - o_i}{\tau_j(E)}, \\
\frac{\mathrm{d}o_i}{\mathrm{d}t} &= \frac{\overline{o}_i(E) - o_i}{\tau_{o_i}(E)}, \\
\frac{\mathrm{d}f_{Ca}}{\mathrm{d}t} &= \frac{\overline{f}_{Ca}(Cai) - f_{Ca}}{\tau_{f_{Ca}}}, \\
\frac{\mathrm{d}Cai}{\mathrm{d}t} &= \frac{B1}{B2}, \\
B1 &= (2FV_i)^{(-1)}(2I_{NaCa}(E, Cai) - I_{p,Ca}(Cai) - I_{Ca,L}(E, \overline{d}, f_{Ca}) \\
&\quad - I_{b,Ca}(E, Cai)) + (V_i)^{(-1)}(V_{up}(0.000496 - I_{up}(Cai)) \\
&\quad + I_{rel}(Carel, u(t), v(t), \overline{w}(E))V_{rel}), \\
B2 &= 1 + \frac{[Trpn]_{max}K_{m,Trpn}}{(Cai + K_{m,Trpn})^2} + \frac{[Cmdn]_{max}K_{m,Cmdn}}{(Cai + K_{m,Cmdn})^2}, \\
\frac{\mathrm{d}Carel}{\mathrm{d}t} &= \frac{(I_{tr}(Carel) - I_{rel}(Carel, u(t), v(t), \overline{w}(E)))}{\left(1 + \frac{[Csqn]_{max}K_{m,Csqn}}{(Carel + K_{m,Csqn})^2}\right)}.
\end{aligned} \tag{6.22}$$

We have a sixth-order system (6.22) and we draw the graphs of CRN-8 and CRN-6 for E, Cai, $Carel$, j, o_i and f_{Ca} once I_{Na} is over. So we have new initial conditions y_1 to see if there is any difference between the two systems. Figure 6.35 shows that there is no change in E, j and o_i and there is little change in $Carel$ and f_{Ca}, and Cai is higher.

6.4.3 Neglecting the minor currents

We want to be able to eliminate the currents that are small compared to I_{to} and $I_{Ca,L}$. We found that we could eliminate I_{K_1}, I_{Kr}, I_{Ks}, $I_{Na,Ca}$, and I_{tr} and replace the other currents with constant values, $I_{Na,K}$=22.4544, $I_{p,Ca}$=17.7916,

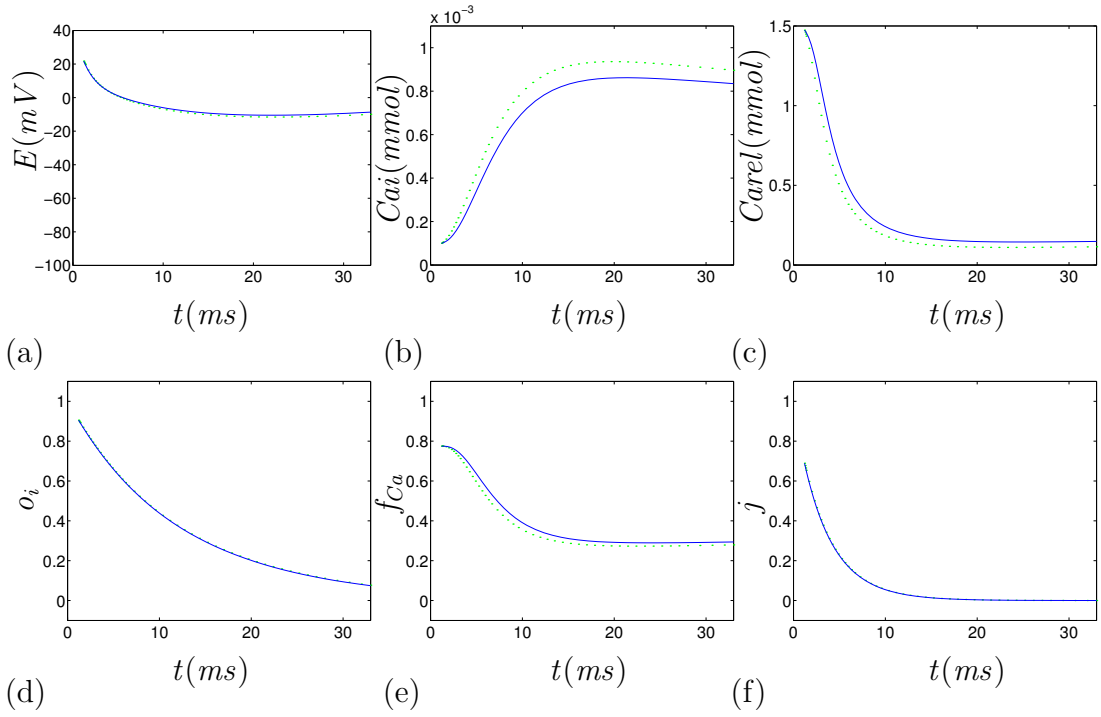

Figure 6.35: Graphs of CRN-8, system (6.21), (-) and CRN-6, system (6.22), (.) for t=[1.2, 33] and (a) E, (b) Cai, (c) $Carel$, (d) o_i, (e) f_{Ca} and (f) j.

$I_{b,Na}$=−5.3323, $I_{b,Ca}$=−12.7536 and I_{up}=$3.2 * 10^{-3}$. These values were found empirically to give us an accurate approximation.

So the system looks like this now:

$$
\begin{aligned}
\frac{\mathrm{d}E}{\mathrm{d}t} &= -\frac{(I_{to}(E,\overline{o}_a(E),o_i)+I_{Kur}(E,\overline{u}_a(E))+A)}{C_M} \\
&\quad +\frac{I_{Ca,L}(E,\overline{d}(E),f_{Ca}(Cai))}{C_M}, \\
\frac{\mathrm{d}j}{\mathrm{d}t} &= \frac{\overline{j}(E)-j}{\tau_j(E)}, \\
\frac{\mathrm{d}o_i}{\mathrm{d}t} &= \frac{\overline{o}_i(E)-o_i}{\tau_{o_i}(E)}, \\
\frac{\mathrm{d}f_{Ca}}{\mathrm{d}t} &= \frac{\overline{f}_{Ca}(Cai)-f_{Ca}}{\tau_{f_{Ca}}}, \\
\frac{\mathrm{d}Cai}{\mathrm{d}t} &= \frac{B1}{B2}, \\
B1 &= (2FV_i)^{(-1)}(B-I_{Ca,L}(E,\overline{d}(E),f_{Ca}(Cai)))+(V_i)^{(-1)}(V_{up}C \\
&\quad +I_{rel}(Carel,u,v,\overline{w}(E))V_{rel}), \\
B2 &= 1+\frac{[Trpn]_{max}K_{m,Trpn}}{(Cai+K_{m,Trpn})^2}+\frac{[Cmdn]_{max}K_{m,Cmdn}}{(Cai+K_{m,Cmdn})^2},
\end{aligned}
\tag{6.23}
$$

$$\frac{\mathrm{d}Carel}{\mathrm{d}t} = \frac{-I_{rel}(Carel,u,v,\overline{w}(E))}{\left(1+\frac{[Csqn]_{max}K_{m,Csqn}}{(Carel+K_{m,Csqn})^2}\right)},$$

where A=22.1601, B=−5.0380 and C=−0.0027.

Figure 6.36 shows that these changes don't make much difference to the system, it only brings Cai closer to its CRN-8 solution. So by eliminating these currents we make the number of currents in I_{ion} less.

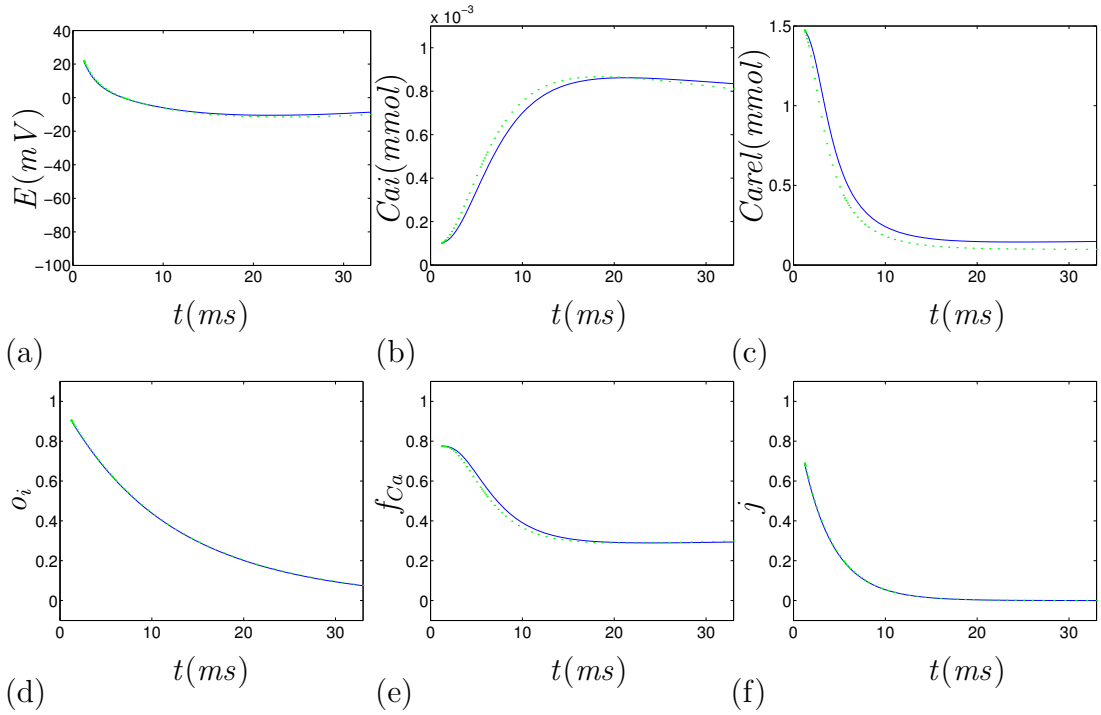

Figure 6.36: Graphs of CRN-8, system (6.21), (-) and CRN-6, system (6.23), (.) for t=[1.2, 33] and (a) E, (b) Cai, (c) $Carel$, (d) o_i, (e) f_{Ca} and (f) j.

6.4.4 Iterations for constant E=E_0

Now that we have eliminated the minor currents we want to see if we can replace E with a constant, E_0, that will make no difference to j, o_i, f_{Ca}, Cai and $Carel$ in system (6.23). We can only do this for the scale [4.1, 33] where we can cut off the beginning of the action potential, see Fig. 6.35(a). So we chose the value of E_0 at t=33 and this is E_0=−10.8425. So the new system is:

$$\begin{aligned} E_0 &= -10.8425, \\ \frac{\mathrm{d}j}{\mathrm{d}t} &= \frac{\overline{j}(E_0)-j}{\tau_j(E_0)}, \end{aligned} \tag{6.24}$$

$$
\begin{aligned}
\frac{\mathrm{d}o_i}{\mathrm{d}t} &= \frac{\overline{o}_i(E_0) - o_i}{\tau_{o_i}(E_0)}, \\
\frac{\mathrm{d}f_{Ca}}{\mathrm{d}t} &= \frac{\overline{f}_{Ca}(Cai) - f_{Ca}}{\tau_{f_{Ca}}}, \\
\frac{\mathrm{d}Cai}{\mathrm{d}t} &= \frac{B_1}{B_2}, \\
B_1 &= (2FV_i)^{(-1)}(B - I_{Ca,L}(f_{Ca})) + (V_i)^{(-1)}(V_{up}C + I_{rel}(Carel, u, v)V_{rel}), \\
B_2 &= 1 + \frac{[Trpn]_{max}K_{m,Trpn}}{(Cai + K_{m,Trpn})^2} + \frac{[Cmdn]_{max}K_{m,Cmdn}}{(Cai + K_{m,Cmdn})^2}, \\
\frac{\mathrm{d}Carel}{\mathrm{d}t} &= \frac{-I_{rel}(Carel, u, v)}{\left(1 + \frac{[Csqn]_{max}K_{m,Csqn}}{(Carel + K_{m,Csqn})^2}\right)},
\end{aligned}
$$

where B=−5.0380, C=−0.0027 and $\overline{w}$=0.9522.

As we can see from this system we can replace $\dot{o}_i$ and $\dot{j}$ with an exponential function using the initial conditions for t, j and o_i to give us a system of three equations (f_{Ca}, Cai, $Carel$).

$$
\begin{aligned}
j_0 &= \overline{j}(E_0) + (j(t_0) - \overline{j}(E_0))e^{-(t-t_0)/\tau_j(E_0)}, \\
o_{i_0} &= \overline{o}_i(E_0) + (o_i(t_0) - \overline{o}_i(E_0))e^{-(t-t_0)/\tau_{o_i}(E_0)}.
\end{aligned}
$$

We draw system (6.24) using the initial conditions y_2 taken at t=4.2703. In Fig. 6.37 we draw each equation against the equations in system (6.23) to see if there is any difference. There was no difference in the graphs, so we can consider E as a slow variable for t=[4.2703, 33]. The initial conditions at t=4.2703 are:

$$
\begin{aligned}
y_2 &= (E, Cai, Carel, j, o_i, f_{Ca}), \\
&= (3.1006, 0.0003, 0.6157, 0.2785, 0.7001, 0.6473).
\end{aligned}
$$

We now draw the action potential of system (6.25) with E_0=−10.8425 and the solutions from system (6.24), Fig. 6.37, for E_1, to see if it makes any difference to the action potential, if it doesn't then we can say that E is a constant for the time period [4.2703, 33]. We see from Fig. 6.38 that there isn't much change here so therefore the assumption that we made is correct.

$$
\begin{aligned}
j_0 &= \overline{j}(E_0) + (j(t_0) - \overline{j}(E_0))e^{-(t-t_0)/\tau_j(E_0)}, \\
o_{i_0} &= \overline{o}_i(E_0) + (o_i(t_0) - \overline{o}_i(E_0))e^{-(t-t_0)/\tau_{o_i}(E_0)},
\end{aligned}
\tag{6.25}
$$

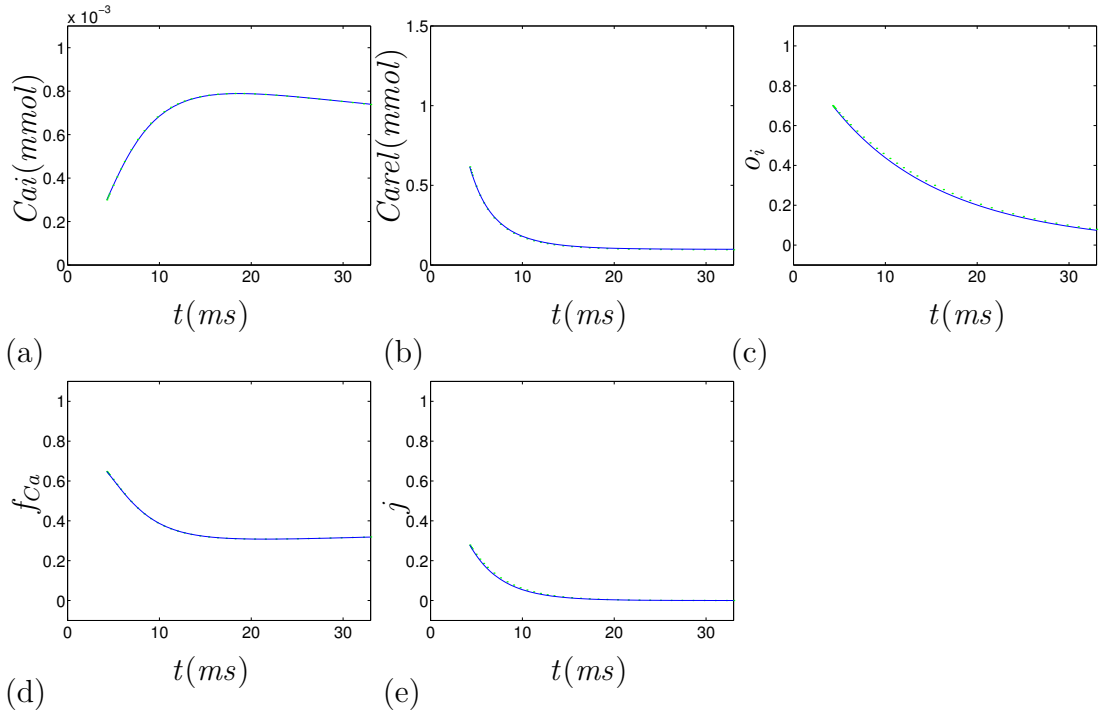

Figure 6.37: Graphs of CRN-6, system (6.23), (-) and CRN-5, system (6.24), (.) for t=[4.2703, 33] and (a) Cai, (b) $Carel$, (c) o_i (d) f_{Ca} and (e) j.

$$
\begin{aligned}
f_{Ca_0} &= \overline{f}_{Ca}(Cai_0) + (f_{Ca}(t_0) - \overline{f}_{Ca}(Cai_0))e^{-(t-t_0)/\tau_{f_{Ca}}}, \\
\frac{\mathrm{d}Cai_0}{\mathrm{d}t} &= \frac{B_1}{B_2}, \\
B_1 &= (2FV_i)^{(-1)}(B - I_{Ca,L}(f_{Ca_0})) + (V_i)^{(-1)}(V_{up}C + I_{rel}(Carel_0, u, v)V_{rel}), \\
B_2 &= 1 + \frac{[Trpn]_{max}K_{m,Trpn}}{(Cai_0 + K_{m,Trpn})^2} + \frac{[Cmdn]_{max}K_{m,Cmdn}}{(Cai_0 + K_{m,Cmdn})^2}, \\
\frac{\mathrm{d}Carel_0}{\mathrm{d}t} &= \frac{-I_{rel}(Carel_0, u, v)}{\left(1 + \frac{[Csqn]_{max}K_{m,Csqn}}{(Carel_0 + K_{m,Csqn})^2}\right)}, \\
\frac{\mathrm{d}E_1}{\mathrm{d}t} &= -\frac{I_{to}(E_1, \overline{o}_a(E_1), o_{i_0}) + I_{Kur}(E_1, \overline{u}_a(E_1)) + I_{Ca,L}(E_1, \overline{d}(E_1), f_{Ca_0}) + A}{C_M},
\end{aligned}
$$

where B=−5.0380, C=−0.0027 and $\overline{w}$=0.9522.

From Fig. 6.38 we see that the action potential goes to a straight line, so maybe it could be going to an equilibrium point. To find this out we draw the graphs of the variables and currents in system (6.23) to check this.

What we see in Fig. 6.39 is that there is no equilibrium point, but a local minimum, so therefore our conjecture that there is an equilibrium point is incorrect.

Now we know we can recreate the action potential by making the voltage a constant between t=[4.2703, 33]. Lets see if we can use the same method again, but this time without knowing the value of E_0 at t=33. We know the value of

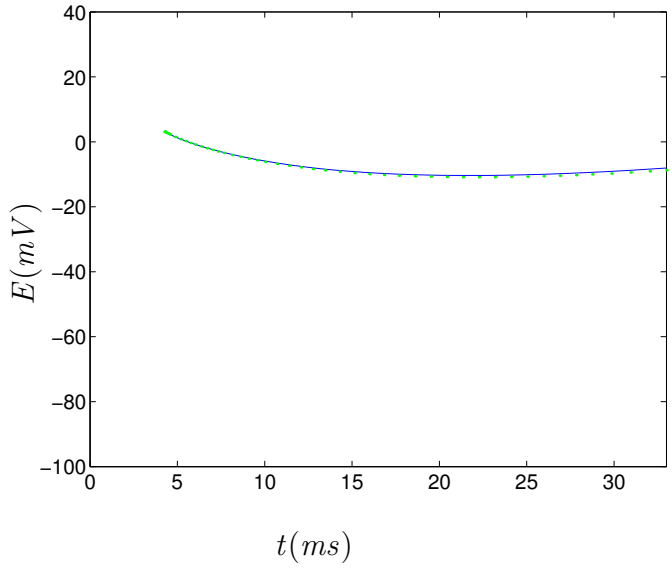

Figure 6.38: Action potential of CRN-6, E, system (6.23), (-) and CRN-6, E_1, system (6.25), (.) with solutions for Cai_0, $Carel_0$, j_0, o_{i_0} and f_{Ca_0} for t=[4.2703, 33] and E_0=−10.8425.

E_0 at t=1.2 is 21.778. So we use the initial conditions y_1 and E_0=21.7785, then we draw the six variables, system (6.25), for t=[1.2, 33] against its equation in system (6.23). We see from Fig. 6.40 that there is either no difference or little difference between the graphs.

We see that the Cai_0 graph, Fig. 6.40(b), drops below the CRN-6 Cai graph. So it was decided to see if we can obtain a better approximation for Cai by adding to the iterations an extra equation of Cai_1, system (6.26), and drawing Cai_1 against CRN-6's Cai and see if it is more accurate. The iterations become:

$$
\begin{aligned}
E_0 &= 21.7785, \qquad (6.26)\\
j_0 &= \overline{j}(E_0) + (j(t_1) - \overline{j}(E_0))e^{-(t-t_1)/\tau_j(E_0)},\\
o_{i_0} &= \overline{o}_i(E_0) + (o_i(t_1) - \overline{o}_i(E_0))e^{-(t-t_1)/\tau_{o_i}(E_0)},\\
f_{Ca_0} &= \overline{f}_{Ca}(Cai_0) + (f_{Ca}(t_1) - \overline{f}_{Ca}(Cai_0))e^{-(t-t_1)/\tau_{f_{Ca}}},\\
\frac{\mathrm{d}Cai_0}{\mathrm{d}t} &= \frac{B_1}{B_2},\\
B_1 &= (2FV_i)^{(-1)}(B - I_{Ca,L}(f_{Ca_0})) + (V_i)^{(-1)}(V_{up}C + I_{rel}(Carel_0, u, v)V_{rel}),\\
B_2 &= 1 + \frac{[Trpn]_{max}K_{m,Trpn}}{(Cai_0 + K_{m,Trpn})^2} + \frac{[Cmdn]_{max}K_{m,Cmdn}}{(Cai_0 + K_{m,Cmdn})^2},\\
\frac{\mathrm{d}Carel_0}{\mathrm{d}t} &= \frac{-I_{rel}(Carel_0, u, v)}{\left(1 + \frac{[Csqn]_{max}K_{m,Csqn}}{(Carel_0 + K_{m,Csqn})^2}\right)},
\end{aligned}
$$

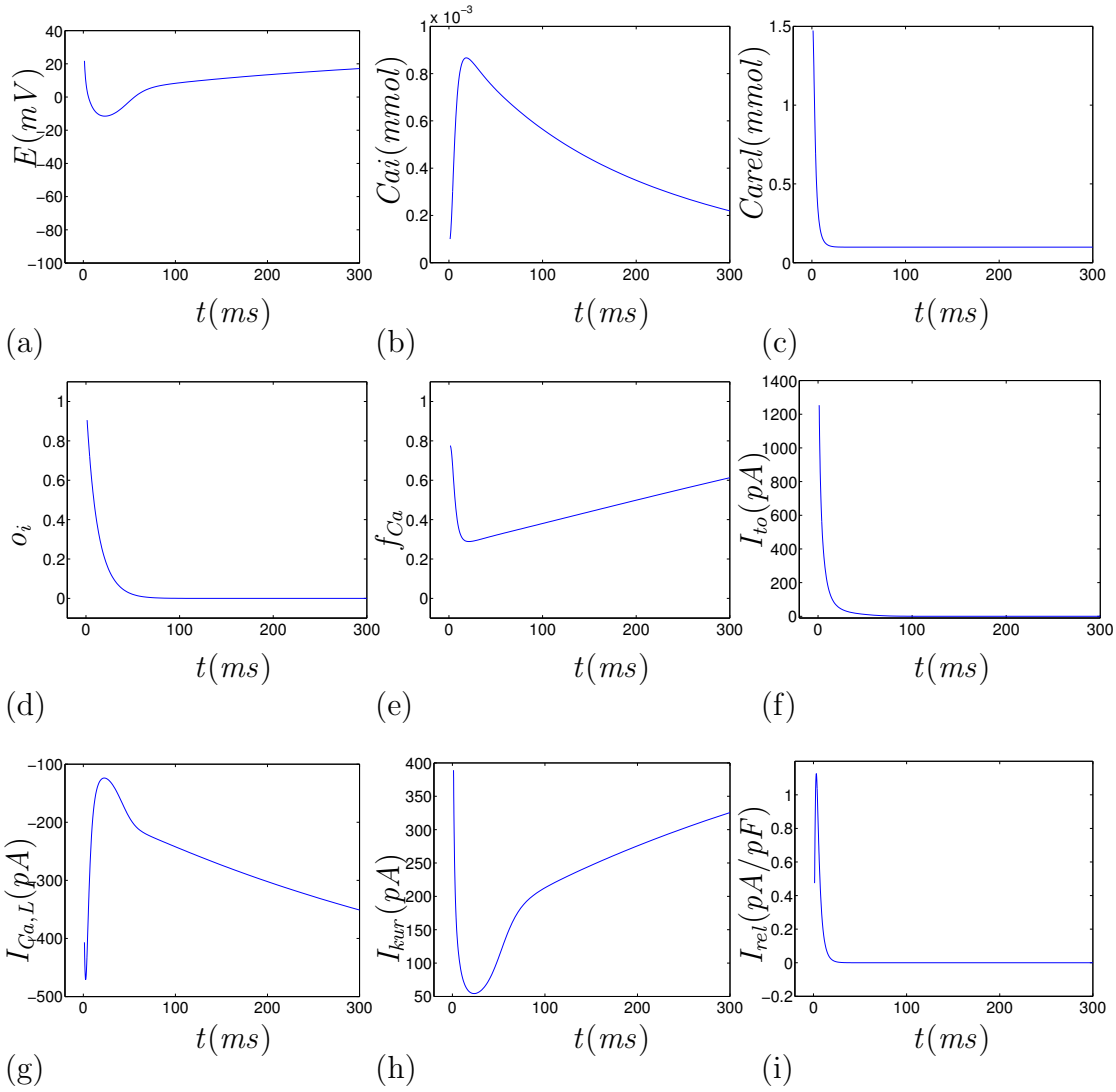

Figure 6.39: Graphs of CRN-6, system (6.23), (-) for t=[1.2, 300] and (a) E, (b) Cai, (c) $Carel$, (d) o_i (e) f_{Ca}, (f) I_{to}, (g) $I_{Ca,L}$, (h) I_{kur} and (i) I_{rel}.

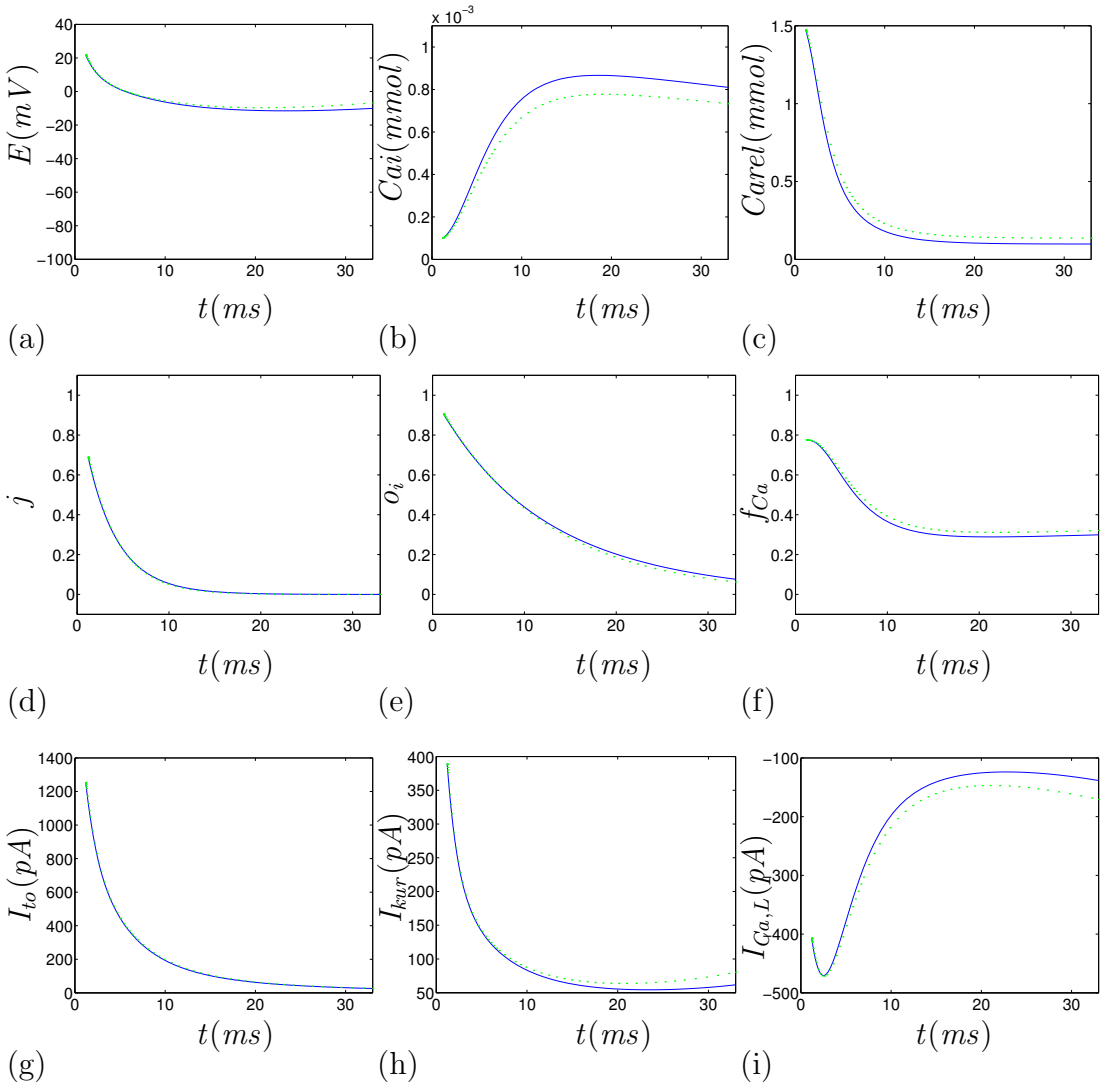

Figure 6.40: Graphs of CRN-6, system (6.23), (-) and CRN-6, system (6.25), (.) for t=[1.2, 33] and E_0=21.7785 for (a) E_1 with solutions for Cai_0, $Carel_0$, j_0, o_{i_0} and f_{Ca_0}, (b) Cai_0, (c) $Carel_0$, (d) j_0 (e) o_{i_0}, (f) f_{Ca_0}, (g) I_{to}, (h) I_{kur} and (i) $I_{Ca,L}$.

$$
\begin{aligned}
\frac{\mathrm{d}E_1}{\mathrm{d}t} &= -\frac{I_{to}(E_1,\overline{o}_a(E_1),o_{i_0})+I_{Kur}(E_1,\overline{u}_a(E_1))+I_{Ca,L}(E_1,\overline{d}(E_1),f_{Ca_0})+A}{C_M},\\
\frac{\mathrm{d}Cai_1}{\mathrm{d}t} &= \frac{B_{11}}{B_{21}},\\
B_{11} &= (2FV_i)^{(-1)}(B-I_{Ca,L}(f_{Ca_0}))+(V_i)^{(-1)}(V_{up}C+I_{rel}(Carel_0,u,v)V_{rel}),\\
B_{21} &= 1+\frac{[Trpn]_{max}K_{m,Trpn}}{(Cai_1+K_{m,Trpn})^2}+\frac{[Cmdn]_{max}K_{m,Cmdn}}{(Cai_1+K_{m,Cmdn})^2},
\end{aligned}
$$

where B=−5.0380, C=−0.0027 and $\overline{w}$=0.9522.

We see from Fig. 6.41(a) that Cai_1 is higher than before, compared to Fig. 6.40(b). So we also add $Carel_1$ to Cai_1, system (6.27), as $\frac{\mathrm{d}Cai_1}{\mathrm{d}t}$ is a function of $Carel_1$. Therefore we have reduced CRN-6 to a system of one equation CRN-1, because we can solve all the equations in quadratures except E_1 because E_1 is too complicated to solve and approximations cannot reproduce the accuracy of the differential equation. If we find a numerical solution for E_1 though, then we can solve all the other equations in quadratures.

$$
\begin{aligned}
E_0 &= 21.7785, \qquad (6.27)\\
j_0 &= \overline{j}(E_0)+(j(t_1)-\overline{j}(E_0))e^{-(t-t_1)/\tau_j(E_0)},\\
o_{i_0} &= \overline{o}_i(E_0)+(o_i(t_1)-\overline{o}_i(E_0))e^{-(t-t_1)/\tau_{o_i}(E_0)},\\
f_{Ca_0} &= \overline{f}_{Ca}(Cai_0)+(f_{Ca}(t_1)-\overline{f}_{Ca}(Cai_0))e^{-(t-t_1)/\tau_{f_{Ca}}},\\
&\int_{Cai(t_1)}^{Cai_0}B_2(Cai_0)\mathrm{d}Cai_0=\int_{t_1}^{t}B_1(t)\mathrm{d}t,\\
B_1 &= (2FV_i)^{(-1)}(B-I_{Ca,L}(f_{Ca_0}(t)))+(V_i)^{(-1)}(V_{up}C\\
&+I_{rel}(Carel_0(t),u(t),v(t))V_{rel}),\\
B_2 &= 1+\frac{[Trpn]_{max}K_{m,Trpn}}{(Cai_0+K_{m,Trpn})^2}+\frac{[Cmdn]_{max}K_{m,Cmdn}}{(Cai_0+K_{m,Cmdn})^2},\\
&\int_{Carel(t_1)}^{Carel_0}\frac{\left(1+\frac{A}{(Carel_0+B)^2}\right)}{Carel_0}\mathrm{d}Carel_0=-K_{rel}\overline{w}(E_0)\int_{t_1}^{t}u^2(t)v(t)\mathrm{d}t,\\
\frac{\mathrm{d}E_1}{\mathrm{d}t} &= -\frac{I_{to}(E_1,\overline{o}_a(E_1),o_{i_0})+I_{Kur}(E_1,\overline{u}_a(E_1))+I_{Ca,L}(E_1,\overline{d}(E_1),f_{Ca_0})+A}{C_M},\\
&\int_{Cai(t_1)}^{Cai_1}B_{12}(Cai_1)\mathrm{d}Cai_1=\int_{t_1}^{t}B_{11}(t)\mathrm{d}t,\\
B_{11} &= (2FV_i)^{(-1)}(B-I_{Ca,L}(f_{Ca_0}))+(V_i)^{(-1)}(V_{up}C\\
&+I_{rel}(Carel_1,u(t),v(t))V_{rel}),\\
B_{21} &= 1+\frac{[Trpn]_{max}K_{m,Trpn}}{(Cai_1+K_{m,Trpn})^2}+\frac{[Cmdn]_{max}K_{m,Cmdn}}{(Cai_1+K_{m,Cmdn})^2},\\
&\int_{Carel(t_1)}^{Carel_1}\frac{\left(1+\frac{A}{(Carel_1+B)^2}\right)}{Carel_1}\mathrm{d}Carel_1=-K_{rel}\overline{w}(E_1)\int_{t_1}^{t}u^2(t)v(t)\mathrm{d}t,
\end{aligned}
$$

where B=−5.0380, C=−0.0027 and $\overline{w}$=0.9522.

We see from Fig. 6.41(b) that now we have no difference between CRN-6's Cai and Cai_1.

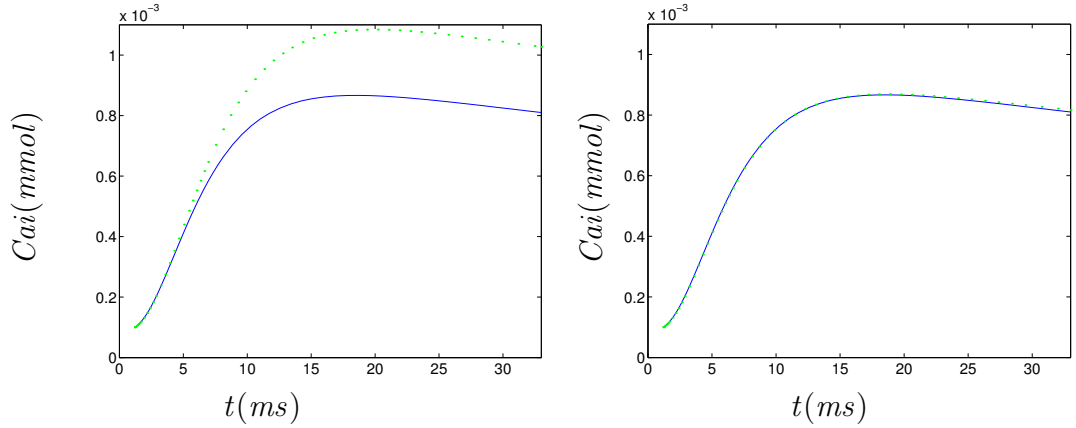

(a) (b)

Figure 6.41: Graphs of CRN-6, system (6.23), (-) for t=[1.2, 33] for E_0=21.7785 for (a) Cai_1, system (6.26), with E_1, (.) and (b) Cai_1, system (6.27), with E_1 and $Carel_1$ (.).

Therefore we can summarize that from drawing system (6.25), with putting j_0, o_{i_0}, f_{Ca_0}, Cai_0 and $Carel_0$ in E_1, we see that Cai drops below CRN-6's Cai, Fig. 6.40, and this stems from using the initial value E_0=21.7785. We see that by using E_0=−10.8425 we have no change in the graphs of Cai, so this is to do with using a different value for E_0. Therefore we see that by drawing Cai_1, system (6.26), instead of Cai_0, system (6.25), against CRN-6's Cai, system (6.23), then Cai_1 is above CRN-6's Cai, Fig. 6.41(a). We also know that $\frac{\mathrm{d}Cai}{\mathrm{d}t}$ is a function of $Carel$ and therefore if we replace $Carel$ with $Carel_1$ in $\frac{\mathrm{d}Cai_1}{\mathrm{d}t}$, system (6.27), and draw Cai_1 against CRN-6's Cai, system (6.23), then we see that there is no difference between them, Fig. 6.41(b).

6.4.5 Dynamics of $Carel$

We take system (6.24) where E_0=21.7785 not −10.8425 as we are taking E_0 at t=1.2, and we see that $\frac{\mathrm{d}Carel}{\mathrm{d}t}$ is a function of t and $Carel$ only, so we want to find an explicit solution for $Carel$. Therefore we integrate $\frac{\mathrm{d}Carel}{\mathrm{d}t}$:

$$\frac{\mathrm{d}Carel}{\mathrm{d}t} = -\frac{I_{rel}(Carel, u, v, \overline{w}(E_0))}{\left(1 + \frac{[Csqn]_{max} K_{m,Csqn}}{(Carel + K_{m,Csqn})^2}\right)}, \quad (6.28)$$

$$\frac{\mathrm{d}Carel}{\mathrm{d}t} = -\frac{K_{rel}u^2v\overline{w}(E_0)Carel}{\left(1+\frac{A}{(Carel+B)^2}\right)},$$

$$\int_{Carel_0}^{Carel}\frac{\left(1+\frac{A}{(Carel+B)^2}\right)}{Carel}\mathrm{d}Carel = -K_{rel}\overline{w}(E_0)\int_{t_0}^{t}u^2v\mathrm{d}t,$$

where A=$[Csqn]_{max}K_{m,Csqn}$ and B=$K_{m,Csqn}$.

Say γ_u=$1/\tau_u$, γ_v=$1/\tau_v$ and the initial conditions are $(t_0, Carel_0)$, then we use partial fractions to find the solution.

Say p=$e^{-t\gamma_v}$, r=$e^{-t\gamma_u}$, q=$e^{-t_0\gamma_v}$ and s=$e^{-t_0\gamma_u}$.

So,

$$\ln\left(\frac{(Carel)^{\frac{(B^2+A)}{B^2}}}{(Carel+B)^{\frac{A}{B^2}}}\right)+\frac{A}{B(Carel+B)} = K_{rel}\overline{w}(E_0)\left(\frac{p-q}{\gamma_v}+\frac{2(qs-rp)}{\gamma_u+\gamma_v}+\frac{pr^2-qs^2}{2\gamma_u+\gamma_v}\right) +D,$$

where D=$\ln\left(\frac{(Carel_0)^{\frac{(B^2+A)}{B^2}}}{(Carel_0+B)^{\frac{A}{B^2}}}\right)+\frac{A}{B(Carel_0+B)}$, which is a constant.

To obtain an explicit solution for $Carel(t)$, which is not possible by rearranging the above equation, we have to use iterations.

Say, G=$K_{rel}\overline{w}(E_0)\left(\frac{p-q}{\gamma_v}+\frac{2(qs-rp)}{\gamma_u+\gamma_v}+\frac{pr^2-qs^2}{2\gamma_u+\gamma_v}\right)+D$, so

$$\ln\left(\frac{(Carel)^{\frac{(B^2+A)}{B^2}}}{(Carel+B)^{\frac{A}{B^2}}}\right)+\frac{A}{B(Carel+B)} = G,$$

$$\ln(Carel^{(B^2+A)/B^2})-\ln(Carel+B)^{A/B^2}+\frac{A}{B(Carel+B)} = G,$$

$$\ln(Carel) = \frac{B^2}{(B^2+A)}\left(G+\frac{A}{B^2}\ln(Carel+B)-\frac{A}{B(Carel+B)}\right),$$

$$Carel_{n+1} = (Carel_n+B)^{A/(B^2+A)}e^{\frac{B^2G-AB/(Carel_n+B)}{(B^2+A)}}.$$

To check this we use the initial value of $Carel$ at t=0, which is $Carel_0$=1.488, and we put it in the recurrence relation. Figure 6.42 shows that we need seven iterations to obtain an accurate solution close to the original solution for $Carel$ from system (6.24).

6.4.6 Finding a simpler approximation for $Carel$

We have found an approximation for $Carel$ using iterations, but the equation we obtained only gives one approximation for $Carel$, so we want to see if we can

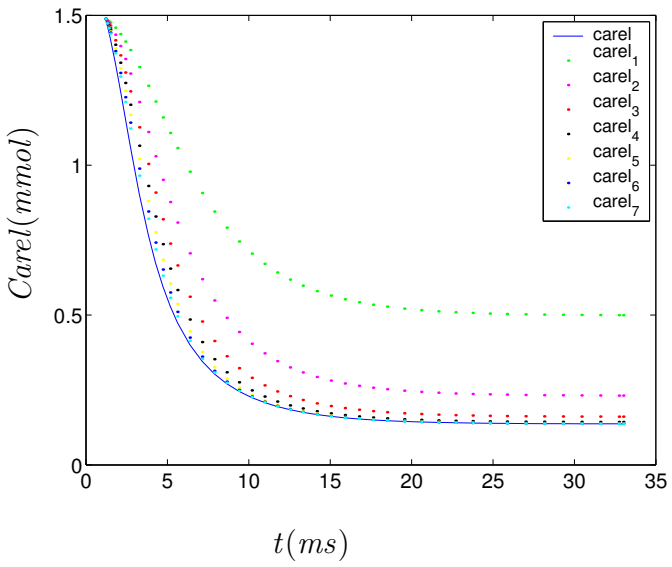

Figure 6.42: Graph of iterations for $Carel$ (6.24) for the initial point $Carel_0$=1.488.

find a simpler approximation, that approximates the solution of the integral as a function of G.

So we have the following equation for $Carel$:

$$G(Carel) = K_{rel}\overline{w}(E_0)\left(\frac{p-q}{\gamma_v} + \frac{2(qs-rp)}{\gamma_u+\gamma_v} + \frac{pr^2-qs^2}{2\gamma_u+\gamma_v}\right) + D, \qquad (6.29)$$

where $G(Carel)$ is defined as:

$$G(Carel) = \ln\left(\frac{(Carel)^{\frac{(B^2+A)}{B^2}}}{(Carel+B)^{\frac{A}{B^2}}}\right) + \frac{A}{B(Carel+B)}.$$

Figure 6.43 shows the graphs of G against $Carel$ and the inverse of this for equation (6.29), so we can determine which approximation we can use.

We have two approximations for this equation, $Carel$=ae^{bG} and $Carel = c(-G)^{-d}$. So we evaluate these two approximations to see which one is the best for our function. We also found two different values for a, b, c and d as well, where one set of values joins the two endpoints together and the other set of values are the ones obtained through a computer approximation using the Marquardt-Levenberg procedure for best fit.

The approximations using the endpoints are:

$$\begin{aligned} Carel &= 1.6323e^{0.1613G}, \\ Carel &= 1.0499(-G)^{-0.7460}, \end{aligned}$$

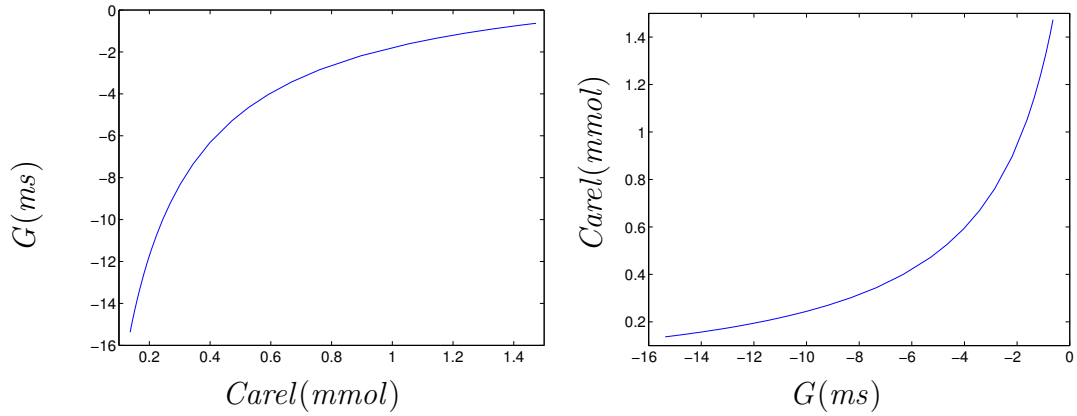

(a) (b)

Figure 6.43: Graphs of (a) G against $Carel$ and (b) $Carel$ against G for equation (6.29).

and the approximations using the Marquardt-Levenberg procedure are:

$$\begin{aligned} Carel &= 1.53814e^{0.192407G}, \\ Carel &= 1.20435(-G)^{-0.652733}. \end{aligned}$$

We draw the graphs of $Carel$ against G for all approximations and compare them with the original graph of $Carel(G)$. Figure 6.44(a) shows the approximations for $Carel{=}ae^{bG}$, Fig. 6.44(b) shows the approximations for $Carel{=}c(-G)^{-d}$; Fig. 6.44(c) shows the computer approximations, using the Marquardt-Levenberg procedure, against $Carel(G)$; this shows us that the two approximations swap at the middle points of the graph and one is above the original curve and one is below the original curve. Figure 6.44(d) shows the approximations using the endpoints against $Carel(G)$ and this shows that one curve is above and one curve is below the original curve. From this analysis we could take either of the endpoint approximations, as these are more accurate than the computer approximations using the Marquardt-Levenberg procedure, as they do incorporate the beginning and endpoints of the curve. The approximation where $Carel{=}1.6323e^{0.1613G}$ looks the best as it is closer to the original curve.

6.4.7 Summary

The end value of the time period, for the intermediate stage, is found where $\overline{u}$ and τ_v switch their values. We checked that $\overline{u}$ can be replaced with the Heaviside

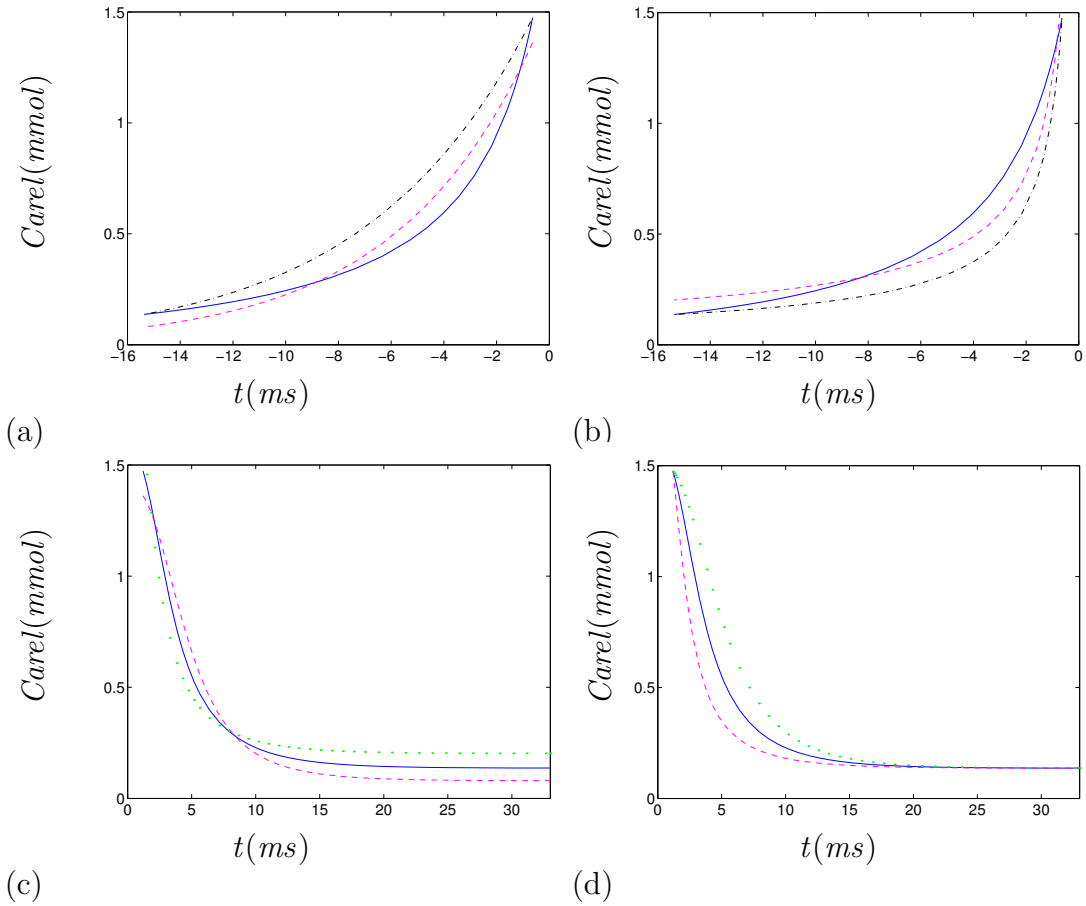

Figure 6.44: Graph of equation (6.29) drawn for (a) $Carel$ against G (-) with the approximations $Carel$=1.6323$e^{0.1613G}$ (-.) and $Carel$=1.53814$e^{0.192407G}$ (- -), (b) $Carel$ against G with the approximations $Carel$=1.0499$(-G)^{-0.7460}$ (-.) and $Carel$=1.20435$(-G)^{-0.652733}$ (- -), (c) $Carel$ against t with the computer approximations $Carel$=1.53814$e^{0.192407G}$ (- -) and $Carel$=1.20435$(-G)^{-0.652733}$ (.) and (d) $Carel$ against t with the endpoint approximations $Carel$=1.6323$e^{0.1613G}$ (.) and $Carel$=1.0499$(-G)^{-0.7460}$ (- -).

function and found that this is a good approximation for $E(T)$.

We found that we can eliminate the minor currents from CRN-6, so that the equation for $Carel$ only contains $Carel$ and t, therefore it is a separable equation and can be solved in quadratures. Then we used the method of iterations to find an analytical equation for $Carel$. We found that the method of iterations worked well and gave us an equation for $Carel$, but if we wanted to put that equation in $\frac{\mathrm{d}Cai}{\mathrm{d}t}$, to integrate with respect to Cai, to find an equation for Cai, then the equation for $Carel$ is complicated to integrate. So we wanted to find a simpler equation for $Carel$, that is why we tried different approximations for $Carel$. From these approximations we found that there wasn't a good approximation for $Carel$.

We also found that we could obtain analytical solutions for j_0, f_{Ca_0}, o_{i_0}, Cai_0, $Carel_0$, E_1, Cai_1 and $Carel_1$, if we replaced E=E_0, even though some of the solutions are in the form of quadratures.

Before we did any iterations we had obtained an accurate system. So the accurate system for the intermediate stage is a system of six equations $(5+1)$, because j is a separate equation that splits away from the other five equations. We compare this with the fast stage and see that we have a system of four equations $(2+2)$, where o_a and d split away.

6.5 The Slow Stage $[t_2, \infty]$

The system is CRN-11 (6.20) which is valid both in the intermediate and slow stage:

$$
\begin{aligned}
\frac{\mathrm{d}E}{\mathrm{d}t} &= -\frac{I_{ion}}{C_M}, \qquad (6.30)\\
I_{ion} &= I_{K1}(E) + I_{to}(E,\overline{o}_a,o_i) + I_{Kur}(E,\overline{u}_a) + I_{Kr}(E,x_r) + I_{Ks}(E,x_s)\\
&\quad + I_{Ca,L}(E,\overline{d},f,f_{Ca}) + I_{p,Ca}(Cai) + I_{Na,K}(E) + I_{NaCa}(E,Cai)\\
&\quad + I_{b,Na}(E) + I_{b,Ca}(E,Cai),\\
\frac{\mathrm{d}y}{\mathrm{d}t} &= \frac{\overline{y}-y}{\tau_y}, \qquad y = j, o_i, x_r, x_s, f, f_{Ca}, u, v,\\
\frac{\mathrm{d}Cai}{\mathrm{d}t} &= \frac{B1}{B2},\\
B1 &= (2FV_i)^{(-1)}(2I_{NaCa}(E,Cai) - I_{p,Ca}(Cai) - I_{Ca,L}(E,\overline{d},f,f_{Ca})\\
&\quad - I_{b,Ca}(E,Cai)) + (V_i)^{(-1)}(V_{up}(0.000496 - I_{up}(Cai))\\
&\quad + I_{rel}(Cai,Carel,u,v,\overline{w})V_{rel}),
\end{aligned}
$$

$$
\begin{aligned}
B2 &= 1+\frac{[Trpn]_{max}K_{m,Trpn}}{(Cai+K_{m,Trpn})^2}+\frac{[Cmdn]_{max}K_{m,Cmdn}}{(Cai+K_{m,Cmdn})^2},\\
\frac{\mathrm{d}Carel}{\mathrm{d}t} &= \frac{(I_{tr}(Carel)-I_{rel}(Cai,Carel,u,v,\overline{w}))}{\left(1+\frac{[Csqn]_{max}K_{m,Csqn}}{(Carel+K_{m,Csqn})^2}\right)}.
\end{aligned}
$$

We draw the graph of the τ's, Fig. 6.45, using the initial values at t=33, which are the final values of the intermediate stage and are:

$$
\begin{aligned}
&(E, Cai, Carel, j, o_i, x_r, x_s, f, f_{Ca}, u, v) =\\
&(-12.2830, 0.0008, 0.1478, 0.0001, 0.0779, 0.0919, 0.0438, 0.8770, 0.2956,\\
&0.9829, 0.0002).
\end{aligned}
$$

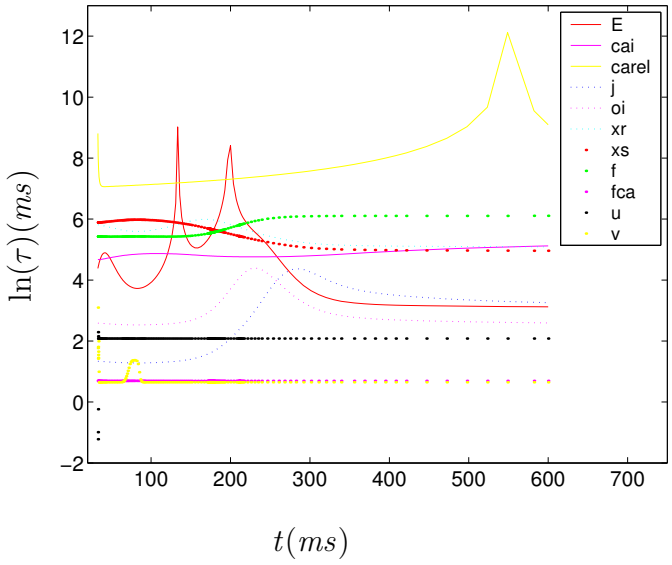

Figure 6.45: Graph of the τ's for CRN-11, system (6.30), for the time scale $[33, 600]$.

We see from the graph that the fast variables are f_{Ca}, u, v, o_i and j. The intersecting variables are Cai, $Carel$, f, x_s and x_r.

We also replace $(Carel - Cai)$ with $Carel$ in I_{rel} and see that there is no change in the action potential, Fig. 6.46.

We draw the fast variables against their quasi-stationary values for two time periods $[33, 600]$ and $[33, 63]$ to see how close they are to their quasi-stationary values. We see from Figs. 6.47 and 6.48 that f_{Ca} is exactly like its quasi-stationary value and therefore can be replaced with its quasi-stationary value, u is close to its quasi-stationary value and is exactly the same after t=110. Between 33 and 110 it can be replaced at different stages with exponential functions. Variable v

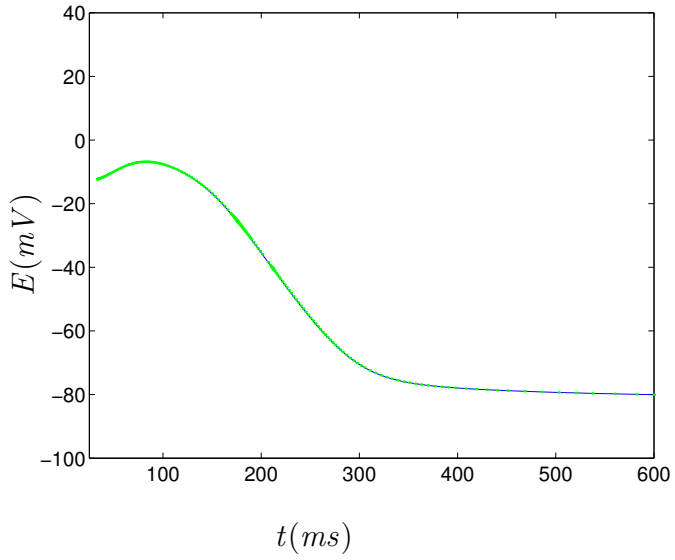

Figure 6.46: Action potential of CRN-11, system (6.30), (-) and CRN-11 with $(Carel - Cai) \approx Carel$ in I_{rel} (.).

is exactly the same as its quasi-stationary value and therefore can be replaced with it. Variable o_i is close to its quasi-stationary value and so is j. Variable f is not close to its quasi-stationary value and neither are x_r or x_s.

If we put $1/\epsilon$ in front of the fast variables the system will look like:

$$
\begin{aligned}
\frac{\mathrm{d}E}{\mathrm{d}t} &= -\frac{I_{ion}}{C_M}, \qquad (6.31)\\
I_{ion} &= I_{K1}(E) + I_{to}(E,\overline{o}_a,o_i) + I_{Kur}(E,\overline{u}_a) + I_{Kr}(E,x_r) + I_{Ks}(E,x_s)\\
&\quad + I_{Ca,L}(E,\overline{d},f,f_{Ca}) + I_{p,Ca}(Cai) + I_{Na,K}(E) + I_{NaCa}(E,Cai)\\
&\quad + I_{b,Na}(E) + I_{b,Ca}(E,Cai),\\
\frac{\mathrm{d}y}{\mathrm{d}t} &= \frac{\overline{y}-y}{\tau_y}, \qquad y = x_r, x_s, f,\\
\frac{\mathrm{d}y}{\mathrm{d}t} &= \frac{1}{\epsilon}\frac{\overline{y}-y}{\tau_y}, \qquad y = j, o_i, f_{Ca}, u, v,\\
\frac{\mathrm{d}Cai}{\mathrm{d}t} &= \frac{B1}{B2},\\
B1 &= (2FV_i)^{(-1)}(2I_{NaCa}(E,Cai) - I_{p,Ca}(Cai) - I_{Ca,L}(E,\overline{d},f,f_{Ca})\\
&\quad - I_{b,Ca}(E,Cai)) + (V_i)^{(-1)}(V_{up}(0.000496 - I_{up}(Cai))\\
&\quad + I_{rel}(Cai,Carel,u,v,\overline{w})V_{rel}),\\
B2 &= 1 + \frac{[Trpn]_{max}K_{m,Trpn}}{(Cai+K_{m,Trpn})^2} + \frac{[Cmdn]_{max}K_{m,Cmdn}}{(Cai+K_{m,Cmdn})^2},\\
\frac{\mathrm{d}Carel}{\mathrm{d}t} &= \frac{(I_{tr}(Carel) - I_{rel}(Cai,Carel,u,v,\overline{w}))}{\left(1 + \frac{[Csqn]_{max}K_{m,Csqn}}{(Carel+K_{m,Csqn})^2}\right)}.
\end{aligned}
$$

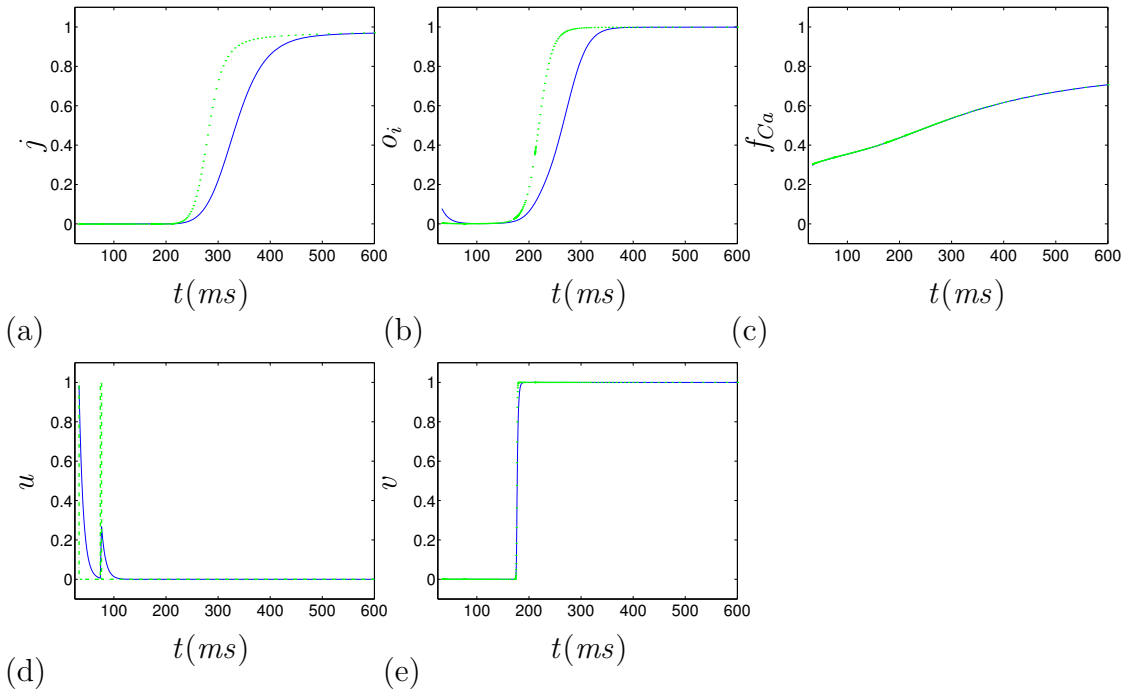

Figure 6.47: Graphs of the fast variables (-) and their quasi-stationary values (-.) and (.) for CRN-11, system (6.30), for t=[33, 600]. (a) j, (b) o_i, (c) f_{Ca}, (d) u and (e) v.

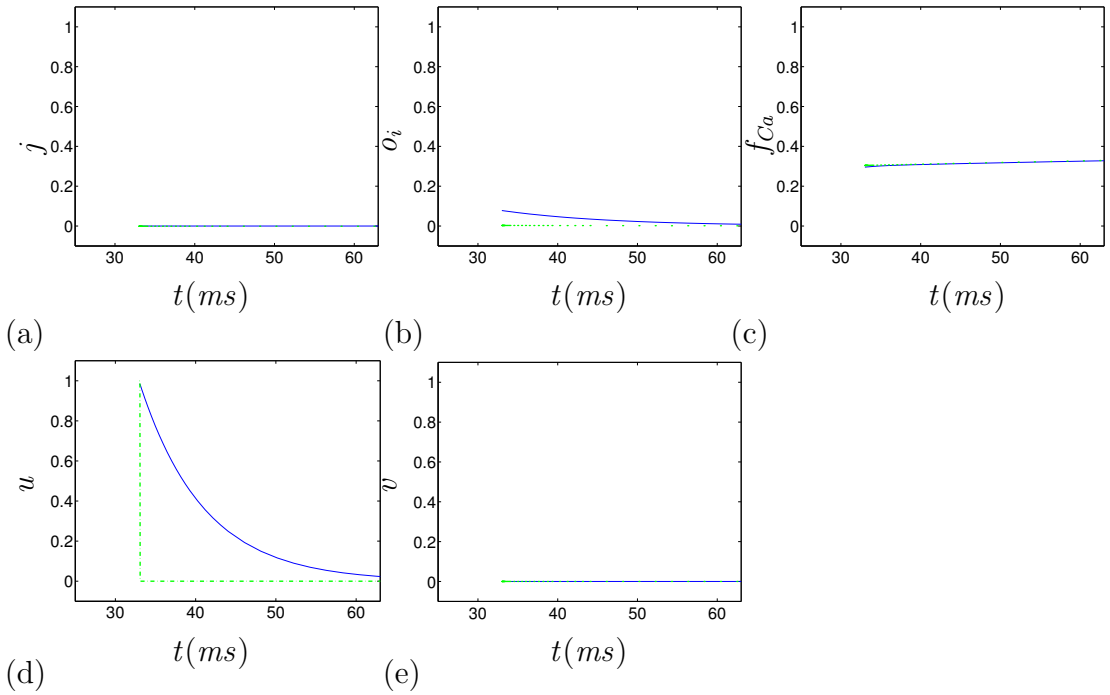

Figure 6.48: Graphs of the fast variables (-) and their quasi-stationary values (-.) and (.) for CRN-11, system (6.30), for t=[33, 63]. (a) j, (b) o_i, (c) f_{Ca}, (d) u and (e) v.

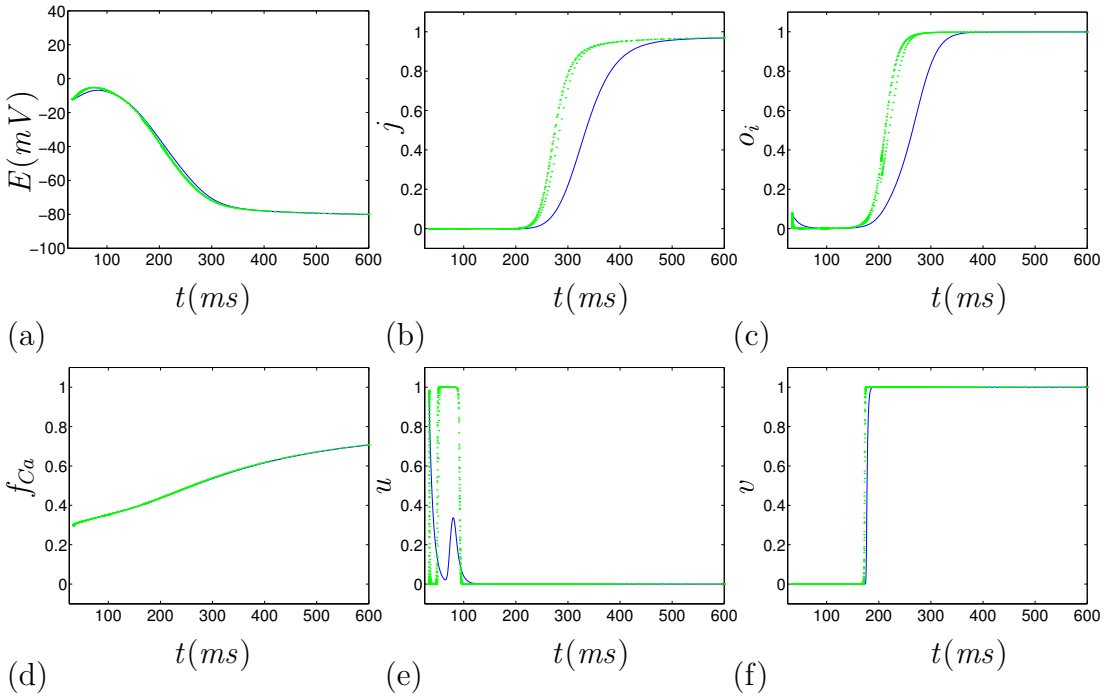

Figure 6.49: Graphs of CRN-11, system (6.30) ϵ=1, (-) and CRN-11, system (6.31) $\epsilon \to 0$, (.) for the variables (a) E, (b) j, (c) o_i, (d) f_{Ca}, (e) u and (f) v.

As we tend ϵ to zero we see from Fig. 6.49 that the action potential is similar to CRN-11, there is only a slight change in the return. We see that from drawing the action potential of system (6.32) against CRN-11, system (6.30), Fig. 6.50, o_i causes this slight change in the action potential, so it is not a fast variable. So we take $\frac{1}{\epsilon}$ from in front of o_i and obtain our new system:

$$
\begin{aligned}
\frac{\mathrm{d}E}{\mathrm{d}t} &= -\frac{I_{ion}}{C_M}, \qquad (6.32)\\
I_{ion} &= I_{K1}(E) + I_{to}(E,\overline{o}_a,o_i) + I_{Kur}(E,\overline{u}_a) + I_{Kr}(E,x_r) + I_{Ks}(E,x_s)\\
&\quad + I_{Ca,L}(E,\overline{d},f,f_{Ca}) + I_{p,Ca}(Cai) + I_{Na,K}(E) + I_{NaCa}(E,Cai)\\
&\quad + I_{b,Na}(E) + I_{b,Ca}(E,Cai),\\
\frac{\mathrm{d}y}{\mathrm{d}t} &= \frac{\overline{y}-y}{\tau_y}, \qquad y = o_i, x_r, x_s, f,\\
\frac{\mathrm{d}y}{\mathrm{d}t} &= \frac{1}{\epsilon}\frac{\overline{y}-y}{\tau_y}, \qquad y = j, f_{Ca}, u, v,\\
\frac{\mathrm{d}Cai}{\mathrm{d}t} &= \frac{B1}{B2},\\
B1 &= (2FV_i)^{(-1)}(2I_{NaCa}(E,Cai) - I_{p,Ca}(Cai) - I_{Ca,L}(E,\overline{d},f,f_{Ca})\\
&\quad - I_{b,Ca}(E,Cai)) + (V_i)^{(-1)}(V_{up}(0.000496 - I_{up}(Cai))
\end{aligned}
$$

$$
\begin{aligned}
& +I_{rel}(Cai, Carel, u, v, \overline{w})V_{rel}), \\
B2 &= 1 + \frac{[Trpn]_{max}K_{m,Trpn}}{(Cai + K_{m,Trpn})^2} + \frac{[Cmdn]_{max}K_{m,Cmdn}}{(Cai + K_{m,Cmdn})^2}, \\
\frac{\mathrm{d}Carel}{\mathrm{d}t} &= \frac{(I_{tr}(Carel) - I_{rel}(Cai, Carel, u, v, \overline{w}))}{\left(1 + \frac{[Csqn]_{max}K_{m,Csqn}}{(Carel + K_{m,Csqn})^2}\right)}.
\end{aligned}
$$

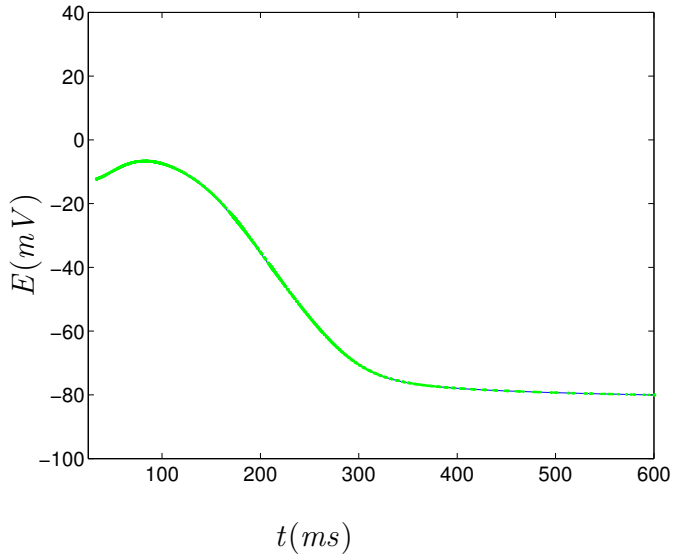

Figure 6.50: Action potential of CRN-11, system (6.30), (-) and CRN-11, system (6.32) $\epsilon \to 0$, (.).

If we use the change of variable $T = \frac{t}{\epsilon}$ we obtain:

$$
\begin{aligned}
\frac{\mathrm{d}E}{\mathrm{d}T} &= -\epsilon\frac{I_{ion}}{C_M}, \qquad (6.33) \\
I_{ion} &= I_{K1}(E) + I_{to}(E, \overline{o}_a, o_i) + I_{Kur}(E, \overline{u}_a) + I_{Kr}(E, x_r) + I_{Ks}(E, x_s) \\
& +I_{Ca,L}(E, \overline{d}, f, f_{Ca}) + I_{p,Ca}(Cai) + I_{Na,K}(E) + I_{NaCa}(E, Cai) \\
& +I_{b,Na}(E) + I_{b,Ca}(E, Cai), \\
\frac{\mathrm{d}y}{\mathrm{d}T} &= \epsilon\frac{\overline{y} - y}{\tau_y}, \qquad y = o_i, x_r, x_s, f, \\
\frac{\mathrm{d}y}{\mathrm{d}T} &= \frac{\overline{y} - y}{\tau_y}, \qquad y = j, f_{Ca}, u, v, \\
\frac{\mathrm{d}Cai}{\mathrm{d}T} &= \epsilon\frac{B1}{B2}, \\
B1 &= (2FV_i)^{(-1)}(2I_{NaCa}(E, Cai) - I_{p,Ca}(Cai) - I_{Ca,L}(E, \overline{d}, f, f_{Ca}) \\
& -I_{b,Ca}(E, Cai)) + (V_i)^{(-1)}(V_{up}(0.000496 - I_{up}(Cai)) \\
& +I_{rel}(Cai, Carel, u, v, \overline{w})V_{rel}), \\
B2 &= 1 + \frac{[Trpn]_{max}K_{m,Trpn}}{(Cai + K_{m,Trpn})^2} + \frac{[Cmdn]_{max}K_{m,Cmdn}}{(Cai + K_{m,Cmdn})^2},
\end{aligned}
$$

$$\frac{\mathrm{d}Carel}{\mathrm{d}T} = \epsilon \frac{(I_{tr}(Carel) - I_{rel}(Cai, Carel, u, v, \overline{w}))}{\left(1 + \frac{[Csqn]_{max} K_{m,Csqn}}{(Carel + K_{m,Csqn})^2}\right)}.$$

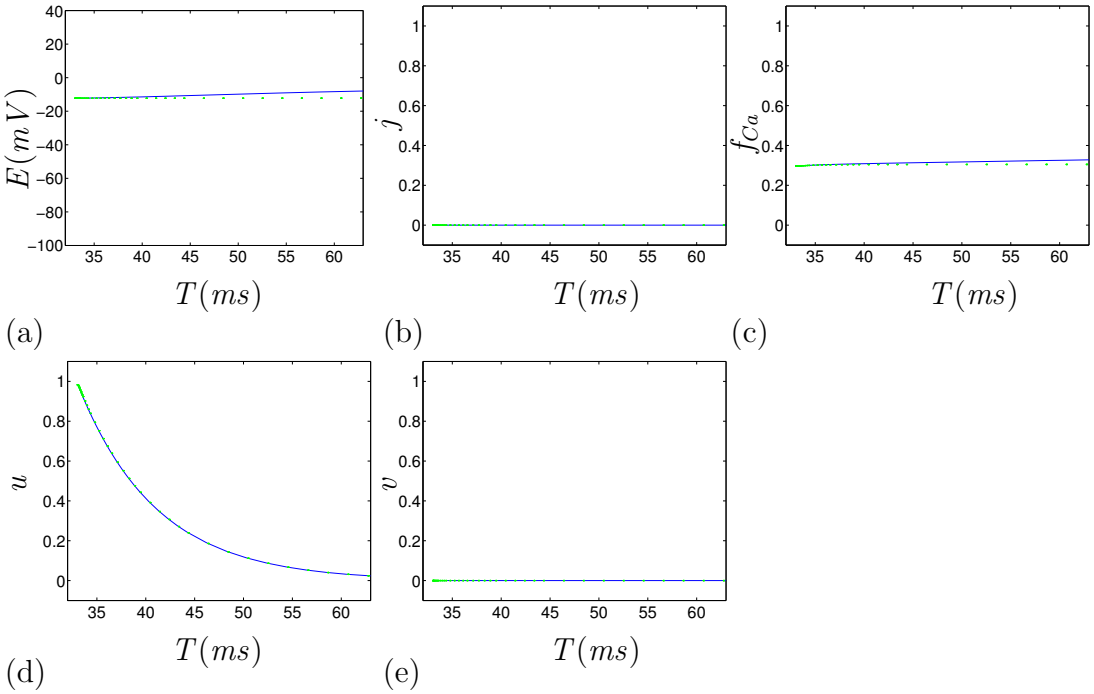

Figure 6.51: Graphs of CRN-11, system (6.30) ϵ=1, (-) and CRN-11, system (6.33) $\epsilon \to 0$, (.) for T=[33, 63] for the variables (a) E, (b) j, (c) f_{Ca}, (d) u and (e) v.

As we tend ϵ to zero for the fast time we draw the action potential for T=[33, 63], Fig. 6.51(a) and see that near the end, as the action potential starts its return, the action potential drops lower than CRN-11. We also draw the other variables in the system, Figs. 6.51 and 6.52, to see what happens to them as $\epsilon \to 0$ for system (6.33).

6.5.1 Analysis of u and $\overline{u}$

We know from the previous section that $\overline{u}$ can be replaced with the Heaviside function. We also see from Fig. 6.49(e) that we have an extra opening in u and this is caused by the approximations that we have done so far. We want to analyse this extra opening to see if it is significant. So we draw the graphs of u and $\overline{u}$ for its original equation and the Heaviside function. Figure 6.53(a) shows u and $\overline{u}$ and this shows what happens to them both for CRN-11.

We see that because of this extra opening on u, then we also have an extra opening for $\overline{u}$ if it is the Heaviside function, we didn't want this as we wanted

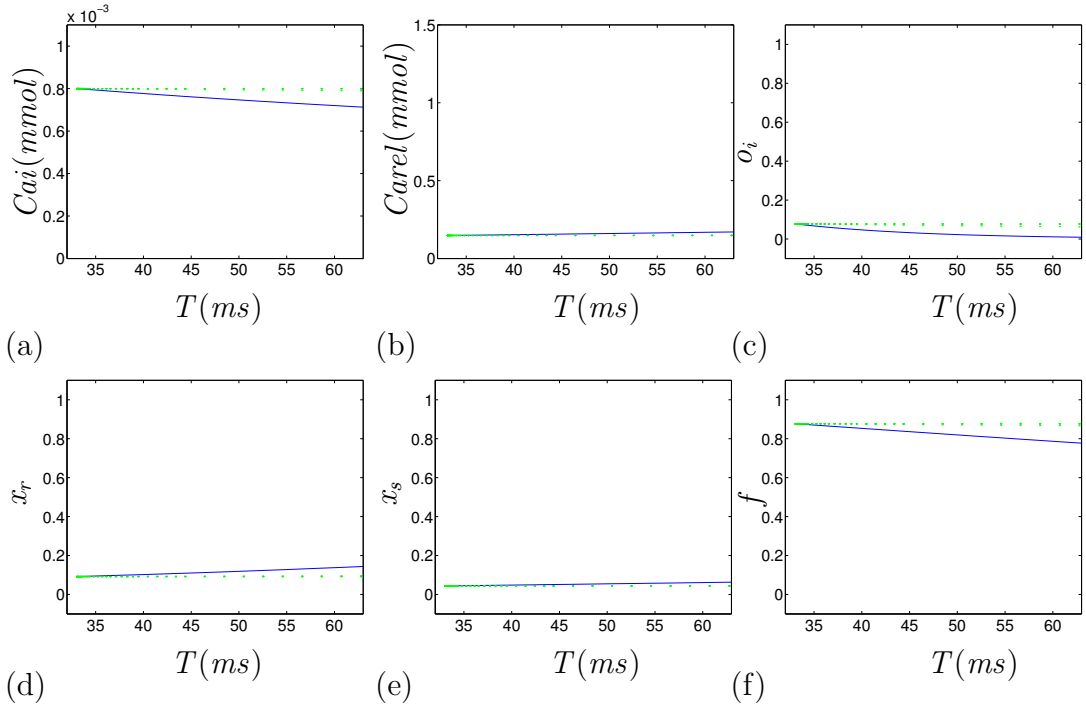

Figure 6.52: Graphs of CRN-11, system (6.30) ϵ=1, (-) and CRN-11, system (6.33) $\epsilon \to 0$, (.) for the variables (a) Cai, (b) $Carel$, (c) o_i, (d) x_r, (e) x_s and (f) f.

a step function. So our approximation is not very good or robust because a is smaller than F_1 by a factor of 230. Despite this fact we know that the action potential doesn't change else we wouldn't have replaced $\overline{u}$ with the Heaviside function in the beginning. This doesn't change any of the other variables either, because u only appears in product with v, and v is closed in that time interval anyway.

So we want to eliminate this second opening and therefore $\overline{u}$ will be zero after t=33 always. We know that $\overline{u}$ depends on F_n and that F_n depends on Cai, so we can vary the initial value of Cai by 1% either way and see what affect this has on the graphs of u and $\overline{u}$. We see from Fig. 6.53 that if we do this we can eliminate the second opening and obtain the graphs of u and $\overline{u}$.

Therefore we can replace u with $\overline{u}$=0 as we know that it will be zero always now, even though the second opening did not affect the action potential, and we can replace v with $\overline{v}$=1, which will give us I_{rel}=0. So we have adiabatically eliminated two variables and have eliminated a calcium current as well. We can also adiabatically eliminate f_{Ca} and j to obtain the following system of seven equations:

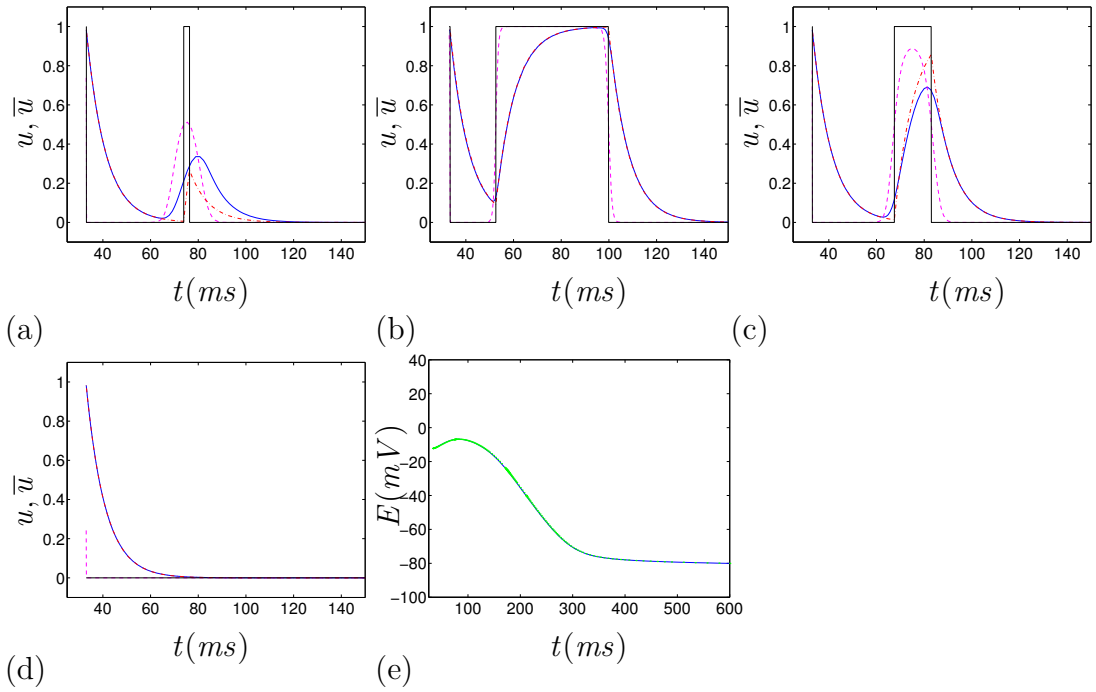

Figure 6.53: Graphs of u (-blue) and $\overline{u}$ (- -) for the original function and u (-.) and $\overline{u}$ (-black) for the Heaviside function for CRN-11, system (6.30), for different initial values for Cai=0.0008^m where (a) m=1, (b) m=1.01, (c) m=1.001, (d) m=0.99 and the action potential of CRN-11, system (6.30), with $\overline{u}$ as its original function (-) and as its Heaviside function (.).

$$
\begin{aligned}
\frac{\mathrm{d}E}{\mathrm{d}t} &= -\frac{I_{ion}}{C_M}, \qquad (6.34)\\
I_{ion} &= I_{K1}(E) + I_{to}(E,\overline{o}_a,o_i) + I_{Kur}(E,\overline{u}_a) + I_{Kr}(E,x_r) + I_{Ks}(E,x_s)\\
&\quad + I_{Ca,L}(E,\overline{d},f,\overline{f}_{Ca}(Cai)) + I_{p,Ca}(Cai) + I_{Na,K}(E) + I_{NaCa}(E,Cai)\\
&\quad + I_{b,Na}(E) + I_{b,Ca}(E,Cai),\\
\frac{\mathrm{d}y}{\mathrm{d}t} &= \frac{\overline{y}-y}{\tau_y}, \qquad y = o_i, x_r, x_s, f,\\
\frac{\mathrm{d}Cai}{\mathrm{d}t} &= \frac{B1}{B2},\\
B1 &= (2FV_i)^{(-1)}(2I_{NaCa}(E,Cai) - I_{p,Ca}(Cai) - I_{Ca,L}(E,\overline{d},f,\overline{f}_{Ca}(Cai))\\
&\quad - I_{b,Ca}(E,Cai)) + (V_i)^{(-1)}(V_{up}(0.000496 - I_{up}(Cai))),\\
B2 &= 1 + \frac{[Trpn]_{max}K_{m,Trpn}}{(Cai+K_{m,Trpn})^2} + \frac{[Cmdn]_{max}K_{m,Cmdn}}{(Cai+K_{m,Cmdn})^2},\\
\frac{\mathrm{d}Carel}{\mathrm{d}t} &= \frac{I_{tr}(Carel)}{\left(1+\frac{[Csqn]_{max}K_{m,Csqn}}{(Carel+K_{m,Csqn})^2}\right)}.
\end{aligned}
$$

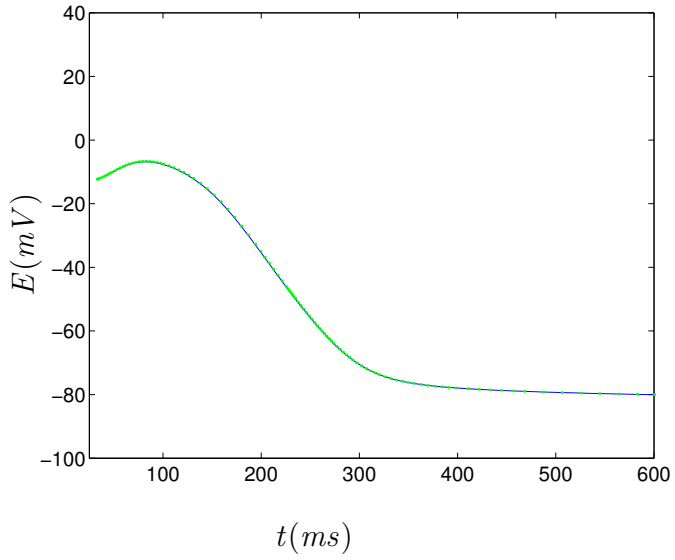

Figure 6.54: Action potential of CRN-11, system (6.30), (-) and CRN-7, system (6.34) (.).

We see from Fig. 6.54 that there is no difference between CRN-11 (6.30) and CRN-7 (6.34).

6.5.2 Eliminating minor currents

We want to see if we can eliminate any minor currents from system (6.34), so we draw the graphs of the currents in $\dot{E}$ and $\dot{Cai}$ for both CRN-11, system (6.30), and CRN-7, system (6.34), Fig. 6.55, to check that the currents look the same for both systems and we see that they do, so Fig. 6.55 shows all the currents in $\dot{E}$ and $\dot{Cai}$.

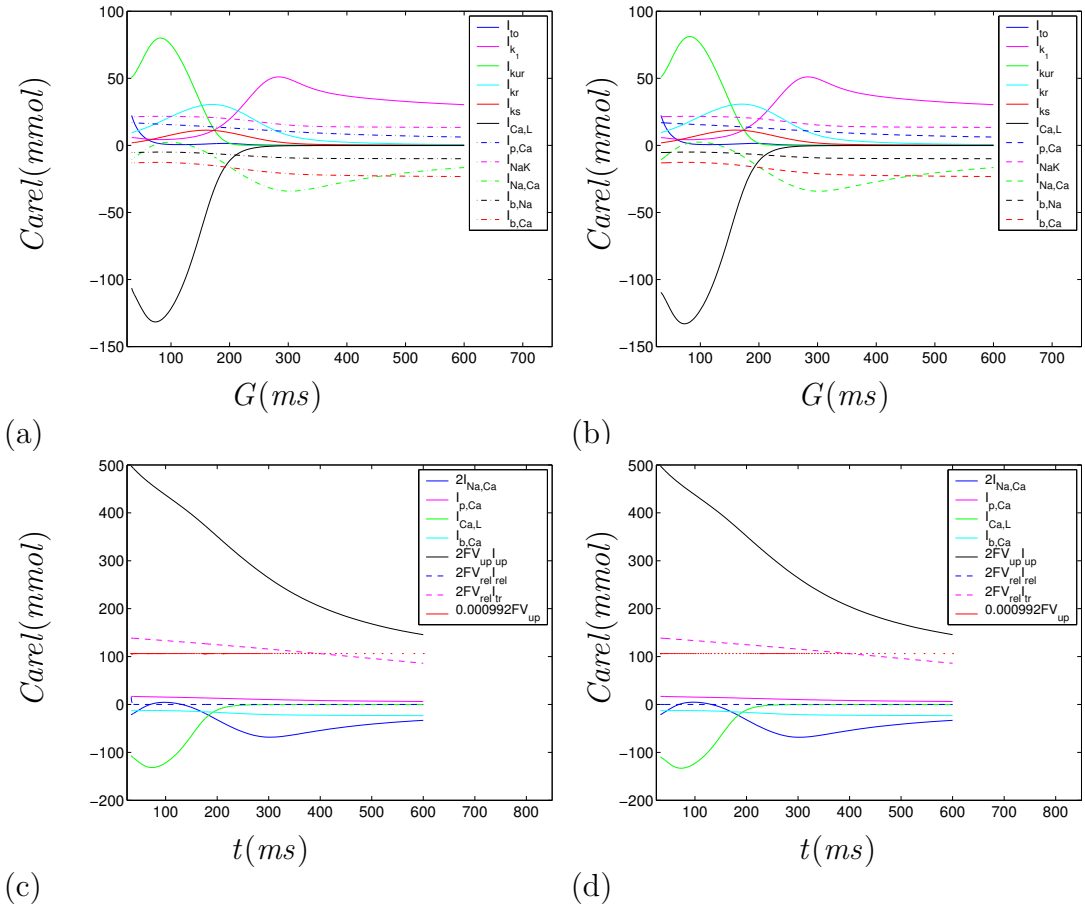

Figure 6.55: Graphs of currents in $\dot{E}$ for (a) CRN-11, system (6.30), and (b) CRN-7, system (6.34). Graphs of currents in $\dot{Cai}$ for (c) CRN-11, system (6.30), and (d) CRN-7, system (6.34).

We found that if we eliminate any of the remaining currents, then this affects the action potential. We know that I_{rel}=0 already, then we found that if we eliminate I_{to} we obtain the action potential to look like CRN-11's action potential, but it is a little higher at the beginning. So if we eliminate I_{to} then o_i doesn't affect the action potential; but the voltage does affect o_i, so we might as well adiabatically eliminate o_i. Therefore we decided to keep CRN-7 as an accu-

rate system where the action potential doesn't change, compared with CRN-11, through the adiabatical eliminations. Then we will have a less accurate system, which is found by adiabatically eliminating another fast variable, using iterations and approximations of other variables, where the resulting action potential is compared with CRN-7.

6.5.3 Iterations for $\frac{\mathrm{d}Carel}{\mathrm{d}t}$

As we see from system (6.34), the equation $\frac{\mathrm{d}Carel}{\mathrm{d}t}$ only contains the variable $Carel$ and none of the other variables. Also the other equations do not contain $Carel$ either. So we can resolve $\frac{\mathrm{d}Carel}{\mathrm{d}t}$ with respect to $Carel$ and t. So we can use the variable separable method and then solve by iterations.

$$\begin{aligned} \frac{\mathrm{d}Carel}{\mathrm{d}t} &= \frac{I_{tr}(Carel)}{\left(1+\frac{[Csqn]_{max}K_{m,Csqn}}{(Carel+K_{m,Csqn})^2}\right)}, \\ \frac{\mathrm{d}Carel}{\mathrm{d}t} &= \frac{Caup-Carel}{\tau_{tr}\left(1+\frac{A}{(Carel+B)^2}\right)}, \end{aligned} \tag{6.35}$$

where A=$[Csqn]_{max}K_{m,Csqn}$ and B=$K_{m,Csqn}$. Using partial fractions, the initial conditions $(t_0, Carel_0)$, p=$Caup+B$, and q=$AB^2-A(Caup+B)^2+ACaup(B+Caup)$ to find the solution.

$$\begin{aligned} &\int_{Carel_0}^{Carel}\frac{\left(1+\frac{A}{(Carel+B)^2}\right)}{(Caup-Carel)}\mathrm{d}Carel=\int_{t_2}^{t}\frac{1}{\tau_{tr}}\mathrm{d}t, \\ &\ln|(Carel-Caup)^{\frac{(p^2+A)}{p^2}}(Carel+B)^{\frac{q}{p^2BCaup}}|+\frac{A}{p(Carel+B)} \\ &=-\frac{(t-t_2)}{\tau_{tr}}+\frac{A}{p(Carel_0+B)}+\ln|(Carel_0-Caup)^{\frac{(p^2+A)}{p^2}}(Carel_0+B)^{\frac{q}{p^2BCaup}}|. \end{aligned}$$

Rearranging with respect to t, we obtain:

$$\begin{aligned} t &= \tau_{tr}\left(\frac{A}{p(Carel_0+B)}+\ln|(Carel_0-Caup)^{\frac{(p^2+A)}{p^2}}(Carel_0+B)^{\frac{q}{p^2BCaup}}|\right. \\ &\quad \left.-\frac{A}{p(Carel+B)}\right)-\tau_{tr}\left(\ln|(Carel-Caup)^{\frac{(p^2+A)}{p^2}}(Carel+B)^{\frac{q}{p^2BCaup}}|\right)+t_2. \end{aligned}$$

Again quadratures produce an implicit solution for $Carel(t)$, like we found for the iterations in the intermediate stage.

Let us solve this for $Carel$ explicitly using iterations, say

$$G = -\frac{(t-t_2)}{\tau_{tr}} + \frac{A}{p(Carel_0+B)} + \ln|(Carel_0 - Caup)^{\frac{(p^2+A)}{p^2}}(Carel_0+B)^{\frac{q}{p^2BCaup}}|.$$

So,

$$\begin{aligned} G &= \ln|(Carel - Caup)^{\frac{(p^2+A)}{p^2}}(Carel+B)^{\frac{q}{p^2BCaup}}| + \frac{A}{p(Carel+B)}, \\ Carel &= \frac{A}{p(G - \ln|(Carel - Caup)^{\frac{(p^2+A)}{p^2}}(Carel+B)^{\frac{q}{p^2BCaup}}|)} - B. \end{aligned}$$

So for iterations we have:

$$Carel_{n+1} = \frac{A}{p(G - \ln|(Carel_n - Caup)^{\frac{(p^2+A)}{p^2}}(Carel_n+B)^{\frac{q}{p^2BCaup}}|)} - B.$$

We can start the iterations from $Carel_0$ which is the vector of $Carel$ taken from equation (6.35).

To see if the iterations tend to a value we compare the values at t=600. The iterations converge immediately.

So lets try the iterations as if we don't know what $Carel_0$ is. We use the initial point of $Carel$ at t=33, which is $Carel_0$=0.1478, and we see if the iterations converge. We found that the iterations didn't converge.

Also we try the following approximation, $(Caup - Carel) \approx Caup$ in the equation $\frac{\mathrm{d}Carel}{\mathrm{d}t}$ to see if this approximation is close to the original graph of $Carel$, as if it is then the workings out using the variable separable method will be much simpler. Unfortunately as Fig. 6.56 shows this replacement doesn't work. The approximation gives a curve that is moving away from the original curve for $Carel$.

We want to obtain a simple approximation for $Carel$ that is also close to the original graph of $Carel$, so we take the following equation and draw the graph of G against $Carel$ to see if we can approximate this function.

$$\phi(Carel) = \ln|(Carel - Caup)^{\frac{(p^2+A)}{p^2}}(Carel+B)^{\frac{q}{p^2BCaup}}| + \frac{A}{p(Carel+B)} = G.$$

We see from Fig. 6.57(a) that we can approximate this function with a linear function. So we do this and obtain the following approximation:

$$Carel = -0.15851G + 0.8557.$$

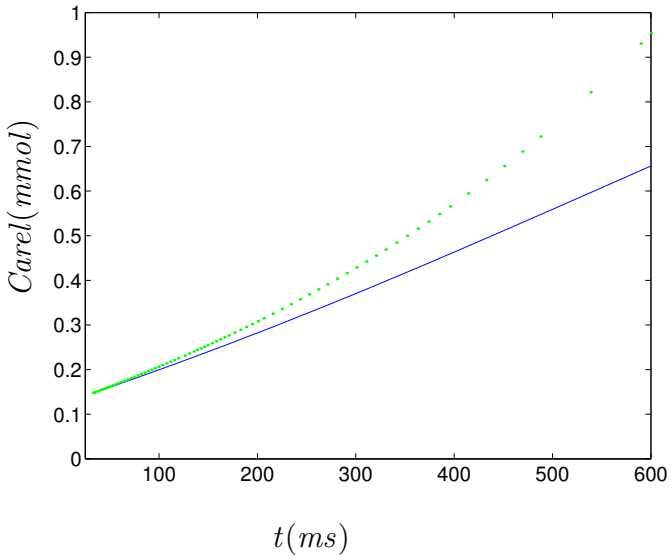

Figure 6.56: Graph of $Carel$ from system (6.34) (-) and the approximation $(Caup - Carel) \approx Caup$ in the equation $\frac{\mathrm{d}Carel}{\mathrm{d}t}$ in system (6.34)) (.).

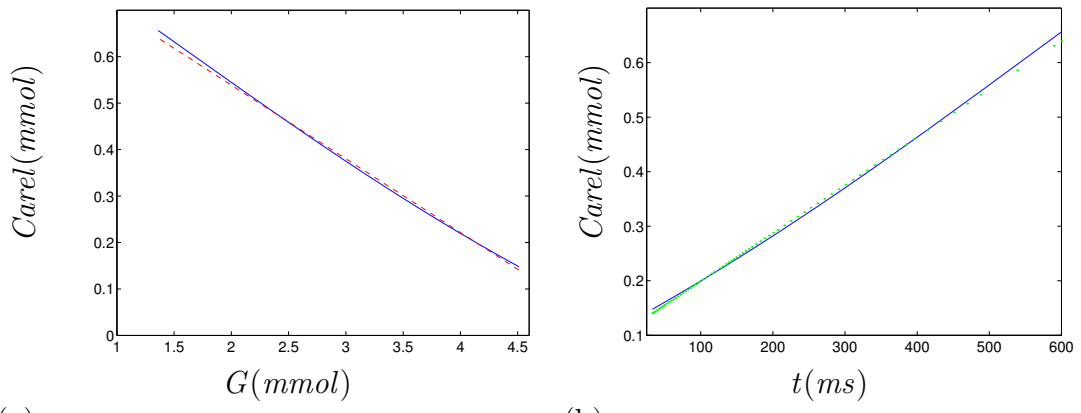

(a) (b)

Figure 6.57: Graph of $Carel$, system (6.34) (-) and approximation $Carel{=}-0.15851G + 0.8557$ (- -) and (.) drawn against (a) G and (b) t.

So we draw our new function against time and compare it with CRN-7's $Carel$ to see how well it is approximated and Fig. 6.57(b) shows that it is a good approximation as it is very close to the original curve of $Carel$.

Even though we have found a good approximation for $Carel$ as a function of t, we still want to see if we can make the answer simpler by approximating the $\frac{\mathrm{d}Carel}{\mathrm{d}t}$ equation before we do any calculations to it. So we tried three more approximations and found that none of the approximations are close to the original solution for $Carel$, therefore we conclude that the answer that we obtained for $Carel$ as a function of t is still the best solution.

6.5.4 Finding a good reduction for CRN-7

We want to reduce CRN-7 to a system of three equations, so we have a system that we can analyse better. This system won't be exactly the same as CRN-7, but that system is our accurate system and any system after that is less accurate, but is still a good approximation of CRN-7.

The first reduction we tried is to neglect I_{to}, I_{kr} and I_{ks} from CRN-7, because these three currents contain gating variables. We can't eliminate $I_{Ca,L}$ as this current depends on Cai which we want to keep. So we have a system of three equations, CRN-3, that is less accurate than CRN-7, but within 10% of CRN-7.

We drew solutions for CRN-3 and compared them with the solutions for CRN-7. We saw that for the action potential there is a big change on the return, the shape becomes more dome like and also there is a noticeable change for Cai, and f, so this is not a good reduction.

Therefore we decided on another reduction. We take CRN-7 and we adiabatically eliminate o_i and also eliminate $Carel$, because the $Carel$ equation only contains $Carel$ and is not affected by any other variables in the system, and no other variables in the system contain $Carel$ so we consider this equation separately.

So now we collect all the terms that only contain E together and all the terms that contain other variables together in the $\frac{\mathrm{d}E}{\mathrm{d}t}$ equation. We do the same for the $\frac{\mathrm{d}Cai}{\mathrm{d}t}$ equation, but here we collect all the terms that contain only calcium together. The system will be CRN-5a:

$$\frac{\mathrm{d}E}{\mathrm{d}t} = -\frac{(I_1(E) + I_2(E, Cai, f, \overline{f}_{Ca}(Cai), x_r, x_s))}{C_M}, \tag{6.36}$$

$$
\begin{aligned}
\frac{\mathrm{d}y}{\mathrm{d}t} &= \frac{\overline{y}(E)-y}{\tau_y(E)}, \qquad y = x_r, x_s, f, \\
\frac{\mathrm{d}Cai}{\mathrm{d}t} &= \frac{(I_3(Cai)+I_4(E,Cai,f,\overline{f}_{Ca}(Cai)))}{2FV_iB2}, \\
B2 &= 1+\frac{[Trpn]_{max}K_{m,Trpn}}{(Cai+K_{m,Trpn})^2}+\frac{[Cmdn]_{max}K_{m,Cmdn}}{(Cai+K_{m,Cmdn})^2},
\end{aligned}
$$

where

$$
\begin{aligned}
I_1(E) &= I_{to}(E,\overline{o}_a,\overline{o}_i)+I_{K1}(E)+I_{Kur}(E,\overline{u}_a)+I_{Na,K}(E) \\
&\quad +I_{b,Na}(E), \\
I_2(E,Cai,f,x_r,x_s) &= C_M(\frac{g_{Kr}x_r(E-E_K)}{1+e^{\frac{(E+15)}{22.4}}}+g_{Ks}x_s^2(E-E_K) \\
&\quad +g_{Ca,L}\overline{d}(E)f\overline{f}_{Ca}(Cai)(E-65.0) \\
&\quad +I_{p,Ca(max)}\left(\frac{Cai}{0.0005+Cai}\right)+\frac{ae^{kE}-b\,Cai\,e^{-mE}}{B(1+K_{sat}e^{-mE})} \\
&\quad +g_{b,Ca}(E-E_{Ca})), \\
I_3(Cai) &= 2FV_{up}(0.000496-I_{up})-I_{p,Ca}, \\
I_4(E,Cai,f) &= C_M(2\frac{ae^{kE}-b\,Cai\,e^{-mE}}{B(1+K_{sat}e^{-mE})}-g_{b,Ca}(E-E_{Ca}) \\
&\quad -g_{Ca,L}\overline{d}(E)f\overline{f}_{Ca}(Cai)(E-65.0)),
\end{aligned}
$$

where B=$(K^3_{m,Na}$+$Nao^3)(K_{m,Ca}$+$Cao)$, a=$I_{NaCa(max)}Nai^3Cao$, k=$\frac{\gamma F}{RT^o}$, b=Nao^3 and m=$\frac{(\gamma-1)F}{RT^o}$.

We now draw the solutions for our new system and compare them with the solutions from CRN-7. The only approximation we use to obtain CRN-5a is that we adiabatically eliminate o_i. So Fig. 6.58 shows the solutions for E, Cai, f, x_r and x_s for both systems.

We see that there is a slight change in the action potential. There is a slight change for x_r and f, but no change for Cai and x_s. So this reduction is not perfect, but it is still a good reduction.

We also draw the variables with their quasi-stationary values to see if any of the gating variables are close to their quasi-stationary values and if they are then we can call these variables fast variables and replace them with their quasi-stationary values. We see from Fig. 6.59 that this is not the case for this system.

We draw the τ's for CRN-5a to see if there are any variables that are not intersecting with E, but we see from Fig. 6.60 that all τ's intersect with τ_E so we can't say that any are fast or slow variables.

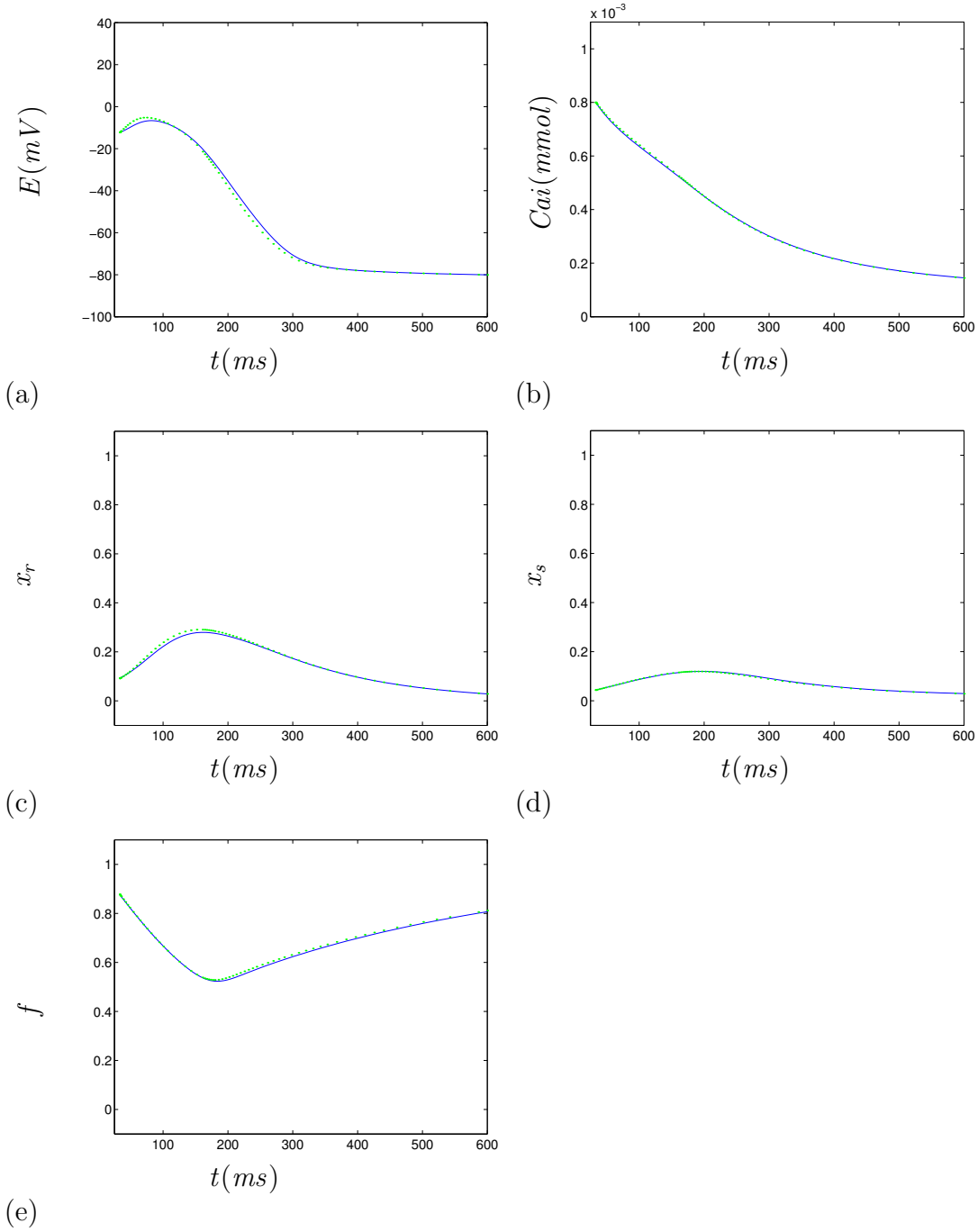

Figure 6.58: Graphs CRN-7, system (6.34), (-) and CRN-5a, system (6.36), (.) for the variables (a) E, (b) Cai, (c) x_r, (d) x_s and (e) f.

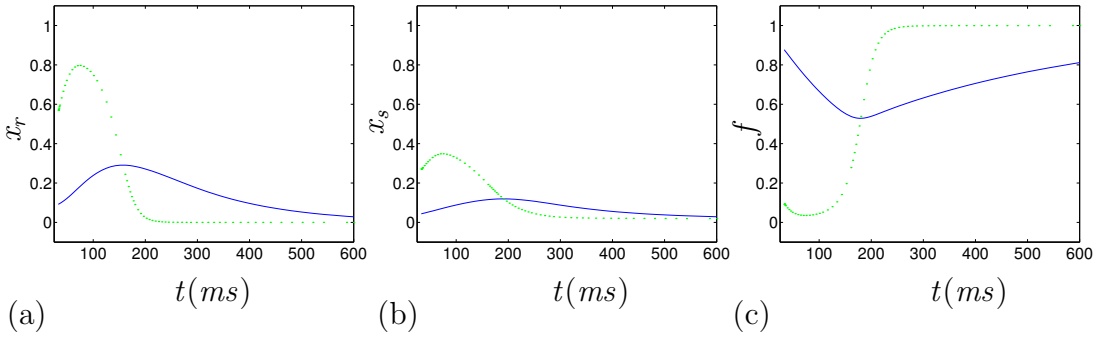

Figure 6.59: Graphs of CRN-5a, system (6.36), for the gating variables (-) and their quasi-stationary values (.). (a) x_r, (b) x_s and (c) f.

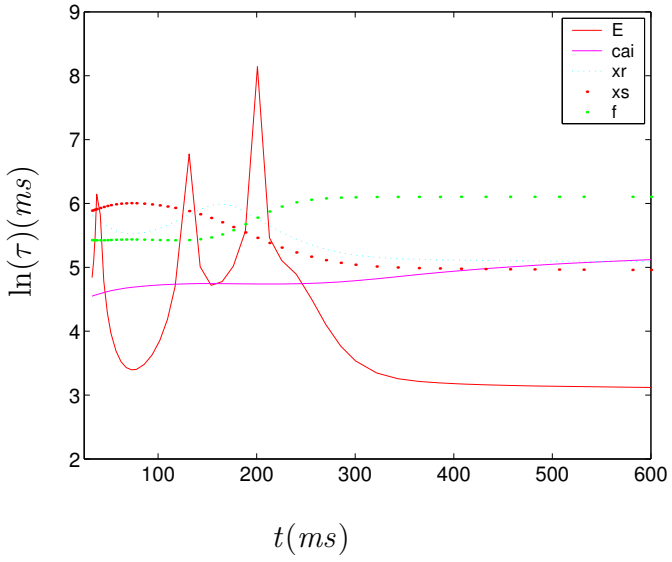

Figure 6.60: Graph of the τ's for system (6.36).

We also draw the graphs of the currents I_1, I_2, I_3 and I_4 to see what these look like and we see from Fig. 6.61(a) that currents I_1 and I_2 are mirror images of each other. We also draw I_1 against E and I_3 against Cai to see how they look.

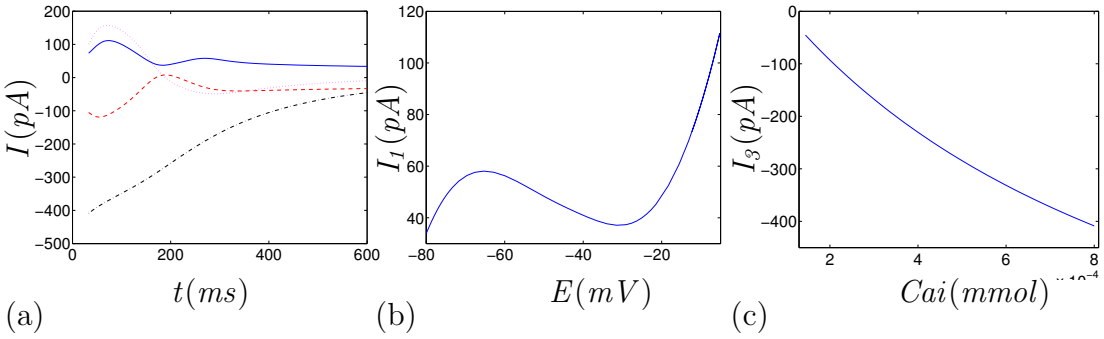

Figure 6.61: Graphs of currents in CRN-5a, system (6.36), for (a) I_1 (-), I_2 (- -), I_3 (-.) and I_4 (:) against t, (b) I_1 against E and (c) I_3 against Cai.

We want to see what regions of stability we obtain for the equation $\frac{\mathrm{d}E}{\mathrm{d}t}$ for this time period t=[33, 600]. So we draw $\frac{\mathrm{d}E}{\mathrm{d}t}$ against E and see how many solutions there are and if they are stable or unstable. So we see from Fig. 6.62 that $\frac{\mathrm{d}E}{\mathrm{d}t}$ starts off in the monostability region, one stable solution, then at t=45.1709 it moves into the bistability region, three solutions, two stable and one unstable, then at t=87.6649 it moves back into the monostability region and finally at t=244.1889 it returns to the bistability region. So this shows that $\frac{\mathrm{d}E}{\mathrm{d}t}$ moves between the two regions, which is similar to the FitzHugh model and Noble's 1962 model, because those two systems do the exact same thing for the slow manifold.

So the reason that the action potential has a slow recovery is that E is actually not a fast variable in this time period.

6.5.5 Empirical elimination of x_r and x_s from CRN-5a

We saw previously that by just eliminating I_{ks} and I_{kr} from CRN-7 we don't obtain a good approximation for CRN-7, so we try to eliminate x_r and x_s from CRN-5a instead. We choose these two gating variables, and not f, because the current $I_{Ca,L}$, that contains f, also contains Cai and E. So we wouldn't make this current a function of E alone, so we choose x_r and x_s and make them a function of f instead. Then we will obtain a system of three equations containing E, Cai and f.

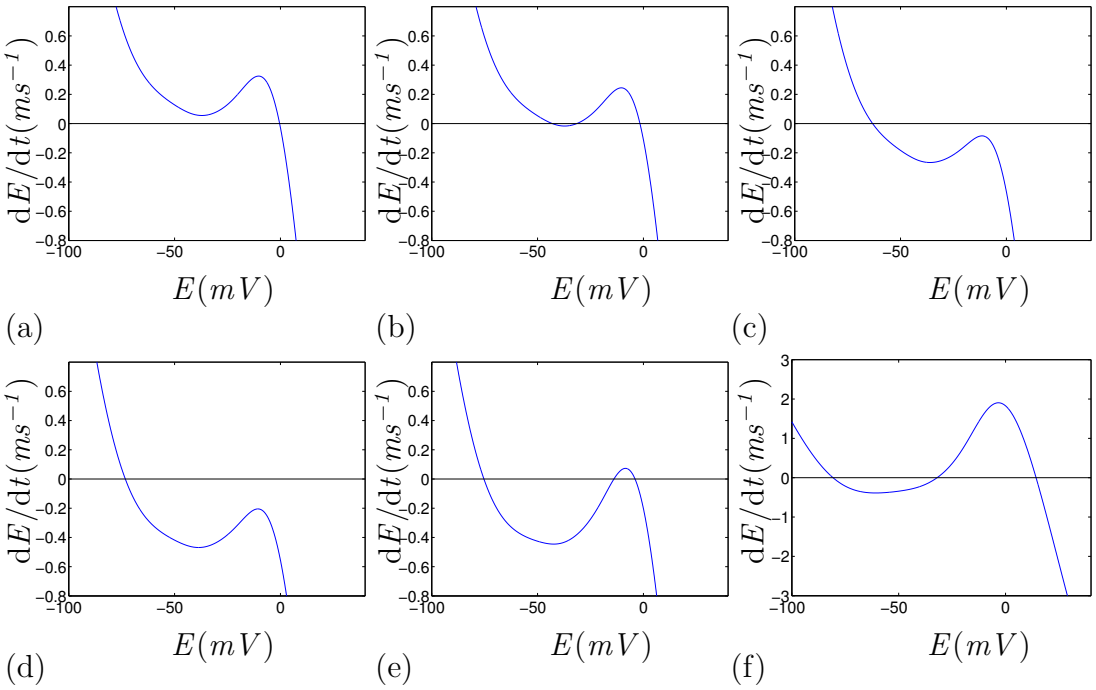

Figure 6.62: Graphs of $\frac{\mathrm{d}E}{\mathrm{d}t}$ in CRN-5a, system (6.36), against E for different points on the action potential corresponding to the following time (a) t=33, (b) t=48.4858, (c) t=100.3814, (d) t=201.8122, (e) t=252.7085 and (f) t=600.

We drew graphs of (f, x_r), (f, x_s) and (x_s, x_r) to see how they looked and this made us decide to eliminate x_r and x_s by replacing them with linear functions of f. We used the computer to approximate these two functions for us into a straight line. Figure 6.63 shows the graphs of (f, x_r), (f, x_s) and (x_s, x_r) with their approximations as well.

Our new approximations are:

$$\begin{aligned} x_r &= 0.5608(1-f), \\ x_s &= 0.2485(1-f). \end{aligned}$$

These are analogous to Krinsky and Kokoz's[8] approximation for $n + h$=G and also similiar to Vinet and Roberge's[47] approximation of x_1 in their paper. We notice a de-facto relationship between the variables and exploit it.

Therefore we have a new system CRN-3:

$$\begin{aligned} \frac{\mathrm{d}E}{\mathrm{d}t} &= -\frac{(I_1(E) + I_2(E, Cai, f))}{C_M}, \\ \frac{\mathrm{d}f}{\mathrm{d}t} &= \frac{\overline{f}(E) - f}{\tau_f(E)}, \end{aligned} \tag{6.37}$$

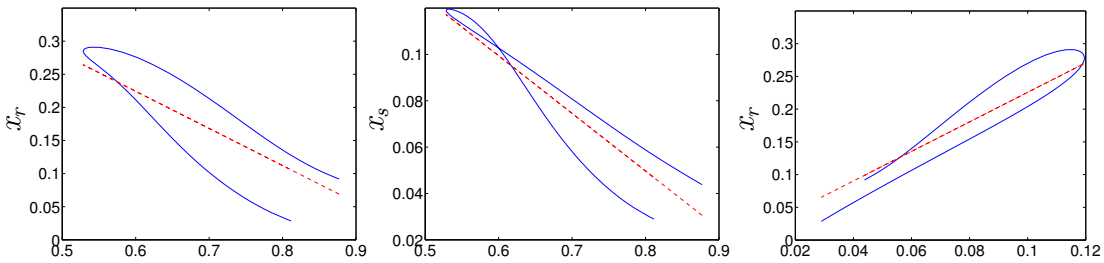

(a) (b) (c)

Figure 6.63: Graphs of CRN-5a, system (6.36), for the following variables with their approximations (a) (f, x_r) (-), x_r=0.5608$(1-f)$ (- -), (b) (f, x_s) (-), x_s=0.2485$(1-f)$ (- -) and (c) (x_s, x_r) (-), x_r=2.2567x_s (- -).

$$\begin{aligned}\frac{\mathrm{d}Cai}{\mathrm{d}t} &= \frac{(I_3(Cai)+I_4(E,Cai,f))}{2FV_iB2},\\ B2 &= 1+\frac{[Trpn]_{max}K_{m,Trpn}}{(Cai+K_{m,Trpn})^2}+\frac{[Cmdn]_{max}K_{m,Cmdn}}{(Cai+K_{m,Cmdn})^2},\end{aligned}$$

where

$$\begin{aligned}I_1(E) &= I_{to}(E,\overline{o}_a,\overline{o}_i)+I_{K1}(E)+I_{Kur}(E,\overline{u}_a)+I_{Na,K}(E)+I_{b,Na}(E),\\ I_2(E,Cai,f) &= C_M\Big(\frac{g_{Kr}x_r(f)(E-E_K)}{1+e^{\frac{(E+15)}{22.4}}}+g_{Ks}x_s^2(f)(E-E_K)\\ &\quad +g_{Ca,L}\overline{d}(E)f\overline{f}_{Ca}(Cai)(E-65.0)+I_{p,Ca(max)}\left(\frac{Cai}{0.0005+Cai}\right)\\ &\quad +\frac{ae^{kE}-b\,Cai\,e^{-mE}}{B(1+K_{sat}e^{-mE})}+g_{b,Ca}(E-E_{Ca})\Big),\\ I_3(Cai) &= 2FV_{up}(0.000496-I_{up})-I_{p,Ca},\\ I_4(E,Cai,f) &= C_M\Big(2\frac{ae^{kE}-b\,Cai\,e^{-mE}}{B(1+K_{sat}e^{-mE})}-g_{Ca,L}\overline{d}(E)f\overline{f}_{Ca}(Cai)(E-65.0)\\ &\quad -g_{b,Ca}(E-E_{Ca})\Big),\end{aligned}$$

where B=$(K_{m,Na}^3$+$Nao^3)(K_{m,Ca}$+$Cao)$, a=$I_{NaCa(max)}Nai^3Cao$, k=$\frac{\gamma F}{RT^o}$, b=Nao^3 and m=$\frac{(\gamma-1)F}{RT^o}$.

We now draw the solutions for our new system and compare them with the solutions from CRN-5a to see if they are different and if they are different, how different. We want to see how good this reduction is. So Fig. 6.64 shows the solutions for E, Cai, f, x_r and x_s for both systems.

We see that for the action potential there is a slight change for all the variables, so this reduction is not perfect, but it is still a good reduction. We draw

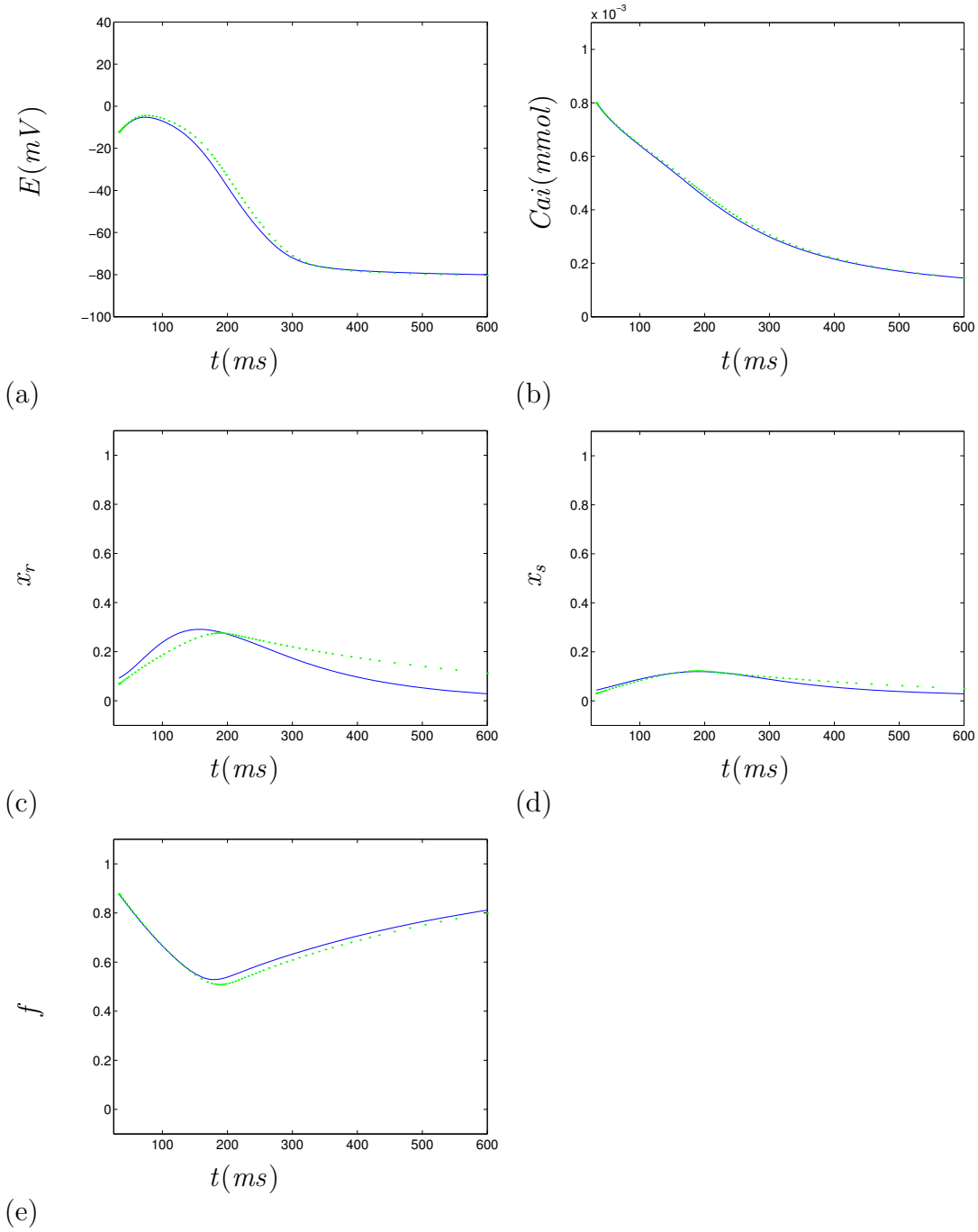

Figure 6.64: Graphs CRN-5a, system (6.36), (-) and CRN-3, system (6.37), (.) for the variables (a) E, (b) Cai, (c) x_r, (d) x_s and (e) f.

I_{ks} and I_{kr} to see how this approximation affects these two currents. Figure 6.65 shows that the curves from CRN-3, system (6.37), is different than the curves for CRN-5a, system (6.36), but they are not different by a lot, so this approximation is still a good approximation.

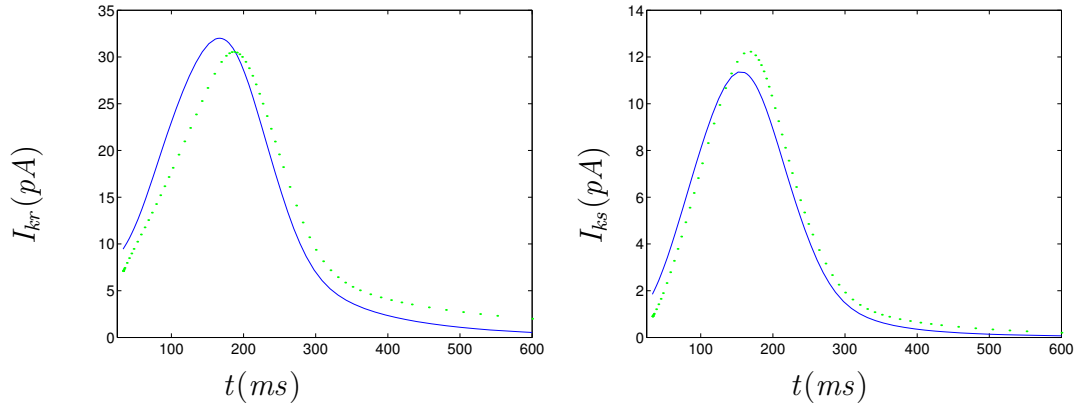

(a) (b)

Figure 6.65: Graphs CRN-5a, system (6.36), (-) and CRN-3, system (6.37), (.) for the currents (a) I_{kr} and (b) I_{ks}.

We draw the τ's for CRN-5 to see if there are any variables that are not intersecting with E, but we see from Fig. 6.66 that all τ's intersect with τ_E so we can't say that any are fast or slow variables.

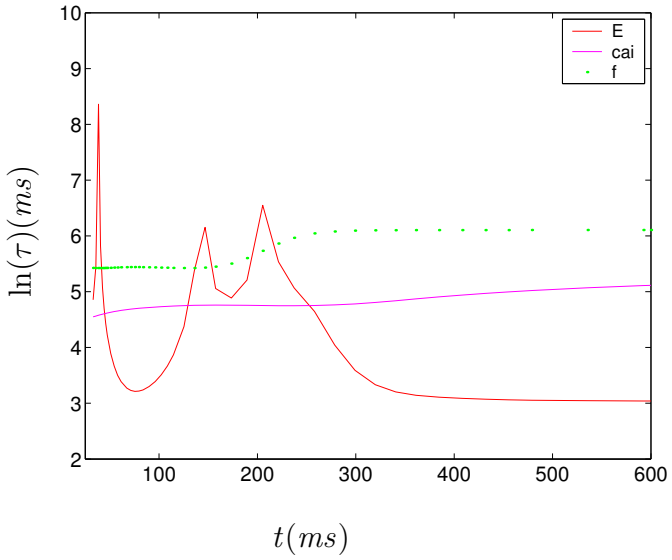

Figure 6.66: Graph of the τ's for system (6.37).

We don't draw the currents again as they look exactly the same as Fig. 6.65.

6.5.6 Replacing $\overline{f}$ and τ_f with a Heaviside function in CRN-3 (system (6.37))

We see from Fig. 6.67(a) that we can replace $\overline{f}$ with a Heaviside function in system (6.37).

The Heaviside function for $\overline{f}$ is:

$$\overline{f} = \theta(-E + E_f),$$

where E_f=−27.7206.

We see from Fig. 6.67(b) that we can also replace τ_f with a Heaviside function in system (6.37).

The Heaviside function for τ_f is:

$$\tau_f = 228 + 220.5993\,\theta(-E + E_f).$$

We draw the solutions of system (6.37) to see if there is any difference with this new replacement. We see that the solutions are slightly different from CRN-3's solutions (6.37) and $f(t)$ has a fracture point now instead of a curve because of introducing the Heaviside function to $\overline{f}$ and τ_f. Even though the solutions are not exactly the same they are still in a good region of percentage error for them to be acceptable.

Hence the analytical solutions for f are:

$$\begin{aligned} E < E_f: &\qquad f = \overline{f} + (f(t_2) - \overline{f})e^{-(t-t_2)/\tau_f}, \\ E > E_f: &\qquad f = f(t_2)e^{-(t-t_2)/\tau_f}. \end{aligned}$$

So we have a system of $(2 + 1)$ variables:

$$\begin{aligned} \frac{\mathrm{d}E}{\mathrm{d}t} &= -\frac{(I_1(E) + I_2(E, Cai, f))}{C_M}, \\ \frac{\mathrm{d}Cai}{\mathrm{d}t} &= \frac{(I_3(Cai) + I_4(E, Cai, f))}{2FV_iB2}, \\ B2 &= 1 + \frac{[Trpn]_{max}K_{m,Trpn}}{(Cai + K_{m,Trpn})^2} + \frac{[Cmdn]_{max}K_{m,Cmdn}}{(Cai + K_{m,Cmdn})^2}, \end{aligned} \tag{6.38}$$

where

$$I_1(E) = I_{to}(E, \overline{o}_a, \overline{o}_i) + I_{K1}(E) + I_{Kur}(E, \overline{u}_a) + I_{Na,K}(E) + I_{b,Na}(E),$$

$$
\begin{aligned}
I_2(E,Cai,f) &= C_M\Big(\frac{g_{Kr}x_r(f)(E-E_K)}{1+e^{\frac{(E+15)}{22.4}}} + g_{Ks}x_s^2(f)(E-E_K) \\
&\quad + g_{Ca,L}\overline{d}(E)f\overline{f}_{Ca}(Cai)(E-65.0) + I_{p,Ca(max)}\left(\frac{Cai}{0.0005+Cai}\right) \\
&\quad + \frac{ae^{kE}-b\,Cai\,e^{-mE}}{B(1+K_{sat}e^{-mE})} + g_{b,Ca}(E-E_{Ca})\Big), \\
I_3(Cai) &= 2FV_{up}(0.000496-I_{up}) - I_{p,Ca}, \\
I_4(E,Cai,f) &= C_M\Big(2\frac{ae^{kE}-b\,Cai\,e^{-mE}}{B(1+K_{sat}e^{-mE})} - g_{Ca,L}\overline{d}(E)f\overline{f}_{Ca}(Cai)(E-65.0) \\
&\quad - g_{b,Ca}(E-E_{Ca})\Big),
\end{aligned}
$$

where $B{=}(K^3_{m,Na}{+}Nao^3)(K_{m,Ca}{+}Cao)$, $a{=}I_{NaCa(max)}Nai^3Cao$, $k{=}\frac{\gamma F}{RT^o}$, $b{=}Nao^3$ and $m{=}\frac{(\gamma-1)F}{RT^o}$.

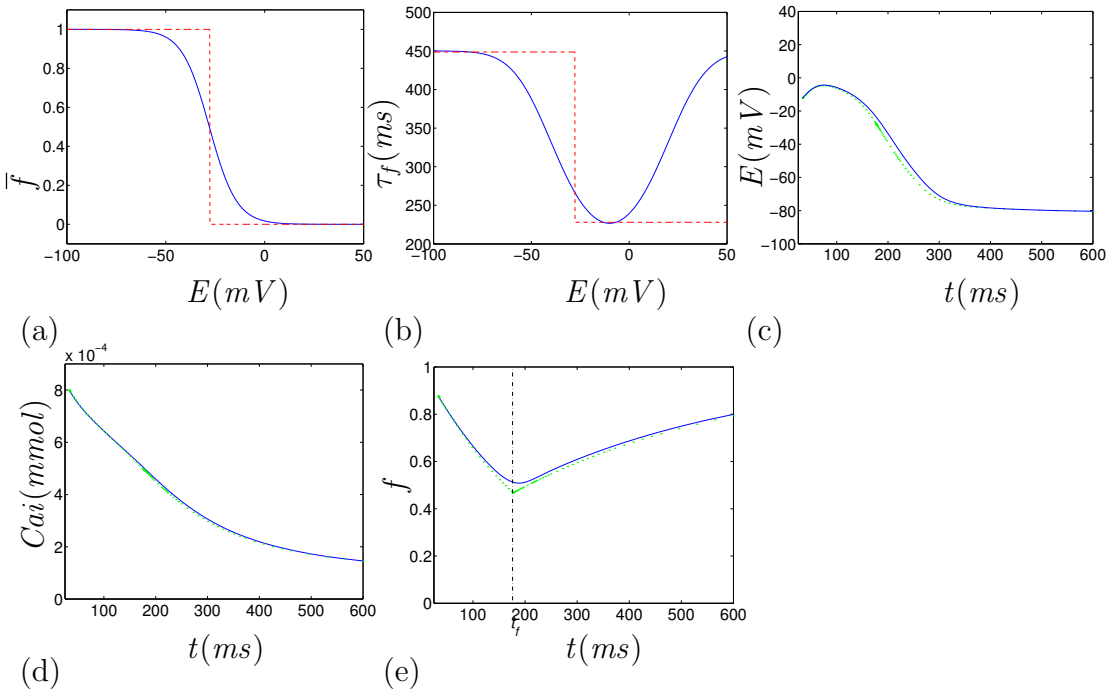

Figure 6.67: (a) Graph of original $\overline{f}$ (-) and Heaviside $\overline{f}$ (- -) for CRN-3, system (6.37). (b) Graph of original τ_f (-) and Heaviside τ_f (- -) for CRN-3. Graphs of CRN-3, with original τ_f, (-) and CRN-3, with Heaviside τ_f and $\overline{f}$, (.) for the variables (c) E, (d) Cai and (e) f.

6.5.7 Summary

The accurate system CRN-7, (6.34), was found by adiabatically eliminating the fast variables j, u and v. Even though CRN-7 is accurate we decided to carry on

reducing it to obtain a system of three variables. This system is less accurate, but can still be used because it is within a good percentage of accuracy.

We obtained a system of three variables CRN-3 (6.37) by adiabatically eliminating the fast variables and from this we were able to find a system of two equations, CRN-2 (6.38).

We were able to find a separate equation for $Carel$ because its differential equation could be separated and integrated, since $Carel$ doesn't affect the solutions of E.

6.6 Properties of Various Reduced Models with Respect to Numerical Simulations

We wanted to measure how successful our reduced systems for the intermediate and slow stages, CRN-6 (6.22) and CRN-7 (6.34) respectively, are compared to the original system. Even though these two systems can only be solved numerically, it is still progress from the original system, because it can be solved faster than the original system.

To check how much faster they are than the original system we have to use a crude, fixed-step "forward Euler solver", (FES). We use this because the FES allows us to control the time step, so we can make a fair comparison.

To test this we take four CRN systems, CRN-21, system (6.1), $[t_0, \infty]$, CRN-14, system (6.6), $[t_0, t_1]$, CRN-11, system (6.12), $[t_1, t_2]$, and CRN-7, system (6.34), $[t_2, \infty]$, and we test different time steps to see what effect it has on the system. We test to see, what is the biggest time step we can use for which each system will be stable, the numbers in table 6.2 are the biggest time step we can have before the system becomes unstable, i.e. at certain points we will have the solution going to infinity. To test to see what is the biggest time step we can have for the system to be accurate, we use the requirement that the time step will be taken for the FES solution to be the same as a high-accuracy Matlab ODE solver to the point that they differ by 1mV.

Table 6.2 shows the values for each system for which time step it was stable and for which time step it was accurate.

We used the FES solver for our comparison, because we wanted to make a fair comparison between the FES and the high-accuracy Matlab ODE solver. We also chose this solver because it is commonly used for modelling the behaviour

System	Stable	Accurate
CRN-21 (complete)	0.1	0.002
CRN-14 (without superfast variables)	0.2	0.004
CRN-11 (after the fast stage)	5	0.1
CRN-7 (the slow stage)	16	2

Table 6.2: Time steps, in ms, admissible for different versions of Courtemanche et al's model.

of excitable cells in cardiac tissue, as cardiac tissue is split up into different cells and to make sure that a fair experiment is being done to study each cell, then the time step in each cell must be the same. So if you reduce the time step in one cell, then you must reduce the time step in every cell and the FES allows you to do this.

Therefore the reduced models are the results of our research and we can see from table 6.2, that by using bigger steps, due to having different time stages, we have accelerated the numerical computations to be fifty times faster than the computations for the original model. So the reduced models can be used for more efficient numerical calculations, even if the analytical solutions are not feasible.

6.7 Main Results

Courtemanche et al's system of 21 equations has been reduced to a system of 14 equations by the following procedures:

Methods

1 Variables Nai, Ki, $Caup$ and u_i are super-slow, and are taken as their initial values. Variables m, u_a and w are super-fast, and are taken as their quasi-stationary values.

Results

- The 14 other variables satisfy system (6.6), CRN-14.

We have split the action potential solution into three time stages, fast intermediate and slow, which correspond to different asymptotic scales. The fast stage is where the sodium current is large. The intermediate stage is where the sodium current is over. The slow stage is where the intermediate stage is over, which happens if F_n reaches it threshold and $\overline{u}$ and τ_v switch from one value to another. The solutions for the three time stages are in the form of two tier answers, i.e. an accurate solution and a less accurate solution, where variables and functions are approximated. For the accurate solution we have used asymptotic methods, e.g. singular perturbation method, and for the less accurate solution we have used non-asymptotic methods, e.g. iterations, which produces cruder results.

The fast stage is for $[t_0, t_1]$. We consider t_0=0 and t_1=1.2 as this is where the sodium current is large. The intermediate stage is for $[t_1, t_2]$. We consider t_1=1.2 and t_2=33 as this is where F_n reaches its threshold. The slow stage is for $[t_2, \infty]$. We consider t_2=33 as this is where the intermediate stage is over for our selected initial conditions.

Methods for the accurate solution for the fast stage

2 Variables Cai, $Carel$, j, o_i, x_r, x_s, f, f_{Ca}, u and v are slow and are taken as their initial values.

Results for the accurate solution for the fast stage

- The four other variables, E, h, o_a and d, satisfy the system (6.9), CRN-4.

Methods for the less accurate solution for the fast stage

3 Quasi-stationary values $\overline{h}$ and $\overline{m}$ are stepwise functions and are replaced with $\overline{h}$=$\theta(E_h - E)$ and $\overline{m}$=$\theta(E - E_m)$, where E_h=−66.6 and E_m=−32.7.

Results for the less accurate solution for the fast stage

- For general $\tau_h(E)$, for $E < E_m$, the explicit solution for h is:

$$h = \overline{h} + (h_0 - \overline{h})e^{-(T-T_0)/\tau_h(E)}.$$

- For general $\tau_h(E)$, for $E > E_m$, the quadrature solution for h is:

$$h = h_0 + \frac{1}{A}\int_{E_0}^{E} \frac{1}{\tau_h(E)(E - E_{Na})}\mathrm{d}E,$$

where A=$g_{Na}j$=7.6245 corresponding to the initial conditions.

- Function $\tau_h(E)$ can be approximated with a constant, which is chosen for E=E_{Na}, $\tau_h(E_{Na})$=0.1301, and the explicit and quadrature solutions are:

$$\begin{aligned} h(E) &= \frac{1}{\tau_h(E_{Na})A}\ln\left(\frac{|E-E_{Na}|}{|E_0-E_{Na}|}\right)+h_0, \\ E(T) &= -(E_0-E_{Na})e^{(A\tau_h(E_{Na})h_0 e^{-\frac{(T-T_0)}{\tau_h(E_{Na})}}-A\tau_h(E_{Na})h_0)}+E_{Na}, \\ o_a &= o_{a_0}+\int_{T_0}^{T}\frac{\overline{o}_a(T)}{\tau_{o_a}(T)}\mathrm{d}T, \\ d &= d_0+\int_{T_0}^{T}\frac{\overline{d}(T)}{\tau_{o_a}(T)}\mathrm{d}T. \end{aligned}$$

4 If $T\to\infty$, $E_\infty(E_0)\approx 33.9247$ for τ_h=constant, and the values for $\overline{o}_a$, $\overline{d}$, τ_{o_a} and τ_d at E_∞ are $\overline{o}_a$=0.9569, τ_{o_a}=1.4467, $\overline{d}$=0.9959, τ_d=0.6493, which are found analytically.

- Variables o_a and d have a quadrature solution for a short interval of time $[t_0, 0.12]$:

$$\begin{aligned} o_a &= \overline{o}_a+(o_{a_0}-\overline{o}_a)e^{\int_{T_0}^{T}1/\tau_{o_a}(T)\mathrm{d}T}, \\ d &= \overline{d}+(d_0-\overline{d})e^{\int_{T_0}^{T}1/\tau_d(T)\mathrm{d}T}. \end{aligned}$$

- Variables o_a and d have an explicit solution for a long interval of time $[0.12, t_1]$:

$$\begin{aligned} o_a &= \overline{o}_a+(o_{a_0}-\overline{o}_a)e^{-(T-T_0)/\tau_{o_a}}, \\ d &= \overline{d}+(d_0-\overline{d})e^{-(T-T_0)/\tau_d}. \end{aligned}$$

Methods for the accurate solution for the intermediate stage

5 Variables h, o_a and d are fast, and are taken as their quasi-stationary values. Current I_{Na} is zero due to either $\overline{m}^3$ or $\overline{h}$ being zero. Variables f, x_r, and x_s are slow, and are taken as their initial values. Gating variables u and v are explicit functions of t.

$$u=1-e^{-t/\tau_u}, \qquad v=e^{-t/\tau_v},$$

where τ_u=8 and τ_v=$2+2\theta(F_n-F_1)\approx 4$.

Current I_{rel} is replaced with $k_{rel}u^2v\overline{w}Carel$.

6 Minor currents I_{K1}, I_{Kr}, I_{Ks}, I_{NaCa}, and I_{tr} can be replaced with zero and some other currrents with constants, $I_{Na,K}$=22.4544, $I_{p,Ca}$=17.7916, $I_{b,Na}$=−5.3323, $I_{b,Ca}$=−12.7536 and I_{up}=$3.2 * 10^{-3}$. These values were found numerically.

Results for the accurate solution for the intermediate stage

- The six variables satisfy system (6.23), CRN-6.

Method and result for the less accurate solution for the intermediate stage

7 CRN-6 can be replaced by an iteration procedure, by a sequence of eight equations, (6.26), of which seven can be solved in quadratures, and only one needs to be solved numerically.

Methods for the accurate solution for the slow stage

8 Variables f_{Ca}, j, u and v are fast, and are taken as their quasi-stationary values and $\overline{u}$=0 and $\overline{v}$=1.

Results for the accurate solution for the slow stage

- The seven other variables satisfy the system (6.34), CRN-7.

Methods for the less accurate solution for the slow stage

9 Variable o_i is fast, and is taken as its quasi-stationary value.

10 Variable $Carel(t)$ has a solution in quadratures:

$$\int_{Carel_0}^{Carel} \frac{(1+\frac{A}{(Carel+B)^2})}{Caup-Carel}\mathrm{d}Carel = \int_{t_0}^{t} \frac{1}{\tau_{tr}}\mathrm{d}t,$$

and it can be approximated by iterations:

$$Carel(t) = -0.15851G(t) + 0.8557,$$

where

$$G(t) = \ln|(Carel-Caup)^{\frac{(p^2+A)}{p^2}}(Carel+B)^{\frac{q}{p^2BCaup}}| + \frac{A}{p(Carel+B)}.$$

11 Variables x_r and x_s are approximated as functions of f; x_r=$0.5608(1-f)$ and x_s=$0.2485(1-f)$.

12 Functions $\overline{f}$ and τ_f are stepwise functions and are replaced with $\overline{f}$=$\theta(-E+E_f)$ and τ_f=$228+220.5993\theta(-E+E_f)$, where E_f=-27.7206.

Results for the less accurate solution for the slow stage

- The $(2+1)$ variables satisfy the system (6.38).

6.7.1 Hierarchy of small parameters for Courtemanche et al's model

In this formal embedding we can summarise all asymptotic methods that we have applied to the CRN-21 system, as opposed to non-asymptotic methods, e.g. iterations and empiric relationships. Therefore we obtain the reduced systems for the three different time stages, fast, intermediate and slow. The hierarchy system below shows how CRN-21 is reduced for each time stage using small parameters, ϵ_j.

The dependence of ϵ_5 in some of the currents represents the cases where we have not been able to obtain an explicit asymptotic embedding. Instead we have used an axiomatic approach to introduce ϵ_5 to the currents to reduce the number of currents in the equations, and to be able to obtain a solution for the CRN model.

$$
\begin{aligned}
\frac{\mathrm{d}E}{\mathrm{d}t} &= -\frac{I_{ion}}{C_M},\\
I_{ion} &= \frac{1}{\epsilon_3}I_{Na}(E,m,h,j) + I_{K1}(E,Ki;\epsilon_5) + I_{to}(E,Ki,o_a,o_i)\\
&\quad + I_{Kur}(E,Ki,u_a,u_i) + I_{Kr}(E,Ki,x_r;\epsilon_5) + I_{Ks}(E,Ki,x_s;\epsilon_5)\\
&\quad + I_{Ca,L}(E,d,f,f_{Ca}) + I_{p,Ca}(Cai;\epsilon_5) + I_{Na,K}(E,Nai;\epsilon_5)\\
&\quad + I_{NaCa}(E,Nai,Cai;\epsilon_5) + I_{b,Na}(E,Nai;\epsilon_5) + I_{b,Ca}(E,Cai;\epsilon_5),\\
\frac{\mathrm{d}u_i}{\mathrm{d}t} &= \epsilon_1\epsilon_5\frac{\overline{u}_i(E)-u_i}{\tau_{u_i}(E)},\\
\frac{\mathrm{d}Nai}{\mathrm{d}t} &= \epsilon_1\epsilon_5(FV_i)^{(-1)}(-3I_{NaK}(E,Nai) + 3I_{NaCa}(E,Nai,Cai)\\
&\quad + I_{b,Na}(E,Nai) + I_{Na}(E,m,h,j)),
\end{aligned}
$$

ϵ	Description
1	distinguishes the super-slow variables from the slow variables, CRN-21 $\rightarrow$ CRN-17 (6.4),
2	distinguishes the super-fast variables from the fast variables, CRN-17 $\rightarrow$ CRN-14 (6.6),
3	distinguishes the fast variables from the intermediate variables, CRN-14 $\rightarrow$ CRN-4 (6.9), and CRN-14 $\rightarrow$ CRN-11 (6.12),
4	sharpness of u and v dependence on Ca flux, small constant a in CRN-11, (6.12), replacement of $\overline{u}$, $\overline{v}$ and τ_v with piecewise functions,
5	distinguishes the intermediate variables from the slow variables, CRN-11 $\rightarrow$ CRN-8, (6.21) and CRN-11 $\rightarrow$ CRN-7 (6.34),
6	sharpness of f dependence on E in CRN-3, (6.38), replacement of $\overline{f}$ and τ_f with piecewise functions.

Table 6.3: Description of the ϵ's and where they are used in Courtemanche et al's model.

$$
\begin{aligned}
\frac{\mathrm{d}Ki}{\mathrm{d}t} &= \epsilon_1\epsilon_5((FV_i)^{(-1)}(2I_{NaK}(E,Nai) - I_{K1}(E,Ki) - I_{to}(E,Ki,o_a,o_i) \\
&\quad -I_{Kur}(E,Ki,u_a,u_i) - I_{Kr}(E,Ki,x_r) - I_{Ks}(E,Ki,x_s) \\
&\quad -I_{b,K}(E,Ki))), \\
\frac{\mathrm{d}Caup}{\mathrm{d}t} &= \epsilon_1\epsilon_5(I_{up}(Cai) - I_{up,leak}(Caup) - I_{tr}(Caup,Carel)\frac{V_{rel}}{V_{up}}), \\
\frac{\mathrm{d}m}{\mathrm{d}t} &= \frac{1}{\epsilon_2\epsilon_3}\frac{\overline{m}(E;\epsilon_3) - m}{\tau_m(E)}, \qquad \overline{m}(E;0) = \theta(E - E_m), \\
\frac{\mathrm{d}u_a}{\mathrm{d}t} &= \frac{1}{\epsilon_2\epsilon_3}\frac{\overline{u}_a(E) - u_a}{\tau_{u_a}(E)}, \\
\frac{\mathrm{d}w}{\mathrm{d}t} &= \frac{1}{\epsilon_2\epsilon_3}\frac{\overline{w}(E) - w}{\tau_w(E)}, \\
\frac{\mathrm{d}h}{\mathrm{d}t} &= \frac{1}{\epsilon_3}\frac{\overline{h}(E;\epsilon_3) - h}{\tau_h(E)}, \qquad \overline{h}(E;0) = \theta(E_h - E), \\
\frac{\mathrm{d}o_a}{\mathrm{d}t} &= \frac{1}{\epsilon_3}\frac{\overline{o}_a(E) - o_a}{\tau_{o_a}(E)}, \\
\frac{\mathrm{d}d}{\mathrm{d}t} &= \frac{1}{\epsilon_3}\frac{\overline{d}(E) - d}{\tau_d(E)}, \\
\frac{\mathrm{d}u}{\mathrm{d}t} &= \frac{\overline{u}(F_n;\epsilon_4) - u}{\tau_u}, \qquad \overline{u}(F_n;0) = \theta(F_n - F_1), \\
\frac{\mathrm{d}v}{\mathrm{d}t} &= \frac{\overline{v}(F_n;\epsilon_4) - v}{\tau_v(F_n;\epsilon_4)}, \qquad \overline{v}(F_n;0) = \theta(F_n - F_2), \\
&\qquad\qquad\qquad\quad \tau_v(F_n;0) = 2 + 2\theta(F_n - F_1),
\end{aligned}
$$

$$
\begin{aligned}
\frac{\mathrm{d}x_r}{\mathrm{d}t} &= \epsilon_5 \frac{\overline{x}_r(E) - x_r}{\tau_{x_r}(E)}, \\
\frac{\mathrm{d}x_s}{\mathrm{d}t} &= \epsilon_5 \frac{\overline{x}_s(E) - x_s}{\tau_{x_s}(E)}, \\
\frac{\mathrm{d}f}{\mathrm{d}t} &= \epsilon_5 \frac{\overline{f}(E;\epsilon_6) - f}{\tau_f(E;\epsilon_6)}, \qquad \overline{f}(E;0) = \theta(E_f - E), \\
& \qquad\qquad\qquad\qquad \tau_f(E;0) = 228 + 220.5993\theta(E_f - E), \\
\frac{\mathrm{d}j}{\mathrm{d}t} &= \frac{\overline{j}(E) - j}{\tau_j(E)}, \\
\frac{\mathrm{d}f_{Ca}}{\mathrm{d}t} &= \frac{\overline{f}_{Ca}(Cai) - f_{Ca}}{\tau_{f_{Ca}}}, \\
\frac{\mathrm{d}o_i}{\mathrm{d}t} &= \frac{\overline{o}_i(E) - o_i}{\tau_{o_i}(E)}, \\
\frac{\mathrm{d}Cai}{\mathrm{d}t} &= \frac{B1}{B2}, \\
B1 &= (2FV_i)^{(-1)}(2I_{NaCa}(E, Nai, Cai; \epsilon_5) - I_{p,Ca}(Cai; \epsilon_5) \\
&\quad -I_{Ca,L}(E, d, f, f_{Ca}) - I_{b,Ca}(E, Cai; \epsilon_5)) \\
&\quad +(V_i)^{(-1)}(V_{up}(I_{up,leak}(Caup) - I_{up}(Cai; \epsilon_5)) \\
&\quad +I_{rel}(Cai, Carel, u, v, w)V_{rel}; \epsilon_5), \\
B2 &= 1 + \frac{[Trpn]_{max}K_{m,Trpn}}{(Cai + K_{m,Trpn})^2} + \frac{[Cmdn]_{max}K_{m,Cmdn}}{(Cai + K_{m,Cmdn})^2}, \\
\frac{\mathrm{d}Carel}{\mathrm{d}t} &= \frac{(I_{tr}(Caup, Carel; \epsilon_5) - I_{rel}(Cai, Carel, u, v, w; \epsilon_5))}{\left(1 + \frac{[Csqn]_{max}K_{m,Csqn}}{(Carel + K_{m,Csqn})^2}\right)},
\end{aligned}
$$

where

$$
\begin{aligned}
F_n &= 10^{-12}V_{rel}I_{rel}(Cai, Carel, u, v, w) \\
&\quad -\frac{5 * 10^{-13}}{F}\left(\frac{1}{2}I_{Ca,L}(E, d, f, f_{Ca}) - \frac{1}{5}I_{Na,Ca}(E, Nai, Cai)\right), \\
\overline{u} &= (1 + He^{-F_n/\epsilon_4 a})^{-1}, \\
\overline{v} &= 1 - (1 + Ge^{-F_n/\epsilon_4 a})^{-1}, \\
F_1 &= \epsilon_4 a \ln G, \\
F_2 &= \epsilon_4 a \ln H.
\end{aligned}
$$

Chapter 7

Conclusion

We now conclude all the results in this thesis together. We deal with excitable systems of equations that are used to describe action potentials of cardiac and nerve tissues.

We have investigated two classical models, the Hodgkin-Huxley model and Noble's 1962 model, which is a modification of Hodgkin-Huxley's model. As this is the case we would expect their asymptotic structures to be similar, but they are not. We see from studying the asymptotic structure in both the Hodgkin-Huxley and Noble systems, that each system has a different number of fast and slow variables compared to each other. In the Hodgkin-Huxley model we have two fast variables and two slow variables, whereas Noble's model has one super-fast, two fast and one slow variable. Since we have a different number of slow variables we have a different geometry of the slow manifold. In Hodgkin-Huxley's model we have a two-dimensional slow manifold and the fast foliation is a two-parameter set of planes h=const and n=const. In Noble's model we have a one-dimensional slow manifold and a two-dimensional fast foliation, which consists of planes.

We had to introduce artificial small parameters ϵ to both models, by using the method of parametric embedding, so that we could consider Tikhonov's method for fast-slow systems of equations, to obtain the slow manifold and fast foliation. This is because both models do not contain small parameters that we can tend to zero. For the Hodgkin-Huxley model we had a one-parameter embedding as we only introduced the small parameter to the fast equations, and for Noble's model we had a two parameter embedding as we introduced parameters to the super-fast and fast equations.

We see from the reductions in both the Hodgkin-Huxley and Noble's models that for the original models we have a smooth return from the action poten-

tials, but as soon as we consider the limit on the small parameters, ϵ_1 and ϵ_2, approaching zero we lose the smooth returns and obtain jump returns. This is an inevitable consequence of representing our systems in the standard form of Tikhonov's fast-slow systems.

Also we conclude that Hodgkin-Huxley's model is similar to Zeeman's "nerve" model, because the reduced Hodgkin-Huxley model has an asymptotic structure of one fast variable and two slow variables, which is the same asymptotic structure as Zeeman's "nerve" model. We chose to draw the solution of the Hodgkin-Huxley model as a three-dimensional phase portrait, and the geometry of both phase portraits is the same because they both contain a two-dimensional surface, which represents the slow manifold; they both have a two-parameter set of planes that represent the fast foliation, and they both have a fold curve that projects a cusp down the z-axis.

The difference between both models is where Zeeman's hypothesis for the cusp catastrophe is concerned. We have partly confirmed Zeeman's hypothesis as the phase portrait shows that a cusp was obtained for this model, as stated above, but the trajectories do not travel around the cusp point. Therefore we obtained a jump return, whereas Zeeman hypothesised the opposite with a smooth return, and this is the part that hasn't been confirmed and the difference between both models. Therefore the hypothesis fails here due to the system exhibiting a jump return. Also we conclude that Noble's model is similar to Zeeman's "heart" model.

We then considered a non-Tikhonov embedding method to study Noble's model, because some qualitative features were not correctly reproduced in the Tikhonov embedding, such as the smooth return. This non-Tikhonov embedding was derived to achieve a smooth return in the reduced model. This method was to consider the fast variables E and h of the reduced model and introduce the parametric embedding to the $\dot{E}$ and $\dot{h}$ equations; for E we only introduced $1/\epsilon$ to the fast sodium current and not to any of the other currents. Whereas for Noble's model, using Tikhonov's approach, we introduced $1/\epsilon$ as a factor of the whole of the right-hand side of the $\dot{E}$ equation. Also, we noticed that the sodium current gates exhibit near perfect switch behaviour and therefore we replaced the sodium gates' quasi-stationary values with Heaviside functions.

This then lead to the following mathematical features in the asymptotic analysis. These features are that E is both a fast and slow variable, but not at the

same time, and the equilibria in the fast subsystem are not isolated. These are features of the non-Tikhonov embedding.

Therefore from analysing this embedding we found that we did retain the qualitative properties of the system, fast onset and smooth return. Since we are mostly interested in excitable systems, we have applied this method to an excitable variant of Noble's model as well as the original oscillatory variant.

We saw that the phase portrait for the slow system, for the non-Tikhonov embedding of the excitable version of Noble's model, is similar to the phase portrait for Tikhonov's embedding for the excitable version of Noble's model. We found that both E nullclines have a branch in the complex plane and that the trajectories travel to the stable equilibrium point, but the one difference between the two variants is that the reduced model in the variant using Tikhonov's embedding does not retain its smooth return and instead has a jump return to equilibrium. In the phase portrait, for the variant using Tikhonov's embedding, this corresponded to an almost vertical jump from the stable piece of the nullcline to the unstable piece, whereas for the variant using the non-Tikhonov embedding we retain the smooth return as in the original model. We also saw that for the fast system, for the non-Tikhonov variant, we have a line of equilibria not an equilibrium point and this implies that each of these equilibria has one zero eigenvalue and therefore are not asymptotically stable.

We conclude the results for Courtemanche et al's system of 21 equations. Courtemanche et al's system was reduced to a system of 14 equations, CRN-14, by eliminating the super-fast and super-slow variables by using a standard Tikhonov embedding. Then we discovered that the system could be split up into three different time scales, according to the speed of the remaining variables at different parts of the action potential. After this we used the same non-Tikhonov embedding that we used in Noble's excitable model to deal with the fast sodium current here, which we called the sodium embedding.

With these separate time stages we have reduced the system further. So for the fast stage we have reduced CRN-14 to CRN-4, which has a $(2 + 2)$ structure, because we had two equations that didn't affect the voltage equation, but the voltage equation affected them, e.g. the two equations were functions of voltage, but voltage wasn't a function of them. So we could then describe CRN-4's properties by using a two-dimensional phase portrait, which is similar to the phase portrait for the fast embedding for Noble's excitable model. Also

we have found analytical solutions for the trajectories for CRN-4 by replacing τ_h with various functions of voltage. We replaced τ_h with a constant and found analytical solutions for voltage and the gating variable h, and then we found analytical solutions and solutions in quadratures for the gating variables o_a and d. The solutions for o_a and d depends on what the values are for the quasi-stationary and τ terms at different time intervals along the fast stage, because for certain time intervals we can either have analytical solutions or solutions in quadratures.

Once the fast stage is over we have the intermediate stage which starts with CRN-11, where all the fast variables are replaced with their quasi-stationary values. We found that CRN-11 contained a calcium subsystem, and from this subsystem we obtained phase portraits that were similar to the phase portraits for Zeeman's "nerve" model and Hodgkin-Huxley's model. These phase portraits contained a surface, which represented the slow manifold, a fold curve and trajectories that travel around the fold curve and the surface representing a smooth return. The differences between the calcium phase portraits and Zeeman's "nerve" model and Hodgkin-Huxley's model, is that they involve completely different variables, which describe different processes, and for the calcium model we do have a cusp projected to the $(K, I_{Ca,L})$ plane, but instead of being in a 3/2 parabola shape, we have a right angle shape. This is because we treat the small parameter a to be zero. If the parameter is considered positive then the cusp can be seen in the standard 3/2 parabola shape.

CRN-11 was reduced to CRN-6 with accuracy, and CRN-1 with less accuracy, as we did some regular perturbations and non-asymptotic approximations to CRN-6, which resulted with solutions in quadratures of all the equations in this system except one. Then the slow stage started after the intermediate stage, this is where F_n exceeds its threshold and $\overline{u}$ and τ_v switch from one value to another. System CRN-11 was used for this stage and it was reduced to CRN-7 with accuracy, and CRN-3 with less accuracy, as we did some regular perturbations and non-asymptotic approximations to CRN-7, which resulted with a solution in quadratures and an empirical approximation of two of the variables. CRN-11 is used for both the intermediate and slow time stages, because each time stage has different sets of fast and slow variables.

Therefore each time stage was reduced to an accurate system of equations, and to a less accurate system of equations that is within 10% accuracy of the

original system, by using a six-parametric embedding. We were able to reduce the systems even further, but the results were not as accurate as the original Courtemanche et al system, but still retained the qualitative behaviour.

So we have seen that by using Tikhonov, and non-Tikhonov methods solutions can be obtained for a more complicated system of equations that are used to describe cardiac activity.

Bibliography

[1] M. Courtemanche, R. J. Ramirez, and S. Nattel. Ionic mechanisms underlying human atrial action potential properties: Insights from a mathematical model. *Am J Physiol Heart Circ Physiol*, 275:H301–H321, 1998.

[2] A. L. Hodgkin and A. F. Huxley. A quantitative description of membrane current and its application to conduction and excitation in nerve. *J. Physiol.*, 117:500–544, 1952.

[3] D. Noble. A modification of the Hodgkin-Huxley equations applicable to Purkinje fibre action and pace-maker potentials. *J. Physiol.*, 160:317–352, 1962.

[4] R. FitzHugh. Impulses and physiological states in theoretical models of nerve membrane. *Biophys J*, 1:445–456, 1961.

[5] A. N. Tikhonov. Systems of differential equations, containing small parameters at the derivatives. *Mat. Sbornik*, 31(3):575–586, 1952.

[6] E. C. Zeeman. *Differential Equations for the Heartbeat and Nerve Impulse.* Mathematics Institute, University Of Warwick, Coventry, 1972.

[7] E. C. Zeeman. *Catastrophe Theory. Selected Papers 1972-1977.* Addison-Wesley, Reading, MA, 1977.

[8] V. I. Krinsky and Yu. M. Kokoz. Analysis of equations of excitable membranes I: Reduction of the Hodgkin-Huxley equations to a second order system. *Biofizika*, 18(3):506–511, 1973.

[9] V. I. Krinsky and Yu. M. Kokoz. Analysis of equations of excitable membranes II: Method of analysing the elextrophysiological characteristics of the Hodgkin-Huxley membrane from graphs of the zero-isoclines of a second order system. *Biofizika*, 18(5):887–885, 1973.

[10] V. I. Arnold, V. S. Afrajmovich, Yu. S. Il'yashenko, and L. P. Shil'nikov. *Dynamical Systems V, Bifurcation Theory And Catastrophe Theory*. Springer-Verlag, 1994.

[11] A Sjöberg and E Pärt-Enander. *The Matlab* 5 *Handbook*. Prentice Hall, 1999.

[12] D. Noble. Modelling the heart: Insights, failures and progress. *BioEssays*, 24(12):1155–1163, 2002.

[13] E. Marder and A. Prinez. Modelling stability in neuron and network function: The role of activity in homeostasis. *BioEssays*, 24(12):1145–1154, 2002.

[14] R. E. McAllister, D. Noble, and R. W. Tsien. Reconstruction of the electrical activity of cardiac Purkinje fibres. *J. Physiol*, 251:1–59, 1975.

[15] H. Reuter. The dependence of the slow inward current in Purkinje fibres on the extracellular calcium concentration. *J. Physiol*, 192:479–492, 1967.

[16] L. Ebihara and E. A. Johnson. Fast sodium current in cardiac muscle. *Biophys J*, 32:779–790, 1980.

[17] D. DiFrancesco and D. Noble. A model of cardiac electrical activity incorporating ionic pumps and concentration changes. *Phil. Trans. R. Soc. Lond. B*, 307:353–398, 1985.

[18] D. W. Hilgemann and D. Noble. Excitation-contraction coupling and extracellular calcium transients in rabbit atrium: Reconstruction of basic cellular mechanisms. *Proc. R. Soc. Lond. B*, 230:163–205, 1987.

[19] J. P. Drouhard and F. A. Roberge. Revised formulation of the Hodgkin-Huxley representation of the sodium current in cardiac cells. *Comp. Biomed. Res.*, 20(4):333–350, 1987.

[20] G. W. Beeler and H. Reuter. Reconstruction of the action potential of ventricular myocardial fibers. *J. Physiol.*, 268:177–210, 1977.

[21] Y. E. Earm and D. Noble. A model of the single atrial cell: Relation between calcium current and calcium release. *Proc. R. Soc. Lond. B*, 240:83–96, 1990.

[22] C. H. Luo and Y. Rudy. A model of the ventricular cardiac action potential: Depolarization, repolarization, and their interaction. *Circ. Res*, 68(6):1501–1526, 1991.

[23] C. H. Luo and Y. Rudy. A dynamic model of the cardiac ventricular action potential I: Simulations of ionic currents and concentration changes. *Circ. Res*, 74(6):1071–1097, 1994.

[24] C. H. Luo and Y. Rudy. A dynamic model of the cardiac ventricular action potential II: Afterdepolarizations, triggered activity and potentiation. *Circ. Res*, 74(6):1097–1113, 1994.

[25] J. Zeng, K. R. Laurita, D. S. Rosenbaum, and Y. Rudy. Two components of the delayed rectifier K^+ current in ventricular myocytes of the guinea pig type: Theoretical formulation and their role in repolarization. *Circ . Res*, 77(1):140–152, 1995.

[26] P. C. Viswanathan, R. M. Shaw, and Y. Rudy. Effects of i_{Kr} and i_{Ks} heterogeneity on action potential duration and it's rate dependence: A simulation study. *Circulation*, 99:2466–2474, 1999.

[27] G. M. Faber and Y. Rudy. Action potential and contractility changes in $[Nai^+]_i$ overloaded cardiac myocytes: A simulation study. *Biophys J*, 78(5):2392–2404, 2000.

[28] A. Nygren, L. J. Leon, and W. R. Giles. Simulations of the human atrial action potential. *Phil. Trans. R. Soc. Lond. A*, 359:111–1125, 2001.

[29] A. Nygren, C. Fiset, L. Firek, J. W. Clark, D. S. Lindblad, R. B. Clark, and W. R. Giles. Mathematical model of an adult human atrial cell: The role of K^+ currents in repolarization. *Circ Res*, 82:63–81, 1998.

[30] D. Noble, A. Varghese, P. Kohl, and P. Noble. Improved guinea-pig ventricular cell model incorporating a diadic space i_{Kr} and i_{Ks}, and length-and tension-dependent processes. *Can J Cardiol*, 14(1):123–134, 1998.

[31] J. R. Clay. Excitability of the squid giant axon revisited. *J. Neurophysiol*, 80(2):903–913, 1998.

[32] D. Noble and Y. Rudy. Models of cardiac ventricular action potentials: Iterative interaction between experiment and simulation. *Phil. Trans. R. Soc. Lond. A*, 359:1127–1142, 2001.

[33] D. Noble. *The Initiation Of The Heartbeat*. Oxford University Press, 1975.

[34] R. FitzHugh. Thresholds and plateaus in the Hodgkin-Huxley nerve equations. *J Gen Physiol*, 43:867–896, 1960.

[35] L. S. Pontryagin. The asymptotic behaviour of systems of differential equations with a small parameter multiplying the highest derivatives. *Izv. Akad. Nauk SSSR, Ser. Mat.*, 21(5):605–626, 1957.

[36] W. R. Wasow. *Asymptotic Expansions For Ordinary Differential Equations*. Interscience, New York, 1965.

[37] A. B. Vasil'eva, V. F. Butuzov, and L. V. Kalachev. *The Boundary Function Method For Singular Perturbation Problems*. SIAM, 1995.

[38] B. A. Dubrovin, Formenko A. T., and Novikov S. P. *Modern Geometry-Methods And Applications: Part II: Geometry And Topology Of Manifolds*. Springer-Verlag, 1985.

[39] V. I. Arnold. *Ordinary Differential Equations*. The MIT Press, 1973.

[40] J. Guckenheimer and Yu. Ilyashenko. The duck and the devil: Canards on the staircase. *Moscow Mathematical Journal*, 1(1):27–47, 2001.

[41] V. I. Arnold, S. M. Gusein-Zade, and A. N. Varchenko. *Singularities Of Differentiable Maps Volume I*. Birkhäuser, 1985.

[42] V. I. Krinsky and Yu. M. Kokoz. Analysis of equations of excitable membranes III: Membrane of the Purkinje fibre. reduction of the Noble equations to a second order system. analysis of automation by the graphs of zero-isoclines. *Biofizika*, 18(6):1067–1073, 1973.

[43] V. I. Krinsky and Yu. M. Kokoz. Analysis of equations of excitable membranes IV: Use of the method of zero-isoclines for analysing the membrane of the Purkinje fibre (anodic and cathodic stimulation, extrasystoles). *Biofizika*, 19(3):493–497, 1974.

[44] C. Meunier. Two and three-dimensional reductions of the Hodgkin-Huxley system: Separation of tine scales and bifurcation schemes. *Biol. Cybern*, 67(5):461–468, 1992.

[45] G. S. Cymbalyuk and R. L. Calabrese. A model of slow plateau-like oscillations based upon the fast Na^+ current in a window mode. *Neurocomputing*, 38-40:159–166, 2001.

[46] R. J. Butera, Jr., J. Rinzel, and J. C. Smith. Models of respiratory rhythm generation in the pre-Bötzinger complex I. Bursting pacemaker neurons. *J. Neurophysiol*, 82(1):382–397, 1999.

[47] A. Vinet and F. A. Roberge. Excitability and repolarization in an ionic model of the cardiac cell membrane. *J. Theor. Biol*, 170:183–199, 1994.

[48] J. S. Enns-Ruttan. *Analysis Of Electrophysiological Models Of Spontaneous Secondary Spiking And Triggered Activity.* PhD thesis, The University Of British Columbia, 1998.

[49] T. B. Kepler and E. Marder. Spike initiation and propagation on axons with slow inward currents. *Biol Cybern*, 68:209–214, 1993.

[50] O. Bernus, R. Wilders, C. W. Zemlin, H. Verschelde, and A. V. Panfilov. A computationally efficient electrophysiological model of human ventricular cells. *Am J Physiol Heart C*, 282(6):H2296–H2308, 2002.

[51] L. Priebe and J. Beuckelmann. Simulation study of cellular electric properties in heart failure. *Circ Res*, 82:1206–1223, 1998.

[52] F. Fenton and A. Karma. Vortex dynamics in three-dimensional continuous myocardium with fiber rotation: Filament instability and fibrillation. *Chaos*, 8(1):20–47, 1998.

[53] G. Duckett and D. Barkely. Modelling the dynamics of cardiac action potentials. *Phys. Rev. Lett*, 85(4):884–887, 2000.

[54] R. R. Aliev and A. V. Panfilov. A simple two-variable model of cardiac excitation. *Chaos, Solitons Fractals*, 7(3):293–301, 1996.

[55] R. Hinch. An analytical study of the physiology and pathology of the propagation of cardiac action potentials. *Prog Biophys Mol Bio*, 78(1):45–81, 2002.

[56] C. C. Mitchell and D. G. Schoeffer. A two-current model for the dynamics of cardiac membrane. *B Math Bio*, 65:767–793, 2003.

[57] G. S. Cymbalyuk, Q. Gaudry, M. A. Masino, and R. L. Calabrese. Bursting in leech heart interneurons: Cell-autonomous and network-based mechanisms. *J. Neurosci*, 22(24):10580–10592, 2002.

[58] V. N. Biktashev. Dissipation of the excitation wavefronts. *Phys. Rev. Lett*, 89(16):168102, 2002.

[59] V. N. Biktashev. A simplified model of propagation and dissipation of excitation fronts. *Int. J. Of Bifurcation And Chaos*, 13(12):3605–3619, 2003.

[60] D. Attwell, I. Cohen, D. Eisner, M. Ohba, and C. Ojeda. The steady state TTX-sensitive ("window") sodium current in cardiac Purkinje fibres. *Pflugers Arch*, 379:137–142, 1979.

[61] N. Friedman. *Étude d'un nouveau modèle du myocyte cardiaque incorporant une régulation du calcium intracellulaire.* Master's thesis, Montreal: Ecole Polytechnique de Montréal, Université de Montréal, 1996.

[62] N. Friedman, A. Vinet, and F. A. Roberge. A study of a new model of the cardiac ventricular cell incorporating myoplasmic calcium regulation. *Proc XXII Comput. Med. Biomed. Eng. Soc. Conf.*, pages 92–93, 1996.